Epitaxy and Physical Properties of Group-III Sesquioxide Alloys

Der Fakultät für Physik und Geowissenschaften
der Universität Leipzig
eingereichte

D I S S E R T A T I O N

zur Erlangung des akademischen Grades
Doctor rerum naturalium
Dr. rer. nat.,

vorgelegt
von M. Sc. Anna Hassa
geboren am 01.05.1991 in Görlitz

Gutachter: Prof. Dr. Marius Grundmann (Universität Leipzig)
Prof. Stephen Pearton (University of Florida)

Tag der Verleihung: 21.06.2021

Vorwort

Die vorliegende Arbeit wurde im Rahmen der "Nachwuchsforschergruppe Oxid-Heterostrukturen" bearbeitet und fertiggestellt. An dieser Stelle möchte ich all denjenigen Personen danken, die zum Gelingen dieser Arbeit beigetragen haben.
Insbesondere Herrn Prof. Dr. Marius Grundmann danke ich herzlich für die Vergabe des Dissertationsthemas, seinem wissenschaftlichen Rat und die großzügige wissenschaftliche Freiheit, die er mir in seiner Arbeitsgruppe gewährte, um diese Dissertation anzufertigen.
Weiterhin gilt mein herzlicher Dank Herrn PD Dr. habil Holger von Wenckstern für eine Vielzahl wissenschaftlicher Diskussionen, welche die Arbeit stets beförderten und die Qualität der Arbeit gewährleistete. Außerdem danke ich dem Leiter der "Nachwuchsforschungsgruppe" Dr. Daniel Splith, sowie meinem Kollegen Dr. Max Kneiß, für die hilfreichen Gespräche während unserer gemeinsamen Zeit in der Halbleiterphysik Arbeitsgruppe an der Universität Leipzig. Ihnen und auch Dr. Peter Schlupp danke ich auch sehr für das Gegenlesen dieser Arbeit.
Außerdem möchte ich mich bei allen Kooperationspartnern für die Möglichkeit der institutsübergreifenden Zusammenarbeit bedanken sowie den Mitgliedern der Arbeitsgruppe, insbesondere meinen Zimmerkollegen, für ein angenehmes und herzliches Arbeitsklima.
Meinen Eltern, Großeltern und meinem Mann danke ich aus tiefsten Herzen für ihre bedingungslose Unterstützung. Ihnen widme ich diese Dissertation.

Bibliographische Beschreibung

Hassa (geb. Werner), Anna:
Epitaxy and Physical Properties of Group-III Sesquioxide Alloys
Universität Leipzig, Dissertation
140 Seiten, 202 Zitate, 17 Abbildungen, 2 Tabellen (exklusive des kummulativen Teils)

Referat:

In der vorliegenden Arbeit werden das Wachstum und Materialeigenschaften von Galliumoxid (Ga_2O_3) sowie deren Legierungen mit Indium- oder Aluminiumoxid (In_2O_3/ Al_2O_3) untersucht. Ga_2O_3 kann in verschiedenen Polymorphen (α, β, γ oder κ) auftreten, in denen die fundamentale Bandlücke zwischen 4.6 und 5.3 eV variieren kann. Die Legierung von In_2O_3 oder Al_2O_3 führt zu einer Verringerung oder Vergrößerung der Bandlücke und damit zu einem Bandlückenbereich von 3.7 bis 8.8 eV. Aufgrund variierender Materialeigenschaften der Polymorphe, können eine Vielzahl an Anwendungen umgesetzt werden. Zum Beispiel erlaubt die spontane Polarisaton bei κ-Ga_2O_3 eine hohe 2DEG an der Grenzfläche von Heterostrukturen, wodurch die κ-Phase ein geeigneter Kandidat für die Herstellung von Transistoren mit hoher Elektronenbeweglichkeit ist. Dadurch, dass β-Ga_2O_3 auch als Substrate erhältlich sind, ist diese Modifikation interresant für Hochleistungselektronik. Alle der Gruppe-III Sesquioxide können in der α-Phase kristallisieren, so dass diese besonders geeignet für die Herstellung von wellenselektiven Photodetektoren. Um den Wachstumsprozess und die Eigenschaften der verschiedenen Polymorphe zu untersuchen, wurden die in dieser Arbeit untersuchten Proben mittels gepulster Laserabscheidung (PLD) hergestellt. Die Wachstumsbedingungen, wie der Sauerstoffpartialdruck $p(O_2)$, wurden dafür systematisch variiert und deren Einfluss auf den Kationeneinbau und damit auch die Materialkomposition von $(Al,Ga)_2O_3$ und $(In,Ga)_2O_3$ untersucht. Zum Beispiel verstärkt eine sauerstoffarme Umgebung, was einem geringen $p(O_2)$ entspricht, die Bildung und anschließende Desorption flüchtiger Suboxide. Da sich die Sauerstoffbindungsenergien der untersuchten Materialien voneinander unterscheiden, verursacht einen bevorzugten Einbau von Al in $(Al,Ga)_2O_3$ oder von Ga in $(In,Ga)_2O_3$. Aufgrund einer vorausgesagten großen spontanen Polarisation von κ-Ga_2O_3 basierten Heterostruckturen, wurden anschließend die κ-$(Al,Ga)_2O_3$ und κ-$(In,Ga)_2O_3$ Legierungen in Abhängigkeit der Kompositionszusammensetzung untersucht. Der bisher höchste erreichte In-Gehalt von 35 at.% in κ-$(In,Ga)_2O_3$ ermöglicht in Kombination mit dem maximal errreichten Al-Gehalt von 46 at.% in κ-$(Al,Ga)_2O_3$ eine Bandlückenvariation von 4.3 bis 5.9 eV. Weiterhin wird die erfolgreiche Herstellung von α-$(Al,Ga)_2O_3$ über den gesamten Kompositionsbereich gezeigt. Am Ende wird ein Überblick über aktuelle Mischungsgrenzen, Bandlückenvariationen und Gitterkonstanten abhängig von der Zusammensetzung für die α-, β-, κ-Phase der Sesquioxide sowie der kubischen Bixbyte-Struktur gegeben. Dazu werden aktuelle Ergebnisse aus der Literatur sowie die im Rahmen dieser Arbeit erzielten Ergebnisse zusammengefasst.

Bibliographic Description

Hassa (geb. Werner), Anna:
Epitaxy and Physical Properties of Group-III Sesquioxide Alloys
Universität Leipzig, Dissertation
140 pages, 202 references, 17 figures, 2 tables (all excluding cumulative part)

Abstract:

This thesis focuses on the growth and the determination of physical properties of gallium oxide (Ga_2O_3) and related alloys. Ga_2O_3 may crystallize in various polymorphs (namely α, β, γ or κ) and hence the fundamental bandgap varies between 4.6 and 5.3 eV. An alloy with In_2O_3 or Al_2O_3 reduces or enhance the optical bandgap, which potentially enables bandgap engineering between 3.7 and 8.8 eV. Due to several material properties of the distinct Ga_2O_3 polymorphs, a wide range of applications can be realized. For example, the κ-polymorph possesses a spontaneous polarization, which enables extremely high 2DEG densities at the interface of heterostructures and thus the κ-phase is a suitable candidate for the realization of high-electron mobility transistors. The availability of β-Ga_2O_3 substrates renders this phase interesting for the implementation of high performance power devices. Since each of the group-III sesquioxides may crystallize in the α-phase, this polymorph is especially suited for the fabrication of wavelength-selective photodetectors. In order to study the growth process and the material properties of the different polymorphs, the samples studied in this thesis were prepared by pulsed laser deposition (PLD). For this purpose, several growth conditions, such as oxygen pressure $p(O_2)$, and their influence on the cation incorporation and thus the alloy composition of $(Al,Ga)_2O_3$ and $(In,Ga)_2O_3$ were analyzed systematically. For instance, an oxygen poor ambient, corresponding to low $p(O_2)$ in the PLD chamber causes the formation and subsequent desorption of volatile suboxides. The dissociation energies of the oxygen bonds differs for the materials investigated and induces a preferred incorporation of Al into $(Al,Ga)_2O_3$ or Ga into $(In,Ga)_2O_3$. The κ-polymorph has attracted increasing scientific interest due to a predicted large polarization, the κ-$(Al,Ga)_2O_3$ and κ-$(In,Ga)_2O_3$ alloy was in the focus of the further course. The samples were fabricated with a continuous composition spread to enable investigations of the material properties as a function of the alloy composition. To date, the highest In-content into κ-Ga_2O_3 of 35 at.% is achieved. In combination with the maximum Al-content of 46 at.%, bandgap engineering from 4.3 to 5.9 eV is possible. In addition, α-$(Al,Ga)_2O_3$ was successfully fabricated in the entire composition range. Investigations of the lattice constants reveals relaxed growth for Al contents below 55 at.% and otherwise pseudomorphic growth. In the last part, an overview about current miscibility limits, the variation of bandgap and lattice constants in dependence on the alloy composition for the α-, β-, κ-phase of the sesquioxides as well as of the cubic bixbyte structure is given. Therefore, the data obtained and latest literature data are summarized in this thesis.

Contents

CHAPTER 1

Introduction

Semiconductor-based technology has become an indispensable part of modern life and is used in smartphones and tablets, among other things. Silicon, the primary semiconductor used, has reached its fundamental technological limits in some, more specialized, applications, such as the detection of high energetic ultraviolet (UV) radiation, which brought attention to ultra-wide bandgap semiconductors. Compared to already established materials such as SiC and GaN, the transparent-appearing semiconductor Ga_2O_3 has an ultra-wide bandgap of about 4.6–5.3 eV [1, 2], which is more than 1 eV larger compared to that of SiC (3.3 eV [3]) or GaN (3.4 eV [4]). An alloying with other group-III sesquioxides, namely Al_2O_3 (8.8 eV [5]) or In_2O_3 (3.7 eV [6]), can further enlarge or reduce the possible optical bandgap of Ga_2O_3. Along with a large Baliga's figure of merit, which is approximately four times larger than for GaN or a large breakdown field of 8 MV cm^{-1} [7] being about three times larger than for SiC or GaN, Ga_2O_3 is a particularly promising candidate for next generation power electronic devices. Possible fields of application are high-power electronics [1, 8-10], solar-blind UV-photodetectors (PDs) [11-13], gas sensors [14], or thin film transistors [15]. Touch panel displays, solar cells and applications in optical communication [1, 9, 10] can also be implemented.

Ga_2O_3 can appear in various polymorphs, called α, β, κ and γ assigned to a rhombohedral, monoclinic, orthorhombic or defective spinel crystal structure. The thermodynamical stability of these phases can be ranked by $\beta > \kappa > \alpha > \gamma$ [16]. After Higashiwaki *et al.* introduced a functional metal-semiconductor field-effect transistor based on monoclinic β-Ga_2O_3 in 2012 [7], scientific interest focused on this modification, whereby the lion's share of Ga_2O_3 related scientific publications and especially reviews refer to the β-gallia structure [1, 9, 10, 17]. Due to a predicted large spontaneous electrical polarization P of 23–26 µC/cm^2 [18-20] occurring in the orthorhombic κ-phase, this modification recently moved even further into scientific focus. At the in-

terface of heterostructures (e.g. $Ga_2O_3/(Al_xGa_{1-x})_2O_3$) cause a discontinuous change of the polarization P, which potentially results in extremely high two-dimensional electron gas (2DEG) densities [21] enabling applications in high-electron mobility transistors (HEMTs) or quantum-well infrared photodetectors (QWIPs) [E1]. Since Al_2O_3 crystallizes in a rhombohedral structure at thermodynamic equilibrium, the α-phase can potentially be stabilized over the entire composition range of the $(Al,Ga)_2O_3$ alloy rendering this structure particularly suitable for the realization of wavelength-selective PDs, such as deep UV-PDs or QWIPs [22, 23]. However, for the remaining Ga_2O_3 polymorphs, alloys with Al_2O_3 or In_2O_3 are only possible up to certain cation compositions. When these compositions are exceeded, phase separation occurs resulting a change in physical properties. Accordingly, this must be taken into account in the fabrication of sesquioxide alloy based devices. An exact determination of the miscibility gaps, the resulting bandgap limits and the material properties depending on the alloy composition is therefore essential for the realization of such devices.

The in this thesis presented and discussed samples were prepared by pulsed laser deposition (PLD). A part of the thin films were deposited using single segmented ceramic targets with a distinct chemical composition. The other portion of the samples were grown employing a combinatorial PLD-approach, called continuous composition spread (CCS) approach, which was introduced by von Wenckstern *et al.* from the semiconductor physics group of the University Leipzig [24]. The target used for this approach has to be two-fold azimuthally segmented, consisting either of Ga_2O_3/Al_2O_3 or of Ga_2O_3/In_2O_3, to fabricate $(Al,Ga)_2O_3$ or $(In,Ga)_2O_3$ thin films with a lateral varying cation composition. When preparing thin films by PLD, growth conditions, such as substrate temperature (T_g) or the oxygen pressure ($p(O_2)$) in the PLD chamber, can be defined. The choice of T_g and $p(O_2)$ has a significant impact on the formation of Ga_2O_3 thin films, as described in previous publications by Müller *et al.* and Zhang *et al.* [25, 26]. In the study of Müller *et al.* on β-Ga_2O_3 thin films by PLD reveals that an reduced $p(O_2)$ results in lower growth rates [25]. Similar investigations were presented from Vogt and Bierwagen for β-Ga_2O_3 thin films grown by molecular beam epitaxy (MBE) [27,28]. Due to a low oxygen concentration during deposition, increased volatile Ga_2O suboxides are formed, which desorb and do not contribute to the thin film growth. If sufficient oxygen is available all offered Ga atoms are incorporated into the layer. Furthermore, Zhang *et al.* discovered for PLD grown thin films that an increased growth temperature also leads to decreased growth rates, because high T_g intensifies the formation of volatile Ga_2O [26]. Since the various Me-O (Me = Al, Ga, In) bonds have different dissociation energies (E_diss(Al-O) = 5.22) eV, E_diss(Ga-O) = 3.9 eV, E_diss(In-O) = 3.6 eV [29]), the fabrication of $(Al,Ga)_2O_3$ or $(In,Ga)_2O_3$ alloys in an

oxygen-poor growth regime results not only in a reduction of the growth rates, but also in a non-stoichiometric Me cation transfer from target to substrate. More precisely, this means that in $(Al,Ga)_2O_3$ the Al atoms and in $(In,Ga)_2O_3$ the Ga atoms are preferentially incorporated into the layer. That low $p(O_2)$ leads to a non-stoichiometric Ga-to-In or rather Al-to-Ga ratio in β-$(In_xGa_{1-x})_2O_3$ or β-$(Al_xGa_{1-x})_2O_3$ thin films was already investigated in the Semiconductor Physics Group of the University Leipzig and discussed in several theses as the master thesis of M. Purfürst [30] or the master thesis of the author [31]. To fabricate thin films with a reproducible cation target-to-substrate transfer and high growth rates it is mandatory to optimize the growth conditions for the sesquioxides and their various polymorphs.

Taking these potential the potential research areas of Ga_2O_3 based alloys into account, the following objectives result for the present work:

I Investigations of phase formation and desorption processes of $(Al,Ga)_2O_3$ and $(In,Ga)_2O_3$ thin films in dependence on $p(O_2)$ and/or T_g

II Determination of physical properties of κ-$(Al_xGa_{1-x})_2O_3$, κ-$(In_xGa_{1-x})_2O_3$ as well as α-$(Al_xGa_{1-x})_2O_3$ thin films as a function of the cation composition x

III Extension of the phase limits and thus an expanded optical bandgap range

The results of these research aspects were published in a total of six peer-reviewed journal articles forming the cumulative part of this thesis. In the first two, the influence of oxygen pressure and growth temperature on the phase formation of $(Al,Ga)_2O_3$ is discussed in Refs. [E2, E3]. The phase limits and material properties of κ-$(Al_xGa_{1-x})_2O_3$, κ-$(In_xGa_{1-x})_2O_3$ and α-$(Al_xGa_{1-x})_2O_3$ thin films, which exhibit cation composition gradients are published in Refs. [E4-E6] and form the second part of this work. The last part consists of a topical review article [E7] in which published results together with data obtained in the scope of this work on the progression of current miscibility limits, optical band gaps and lattice constants in dependence on the cation alloy of the mentioned sesquioxide alloys is summarized. Additionally, this article deals with the desorption processes that can be observed in an oxygen poor or rich ambient, respectively.

Other studies in which the author has participated deal with different polymorphs of the $(In,Ga)_2O_3$ alloy [E8-E10], κ-Ga_2O_3 and its related alloys [E1, E11-E13] as well as the different combinatorial PLD approaches that are used within the semiconductor working group [E14].

Annotation: The present thesis was prepared in the Semiconductor Physics Group at the Faculty of Physics and Earth Sciences of the University Leipzig. This thesis was funded within the framework of the Young Investigator Group “Oxide Heterostructure” (SAB100310460) and partly by the Deutsche Forschungsgemeinschaft (DFG, German Research Foundation) - project number 31047525, SFB762, project B04, which were acquired by Holger von Wenckstern, Michael Lorenz and Marius Grundmann. The author acknowledges the Leipzig School for Natural Sciences BuildMoNa. Own contributions and contributions of others are summarized as part of this cumulative thesis. References to publications with own contribution are marked with an "E".

CHAPTER2

Group-III Sesquioxides

The materials of the group-III sesquioxides, which include indium, gallium, and aluminum oxide (In_2O_3, Ga_2O_3, Al_2O_3), are characterized by ultra-wide bandgap energies and an appearance transparent to the human eye with absorption edges deep into the ultraviolet (UV) band (see fig. 2.1). The possibility of alloying these materials among each other enables precisely tunable bandgap energies in a broad range and thus the realization of applications where a tailored bandgap is required, such as solar blind UV-photodetectors. The sesquioxides have different thermodynamically stable crystal structures, namely, the corundum-structured α-Al_2O_3, the monoclinic β-Ga_2O_3 or the cubic bixbyte In_2O_3 structure, respectively. As a result, phase separation can occur in the alloys observable at certain cation compositions. The phase limits vary for the different crystal structures and confine the potential bandgap ranges. The following sections cover the polymorphism of the materials mentioned and their physical properties. In addition, for the various alloys, the physical properties as function of the chemical composition are discussed only briefly, since an extensive consideration in the form of a topical review [E7] is part of this cumulative thesis.

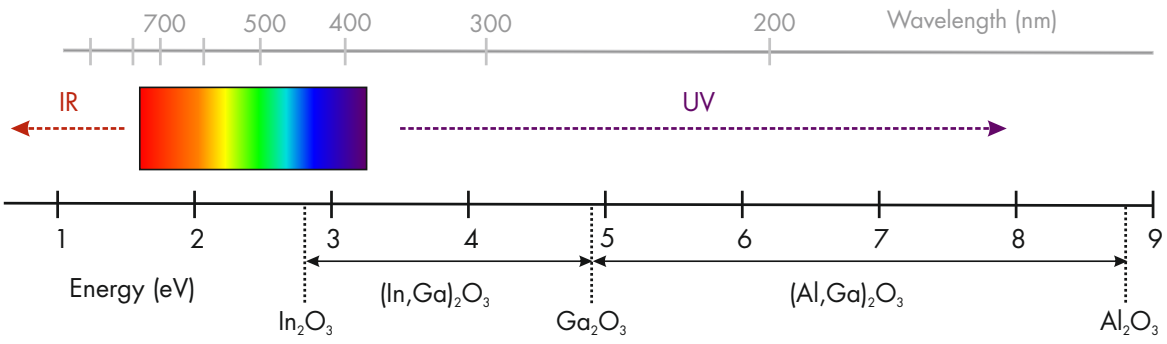

Figure 2.1: Electromagnetic spectrum of light and the optical bandgaps of the sesquioxides in dependence on photon energy (black scale) and wavelength (gray scale). Ranges of infrared (IR) and UV radiation as well as visible light are marked in the graph.

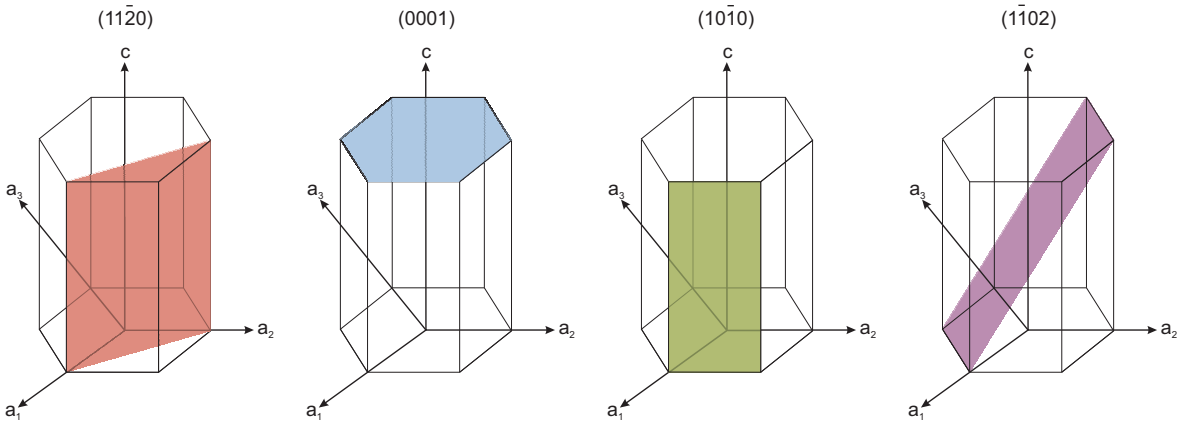

Figure 2.2: Schematic representation of an α-Al_2O_3 hexagon. Different lattice planes displaying possible sapphire cuts are indicated by different colors as labeled. Cutting along the red/blue/green/violet colored lattice plane results in a-/c-/m-/r-plane sapphire.

2.1 Aluminum Oxide

The highest bandgap of the group-III-sesquioxides with an energy of 8.8 eV [5] exhibits the rhombohedral α-polymorph being the thermodynamically most stable phase of Al_2O_3. Due to its optical transparency, electrically insulating behaviour, high temperature stability, high mechanical strength [32] and since it can be produced cost-effective on industrial scale, α-Al_2O_3 is a common substrate for Ga_2O_3 based thin films. The substrates can be obtained by cutting α-Al_2O_3 single crystals along their (11.0)-, (00.1)-, (10.0)- or (01.2)-lattice planes (corresponding to a-/c-/m-/r-plane sapphire), as presented in fig. 2.2. In the rhombohedral lattice structure, the Al cations are octahedrally coordinated (O_h) within a hexagonal close-packed O^{2-} array. The rhombohedral polymorph crystallizes in space group $R\bar{3}c$ with the lattice parameters $a = 4.7617$ Å and $c = 12.995$ Å [2]. Actually, Al_2O_3 is an indirect semiconductor, but is usually referred to as direct one because the difference between the direct and indirect band-to-band transition is so small that the material behaves as a direct semiconductor [33].

2.2 Gallium Oxide

In 1952, Roy *et al.* identified and defined the various polymorphs in which Ga_2O_3 may occur and denoted them as α-, β-, γ-, δ-, and ϵ-polymorph [16]. Later studies by Playford *et al.* revealed that the δ-phase is not a distinct polymorph of Ga_2O_3, but a nanocrystalline form of the ϵ-phase. The monoclinic β-gallia structure is the thermodynamically most stable phase, followed by the metastable orthorhombic κ-

Table 2.1: Space group, lattice parameter, ratio of octahedral to tetrahedral coordinated Ga sites and optical bandgap energies (at RT) for the different gallia polymorphs.

Polymorph (Structure)	**Space group**	**Lattice constants**	O_h:T_d	**Optical bandgap**	**Refs.**
β (monoclinic)	$C2/m$	$a = 12.214$ Å $b = 3.037$ Å $c = 5.798$ Å $\beta = 103.83°$	1:1	4.6-5.0 eV	[1, 34]
κ (orthorhombic)	$Pna2_1$	$a = 5.046$ Å $b = 8.702$ Å $c = 9.283$ Å	3:1	4.9 eV	[35], [E11]
α (rhombohedral)	$R\bar{3}c$	$a = 4.9825$ Å $c = 13.433$ Å	1:0	5.2-5.3 eV	[36, 37]
γ (defective spinel)	$Fd\bar{3}m$	$a = 8.2376$Å	2:1	5 eV	[38, 39]

(also referred to as ϵ-), the rhombohedral α-, and by the defective spinel γ-phase [16]. The crystal structure also determines the size of the band gap energy, which can vary from 4.6 to 5.3 eV depending on the polymorph.

In the crystal lattice, the Ga atoms occupy either octahedrally (O_h, 4-fold coordinated) or tetrahedrally (T_d, 6-fold coordinated) ordered cation sites. The ratio of O_h to T_d differs for the different polymorphs. In tab. 2.1 are these ratios along with the space groups, lattice constants, and optical bandgaps for the different gallia polymorphs summarized.

2.2.1 Monoclinic β-Ga_2O_3

The thermodynamically most stable β-gallia structure, so that the main focus of previous studies was on this polymorph and a large number of reviews have been published so far [1, 9, 10, 40].

In the β-gallia unit cell, the Si atoms typically occupy the tetrahedral lattice sites while Sn rather prefers the octahedral ones [41]. β-Ga_2O_3 belongs to space group $C2/m$ possessing a lattice constants $a = 12.214(3)$ Å, $b = 3.0371(9)$ Å, $c = 5.7981(9)$ Å and $\beta = 103.83°$ with an unit cell volume of $208.85(1)$ Å^3 [34]. The unit cell consists of four Ga_2O_3 molecules with a O_h:T_d ratio of 1:1, as shown in fig. 2.3.

The monoclinic phase can be fabricated by a variety of growth techniques. These include for thin films PLD [25, 26, 43-49], metal organic chemical vapour deposition (MOCVD) [50-58], mist chemical vapour deposition (CVD) [59, 60], MBE [27, 61-63], halide vapor phase epitaxy (HVPE) [41, 64-67], metal organic chemical vapor phase

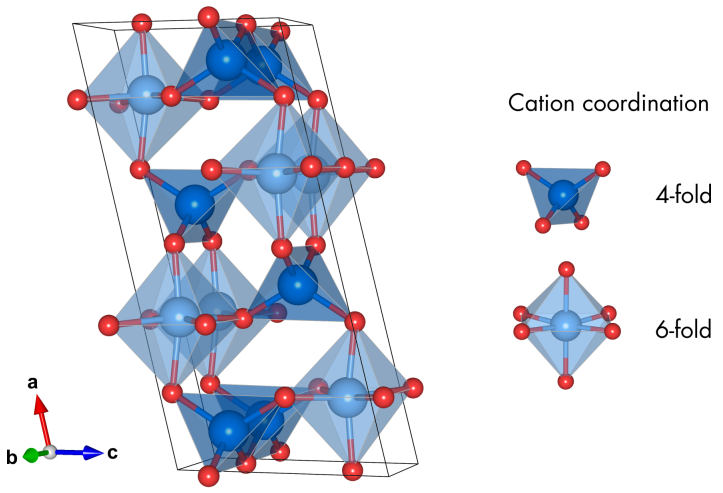

Figure 2.3: Crystal structures of monoclinic β-Ga_2O_3. The oxygen atoms are shown as red and the gallium atoms as blue spheres. The possible cation sites are shown next to the unit cell. The graphics were created with *VESTA3* [42].

epitaxy (MOVPE) [68], and atomic layer deposition (ALD) [69, 70]. Monoclinic single bulk crystals (e.g. substrates) can be synthesized by the floating-zone technique (FZ) [71-73], the edge-defined film-fed growth (EFG) [74] and the Czochralski (CZ) [75, 76] method.

Former studies showed that variations in the growth conditions can influence the thin film thickness and growth rates due to the formation and subsequent desorption of volatile Ga_2O suboxides. During MBE synthesis, Vogt and Bierwagen established a correlation between layer thickness and oxygen- or gallium-flux, respectively [27, 28]. With an increased Ga-flux, a reduced thin film thickness was observed. An enhancement of the O-flux resulted in thin films with increased layer thickness. Similar observations were reported for PLD grown thin films by Müller *et al.*, where decreasing oxygen pressure ($p(O_2)$) cause a reduction in growth rates [25]. Furthermore, Zhang *et al.* demonstrated that high growth temperatures (T_g) results also a reduction in growth rates for PLD grown thin films [26]. This drop in film thickness or the growth rate is caused by the formation and subsequent desorption of volatile suboxides in an oxygen poor growth regime. Figure 2.4 illustrates how the atoms involved behave in an oxygen rich or a poor regime, respectively. While in the former case all offered atoms are incorporated into the thin film layer, in the second case volatile suboxides consisting of two Ga atoms and one O atom are formed due to a lack of oxygen. The suboxides desorb and are not embedded in the layer resulting in a lower film thickness and thus growth rate. Ga_2O suboxides can either be formed in the ambient before thin film crystallization or in the course of an etching process. In the latter case, Ga atoms release O atoms from the layer to form suboxides being desorbed. The formation of

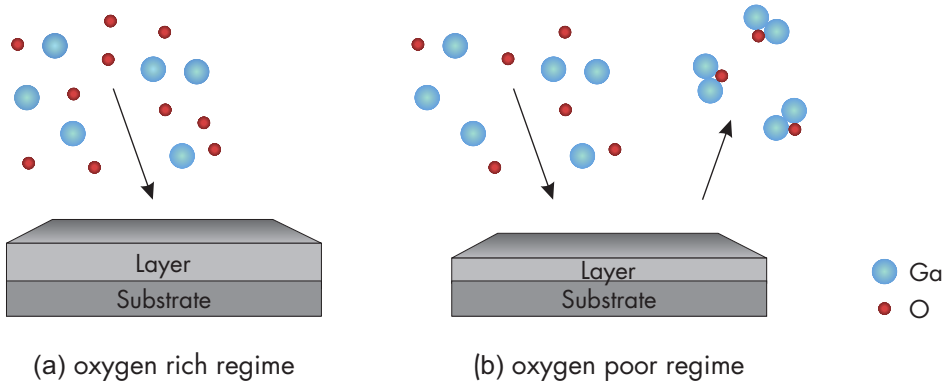

Figure 2.4: Schematic growth mechanism of β-Ga_2O_3 thin films for (a) an oxygen rich regime, where all offered atoms are incorporated into the layer or (b) an oxygen poor regime, where volatile Ga_2O forms and desorbs.

the suboxides (and with that the growth rate/layer thickness) can thus as a side effect be controlled by the growth temperature as well as the oxygen supply in the case of MBE or the oxygen pressure applied in the case of PLD.

So far, many theoretical calculations were published about the electronic structure of β-Ga_2O_3, based on the density functional theory (DFT) approach [37, 77-81]. The results of the calculations are quite similar and show that the conduction band minimum (CBM) is located at the Γ point while the valence band exhibits an almost flat dispersion. He *et al.* demonstrated that the valence band maximum (VBM) occur at the M-point leading to an indirect bandgap with an energy of 4.66 eV as well as a slightly lower direct bandgap of 4.69 eV at the Γ-point [37]. Similar calculations were presented from Peelaers *et al.* with an indirect bandgap of 4.84 eV and a direct one of 4.88 eV or Varley *et al.* with an indirect bandgap of 4.83 eV and a direct one of 4.87 eV [79, 80]. Since the difference between both types of bandgaps is quite small, β-Ga_2O_3 is described as direct semiconductor with an experimentally determined optical bandgap ranging between 4.6-5.0 eV [1]. The asymmetrical crystal structure of the monoclinic β-gallia modification results in an optical anisotropic behaviour. Matsumoto *et al.* conducted a study to systematic investigate the optical anisotropy of vapor grown single crystal platelets of β-Ga_2O_3 at RT [82]. In summary, they reported for light polarized E$\|$b an absorption edge of 4.90 eV, 4.54 eV for E$\|$c and 4.56 eV for E$\perp$b&c [82]. Another study of FZ grown single crystals performed by Ueda *et al.* yields similar values of 4.90 eV for E$\|$b and 4.59 eV for E$\|$c [83].

In addition, the monoclinic phase was extensively electrically characterized, whereby a maximum room temperature (RT) electron mobility of $\mu = 176\,\mathrm{cm}^2/\mathrm{Vs}$ [84] was found for an epitaxial grown and Si-doped thin film. So far, the high theoretical calculated breakdown field of 8 MV/cm [34, 83] could not be reached, but it was possible to

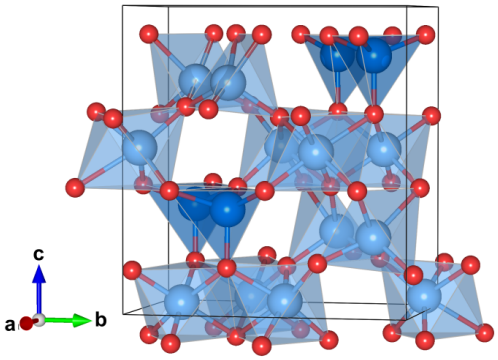

Figure 2.5: Crystal structures of orthorhombic κ-Ga_2O_3. The oxygen atoms are displayed as red and the gallium atoms as blue spheres, wherein the octahedrally bonded atoms are shown brighter than the tetrahedrally bonded Ga atoms. The graphic was created with the software *VESTA3* [42].

fabricate a β-Ga_2O_3 thin film with a breakdownfield of 4.2 MV/cm by low pressure CVD [85] . The charge carrier concentration reaches values up to $1.44 \times 10^{19}\,\mathrm{cm}^{-3}$ for unintentionally doped epitaxial thin films [41] and can be tuned by doping with Sn or Si [86-88].

2.2.2 Orthorhombic κ-Ga_2O_3

In the literature, this polymorph is often denoted as ϵ-phase, but this is mainly associated to a hexagonal lattice structure with space group $P6_3mc$ [16, 89, 90]. However, detailed transmission electron microscopy (TEM) investigations conducted by Cora *et al.* revealed that this polymorph crystallizes in an orthorhombic lattice structure having space group $Pna2_1$ [35]. Due to its isostructurality to the κ-alumina phase, Cora *et al.* suggested the use of the notation of κ-Ga_2O_3. Even though many publications support the orthorhombic structure afterwards, both nominations (κ and ϵ) can be found in literature. Within the semiconductor physics group of the University Leipzig, the notation as κ was decided upon, therefore it is used in this thesis and the related publications.

Figure 2.5 demonstrates the orthorhombic unit cell, formed out of two different stacking layers. The first consists only of octahedrally ordered Ga sites and the other of alternately arranged octahedrally and tetrahedrally ordered Ga sites, resulting in an O_h:T_d ratio of 3:1. The lattice constants of this structure are determined to be $a = 5.046$ Å $b = 8.702$ Å $c = 9.283$ Å [35]. κ-Ga_2O_3 typically grows in a columnar fashion and forms three rotational domains, which are rotated by 120° with respect to each other, which can be clearly distinguished by XRD ϕ-scans [E11].

The electronic band structure of κ-Ga_2O_3 was derived by DFT calculations, demon-

strating a flat valence band, as for β-Ga_2O_3, which results in a bandgap energy of 4.6 eV [20]. With angle-resolved photoemission spectroscopy (ARPES) measurements, a bit higher VBM at the Γ-point was calculated leading to the assumption that the orthorhombic phase offers actually a direct optical bandgap of around 4.4 eV [91]. Further experimentally determinations show slightly higher values of approximately 4.9eV [E11] [35].

So far, κ-Ga_2O_3 has been successful fabricated by mist CVD [92, 93], MOCVD [35, 56, 57, 89, 91, 94-96], HVPE [97, 98], plasma-assisted and tin-assisted MBE [90, 99], tin-assisted PLD [43] [E11], or ALD [100]. To stabilize the κ-phase via MBE or PLD, it is necessary to add tin during growth, otherwise the β-polymorph is formed. Kracht *et al.* proposed that the κ-phase is formed by a metal-exchange catalysis, which can also be mediated by indium [90]. Depth resolved X-ray photoelectron spectroscopy (XPS) measurements found tin only on the layer surface for PLD grown thin films [E11]. Therefore Kneiß *et al.* suggested a surfactant-mediated growth for the synthesis of κ-Ga_2O_3 [E11].

Since tin is not incorporated in these tin-assisted PLD grown samples, it is required to add a further dopant to induce an n-type conductivity. A successful intrinisic Si and extrinsic Sn doping for with charge carrier concentrations of few $10^{18}\,cm^{-3}$ and about $10^{17}\,cm^{-3}$ was achieved by Parisini *et al.* for samples grown by MOVPE [101]. Additionally, the κ-phase is the only polymorph of Ga_2O_3 that exhibits a spontaneous electrical polarization P. Due to the possibility to attain polarization doping, the scientific interest and thus the number of publications on this phase has increased rapidly in the recent years. At the interface of orthorhombic $Ga_2O_3/(Al_xGa_{1-x})_2O_3$ or $Ga_2O_3/(In_xGa_{1-x})_2O_3$ based heterostructures a discontinuous change of the polarization induces a charge accumulation, enabling for instance application in high-electron mobility transistors.

2.2.3 Rhombohedral α-Ga_2O_3

The semi-stable rhombohedral modification is of particular interest, because it possesses the same lattice structure as the most commonly used α-Al_2O_3 substrates, which results in a small lattice mismatch between layer (α-Ga_2O_3) and substrate (α-Al_2O_3). So far, α-Ga_2O_3 can be stabilized on *a*-, *c*-, *m*- and *r*-plane sapphire by mist CVD [36, 59, 102-106], mist epitaxy [107], HVPE [108-111], MOVPE [112], MBE [22], PLD [E6], ALD [23] and the sol-gel method [113]. The usage of an α-Fe_2O_3 buffer layer between substrate and thin film can positively promote the growth [93]. During the deposition of other polymorphs, such as monoclinic or orthorhombic thin films, a small 3-4 monolayers thick α-Ga_2O_3 interlayer between substrate and thin film was

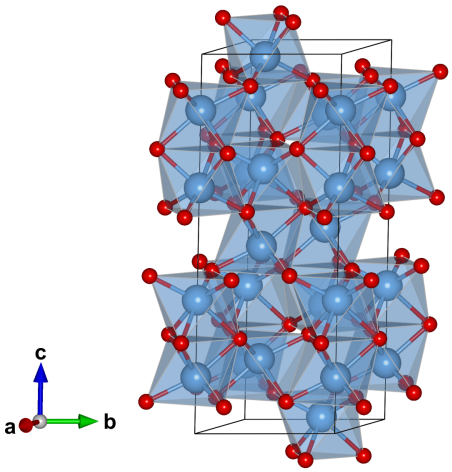

Figure 2.6: Stick-and-ball model of rhombohedral α-Ga_2O_3. The gallium atoms are indicated as blue spheres and the oxygen atoms as red ones. The structure was drawn with the software *VESTA3* [42].

observed and reported for MOVPE, PLD and MBE [114], [E3]. The α-interlayer grows coherently strained up to the point where the strain build up is too large, so that the crystal turns over into β- or κ-phase.

Since the Ga atoms have larger ionic radii (0.62 Å) compared to the Al atoms (0.57 Å), the lattice parameters of α-Ga_2O_3 are larger than those of α-Al_2O_3 and amount to $a = 4.9825$,Å and $c = 13.433$ Å [36]. A rhombohedral unit cell including the octahedral ordered cations and oxygen atoms is presented in fig. 2.6. Of all reported polymorphs, this phase has the highest optical bandgap with energies ranging between 5.0 eV and 5.3 eV [102, 108, 110, 112, 113]. By an additional Sn- [59, 106, 115], Si- [116], or F-doping [117] it is possible to obtain n-type conducting thin films enabling the preparation of highly rectifying Schottky barrier diodes [103, 107, 118].

2.2.4 Defective-spinel γ-Ga_2O_3

The thermodynamically least stable gallia modification is the cubic defective-spinel γ-phase. The space group is $Fd\bar{3}m$ and the lattice constant was determined to $a = 8.2376$Å [38]. The ratio of O_h to T_d ordered Ga sites is 2:1. So far, stabilization of γ-Ga_2O_3 has only been possible with a few techniques, such as mist CVD [39], MOCVD [112] or a solvothermal oxidation of gallium metal in ethano lamine [119]. Furthermore, this polymorph can be obtained by PLD using a Mg-doped target [120]. Via MBE γ-Ga_2O_3 thin films doped with Mn or Fe were reported [121, 122]. The γ-phase can also be achieved by baking κ-Ga_2O_3 at around 820°C [123]. Oshima *et al.* determined a direct bandgap of 5.0 eV [39].

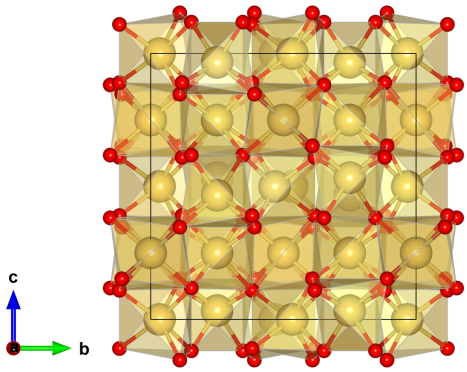

Figure 2.7: Stick-and-ball model of the cubic crystal structure of In_2O_3 created with *VESTA3* [42]. The indium atoms are indicated as yellow spheres and the oxygen atoms as red ones.

2.3 Indium Oxide

Indium oxide crystallizes in thermodynamic equilibrium in the body-centered cubic (bcc) In_2O_3 structure, sometimes referred to as bixbyte structure. Cubic In_2O_3 belongs to space group $Ia3$ with the lattice constant $a = 10.117 \pm 0.001$ Å [124]. Figure 2.7 demonstrates the unit cell of cubic In_2O_3, which consists of 16 molecules or 80 atoms, respectively. The In atoms are six-fold coordinated and can occupy in the unit cell either the Wyckhoff position 8b (cation lies on the space diagonal between two oxygen vacancies) or the Wyckhoff position 24d (within the bcc cell with the oxygen vacancies located on the surface diagonal) with a cation ratio of 1:3.

Binary cubic In_2O_3 can be fabricated by different growth methods such as PLD [125-129], MBE [130-135], MOCVD [136-138], sputtering [139-141], and others. In most reports, YSZ, ZrO_2 (100) or Al_2O_3 (00.6) are employed as substrates.

First optical investigations of Weiher and Ley indicated that In_2O_3 can posses an indirect, forbidden band-to-band transition of 2.62 eV or a direct transition of 3.75 eV [142]. Walsh *et al.* showed later an upper bandgap limit of the direct, parity-forbidden transition of 2.9 eV [143]. Experimental studies discovered the bandgaps energies of about 3.7 eV complying the first dipole allowed band-to-band transition [142, 144].

The semiconductor is intrinsically n-type with a high accumulation of charge carriers near the surface, which has in the early stages been an impediment in the fabrication of Schottky contacts. Nominally undoped In_2O_3 can exhibit free charge carrier concentrations in the range of 10^{18} to $10^{19}\,cm^{-3}$ [126, 145]. The best known doping of In_2O_3 is probably that with Sn, which is already known as ITO finding increased industrial application as a transparent conductive oxide.

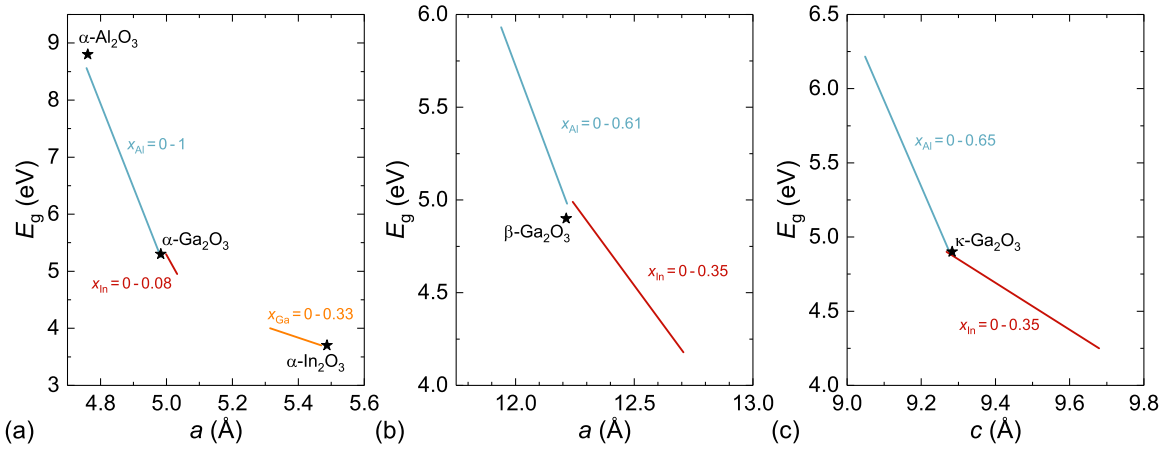

Figure 2.8: Optical bandgap E_g as a function of selected lattice constants for the actual miscibility gaps of the (a) α-, (b) β- and (c) κ-polymorph of the $(Al_xGa_{1-x})_2O_3$ and $(In_xGa_{1-x})_2O_3$ alloys. The actual miscibility gaps are labeled in the graphs. The data are in accordance to Ref.[E7].

2.4 Ternary Alloys of the Group-III Sesquioxides

The opportunity to alloy the group-III sesquioxides with each other, for instance, allows to precisely tailor the optical bandgap. Due to the different crystal ground states of the binary materials, it is required to identify the specific miscibility limits of the particular alloys, since the amount of maximum cation composition defines the possible tunable bandgap range. Usually, phase separation occursfor higher composition ratios. Figure 2.8 depicts the current miscibility limits with the resulting bandgap ranges and evolution of selected lattice constants for the α-, β- and κ-modifications. Characteristic physical properties, such as the evolution of the optical bandgaps or the lattice parameters as a function of the chemical composition in $(Al_xGa_{1-x})_2O_3$ and $(In_xGa_{1-x})_2O_3$ thin films occupy a significant part of the cumulative part of this work, hence only a short insight is given in the following. The growth methods with which the respective ternary alloys could be stabilized to date are summarized in tab. 2.2.

2.4.1 Aluminum Gallium Oxide

First studies of the solubilities of Ga_2O_3 in α-Al_2O_3 as well as Al_2O_3 in β-Ga_2O_3 were carried out by Hill *et al.* in 1952 [146]. In the former case, they showed a maximum cation basis of 25% and for Al_2O_3 in β-Ga_2O_3 a limit of 67%. Later investigations of Mizuno *et al.* and Jaromin *et al.* of solid soultions found solubility limits of Ga_2O_3 in α-Al_2O_3 of 15% or 12%, respectively [147, 148]. The reported maximum Al-contents in β-Ga_2O_3 are 75% or rather 78%. In subsequent experimental investigations

Table 2.2: Selected exemplary growth methods with several references for the rhombohedral, monoclinic, orthorhombic, and cubic polymorphs of the $(Al,Ga)_2O_3$ and $(In,Ga)_2O_3$ alloys.

Polymorph	**Growth method**
α-$(Al,Ga)_2O_3$	mist CVD [2, 151-153], PLD [154], MBE [155]
β-$(Al,Ga)_2O_3$	PLD [156-159], MBE [149, 160-162], sputtering [163]
κ-$(Al,Ga)_2O_3$	mist CVD [164], PLD [E3, E4, E13]
α-$(In,Ga)_2O_3$	mist CVD [2, 165, 166]
β-$(In,Ga)_2O_3$	MOCVD [167], PLD [129, 168-170], [E8], MBE [62, 99, 171], sol gel method [172]
κ-$(In,Ga)_2O_3$	mist CVD [173], PLD [E5, E12]
c-$(In,Ga)_2O_3$	MOCVD [174,175], PLD [169], [E8], MBE [11], sol-gel method [172]

of $(Al_xGa_{1-x})_2O_3$ thin films, Oshima *et al.* found a maximum Al incorporation into the β-gallia structure of 61 at.% [149]. Since Ga_2O_3 can also crystallize in the rhombohedral crystal structure, the α-phase can be stabilized in the entire compositional range [150] [E6]. The orthorhombic κ-phase is a metastable polymorph of Ga_2O_3 as well as of Al_2O_3, so there should be no miscibility gaps. In practice, however, only a maximum incorporation of Al in κ-Ga_2O_3 of 65 at.% has actually been achieved so far [E13]. The reverse case has not yet been investigated.

In the monoclinic and orthorhombic crystal structure, the Al atoms occupy initially the octahedrally coordinated cation sites. If all O_h are occupied, Al occupy the tetrahedrally ordered ones. The incorporation of the smaller aluminum atoms (ionic radius of Al and Ga: $r_{Al} = 0.535\,\text{Å}$ $r_{Ga} = 0.62\,\text{Å}$) into the lattice structure reduces the distances in the unit cells. The change of the lattice parameters is linear (see fig. 2.8) and follows Vegard's law as long as only the octahedral lattice places are occupied. The phase limits and thus the optical bandgap ranges of each polymorph are given in fig. 2.8 and discussed in detail in Ref. [E7] as part of this thesis.

2.4.2 Indium Gallium Oxide

In the ternary alloy of Ga_2O_3 with In_2O_3, phase separations also occur for certain cation compositions due to the different ground states of the materials. Goldschmidt *et al.* were one of the first research groups investigating this alloy in 1925 [176]. They were able to distinguish three different crystal structures: the β-gallia phase, the cubic bixbyite structure and a hexagonal intermediate phase called $InGaO_3$II phase as well. Later investigations of Shannon and Prewitt determined phase stability of the

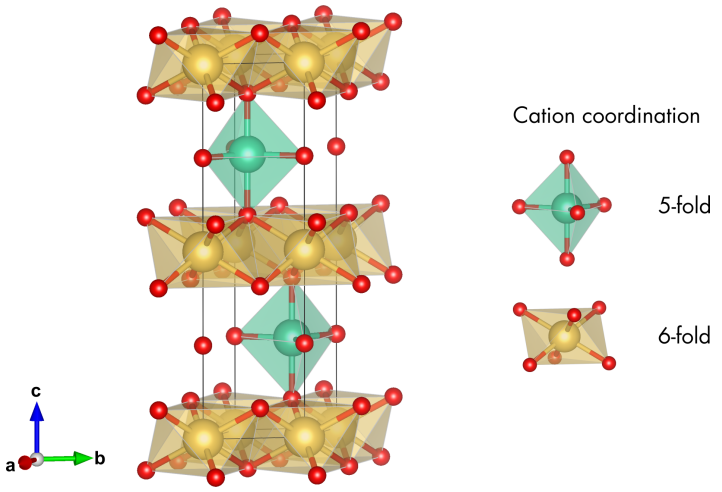

Figure 2.9: Ball-and-stick model of the hexagonal $InGaO_3$II phase created with *VESTA3* [42]. The turquoise spheres indicate the five-fold coordinated Ga sites, the yellow spheres the six-fold coordinated In sites and the red ones the oxygen atoms.

monoclinic structure for $x = 0.25$, $x = 0.33$ and $x = 0.5$ (note, that an impurity phase of bixbyite In_2O_3 was also present in the $x = 0.5$ mixture) and observed at high-pressures the hexagonal structure crystallizing within the $P6_3/mmc$ space group [177]. In this structure, the Ga atoms occupies five-fold and the In atoms six-fold coordinated lattice places. The InO_6 and GaO_5 polyhedra layers alternate along the *c*-direction, as presented in fig. 2.9. The larger In atoms ($r_{In} = 0.8$Å) induce the expansion of the unit cell resulting in increasing lattice constants following Vegard's law as demonstrated in fig. 2.8.

Due to the reduction of the bandgap energy by the incorporation of In atoms, this enables potential bandgap engineering between 4.9 and 3.7 eV. Reports over first electrical transport measurements [168, 172, 175, 178, 179] [E8] are available and the number of publications increased over the years. Starting from the Ga rich side of the phase diagram, the α- and κ-phases were investigated in addition to the β-phase. The maximum solubilities shown so far are $x \leq 0.35$ for the β- and κ-polymorph [11] [E5] and $x \leq 0.08$ and for the α-polymorph [165]. Vice versa, Ga can be incorporated in α-In_2O_3 up to 33 at.% [2] and in cubic In_2O_3 up to 50 at.% [174, 175]. The resulting bandgap ranges of the described polymorphs are summarized in fig. 2.8 and described in chapter 4.

Studies on $(In,Ga)_2O_3$ thin films revealed that in an oxygen poor regime in addition to the formation of Ga_2O, In_2O is also formed [E5, E8] [171]. Because of the stronger Ga-O bond compared to the In-O bond, rather In_2O suboxides are formed and desorbed leading to a comparatively smaller amount of In atoms than Ga atoms in the layer.

A more detailed consideration can be found in chapter 4.

CHAPTER3

Experimental Techniques

The thin films discussed in this thesis were fabricated by pulsed laser deposition (PLD). Due to a high-energy laser, material of a ceramic target is vaporized and interacts with the laser light such that a plasma plume originates, which is directed on an opposing substrate, where the material subsequently condensates and a thin film forms [180]. To create thin films with a lateral varying cation composition, a combinatorial approach for PLD was implemented. The resulting cation ratio was determined by energy dispersive X-ray spectroscopy (EDX) and the crystal structure by X-ray diffraction (XRD). Further structural investigations were partly performed by atomic force microscope (AFM) or transmission electron microscopy (TEM). Optical properties, like bandgap energy or dielectric constants, were investigated by transmission spectroscopy and spectroscopic ellipsometry. The following section will give a brief overview about these techniques.

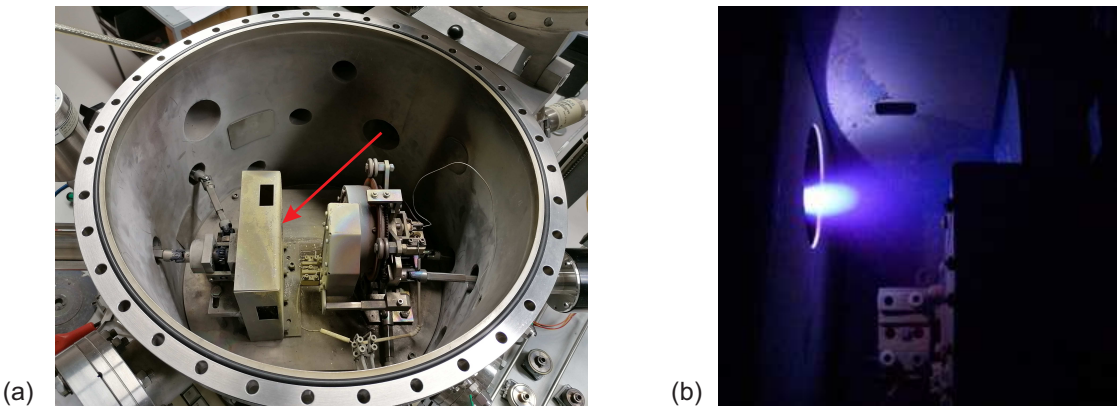

Figure 3.1: Picture of (a) the PLD chamber utilized at the semiconductor physics group of the University Leipzig and (b) of a plasma plume generated by a Ga_2O_3 target. The red arrow indicate the path of the laser beam.

3.1 Thin Film Preparation

Figure 3.1(a) presents an image of the PLD chamber of the semiconductor physics group where all samples discussed in the cumulative part of this thesis were deposited. The corresponding schematic layout is shown in fig. 3.2. A KrF excimer laser (*Coherent LPX Pro 305*, 248 nm) is directed through a quartz window on a ceramic target consisting of the material from which the thin film is later formed. The energy density of the laser beam is 2.6 $\mathrm{Jcm^{-2}}$ on the target surface leading to an evaporation of the target material. Then, the interaction of the laser light with the ablated material creates a plasma state. Due to a pressure gradient the material spreads away from the target in the shape of a plasma plume. This material condenses and forms a thin film when it hits the substrate. Figure 3.1(b) shows such a plasma plume formed using a ceramic Ga_2O_3 target. Target and substrate are mounted rotatable opposite each other at a distance of 10 cm and with a small lateral offset ϵ to each other. ϵ enables a consistent condensation of the plasma material on the substrate and thus the formation of a homogeneous thin film. In addition to the target rotation, a periodic vertical target movement causes an even material removal of the target material. Since the ceramic targets are fabricated within the semiconductor physics group, material alloys, e.g. $(Al,Ga)_2O_3$ or $(In,Ga)_2O_3$ can be synthesized. Before the thin film deposition starts, the PLD chamber is evacuated and a free selectable process gas is inserted with an intended partial pressure. For the deposition of oxide semiconductors, oxygen (O_2) is usually chosen. Furthermore, the chamber and especially the substrate can be heated.

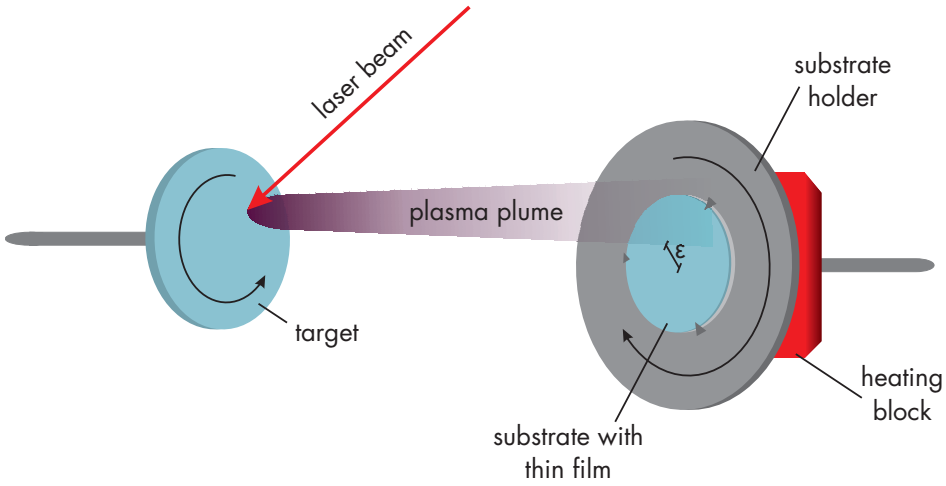

Figure 3.2: Schematic structure of the setup to synthesis a homogeneous thin film by PLD.

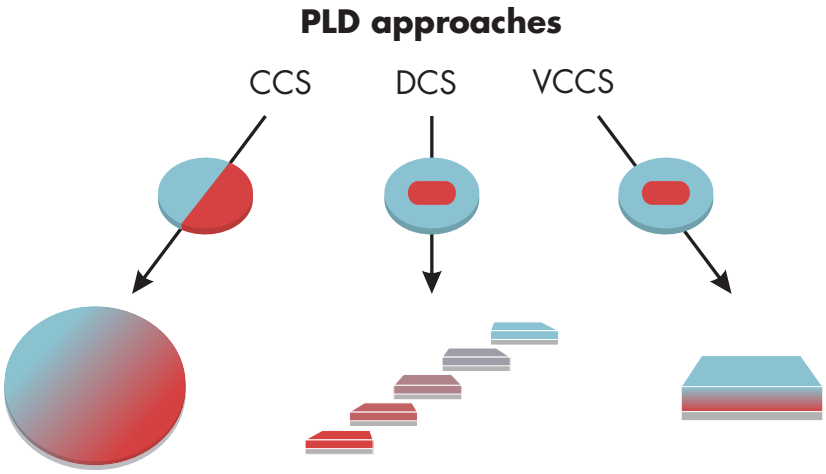

Figure 3.3: Graphical overview about the combinatorial PLD approaches for thin film deposition. A two-fold segmented target (left) can be applied to fabricate a thin film with a lateral varying material composition (CCS). With a radially segmented target, it is possible to create either thin films with a homogeneous cation distribution (DCS) or a thin films having a vertically varying cation composition (VCCS).

Combinatorial thin film synthesis

Ternary alloys with any cation mixtures can be deposited by using different alloyed single ceramic targets, but since the amount of targets required to study an entire composition range is very high, combinatorial approaches are preferred. At the University of Leipzig, especially by Wenckstern *et al.* [24] [E14], methods have been developed and employed where only one segmented target is needed to realize many different alloy compositions. These possibilities lead to a more efficient use of the source materials. Applying a two-fold azimuthally segmented target allows the fabrication of thin films having a lateral CCS, while radially segmented targets offer the possibility to synthesize samples either for a discrete compositional screening (DCS) or a vertical continuous composition spread (VCCS). The target layouts and their resulting alloy distribution maps are depicted in fig. 3.3. The CCS approach is discussed in detail below and the DCS and VCCS approaches are briefly outlined.

(i) CCS approach

One purpose of this work is the systematic investigation of different alloy systems and phases of the group-III sesquioxides. In order to investigate the properties of the different alloys and phases as a function of composition, the CCS approach is mainly applied within the scope of the present work. First, a ceramic target consisting of two halves is produced at the University of Leipzig. One half consists of the material that represents one end of the composition range and the other half consists of the other end of this range. At the beginning of this thesis, two separate targets were manufactured,

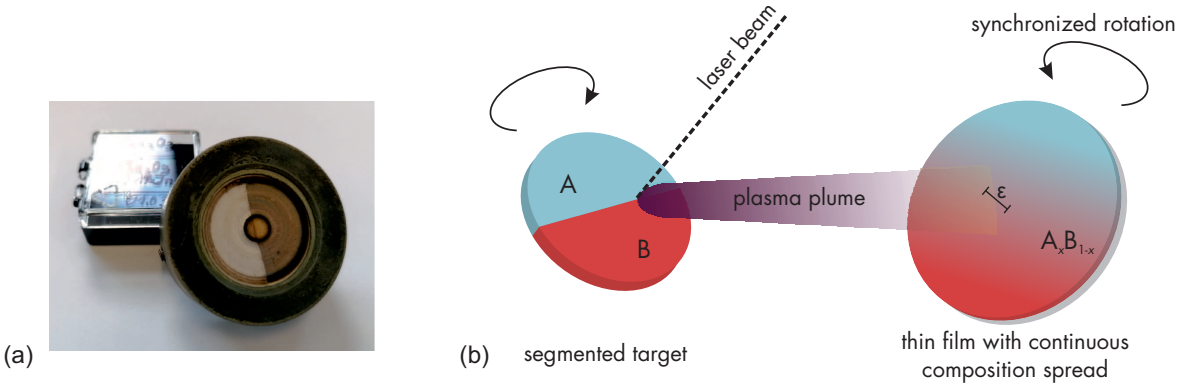

Figure 3.4: (a) Photography of a two-fold azimuthally segmented ceramic PLD target to fabricate thin films by the CCS approach. (b) Schematic representation of the combinatorial CCS-PLD approach. An exactly the same rotational speed of target and substrate ensures the production of a thin film with a lateral varying cation composition.

where each was cut in tow halves and one segment of each material was mounted in the holder. With this method, due to different evaporation rates and shrinkage, targets of different sizes (e.g. thickness and radius) were produced, which made the installation in the target holder challenging. To avoid this, the halves are meanwhile assembled together. The respective material mixtures are pre-sintered individually, then pressed and sintered again together in the target form. Figure 3.4(a) shows a picture of such a two-fold target mounted in a target holder. Opposite the target, a two inch in diameter large substrate is placed with an arbitrary lateral offset ($\epsilon > 0$), related to the position of the target, in the PLD chamber. To deposit a thin film with a laterally changing cation gradient, the rotation speeds of target and substrate must be exactly the same. Due to the target rotation, the chemical composition of the plasma plume, which is created by the laser spot, changes at the interface of both segments and leading at this positions to a mixing of the ablated material.

Figure 3.4(b) shows the schematic representation of the ablation process: When the laser spot is located at material A, this material is ablated and condenses on the substrate. The same process occurs on the other side with material B. As a result of the same rotational speed, material B condenses on the side of the substrate rotated by 180°. At the interface of the segments are partly material A and partly material B ablated. In short, this results in a mixed condensation of the materials (A_xB_{1-x}) depending on the position of the laser spot. The complete process is then repeated until a desired layer thickness is achieved.

The obtainable composition range as well as the thin film thickness depends strongly on the geometric arrangement (ϵ, target-to-substrate distance), the background pressure and temperature in the PLD chamber as well as the materials used, especially their composition and sputter yield [E14]. The expected chemical composition when

producing a CCS thin film can be described for segment A by

$$f_{\mathsf{A}}(r) = \gamma_{\mathsf{A}} \cos\left(\frac{r+\epsilon}{z_{\mathsf{s}}}\right)^{n} \tag{3.1}$$

and for segment B by

$$f_{\mathsf{B}}(r) = \gamma_{\mathsf{B}} \cos\left(\frac{r+\epsilon}{z_{\mathsf{s}}}\right)^{n} \tag{3.2}$$

where γ_{A} and γ_{B} describes the materials transfer coefficients, r the radial position on the substrate, ϵ the lateral offset from the substrate center to the projection of the laser spot, n the influence of the background pressure, and z_{s} the target-to-substrate distance, which is fixed at 10 cm. Note, that $\gamma_{\mathsf{A}} = 1$ is fixed and γ_{B} is variable. The elemental composition to be expected is

$$x(r) = \frac{f_{\mathsf{B}}(r)}{f_{\mathsf{A}}(r) + f_{\mathsf{B}}(r)} \tag{3.3}$$

and the thin film thickness is

$$t(r) = (f_{\mathsf{A}}(r) + f_{\mathsf{B}}(r)) \cdot k \tag{3.4}$$

with k being the amount of ablated material during an experiment. For convenience, k is set to 1 in the following.

Figure 3.5 presents simulated curves for $\epsilon = 10$ mm, $\epsilon = 18$ mm and various n to reveal their influence on the alloy composition x and thin film thickness t. As visible in Fig. 3.5(a), expands the achievable elemental composition range with increasing lateral offset ϵ and decreasing background pressure (increasing n). In addition, it can be observed that the cation gradient gets slightly S-shaped for higher ϵ. Due to an overlap of the plasma plume for a small lateral offset ($\epsilon = 10$ mm), the layer thickness varies significantly over the gradient. For $\epsilon = 18$ mm, the difference in film thickness between substrate center and outside is considerably lower. The variance diminishes further with increasing n, until the thickness in the center of the thin film is smaller than at the outsides.

In the experiments of this work, the influence of the background pressure can be modeled for $(Al_xGa_{1-x})_2O_3$ by $n = 17$ and for $(In_xGa_{1-x})_2O_3$ by $n = 19$. Further, the lateral offset of $\epsilon = 18$ mm was chosen in the experiments to create a preferably homogeneous thin film thickness across the whole sample and to achieve a preferably high composition range as well. Further information and a detailed description of this approach can be found in Refs. [24] and [E14].

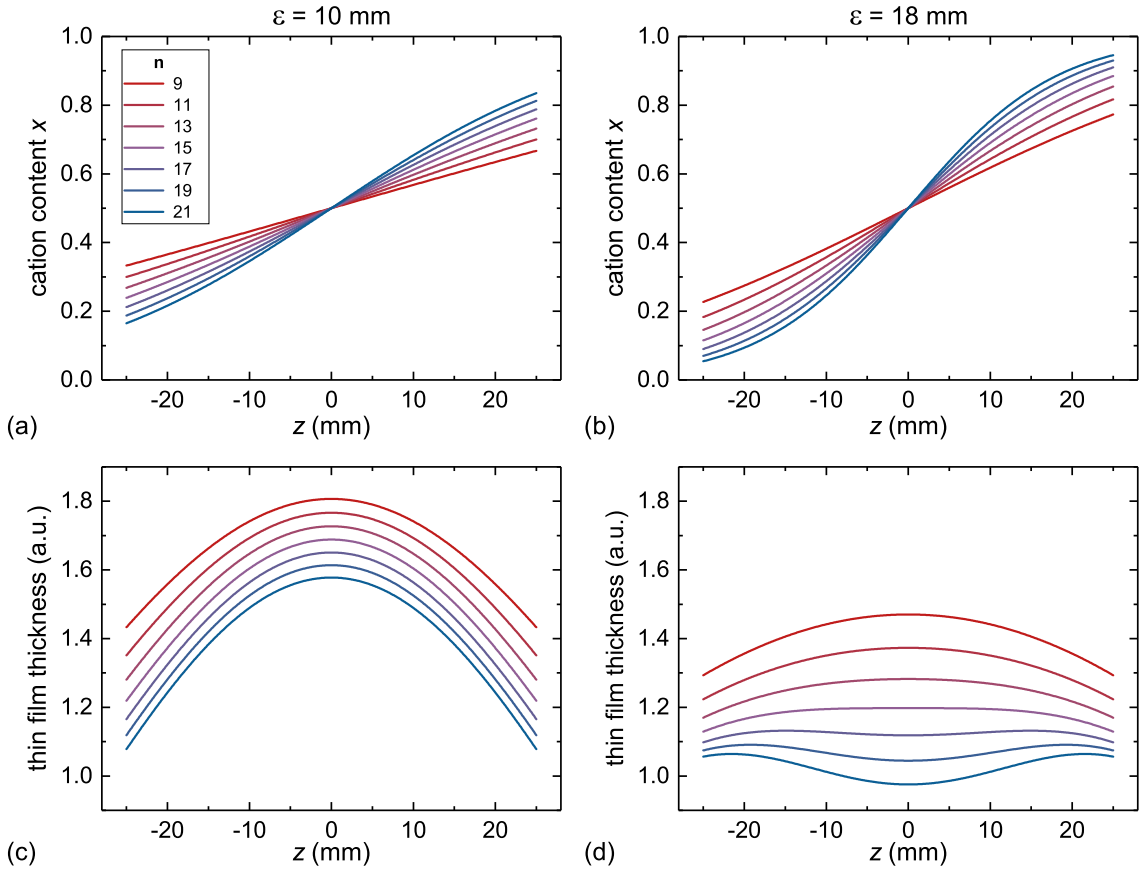

Figure 3.5: (a) presents the chemical composition x and (b) the thin film thickness t as a function of the position on the sample z, where $z = 0\,\text{mm}$ denotes the sample center. The influence of the background pressure on the cation composition x and the thin film thickness is described by the variation of n (low pressure corresponds to high n and vice versa) as marked in the inset of the graphs.

(ii) DCS and VCCS approach

For the synthesis of DCS and VCCS thin films, the same radially segmented ceramic target can be employed, as shown in Fig. 3.3. In contrast to the PLD processes shown so far, the target is not moved in the vertical axis for a thin film created by the DCS approach. Only a constant radial position of the laser spot enables the deposition of a distinct and constant material composition when using this approach. With a fixed radius, the ratio of the inner segment (material A) and the outer segment (material B) remains constant over the ablation period, allowing the fabrication of a thin film with a homogeneous cation composition. In fig. 3.6 an illustrative representation describes the impact of radial position of the laser spot on the alloy composition. A higher distance from the target center implies that the proportionate removal of the outer material increases. Due to the variation of the radial laser spot position, this approach allows the creation of a discrete material library [182].

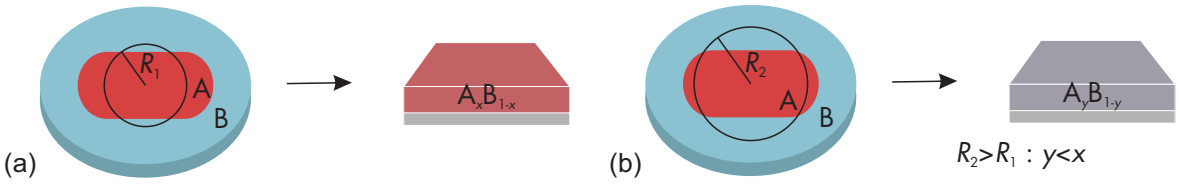

Figure 3.6: Schematic representation of the combinatorial VCCS-PLD approach. (a) displays the creation of a homogeneous thin film using a fixed distance of the laser spot from the target center (R_1). (b) shows that another radial position (R_2) leads to a homogeneous thin films with a slightly different alloy composition. The illustration is created in accordance with Ref. [181].

Further, such a radially segmented target can be used to fabricate thin films with a vertically varying cation distribution by an even change of the radial laser spot position during deposition, hence this approach is abbreviated with VCCS (vertical continuous composition spread). A detailed description of these approaches can be found in Refs. [182] and [E14].

3.2 Thin Film Analysis

3.2.1 Energy Dispersive X-ray Spectroscopy

The elemental composition of the materials can be determined by EDX measurements. Photons from a highly energetic electron beam (several keV) encounter the sample and transmit its energy to the electrons of the inner atomic shells. When the photon energy exceeds the binding energy of the electrons, electrons are released from the inner atomic shells. The more energetic electrons of the outer atomic shells then occupy the vacated positions and emits characteristic X-ray radiation, which is detected by an X-ray detector. Besides the characteristic energy of the X-Ray peak for each element, the additional comparison of the intensity ratios of the peaks allows the determination of the element stoichiometry. Since the photons have to pass through the sample surface, photoelectric absorption can occur, which leads to an intensity reduction of all photon energies. Furthermore, the penetration depth of the X-rays depends on the applied acceleration voltage and can reach several µm. The conducted EDX measurements carried out in this thesis were performed using a *FEI Nova Nanolab 200 equipped with an Ametek EDAX detector*. Further information can be found in Ref. [183].

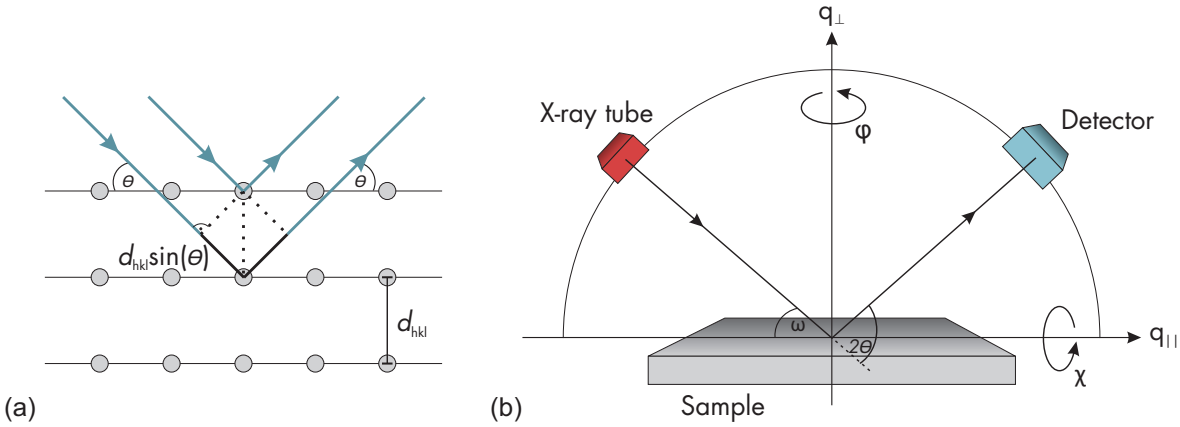

Figure 3.7: Schematic structure of (a) lattice planes in a crystal to deduce the Bragg equation and (b) possible measurement directions of the XRD setup.

3.2.2 X-ray Diffraction

Crystal structure investigations using XRD exploit the interaction of electrons with X-rays leading to diffraction, interference and scattering phenomena. The crystal acts as a diffraction lattice with lattice plane distances (d_{hkl}) of a few Å. In a X-ray tube accelerated electrons (several 10 keV) hit the atomic shells under a distinct angle of incidence leading to the excitation of core electrons. The free electron levels will be refilled by electrons from outer shells. The subsequent detection of the X-rays results in a characteristic diffractogram, which is unique for each crystalline material. Usually, a Cu K_α radiation of $\lambda \approx 1.54$ Å is applied.

The most common methods and arrangements can be described with the help of the Bragg equation, which can be modeled by constructive interference between two X-rays, scattered on two lattice planes, as sketched in fig. 3.7(a). The resulting path difference must be a multiple ($n \in \mathbb{N}$) of the wavelength for constructive interference and is expressed by:

$$n\lambda = 2\, d_{hkl}\, \sin(\theta) \tag{3.5}$$

where 2θ describes the angle between incident and scattered beam. The lattice planes are characterized by the Miller indices $\{hkl\}$. The three main measurement options used in this thesis are briefly described below and were measured by a *PANalytical X'pert PRO MRD diffractometer* equipped with a *PIXcel*^{3D} *detector* operating in 1D scanning line mode with 255 channels (for 2θ-ω scans), receiving slit mode (for ϕ-scans) and fast 2D frame based mode (for RSMs).

2θ-ω scans:

The crystal structure of the sample, can be deduced by acquiring 2θ-ω scans. There-

fore, the X-ray tube (see fig. 3.7(b)) is rotated by $\Delta\omega$, which is the incident angle regarding the surface normal, while the detector is rotated at twice the amount of the 2θ angle, simultaneously. The received XRD pattern reveals the positions of the reflection peaks, which are characteristic for each crystal structure. In addition, the lattice plane distances can be obtained due to the Bragg's equation.

ϕ scans:

To investigate the epitaxial growth of the thin film as well as the epitaxial relation between thin film and substrate, ϕ-scans are required. For this, the XRD setup has approached to the angular position of an asymmetric or a skew-symmetric reflex of the crystal structure for which the 2θ, ω and χ angles has to remain fixed. Subsequent, the sample is rotated around the ϕ-axis.

reciprocal space map (RSM) scans:

In the RSM application, the 2θ and the ω angles are varied so that ω is changed step by step for each 2θ position. The individual scans produce a chart in the reciprocal space, from which the in- and out-of-plane reciprocal space coordinates

$$q_{\parallel} = \frac{1}{\lambda}[\cos\omega - \cos(2\theta - \omega)] \tag{3.6}$$

and

$$q_{\perp} = \frac{1}{\lambda}[\sin\omega + \sin(2\theta - \omega)] \tag{3.7}$$

can be calculated. With the respective intensities, the RSM yields from these data. Based on the RSMs, conclusions can be drawn about relaxed or pseudomorphic growth as well as the size of lattice constants.

3.2.3 Atomic Force Microscopy

Besides elemental composition and crystal structure, the surface morphology of a thin film provides information about structural material properties. The sample surface can be recorded by AFM measurements, either in contact or in non-contact mode. Depending on the size of the surface grains or liquid shreds, both modes can be selected. A cantilever, mounted perpendicular to the sample surface, with a sharp tip (radius of a few nm) can be adjusted in z-dimension (height) and thus be brought close to the surface. An infrared laser beam is directed on the tip, where it is reflected to an four-quadrant photodiode. The tip oscillates close to its resonance frequency and its magnitude and phase will be detected. In contact mode the measuring tip touches the surface causing resonance curve shifts of the tip oscillations. In non-contact mode the

tip hovers briefly above the surface and attractive Van-der-Waals forces and repulsive electrostatic Pauli repulsions affect changes in the oscillations. By moving in x- and y-direction (xy-piezo built into the sample stage), surface morphologies up to several ten µm can be scanned. The measurements were performed using a *Park Systems XE-150 atomic force microscope*. The data were evaluated by Gwyddion [184].

3.2.4 Transmission Spectroscopy

By means of transmission, the optical band edges of the materials can be determined and then the optical band gap can be calculated. For the transmission spectroscopy the light of a deuterium and a halogen lamp is used, allowing measurements in a spectral range of 200–2000 nm. A monochromator filters unintentional radiation and a beam splitter divides the light into a reference and a measuring beam, whereby the latter one is directed to the sample. The transmittance T is described by

$$T = \frac{I_\mathsf{T}}{I_0} = \frac{(1-R)^2 e^{-\alpha d}}{1 - R^2 e^{-2\alpha d}} \tag{3.8}$$

with the incident (transmitted) intensity I_0 (I_T), the reflection R, the absorption coefficient α, and the thin film thickness d.

The light passes through the surface into the thin film and is reflected at the back and front and is reflected between the substrate/film interface and the surface of the film. Since they are parallel to each other and the thickness of the thin film is less than the coherence length of the light, multiple reflections occur. Since the thin film behaves like a Fabry-Perot interferometer, the layer thickness can be calculated out of multi-reflections by

$$\Delta E_\mathsf{ph} = \frac{hc}{2n(\lambda)d}. \tag{3.9}$$

where ΔE_ph is the energetic distance of the transmission maxima, n the refractive index and λ the wavelength of the incident light. The transmitted light as well as the reference beam are detected by a photodiode. Thus the photon Energy E_ph is given by $E_\mathsf{ph} = hc\lambda^{-1}$ with the Planck constant h and the velocity of light c. The absorption coefficient can be derived from Lambert-Beer's law, neglecting the reflection:

$$I_\mathsf{T} = I_0 e^{-\alpha d}. \tag{3.10}$$

For direct semiconductors $\alpha \propto (E_\mathsf{ph} - E_\mathrm{g})^{1/2}$, and for indirect ones $\alpha \propto (E_\mathsf{ph} - E_\mathrm{g} \pm h\nu_\mathsf{ph})^2$ can be applied, where ν_ph defines the phonon frequency [185]. The measurements were performed using an *UV/VIS-dual beam spectrometer Lambda 19* from Perkin-Elmer.

3.2.5 Spectroscopic Ellipsometry

Spectroscopic ellipsometry allows the determination of the optical bandgap, the thin film thickness, the dielectric constant as well as the refractive index by studying the polarization change of light, which is reflected by the thin film investigated.

The optically biaxial thin films can be described by an uniaxial model, where the optical axis is parallel to the surface normal. By using standard ellipsometry [186], the ellipsometric parameters Ψ and Δ can be obtained from

$$\rho = \frac{r_{\mathsf{p}}}{r_{\mathsf{s}}} = \mathsf{tan}\Psi \cdot \mathsf{e}^{i\Delta} \tag{3.11}$$

with the polarization change ρ and the complex reflection coefficients r_{p} and r_{s} of parallel and perpendicular polarized light. In order to reduce the dependence of Ψ and Δ on the angle of incidence, these quantities have to be converted into a pseudo dielectric function (DF) [187]

$$< \epsilon >=< \epsilon_1 > +i < \epsilon_2 >= \sin^2\Phi \left(1 + \tan^2\Phi \left(\frac{1-\rho}{1+\rho}\right)^2\right) \tag{3.12}$$

with Φ being the angle between the sample normal and the incident light. Then, the DF was simulated using a layer stack model, which consists of a substrate layer, a layer describing the thin film and a surface layer. Based on the simulations, optical band gap and thin film thickness can also be obtained. Further, the refractive index n can be described for isotropic and transparent materials by the Cauchy function, i.e. $n = A + B/\lambda^2 + C/\lambda^4$. A dual rotating compensator ellipsometer (*RC2, J.A. Woollam M2000*) with a spot size of about $300 \times 500\,\mu\mathrm{m}^2$ was used to conduct the ellipsometric measurements.

CHAPTER4

Cumulative Part

4.1 Phase Formation and Desorption Processes of β- and κ-$(Al,Ga)_2O_3$ Thin Films

The content of this section has been published in the following two manuscripts:

Reprinted with permission from
A. Hassa, H. von Wenckstern, L. Vines, and M. Grundmann:
Influence of Oxygen Pressure on Growth of Si-Doped β-$(Al_xGa_{1-x})_2O_3$ Thin Films on c-Sapphire Substrates by Pulsed Laser Deposition, ECS Journal of Solid State Science and Technology, volume 8, no. 7, pages Q3217–Q3220 (2019). Copyright 2019 by ECS.
doi:10.1149/2.0411907jss

Reprinted from
A. Hassa, C. Wouters, M. Kneiß, D. Splith, C. Sturm, H. von Wenckstern, M. Albrecht, M. Lorenz, and M. Grundmann:
Control of phase formation of $Al_xGa_{1-x})_2O_3$ thin films on c-plane Al_2O_3, Journal of Physics D: Applied Physics, volume 53, no. 48 (2020). Available under the Creative Commons Attribution 4.0 licence at:
doi:10.1088/1361-6463/abaf7d

JSS Focus Issue on Gallium Oxide Based Materials and Devices

Influence of Oxygen Pressure on Growth of Si-Doped β-$(Al_xGa_{1-x})_2O_3$ Thin Films on c-Sapphire Substrates by Pulsed Laser Deposition

A. Hassa,[1,z] H. von Wenckstern,[1] L. Vines,[2] and M. Grundmann[1]

[1] *Felix Bloch Institute for Solid State Physics, Universität Leipzig, Sachsen 04103, Germany*
[2] *Department of Physics, Centre for Materials Science and Nanotechnology, University of Oslo, Oslo 0316, Norway*

Ga_2O_3 is a deep-UV transparent semiconducting oxide being interesting for solar-blind photo detectors e.g. for flame or missile plume detection. The bandgap of about 4.9 eV can be increased by alloying with Al_2O_3. We have investigated β-$(Al,Ga)_2O_3$ thin films grown by pulsed laser deposition (PLD) on (00.1) Al_2O_3 with regard to the influence of the growth parameters such as growth temperature (T_g) and oxygen partial pressure ($p(O_2)$) on the structural, optical and electrical properties of the samples. The thin films have (-201) orientation and the cation incorporation strongly depends on the deposition parameters. At a given T_g, the incorporation of Al is favored for lower $p(O_2)$ due to higher dissociation energy of the Al-O bond compared to the Ga-O bond. At a given $p(O_2)$, the incorporation of Al is favored for higher T_g due to desorption of gallium sub-oxides during growth.
 [DOI: 10.1149/2.0411907jss]

Manuscript submitted January 16, 2019; revised manuscript received April 5, 2019. Published April 24, 2019. *This paper is part of the JSS Focus Issue on Gallium Oxide Based Materials and Devices.*

The wide bandgap semiconductor gallium oxide is more and more explored for high-power electronics, because of its promising material properties, such as beneficial breakdown voltages and large power semiconductor device figures of merit. Further applications include quantum well infrared photodetectors or deep UV-photodetectors like flame sensors for missile plume detection, biological and chemical sensors for ozone detection or gas sensors. In addition, Ga_2O_3 finds use in touch panel displays, solar cells or optical communications, such as intra- and inter-satellite secured communication systems.[1–3]

Ga_2O_3 occurs in different polymorphs, denoted by α, β, γ, δ, ϵ,[4] and κ.[5] Because of it is thermodynamical stability, the monoclinic β-structure is the most studied phase, so far. The large bandgap energy of the binary oxide ranges between 4.7 and 5.0 eV. The optical anisotropy and dichroism have been investigated in detail in Ref. 6. The gap can be tuned by alloying with In_2O_3 or Al_2O_3.[1–3] Up to now conducting $(In,Ga)_2O_3$ thin films with a tailored bandgap could be produced and devices based on the ternary alloy were realized.[2,7] The most challenging part will be the fabrication of conducting $(Al,Ga)_2O_3$ thin films. Since intrinsic defects such as oxygen vacancies do not contribute to the conduction of Ga_2O_3,[8] extrinsic doping is necessary to realize electrical devices.[9] Possible suitable cations for doping are silicon,[2,10–12] tin[2,13] or germanium[2,14] Hence these cations are part of the present study to create conducting samples. In the β-Ga_2O_3 crystal structure, Al replaces Ga at octahedral sites, which induces changes of the crystal structure and thereby in the lattice constants as reported by Kranert et al.[15] Schmidt-Grund et al. investigated the relating bandgap dependency on the aluminum content x_{Al}, which can be described by the formula $E_g = (4.811 + 2.138\, x_{Al})$ eV for $0.11 \leq x_{Al} \leq 0.55$.[16]

In the fabrication of thin films by means of pulsed laser deposition (PLD) the oxygen pressure $p(O_2)$ and growth temperature T_g influence the growth process and the thin film properties independently. For binary β-Ga_2O_3 thin films, Müller et al. observed decreasing growth rates with decreasing $p(O_2)$[12] and Zha et al. reported decreasing growth rates with increasing T_g.[17] For ternary $(Al,Ga)_2O_3$ thin films, Wang et al. characterized the influence of the growth temperature and showed that for increasing T_g lower growth rates were observed.[18] Wakabayashi et al. showed the influence of $p(O_2)$ on PLD grown $(Al,Ga)_2O_3$ samples.[19] For low oxygen pressures they observed a decrease of the growth rate and a non-stoichiometric transfer of Ga and Al atoms. They showed that this process can be suppressed by using an oxygen-radical atmosphere during growth. As a result the growth rates recovered and a stoichiometric transfer was observed.[19] Further, Feng et al. reported a non-stoichiometric cation transfer from target to sample for PLD grown $(Al,Ga)_2O_3$ thin films, which was attributed to the formation of the volatile suboxide Ga_2O.[20] The choice of oxygen pressure and/or growth temperature during PLD influence the growth rate and cation composition of $(Al,Ga)_2O_3$. Therefore, it is of great importance to understand the growth process and the formation of volatile gallium suboxides as a function of $p(O_2)$ and T_g. The central aspect of this work is the determination of the growth window for which stoichiometric cation incorporation occurs. Furthermore, it summarizes our attempts to fabricate electrically conducting thin films.

Experimental

The samples investigated in this study were grown by pulsed laser deposition (PLD) on (00.1) Al_2O_3. The ceramic targets for PLD consist of Ga_2O_3 with 8.8 at.% Al_2O_3 and were additionally doped with different amounts of tin, silicon or germanium to improve electrical conductivity. The growth temperature and growth pressure were changed in a wide parameter space as can be seen in Table I. For the ablation we used a KrF excimer laser (248 nm) with an energy density of 2 Jcm^{-2} at the target and a frequency of 15 Hz. The target to substrate distance was 10 cm. The number of laser pulses was 30300 and the resulting film thicknesses ranges between 400 and 1200 nm. Moreover, series of samples were implanted with tin or silicon using a 1 MeV Tandem accelerator from NEC. For each sample different implantation energies, for Si, 36, 160 and 600 keV and with fluencies of 1.5×10^{13}, 6×10^{13}, and 1.5×10^{14} cm^{-2}, respectively, were used to obtain a homogeneous implantation profile. For the Sn implanted samples we applied 600 keV

Table I. Range of Growth temperature T_g, oxygen partial pressure $p(O_2)$ and cation composition of the used PLD targets.

Target: Ga_2O_3 + 8.8 at.% Al_2O_3 +	Growth parameters: T_g in °C	$p(O_2)$ in mbar
0.2–4.4 at% SiO_2	490–670	3×10^{-4}–0.04
0.6 at% SnO_2	400–670	3×10^{-4}–0.024
0.9–4 at% GeO_2	420–670	3×10^{-4}–0.02

[z]E-mail: anna.hassa@physik.uni-leipzig.de

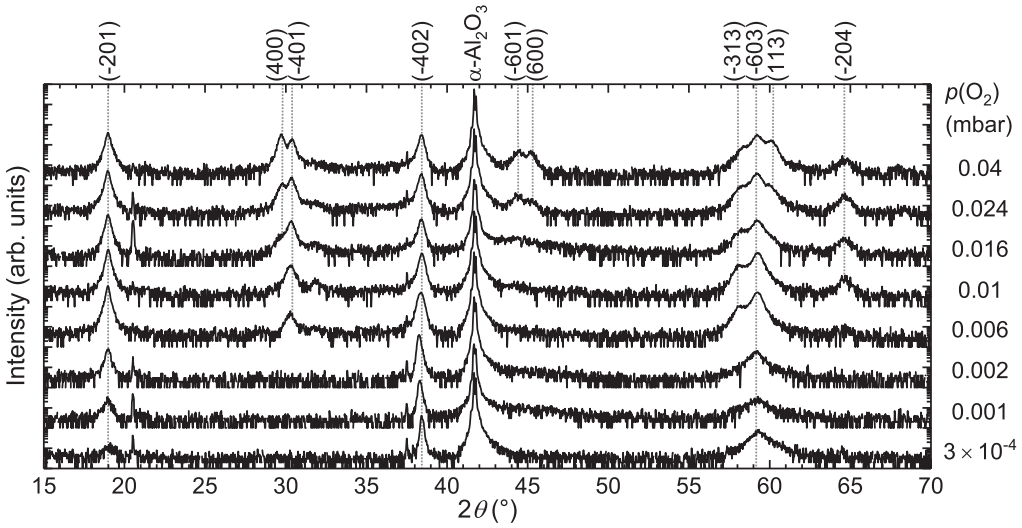

Figure 1. XRD 2θ-ω scans of $(Al,Ga)_2O_3$:Si thin films deposited at a growth temperature of 670°C and different oxygen partial pressures as labeled. The peaks were assigned to reflections at lattice planes as labeled by comparison with JCPDS Card #76-0573.

and 2 MeV and with doses of 5×10^{13} and 1×10^{14} cm^{-2}. To activate the implanted Si and Sn, the samples were annealed at approximately 840°C for one hour in nitrogen ambient. Thin film properties as the alloy composition, structural, optical and electrical properties were investigated by means of energy-dispersive X-ray spectroscopy (EDX), X-ray diffraction (XRD), atomic force microscopy (AFM), and Hall effect measurements. The respective bandgap energies E_g and layer thicknesses d were determined by transmission measurements. By extrapolation of $(\alpha h\nu)^2$ vs. photon energy to zero the bandgap energies were estimated and d can be calculated from observable layer thickness oscillations using a refractive index of $n \approx 2$.[21] There, α describes the absorption coefficient, h the Planck constant and ν the wave frequency. For the transport measurements, ohmic contacts, consisting of 30 nm thick layers of titanium, aluminum and gold (Ti/Al/Au), respectively, were thermally evaporated on the corners of the square samples through a shadow mask. Subsequently, these contacts were annealed at 500°C for 10 minutes in a nitrogen ambient.

Results and Discussion

The influence of the oxygen pressure during growth will be discussed in the following section based on a growth series deposited at a growth temperature of 670°C. The used target consists of 86.8 at.% Ga_2O_3 + 8.8 at.% Al_2O_3 + 4.4 at.% SiO_2 and the oxygen pressure was varied in the range from 0.04 to 3×10^{-4} mbar. XRD patterns, shown in Figure 1, indicate a strong influence of $p(O_2)$ on the crystallinity of the samples. The peak appearing at $2\theta = 41.68°$ can be assigned to reflections on the (00.6) plane of the c-plane sapphire substrate. The remaining visible reflection peaks belong to monoclinic gallium oxide. For Ga_2O_3. For $p(O_2) \leq 0.002$ mbar the thin films grow only in [-201]-direction and show reflection peaks at 2θ angles of 18.9°, 38.4° and 59.2° corresponding to reflections at the (-201) lattice planes. Zhang et al. and Wang et al. already reported that β-$(Al,Ga)_2O_3$ thin films on sapphire substrates grow in [-201]-direction [18,22] as it is the case for binary Ga_2O_3.[2] Nakagomi and Kokubun recognized, that the order of oxygen atoms of the (001) plane of c-sapphire and the corresponding (-201) plane of β-Ga_2O_3 is equal[23] leading to a minor mismatch between both lattice planes. For growth pressure between 0.006 and 0.016 mbar additionally peaks at 30.4°, 58.3° and 64.7° occur and correspond to reflections at the (-401)-, (-313)- and (-204)-planes, respectively. Further reflection peaks at $2\theta = 29.8°$, 44.2°, 45.3°, and 60° are visible for $p(O_2) = 0.024$ - 0.04 mbar and corresponds to the (400)-, (-601)-, (600)-, and (113)-planes.

As the oxygen pressure in the PLD chamber increases, the kinetic energy of the atomic and molecular species arriving at the substrate decreases. The resulting smaller diffusion length leads to the formation of smaller grains, increasing the probability that some of these grains grow in an orientation different from (-201). This effect is in contrast to many other oxide film systems crystallizing in the higher symmetry cubic or hexagonal structure.[24] The correlation of oxygen pressure and crystal growth was reported by Müller et al., who observed for binary Ga_2O_3 similar behavior.[12]

Figure 2a shows the calculated growth rates (r = d/#pulses), bandgap energies and aluminum content from the $(Al_xGa_{1-x})_2O_3$:SiO_2 growth series and its dependence on the growth pressure. The bandgap

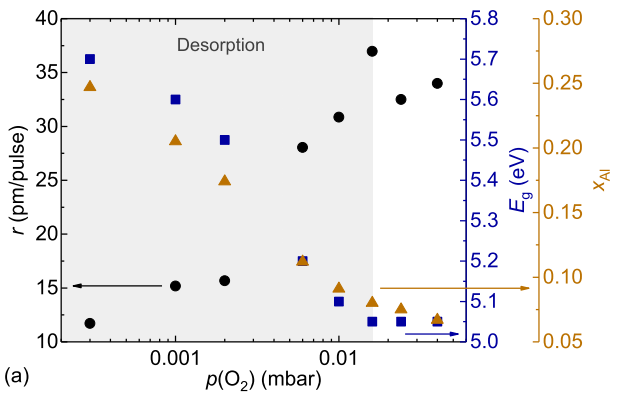

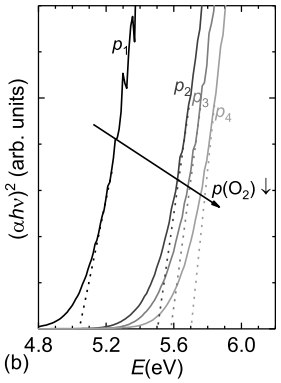

Figure 2. (a) Measured growth rate r, bandgap E_g and aluminum concentration x_{Al} in dependence on the logarithmic oxygen partial pressure $p(O_2)$. The gray shaded area indicates the $p(O_2)$ regime where desorption is essential. (b) Optical transmittance spectra for oxygen pressures of $p_1 = 0.04$ mbar, $p_2 = 0.002$ mbar, $p_3 = 0.001$ mbar, and $p_4 = 3 \times 10^{-4}$ mbar.

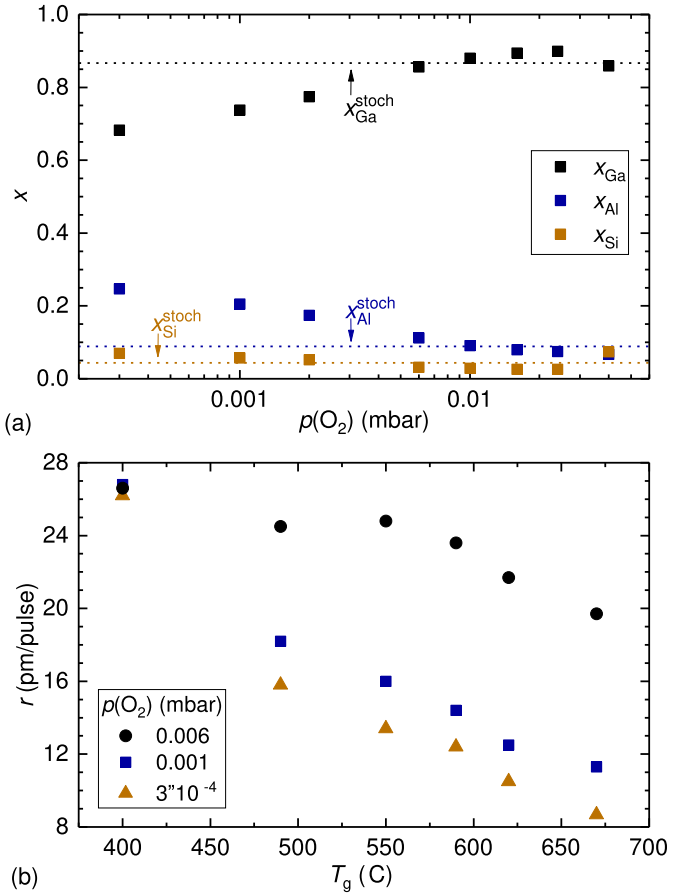

Figure 3. (a) Cation concentration of gallium, aluminum and silicon atoms measured by EDX in dependence of the growth pressure deposited at a growth temperature of 670°C. The dotted lines indicate elemental concentration for a stoichiometric transfer of the target composition being $x_{Ga}^{stoch} = 0.868$, $x_{Al}^{stoch} = 0.088$ and $x_{Si}^{stoch} = 0.044$. (b) Dependency of the growth rate on the growth temperature for three chosen oxygen pressures as labeled in the picture.

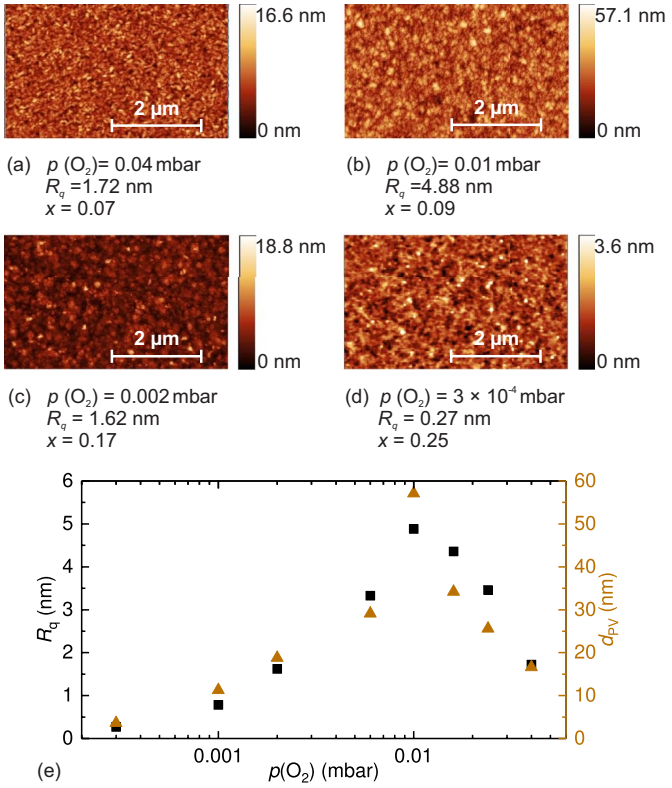

Figure 4. R_q describes the mean square roughness and x the aluminum content. The scale next to the pictures (a) to (d) characterizes the peak-valley-distance (d_{PV}). The thin films are deposited at $T_g = 670°C$ and different oxygen partial pressures as labeled. (e) shows the dependency of R_q and d_{PV} to the oxygen pressure.

energies were calculated from the optical transmittance spectra and are shown for four different oxygen pressures in Fig. 2b. In Fig. 2a a division into two growth regimes ($p(O_2) \geq 0.016$ mbar and $p(O_2) < 0.016$ mbar) is recognizable. For $p(O_2) \geq 0.016$ mbar similar growth rates of 32.5 to 37 pm/pulse, bandgap energies of approximately 5.05 eV and an aluminum content ranging between 0.06 and 0.08 were observed, as well. Below an oxygen pressure of 0.016 mbar the growth rate decreases with decreasing growth pressure up to a value of 12 pm/pulse for 3×10^{-4} mbar. Simultaneously, the bandgap energies and aluminum contents increases up to values of $E_g = 5.7$ eV and $x_{Al} = 0.25$. The influence of the oxygen pressure on the cation composition is illustrated in Figure 3a and show, that with decreasing growth pressure the gallium (aluminum) content x_{Ga} (x_{Al}) decreases (increases) for a given growth temperature of 670°C. The sum of all incorporated cations is always 1 and the silicon proportion ranges between 0.03 and 0.07.

For oxygen pressures between 0.04 and 0.016 mbar a nearly stochiometric transfer of the Ga, Al and Si atoms from target to layer is observed and results in similar growth rates and bandgaps (see Fig. 2). In the oxygen regime below 0.016 mbar, aluminum atoms are preferentially incorporated, because of the higher dissociation energy of the Al-O bond compared to the Ga-O bond.[25] Further, gallium forms volatile sub-oxides being desorbed. As a result, considerably lower amounts of Ga are incorporated into the layers as seen in Figure 3a. The higher aluminum content leads to the observed bandgap increase and the desorption of gallium sub-oxides leads to lower growth rates. Similar desorption processes were reported for molecular beam epitaxy growth of In_2O_3, Ga_2O_3 and $(In_xGa_{1-x})_2O_3$ thin films by Vogt and Bierwagen.[26–28] Since the desorption is a temperature dependent process, we investigated the growth rates of samples deposited at three different oxygen pressures (0.006, 0.001 and 3×10^{-4} mbar) and various growth temperatures (from 400 to 670°C). For deposition of these sample series we used a target consisting of Ga_2O_3 + 8.8 at.% Al_2O_3 + 0.6 at.% SnO_2. The growth rates, depicted in Figure 3b, decreases with increasing temperature showing that the formation of volatile suboxides is favorable at higher growth temperatures. For the highest investigated oxygen pressure of 0.006 mbar saturation of the growth rate with values between 24.5 to 26.2 pm/pulse is observed for growth temperatures below 550°C.

Using AFM on areas of $3 \times 5\ \mu m^2$ the surface morphology and consequently the root mean square surface roughness R_q and peak-valley-distance d_{PV} were examined. Figure 4 displays the R_q and d_{PV} values obtained from the already discussed $(Al_xGa_{1-x})_2O_3$:SiO_2 growth series. The visible surface effects can be divided into two categories for $p(O_2) < 0.01$ mbar and $p(O_2) \geq 0.01$ mbar. For oxygen pressures below 0.01 mbar R_q and d_{PV} depend on the aluminum content. With increasing x_{Al} the surface becomes smoother and the roughness decreases from $R_q = 3.33$ nm for $x_{Al} = 0.11$ to $R_q = 0.27$ nm for $x_{Al} = 0.25$. For $p(O_2) \geq 0.01$ mbar the aluminum content saturates and hence the oxygen pressure is determining the surface morphology. The surface roughness increases from $R_q = 1.72$ nm for 0.04 mbar to $R_q = 4.88$ nm for 0.01 mbar.

Currently, the most challenging task for the growth of ternary heteroepitaxial $(Al,Ga)_2O_3$ thin films is the development of a doping strategy in order to tailor its electrical transport properties. As part of this work various tests were executed to obtain conducting thin films. All samples investigated were electrically insulating. Concerning the doping of the thin films, we doped samples during growth process in situ and additionally we used ion implantation to create

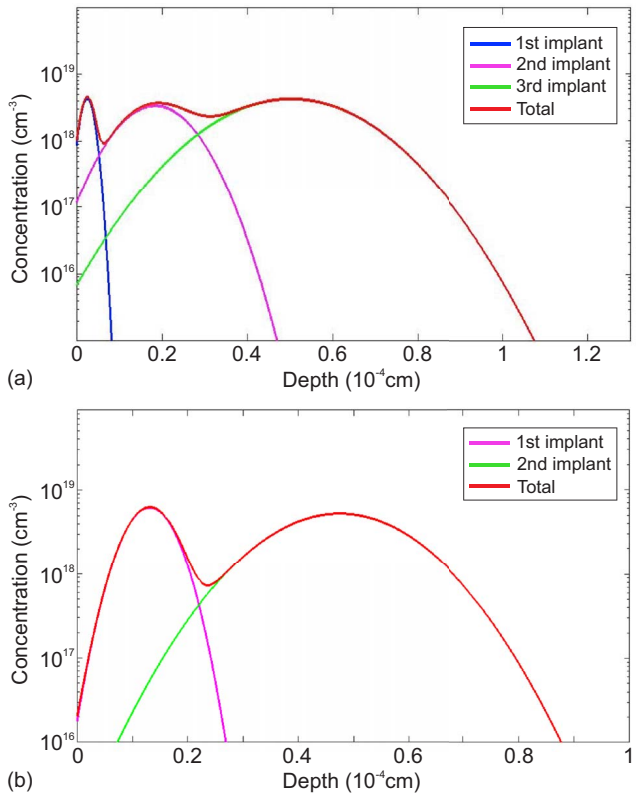

Figure 5. Implantation profile of (a) Si and (b) Sn.

conducting samples, ex situ. For the implantation process a nearly homogeneous dopant concentration of approximately (1–5) $\times 10^{18}$ cm^{-3} was realized for both, Si and Sn, as visible in Fig. 5. Before and after annealing, however, all samples remained insulating as soon as Al was alloyed.

Conclusions

We have discussed the influence of growth conditions on the crystallinity, bandgap energy, growth rate, cation composition and surface morphology of PLD-grown $(Al,Ga)_2O_3$ thin films on c-sapphire substrates. We described that the preferential incorporation of Al was in tendency observed for low oxygen pressures and/or high growth temperature, which was assigned to differences in cation oxygen bond strength and desorption of gallium sub oxide. Decreasing growth pressure lead to decreasing growth rates and low gallium content. Lower growth temperatures favor the stoichiometric cation incorporation into the thin film layer. Further, many different growth conditions were pointed out to produce insulating samples. It can be concluded that it was not possible to produce conductive samples. This issue must be solved prior to the fabrication of devices based on $(Al,Ga)_2O_3$.

Acknowledgments

We thank Monika Hahn for PLD target fabrication, Jörg Lenzner for EDX, and Ulrike Teschner for transmission measurements. This work was supported by European Social Fund within the Young Investigator Group "Oxide Heterostructures" (SAB 100310460) and partly by Deutsche Forschungsgemeinschaft in the Framework of Sonderforschungsbereich 762 "Functionality of Oxide Interfaces". A.H. acknowledges the Leipzig School for Natural Sciences BuildMoNa.

ORCID

A. Hassa https://orcid.org/0000-0002-8087-6592
H. von Wenckstern https://orcid.org/0000-0002-3936-275X
L. Vines https://orcid.org/0000-0001-5759-7192
M. Grundmann https://orcid.org/0000-0001-7554-182X

References

1. S. I. Stepanov, V. I. Nikolaev, V. E. Bougrov, and A. Romanov, *Reviews on Advanced Materials Science*, **44**, 63 (2016).
2. H. von Wenckstern, *Advanced Electronic Materials*, **3**, 1600350 (2017).
3. S. J. Pearton, J. Yang, P. H. Cary, F. Ren, J. Kim, M. J. Tadjer, and M. A. Mastro, *Applied Physics Reviews*, **5**, 011301 (2018).
4. R. Roy, V. G. Hill, and E. F. Osborn, *Journal of the American Chemical Society*, **74**, 719 (1952).
5. H. Y. Playford, A. C. Hannon, E. R. Barney, and R. I. Walton, *Chemistry - A European Journal*, **19**, 2803 (2013).
6. C. Sturm, J. Furthmüller, F. Bechstedt, R. Schmidt-Grund, and M. Grundmann, *APL Materials*, **3**, 106106 (2015).
7. S. J. Pearton, M. A. Mastro, and F. Ren, *Elsevier* (2018).
8. L. Dong, R. Jia, B. Xin, B. Peng, and Y. Zhang, *Scientific Reports*, **7**, 40160 (2017).
9. J. B. Varley, J. R. Weber, A. Janotti, and C. G. Van de Walle, *Applied Physics Letters*, **97**, 142106 (2010).
10. E. G. Víllora, K. Shimamura, Y. Yoshikawa, T. Ujiie, and K. Aoki, *Applied Physics Letters*, **92**, 202120 (2008).
11. D. Splith, S. Müller, F. Schmidt, H. von Wenckstern, J. J. van Rensburg, W. E. Meyer, and M. Grundmann, *Physica Status Solidi (a)*, **211**, 40 (2014).
12. S. Müller, H. von Wenckstern, D. Splith, F. Schmidt, and M. Grundmann, *Physica Status Solidi (a)*, **211**, 34 (2014).
13. N. Suzuki, S. Ohira, M. Tanaka, T. Sugawara, K. Nakajima, and T. Shishido, *Physica Status Solidi (c)*, **4**, 2310 (2007).
14. E. Ahmadi, O. S. Koksaldi, X. Zheng, T. Mates, Y. Oshima, U. K. Mishra, and J. S. Speck, *Applied Physics Express*, **10**, 071101 (2017).
15. C. Kranert, M. Jenderka, J. Lenzner, M. Lorenz, H. von Wenckstern, R. Schmidt-Grund, and M. Grundmann, *Journal of Applied Physics*, **117**, 125703 (2015).
16. R. Schmidt-Grund, C. Kranert, H. von Wenckstern, V. Zviagin, M. Lorenz, and M. Grundmann, *Journal of Applied Physics*, **117**, 165307 (2015).
17. F. Zhang, K. Saito, T. Tanaka, M. Nishio, and Q. Guo, *Journal of Crystal Growth*, **387**, 96 (2014).
18. X. Wang, Z. Chen, F. Zhang, K. Saito, T. Tanaka, M. Nishio, and Q. Guo, *Ceramics International*, **42**, 12783 (2016).
19. R. Wakabayashi, T. Oshima, M. Hattori, K. Sasaki, T. Masui, A. Kuramata, S. Yamakoshi, K. Yoshimatsu, and A. Ohtomo, *Journal of Crystal Growth*, **424**, 77 (2015).
20. Q. Feng, Z. Hu, Z. Feng, X. Xing, Y. Zuo, G. Yan, X. Lu, C. Zhang, H. Zhou, and J. Zhang, *Superlattices and Microstructures*, **120**, 441 (2018).
21. A. Petitmangin, C. Hébert, J. Perrière, B. Gallas, L. Binet, P. Barboux, and P. Vermaut, *Journal of Applied Physics*, **109**, 013711 (2011).
22. F. Zhang, K. Saito, T. Tanaka, M. Nishio, M. Arita, and Q. Guo, *Applied Physics Letters*, **105**, 162107 (2014).
23. S. Nakagomi and Y. Kokubun, *Journal of Crystal Growth*, **349**, 12 (2012).
24. M. Lorenz, *Encyclopedia of Applied Physics*, Wiley-VCH Verlag GmbH & Co. KGaA (Ed.), (2019).
25. Y.-R. Luo, *Comprehensive Handbook of Chemical Bond Energies*, CRC Press (2007).
26. P. Vogt and O. Bierwagen, *Applied Physics Letters*, **106**, 081910 (2015).
27. P. Vogt and O. Bierwagen, *APL Materials*, **4**, 086112 (2016).
28. P. Vogt and O. Bierwagen, *Applied Physics Letters*, **108**, 072101 (2016).

OPEN ACCESS
IOP Publishing
Journal of Physics D: Applied Physics
J. Phys. D: Appl. Phys. **53** (2020) 485105 (9pp)
https://doi.org/10.1088/1361-6463/abaf7d

Control of phase formation of $(Al_xGa_{1-x})_2O_3$ thin films on c-plane Al_2O_3

Anna Hassa[1], Charlotte Wouters[2], Max Kneiß[1], Daniel Splith[1], Chris Sturm[1], Holger von Wenckstern[1], Martin Albrecht[2], Michael Lorenz[1] and Marius Grundmann[1]

[1] Universität Leipzig, Felix-Bloch-Institut für Festkörperphysik, Linnéstraß e 5, 04103 Leipzig, Germany
[2] Leibniz-Institut für Kristallzüchtung, Max-Born-Str. 2, 12489 Berlin, Germany

E-mail: anna.hassa@uni-leipzig.de

Received 16 June 2020, revised 6 August 2020
Accepted for publication 14 August 2020
Published 11 September 2020

Abstract

In this paper, the growth of orthorhombic and monoclinic $(Al_xGa_{1-x})_2O_3$ thin films on (00.1) Al_2O_3 by tin-assisted pulsed laser deposition is investigated as a function of oxygen pressure $p(O_2)$ and substrate temperature T_g. For certain growth conditions, defined by $T_g \geq 580^{\circ}$C and $p(O_2) \leq 0.016$ mbar, the orthorhombic κ-polymorph is stabilized. For $T_g = 540^{\circ}$C and $p(O_2) \leq 0.016$ mbar, the κ-, and the β-, as well as the spinel γ-polymorph coexist, as illustrated by XRD 2θ-ω-scans. Further employed growth parameters result in thin films with a monoclinic β-gallia structure. For all polymorphs, $p(O_2)$ and T_g affect the formation and desorption of volatile suboxides, and thereby the growth rate and the cation composition. For example, low oxygen pressures lead to low growth rates and enhanced Al incorporation. This facilitates the structural engineering of polymorphic, ternary $(Al,Ga)_2O_3$ via selection of the relevant process parameters. Transmission electron microscopy (TEM) studies of a κ - $(Al_{0.13}Ga_{0.87})_2O_3$ thin film reveal a more complex picture compared to that derived from x-ray diffraction measurements. Furthermore, this study presents the possibility of controlling the phase formation, as well as the Al-content, of thin films based on the choice of their growth conditions.

Keywords: Ga_2O_3, crystal growth, $(Al,Ga)_2O_3$

(Some figures may appear in colour only in the online journal)

1. Introduction

Gallium oxide is the focus of research interest, as, given its outstanding properties, such as a wide bandgap, high electrical breakdown field [1] of 8 MVcm^{-1} and large Baliga's figure of merit it is considered to be suitable for a variety of applications, including deep-UV photo detectors [2], gas sensors [3], high power rectifiers, and transistors [4–9]. The band gap ranges between 4.6 eV and 5.3 eV, depending on the respective polymorph, and can be reduced or enlarged by alloying with In_2O_3 or Al_2O_3 to expand the range of possible applications [10]. To date, most of the published studies have dealt with the thermodynamically stable monoclinic β-polymorph, but in recent years, the meta-stable orthorhombic κ-polymorph has garnered increasing interest, owing to its predicted large spontaneous polarization of 23 μC/cm^2 along its c-axis [11]. Extensive studies addressing this polymorph will be required to potentially realize high power and optical devices [12]. Cora *et al* [13] studied the

crystal structure of this polymorph in detail, assigning it to the space group $Pna2_1$, with two distinct cation sites, having a ratio of 1:3 of tetrahedrally and octahedrally coordinated Ga sites. In addition, they compared the orthorhombic with the hexagonal crystal structures, identifying the orthorhombic κ-Ga_2O_3 as a coordinated subgroup of the hexagonal ε-phase [13].

Binary orthorhombic Ga_2O_3 can be realized by a variety of growth techniques, such as halide vapor phase epitaxy HVPE[14, 15], atomic layer deposition[16] (ALD), metal organic chemical vapor deposition [13, 17–21] (MOCVD), mist CVD [22, 23], and plasma-assisted [24] or tin-assisted MBE [25], as well as tin-assisted pulsed laser deposition [26, 27] (PLD). In contrast, ternary alloys containing Al or In have so far only been realized by tin-assisted PLD [28–31] (PLD) on c-sapphire and κ-Ga_2O_3 templates as well as by mist CVD [32, 33] on c-plane AlN templates. With regard to PLD, a certain tin supply is necessary in addition to adequate growth conditions (growth temperature and pressure) in order to stabilize the orthorhombic phase [27]. To date, the highest reported Al content has been $x = 0.46$ for κ-$(Al,Ga)_2O_3$ on $(00.1)Al_2O_3$ [31] which can be enhanced up to $x = 0.65$ by employing an additional κ-Ga_2O_3 thin film template [29]. Kneiß *et al* have described the growth of binary κ-Ga_2O_3 using tin, which is not incorporated into the thin film, but serves as a surfactant [27, 31].

For binary β-Ga_2O_3 thin films, decreasing $p(O_2)$ or increasing T_g (by PLD) or metal-rich regimes (by MBE) leads to decreasing growth rates, caused by the formation and subsequent desorption of volatile Ga_2O suboxides [34–37]. For β-$(Al,Ga)_2O_3$ thin films, the same behaviour has been observed, but with one special feature: a change of the Al/Ga ratio in the thin films [38–40], which is due to the favored incorporation of Al into the layer. In contrast, for β-$(In,Ga)_2O_3$ thin films, the incorporation of Ga atoms is favored, leading to lower In-contents in the case of growth in oxygen-poor conditions [41]. Since growth parameters have such a significant impact on the material properties of β-Ga_2O_3-based thin films, a systematic study of the influence of these growth parameters for the less investigated orthorhombic phase is mandatory. In this paper, we present a detailed structural characterization on the nanoscale, in conjunction with a detailed description of the phase formation of $(Al,Ga)_2O_3$ thin films on c-plane sapphire, as well as the influence of T_g and $p(O_2)$ on this. Moreover, we illustrate the effect of the formation of volatile suboxides on cation incorporation, and therefore on the change of the cation composition in the layer and the growth rate of the thin film.

For this purpose, we deposited $(Al,Ga)_2O_3$ thin films on c-sapphire substrates under various growth conditions. The experiments reveal that orthorhombic $(Al,Ga)_2O_3$ can be stabilized only under certain growth conditions. This requires growth temperatures above 540 °C and oxygen pressures below 0.024 mbar, except for the highest investigated growth temperature of 670 °C, where $p(O_2) = 0.024$ mbar still leads to κ-phase thin films. For $T_g = 540$ °C and $p(O_2) \leq 0.016$ mbar, as well as for 620 °C and 0.024 mbar, the coexistence of κ-, β- and γ-polymorphs is observed. Other growth parameters can lead to monoclinic thin films. The crystal structure of one κ-$(Al_{0.13}Ga_{0.87})_2O_3$ thin film and one $(Al_{0.11}Ga_{0.89})_2O_3$ thin film exhibiting phase separation (κ and $\beta + \gamma$) are investigated in detail, using TEM measurements.

Table 1. Growth temperature T_g, oxygen pressure $p(O_2)$, measured Al content x by EDX, and polymorph for samples A, B and C.

label	T_g (°C)	$p(O_2)$ (mbar)	x	polymorph
A	620	0.002	0.13	κ
B	540	0.001	0.11	phase separation
C	500	0.002	0.10	β

2. Results and discussion

2.1. Crystal structure

The influence of growth parameters on the formation of κ-$(Al_xGa_{1-x})_2O_3$ thin films was analyzed by varying T_g and $p(O_2)$ during PLD growth, utilizing the same ceramic PLD target for all prepared samples. The thin films were also examined under x-ray diffraction, revealing the crystal structure to be monoclinic, orthorhombic, or a coexistence of both. In figure 1, representative 2θ-ω scans ($2\theta = 15$–65°) of $(Al_xGa_{1-x})_2O_3$ thin films are depicted, revealing characteristic reflection peaks, which can be assigned either to the β- or the κ-phase. Peaks corresponding to both phases are present for samples exhibiting phase separation. The growth conditions, Al-content and identified phase of these $(Al_xGa_{1-x})_2O_3$ thin films are presented in table 1. These samples will be referred to as samples A, B, and C below.

At the bottom of figure 1, the XRD pattern of sample C, a polycrystalline β-$(Al_xGa_{1-x})_2O_3$ thin film grown at 500 °C and 0.002 mbar, reveals the growth along the (-201) n lattice plane. This is indicated by the lattice plane reflection peaks observable at $2\theta = 18.82$°, 38.21°, and 59.10°. The growth along the (-201) lattice plane on c-plane sapphire has already been reported several times in relation to β-$(Al_xGa_{1-x})_2O_3$ [39, 40, 42, 43]. Aside from the $(-201)_\beta$ orientation, two additional orientations of the β-phase are visible in the scan: the $(-401)_\beta$ at $2\theta = 30.13$°, and the $(-601)_\beta$ at $2\theta = 44.26$°. The XRD pattern of sample A (top panel of figure 1), which was grown at 620 °C and 0.002 mbar, reveals reflection peaks at $2\theta = 19.26$°, 39.03° and 60.11°, which can be assigned to the (002) n lattice planes of κ-$(Al_xGa_{1-x})_2O_3$. These reflection peaks occur at slightly higher angles compared to those of the β-thin film described above, which is typical for binary κ-Ga_2O_3 [27], as well as its ternary alloys (κ-$(In,Ga,Al)_2O_3$) [28–31]. The thin film B, shown in the middle of figure 1, was grown at 540 °C and 0.001 mbar. The XRD pattern for this sample contains all previously described peaks, indicating phase separation. In addition, a peak shoulder appearing at $2\theta = 58.02$° is observed for B and

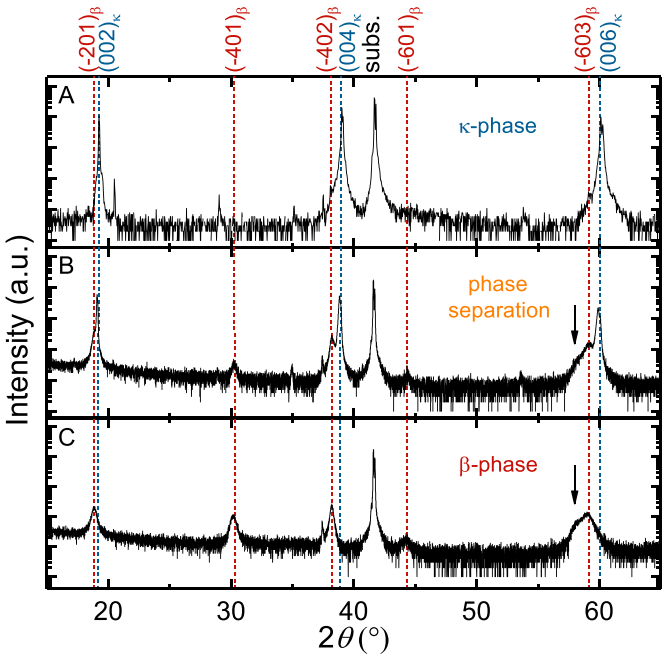

Figure 1. XRD patterns of an orthorhombic κ- (A), a monoclinic β-$(Al_xGa_{1-x})_2O_3$ thin film (C), and a thin film exhibiting a coexistence of both (B). The growth directions of the respective samples are labeled in red for the monoclinic, and blue for the orthorhombic lattice planes. The shoulders highlighted by the arrow can be assigned either to $(-313)_\beta$ or $(333)_\gamma$ lattice planes. The peak positions were assigned according to JCPDS card nos. 76-0573, 20-0426 and 11-0342. The reflection peak visible at 41.68° can be assigned to the (00.6) Al_2O_3 lattice plane (JCPDS PDF card no. 82-1399).

C (marked with an arrow), which cannot be unambiguously assigned to a lattice plane reflection. One possible explanation for this is the presence of reflections at the monoclinic $(-313)_\beta$ and the cubic $(333)_\gamma$ lattice plane, or an convolution of both. The c-plane sapphire (00.6) lattice plane reflection peak appears for all samples at 41.68°. Small peaks at 20.4° and 29.0° can also be observed (e.g. for sample A), emanating from the so-called Umweganregung (x-ray double diffraction) of the substrate. Such an Umweganregung is only observable under certain ϕ rotations, and may therefore occur in some samples [44]. Further visible reflection peaks are due to the K_β (35.2°, 53.9°) or the tungsten L_α (37.4°) spectral lines.

In order to compare the crystalline quality of β- and κ-$(Al,Ga)_2O_3$, the FWHMs of samples A and B were determined for the $(004)_\kappa$ and $(-402)_\beta$ reflection peaks. For the $(-402)_\beta$ reflection, the FWHM amounts to 0.258°, and for $(004)_\kappa$ it is 0.120°, exhibiting a lower broadening, and therefore representing a higher crystalline quality. The thin film thickness does not play a role, since the thickness of the samples is similar (470 nm for sample A, and 510 nm for C). The small differences in thin film thickness are caused by the different growth temperatures and the associated desorption of volatile suboxides [36, 37].

Since the oxygen pressures during growth of the three samples were nearly the same (0.001 or 0.002 mbar, respectively), the difference in growth temperature is accountable for the crystallization of the different phases seen here. Moreover, the growth temperature influences the incorporation of Al into the layers, which increases with increasing T_g. Note that the Al content present in the target is approximately 8.8 at.%. In the layers, values of 10 to 13 at.% were detected (see table 1). A detailed description of this phenomenon maycan be found in the section *Phase Control*. In the next section we want to focus on an atomically resolved description of the orthorhombic thin film (sample A) and the thin film exhibiting phase separation (sample B).

2.2. Growth

TEM investigations were performed for samples A and B and the cross-sectional TEM bright field images are shown in figure 2(a) and (b), respectively. In both layers, two phases of different morphologies can be clearly distinguished: a speckle-contrast region starting from the interface, indicating a highly granular structure, and on top of that a phase with vertically aligned features, indicating columnar-like domains. Selected area electron diffraction (SAED) was performed for each of these regions to identify the crystal structure and the growth orientations. This measurement was performed for two zone axis orientations of the sapphire substrate, $[11\bar{2}0]$ and $[1\bar{1}00]$, for which the data are presented in figure 2(c). With regard to electron diffraction simulations [45], the red circled region is identified as a coexistence of the monoclinic β- and the cubic γ-phase. The γ-Ga_2O_3 phase has a cation-deficient spinel structure ($Fd\bar{3}m$) described in detail by Playford *et al* [46], and similar to that of γ-Al_2O_3. The blue circled region can be identified as the orthorhombic κ-structure in both samples, as shown in figure 2(c). The SAED patterns of the κ- and $\beta+\gamma$-regions of sample A look the same as those presented for sample B. The domain boundaries between the $\beta+\gamma$-part and the κ-phase extend diagonally through the layer. This suggests that the κ-phase starts to nucleate as islands in certain positions, probably due to Sn accumulations, then grows at a higher growth rate than the $\beta+\gamma$-phase until the latter is overgrown. The composition in both phases is the same, as confirmed by STEM-EDXS measurements of the TEM sample. A STEM-EDXS spectrum can be found in the supplemental material (stacks.iop.org/JPD/53/485105/mmedia).

The different phases are investigated in greater detail via Scanning TEM (STEM) imaging. Figure 3(a) shows a STEM image, taken close to the interface in sample B, and including the sapphire substrate and regions with $\beta+\gamma$- and κ-phase. The κ-phase is shown at higher magnification in figure 3(b), where we see that it is growing in narrow columnar domains of a few nanometers in width. The structure exhibits vertical lines of defects, extending through the structure (positions indicated by the white arrows), which are indicative of the vertical domain boundaries. The atomically resolved structure of the κ-phase is displayed in figure 3(c)II, and fits well to the atomic

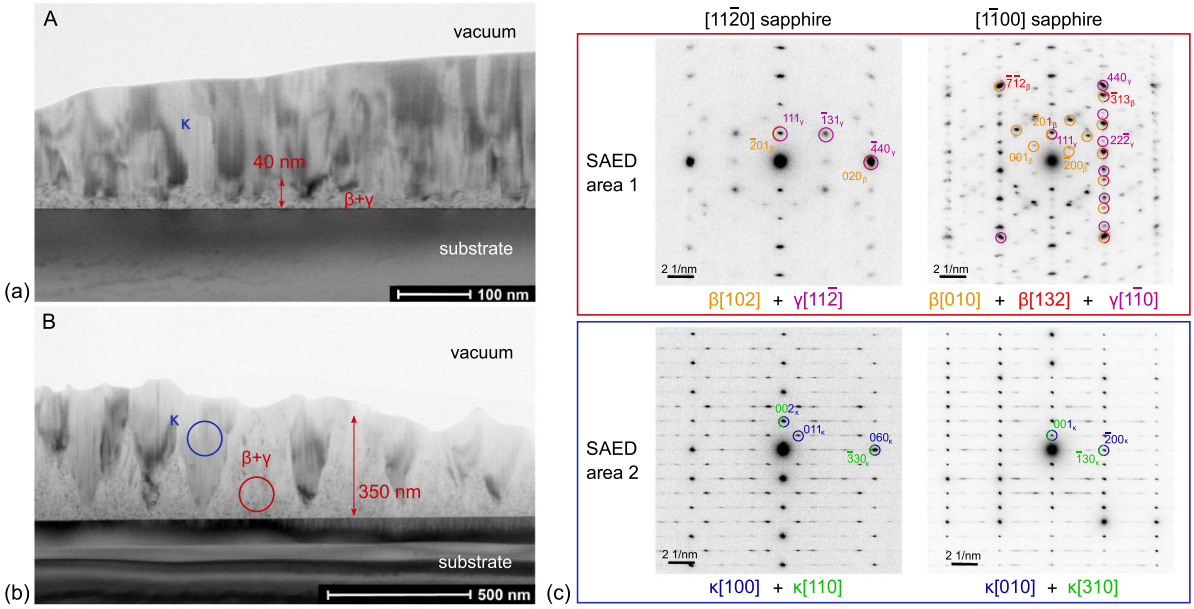

Figure 2. TEM bright field overview images of $(Al_xGa_{1-x})_2O_3$ layers grown at (a) $T_g = 620^\circ$C and $p(O_2) = 0.002$ mbar and (b) $T_g = 540^\circ$C and $p(O_2) = 0.001$ mbar, corresponding respectively to samples A and B, shown in Fig 1. (c) Selected area electron diffraction (SAED, inverted contrast) in two zone axis orientations of the sapphire substrate in the areas indicated by red and blue circle in (b). We note that the streaky horizontal features in the SAED patterns of the κ-phase (blue) are probably caused by the short domain width in this direction, which breaks the periodicity.

model superimposed on the experimental image. Ga columns appear bright in these images, while oxygen atoms are too light to produce a visible contrast. The domains are 60° rotated in plane with respect to each other, and the epitaxial relationships are $(001)_\kappa||(00.1)_s$ and $[010]_\kappa$, $[310]_\kappa||[1\bar{1}00]_s$ and $[100]_\kappa$, $[110]_\kappa||[11\bar{2}0]_s$.

A high magnification image of the interface region (shown in figure 3(c) III) actually reveals the presence of a fourth phase, namely α. It grows pseudomorphically for 3-4 monolayers on the sapphire substrate, with the same crystal structure. This phase is not detectable in XRD, because the layer is buried and too thin. The formation of this α-interlayer has already been shown to be typical for Ga_2O_3 layer growth on sapphire [47].

Close to the interface, small grains (measuring only a few nm) of β- and γ-phase are mixed randomly, while at larger thicknesses the grains grow larger and the β-phase is dominant. Figure 3(c) shows area scans for γ- and a β-phase grains where the structures can be fitted to the stick-and-ball models. Despite these small grains, both β- and γ-phases exhibit an epitaxial relationship with respect to the sapphire. For the out-of-plane orientation, $(\text{-}201)_\beta||(00.1)_s$ and $(111)_\gamma||(00.1)_s$ was found. The spacings of these planes are very close to each other in value ($d((\text{-}201)_\beta) = 4.70$ Å and $d((111)_\gamma) = 4.75$ Å), therefore the phases can hardly be distinguished in the XRD patterns. The in-plane relationship for the γ-phase is $[1\bar{1}0]_\gamma||[1\bar{1}00]_s$. The β-grains grow in different orientations, rotated in-plane by 60° with respect to each other, according to $[010]_\beta$ or $[132]_\beta||[1\bar{1}00]_s$. Since this polycrystalline interlayer is only a few 10 nm thick in sample A, it implies that these grains are even smaller, which could explain the x-ray amorphous behavior of this layer. The formation of the approximately 20–30 nm small and wavy interlayer can be explained by the PLD approach employed here. During the first laser pulses an insufficient amount of tin is ablated, and the required liquid tin layer cannot form instantaneously. Only when this tin layer has formed can the growth of the orthorhombic phase begin.

Investigations of the surface morphology of samples A and C show similar results to comparable samples published previously [29, 31]. Therefore, only the surface morphology of sample B is presented below. AFM measurements show a surface consisting of 3D islands, which has a root mean square surface roughnesses of 8.6 nm. Figure 4(a) shows a $5 \times 5\ \mu m^2$ surface scan, depicting 3D islands, 200–400 nm in diameter. By considering the cross-sectional view, presented in figure 4(b), it can be established that the higher parts of the thin films can be allocated to the orthorhombic phase. The higher growth rates of the κ-phase, compared with those of the β-phase, leads to an overgrowth of the $\beta + \gamma$-part. If the thin film growth were to continue, e.g. by a higher pulse number from the PLD, it may be assumed that the κ-phase proportion would grow further in lateral size and finally overgrow the $\beta + \gamma$-part completely. Such complete

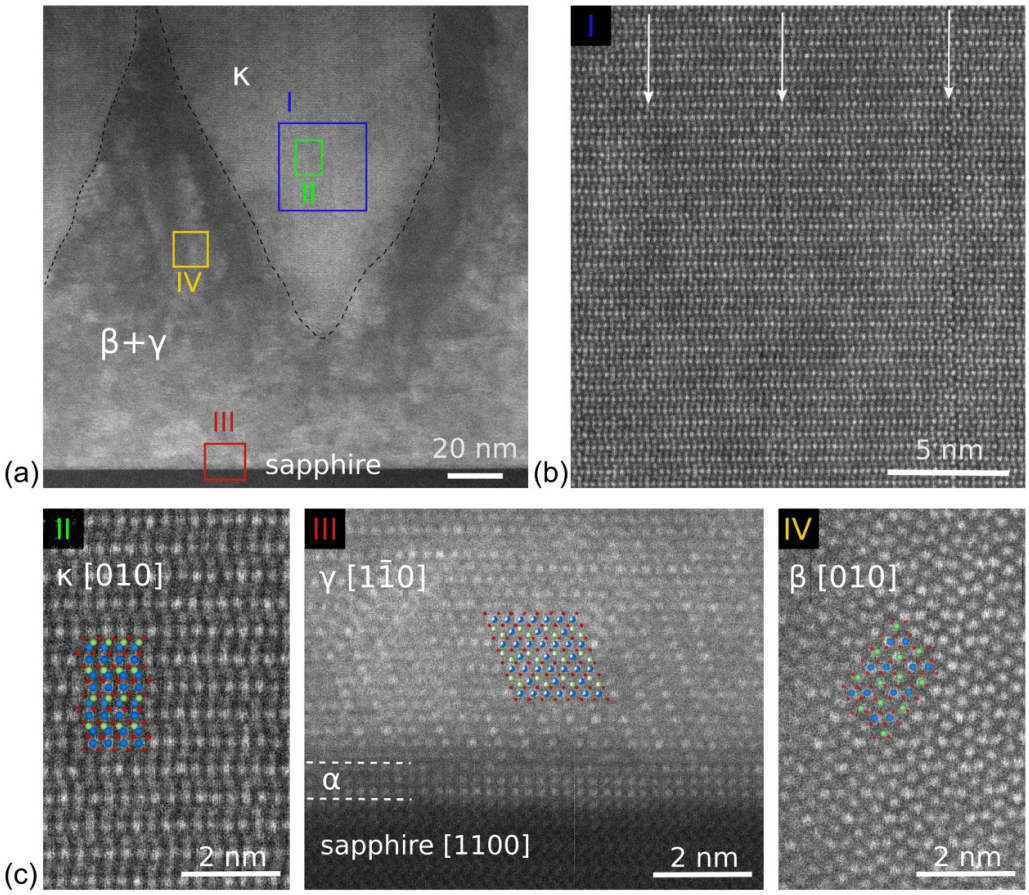

Figure 3. (a) STEM image of an area in sample B ($T_g = 620^\circ$C and $p(O_2) = 0.002$ mbar) showing the substrate, the β+γ-mix phase, and the κ-phase. (b) Higher magnification image of the blue area in (a), showing a defective κ-structure due to many vertical domain boundaries. (c) STEM images of areas II, III and IV in (a), showing the atomically resolved pattern of the κ-, α+γ-, and β-structures, respectively, with the atomic models superimposed (blue & green: 6-fold and 4-fold coordinated Ga respectively, red: O) For the cation-deficient γ-phase, only those cations with the highest occupancy are shown in the model structure.

overgrowth is visible in figure 2(a) for the κ-$(Al,Ga)_2O_3$ thin film.

2.3. Phase control

In addition to the aforementioned samples, thin films were deposited under several growth conditions (various combinations of $p(O_2)$ and T_g) and investigated via XRD to determine their crystal structure, by EDX to define their cation composition, and by spectroscopic ellipsometry to examine their growth rates. Note that the ceramic target employed here consists of Ga_2O_3 doped with 8.8 at.% Al_2O_3. Although TEM images show that the phase distribution is more complicated, below, we will focus only on phases with a high volume fraction, as identified by XRD.

The growth conditions, such as oxygen pressure and substrate temperature, were selected in the ranges of 3×10^{-4} mbar $\leq p(O_2) \leq 0.024$ mbar, and $450^\circ\text{C} \leq T_g \leq 670^\circ$C. Every sample was measured using XRD to determine the respective polymorph. The sample series for $p(O_2) = 0.000\,3$ mbar is depicted in figure 5, showing a change in the crystal structure, dependent on T_g. For temperatures from 670 to 580°C, the κ-phase forms, for 540°C we obtain a mixture of the $\beta+\gamma$- and κ-phases, and for 500-450°C, the β-phase forms. The XRD spectra for the remaining oxygen pressures and growth temperatures can be found in the supplemental material. The evaluation of these detected crystal structures revealed defined growth conditions, among them the κ-modification forms presented in figure 6(a). These specific growth conditions are required for the given amount of tin in the target, due to the surfactant-mediated growth, where a liquid tin layer forms on top of the thin film, inducing the κ-growth below. The tin will not be incorporated into the layer, and desorbs, or rather accumulates at the top, as demonstrated for κ-$(Al,Ga)_2O_3$ [31].

In the oxygen rich regime of 0.024 mbar, and at growth temperatures between 540°C and 580°C, the tin atoms completely oxidize, a liquid tin layer does not form, and hence the formation of the κ-phase is suppressed. To determine the point of transition from the β- to the κ-phase more accurately, thin films were grown between 540°C and 620°C instead of at an oxygen pressure of 0.01 mbar at 0.016 mbar. For temperatures below 500°C, surface-mediated growth cannot be observed, such that the monoclinic polymorph forms across the whole examined pressure range. In a narrow growth window of $T_g = 540^\circ$C and 3×10^{-4} mbar $\leq p(O_2) \leq 0.016$ mbar, as

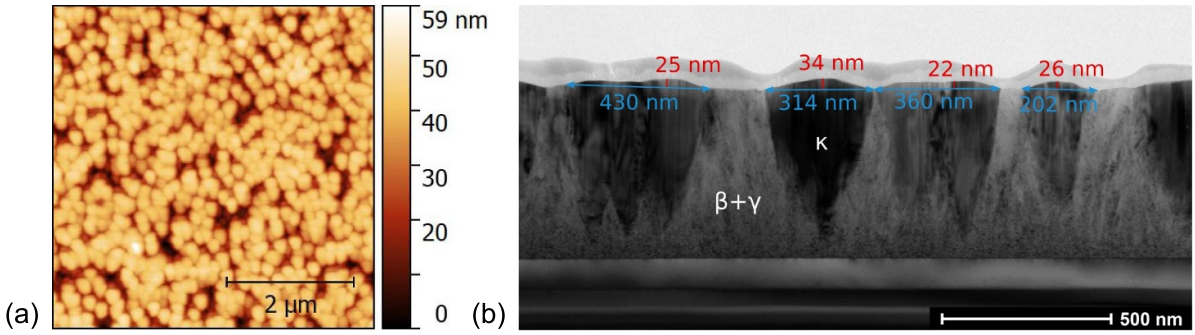

Figure 4. (a) $5\times 5\,\mu m^2$ AFM scan and (b) TEM cross-sectional view of sample B.

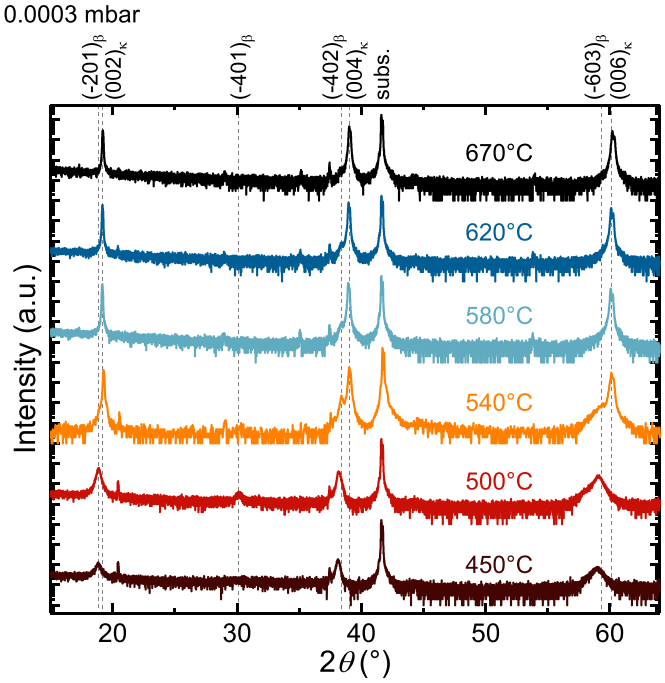

Figure 5. XRD 2θ-ω scans of $(Al_xGa_{1-x})_2O_3$ thin films deposited at $p(O_2) = 0.000\,3$ mbar and various growth temperatures as labeled. The growth directions of the orthorhombic κ- and monoclinic β-samples are indicated in the graphs.

well as for 620 °C and 0.024 mbar, both phases coexist, as described in the previous section. Conceivably, the creation of the liquid tin layer is insufficient and/or small in this growth regime. The cation composition was investigated by means of EDX measurements, and is depicted as a function of the Al content x in figure 6(b). As reported for β-$(Al_xGa_{1-x})_2O_3$ thin films [40], x increases with decreasing oxygen pressure and/or increasing growth temperature up to 2.25 times the amount of material actually offered in the target. In monoclinic thin films, volatile Ga_2O suboxides form at the layer surface, and subsequently desorb. As a result, the Ga_2O species is preferentially formed, due to the lower dissociation energy of the Ga-O bond compared to the Al-O bond. The higher the oxygen deficit (low $p(O_2)$) and/or the higher T_g, the more suboxides form and desorb, leading to a higher Al concentration in the thin film. Since for the κ-polymorph grown by PLD, surface-mediated growth was reported [27, 31], the desorption process should be influenced by the existence of the liquid tin layer on the thin film's surface. The exact growth and desorption mechanism should be the focus of future research projects. However, the Al incorporation for the κ-, β- and the samples exhibiting phase separation is presented in figure 6(b) in relation to its dependence on $p(O_2)$ and T_g. Regarding the T_g series, it is observable that the desorption process diminishes for decreasing T_g. The growth pressure, where a stoichiometric target-to-layer cation transfer can be monitored, shifts continuously to lower $p(O_2)$. The stoichiometric cation transfer is $x = 0.088$, and is marked in figure 6(b). For $T_g = 670$ °C, this point is reached at $p(O_2) = 0.01$ mbar, for 580 °C at around 0.006 mbar, for 540 °C and 500 °C at 0.003 mbar, and for 450 °C a stoichiometric cation transfer was observed between 3×10^{-4} and 0.002 mbar. Since the Al content of the samples grown at 500 °C and 450 °C shows only a small change or no change in x, no additional thin films were grown. In an oxygen rich regime, $p(O_2) \geq 0.016$ mbar, the cation transfer of Al is $x = 0.07$, because the lighter Al ions are more widely scattered than the heavier Ga ions. For high $p(O_2)$, x remains constant and increases are no longer as visible at 620 °C, 580 °C, and 500 °C, indicating that the formation of volatile Ga_2O is suppressed [36, 37]. Nevertheless, the surface-mediated growth reduces the desorption process compared to the monoclinic phase. To demonstrate this, the κ-$(Al_xGa_{1-x})_2O_3$ thin films grown at 670 °C can be compared with β-$(Al_xGa_{1-x})_2O_3$ thin films published before [40]. The target used for both sample series consists of an admixture of 8.8 at.% Al_2O_3, and the samples are grown at 670 °C and at various oxygen pressures. The monoclinic thin films show systematically higher x for all oxygen pressures. Another indication of the lower incorporation of Ga into the layer due to desorption of volatile Ga_2O is a decrease in the growth rate r, which was determined by spectroscopic ellipsometry and presented in figure 6(c). The graph shows a dependency on the growth conditions. With decreasing $p(O_2)$ and/or increasing T_g, the growth rate also decreases. The behaviour of r is in accordance with an increased desorption of volatile Ga_2O, which is indicated by the inset of figure 6(c), where r is plotted against x: r decreases approximately linearly with increasing x. The lowest r is about 19 pm/pulse for the lowest investigated oxygen pressure (3×10^{-4} mbar), the highest temperature (670 °C) and the lowest Ga content

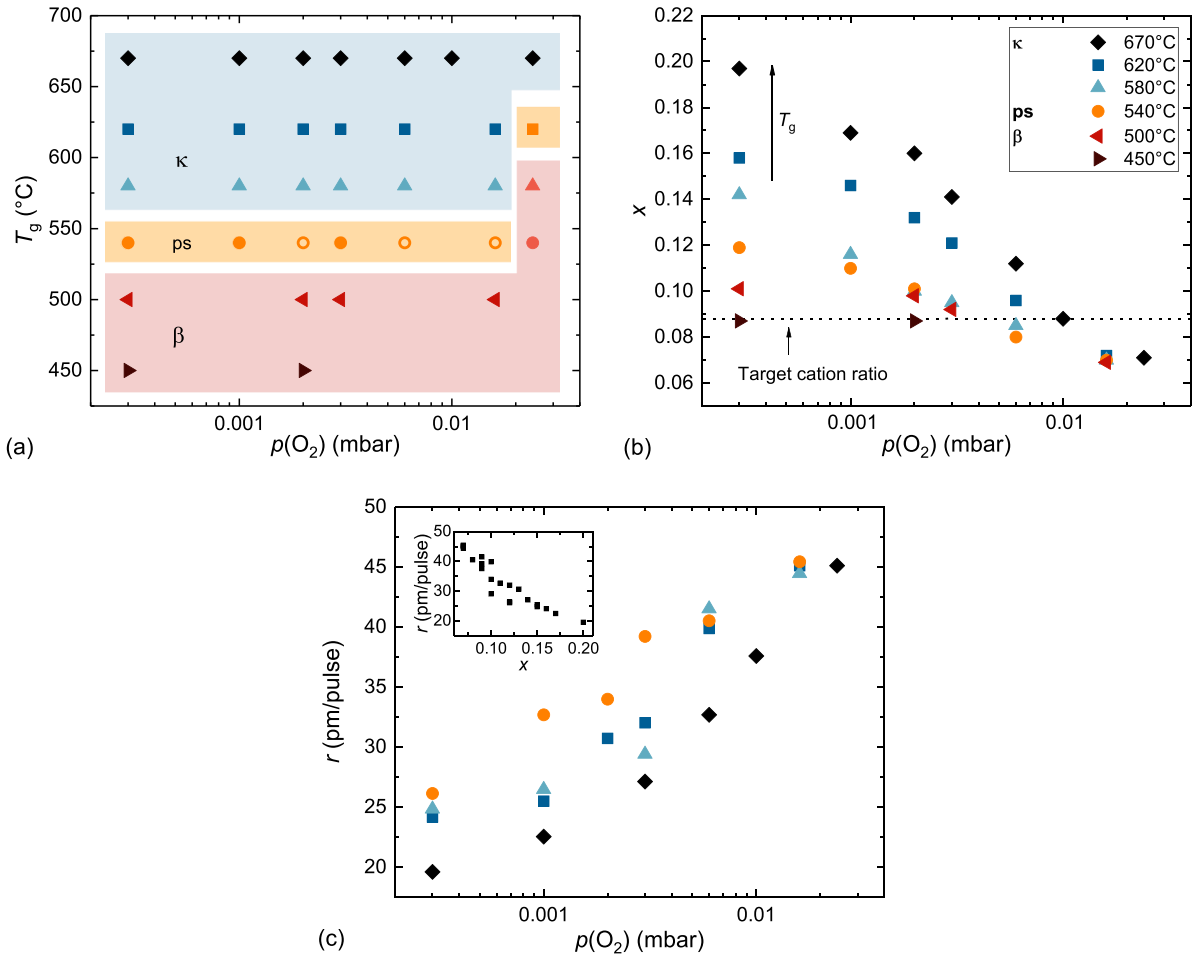

Figure 6. (a) Influence of the growth conditions ($p(O_2)$ & T_g) on the formation of orthorhombic κ- and monoclinic β-$(Al_xGa_{1-x})_2O_3$. The different line widths of the sample exhibiting phase separation (ps) indicate the intensity of the observable β-reflection peaks: a larger width means a more intense peak. (b) Al content x by EDX as a function of the oxygen pressure for the different polymorphs and growth temperatures, as labeled. The dotted line denotes the cation ratio from the target. (c) Growth rate r vs dependence on $p(O_2)$. The inset shows the dependence on the Al-content.

(1-x = 0.8). For the highest investigated oxygen pressures (0.016 mbar and 0.024 mbar), the growth rates seem to saturate for all investigated T_g between 45 - 46.5 pm/pulse. Interestingly, this is the growth region where fewer Al atoms are present, as they were incorporated into the thin film, suggesting that deposition kinematics, such as scattering, play a minor role compared to the forming and desorption of volatile suboxides.

3. Conclusion

In this work, $(Al,Ga)_2O_3$ thin films were deposited under various growth conditions, leading to the crystallization of orthorhombic or monoclinic polymorphs, or a coexistence of both, in addition to cubic defect spinel phases. This allows for the dedicated preparation of a desired crystal structure by means of selecting the relevant growth parameters. The orthorhombic structure forms under higher growth temperatures, and the monoclinic structure at high oxygen pressures and/or low growth temperatures. A coexistence of these phases and the γ-phase can only be observed for $p(O_2) \leq 0.016$ mbar and $T_g = 540^\circ$C, as well as for 0.024 mbar and 620°C. Furthermore, we have shown that under low $p(O_2)$ and/or high T_g, volatile suboxides form and desorb, which leads systematically to increasing Al contents and decreasing growth rates. Here, surfactant-mediated growth is suggested to be the growth mechanism for κ-$(Al,Ga)_2O_3$. Volatile suboxides are formed independent of the polymorph; it seems that the liquid tin layer reduces this process to some extent, as indicated by the cation composition evolution. For a sample grown at $T_g = 620^\circ$C and $p(O_2) = 0.002$ mbar, TEM results reveal that a 3-4 monolayer thick α - $(Al_xGa_{1-x})_2O_3$ layer grew first on the substrate, with a thin polycrystalline $\beta+\gamma$ - $(Al_xGa_{1-x})_2O_3$ layer and the κ - $(Al_xGa_{1-x})_2O_3$ thin film on top. Neither α - nor $\beta+\gamma$ - layers were observed by x-ray diffraction measurements for this sample. Furthermore, TEM and AFM measurements of a sample grown in a phase mixture have been demonstrated. The side-by-side growth of the κ - and $\beta+\gamma$ - phase could be caused by an insufficient and/or a small liquid tin layer on top of the sample.

4. Experimental

The $(Al_xGa_{1-x})_2O_3$ thin films presented here were grown by PLD on 10×10 mm^2 sized c-sapphire substrates at various growth temperatures, ranging between 550 °C and 670 °C, as well as at oxygen partial pressures between 3×10^{-4} mbar and 0.024 mbar. The given growth temperatures were estimated from the heater block temperatures, measured by a thermocouple, minus a constant temperature drop of 50 K due to the radiative heating of the substrate without direct contact to the heater block [48]. All samples were grown using the same target, consisting of Ga_2O_3 (purity 99.999%, Alfa Aeser) with an Al_2O_3 admixture of 8.8 at.% (purity 99.997%, Alfa Aeser) and a SnO_2 (99.9% purity, Alfa Aesar) admixture of 0.6 at.% to induce the growth of the κ-modification [25, 27]. The KrF excimer laser beam (248 nm) has an energy density of 2.6 Jcm^{-2} on the target surface, and the target-to-substrate distance is 10 cm. The total applied pulse number for every thin film sample was 15 300. The first 300 pulses, with a pulse frequency of 1 Hz, were used to create a nucleation layer. The repetition rate for the subsequent 15 000 pulses was 10 Hz. The chemical cation composition was studied by energy-dispersive x-ray spectroscopy (EDX), using a FEI Nova Nanolab 200, equipped with an Ametek EDAX detector. X-ray diffraction (XRD) measurements were acquired using a PANalytical X'pert PRO MRD diffractometer, equipped with a PIXcel^{3D} detector, and operating in 1D scanning line mode with 255 channels. Transmission electron microscopy (TEM) measurements were performed with an aberration corrected FEI Titan 80-300 electron microscope, operating at 300 kV. The TEM samples were prepared in cross-section view along the $<1\bar{1}00>$ and $<11\bar{2}0>$ zone-axis directions of the sapphire substrate. The thin film thickness (d) was determined by spectroscopic ellipsometry, employing a dual rotating compensator ellipsometer (RC2, J.A. Woollam M2000) with a spot size of about $300 \times 500\ \mu$m^2. Subsequently, the growth rate r was calculated by dividing d by the number of pulses during deposition ($r = d/15300$).

Acknowledgments

We thank Monika Hahn for PLD target fabrication, Jörg Lenzner for EDX measurements, and Ulrike Teschner for transmission measurements. This work was supported by the European Social Fund within the Young Investigator Group "Oxide Heterostructures" (No. SAB 100 310 460), and partly by Deutsche Forschungsgemeinschaft in the Framework of Sonderforschungsbereich 762 "Functionality of Oxide Interfaces". A Hassa and M Kneiß acknowledge the Leipzig School for Natural Sciences BuildMoNa. We acknowledge support from the German Research Foundation (DFG) and the Universität Leipzig, within the program of Open Access Publishing.

ORCID iDs

Anna Hassa https://orcid.org/0000-0002-8087-6592
Charlotte Wouters https://orcid.org/0000-0002-0742-168X
Max Kneiß https://orcid.org/0000-0002-8350-7346
Daniel Splith https://orcid.org/0000-0001-5434-2194
Holger von Wenckstern https://orcid.org/0000-0002-3936-275X
Martin Albrecht https://orcid.org/0000-0003-1835-052X
Michael Lorenz https://orcid.org/0000-0003-2774-6040
Marius Grundmann https://orcid.org/0000-0001-7554-182X

References

[1] Higashiwaki M, Sasaki K, Kuramata A, Masui T and Yamakoshi S 2012 Gallium oxide (Ga_2O_3) metal-semiconductor field-effect transistors on single-crystal β-Ga_2O_3 (010) substrates *Appl. Phys. Lett.* **100** 013504
[2] Zhang Z, von Wenckstern H and Grundmann M 2014 Monolithic multichannel ultraviolet photodiodes based on (Mg,Zn)O thin films with continuous composition spreads *Sel. Top. Quantum Electron. IEEE J.* **20** 106–11
[3] Bierwagen O 2015 Indium oxide - a transparent, wide-band gap semiconductor for (opto)electronic applications *Semicond. Sci. Technol.* **30** 024001
[4] Grundmann M, Frenzel H, Lajn A, Lorenz M, Schein F and von Wenckstern H 2010 Transparent semiconducting oxides: materials and devices *phys. stat. sol. (a)* **207** 1437–49
[5] Higashiwaki M, Kuramata A, Murakami H and Kumagai Y 2017 State-of-the-art technologies of gallium oxide power devices *J. Phys. D: Appl. Phys.* **50** 333002
[6] Stepanov S I, Nikolaev V I, Bougrov V E and Romanov A 2016 Gallium oxide: Properties and applications - A review *Rev. Adv. Mater. Sci.* **44** 63–86
[7] Holger von W 2017 Group-III Sesquioxides: Growth, Physical Properties and Devices *Adv. Electron. Mater.* **3** 1600350
[8] Pearton S J, Jiancheng Yang P H Ren C, F, Kim J, Tadjer M J and Mastro M A 2018 A review of Ga_2O_3 materials, processing and devices *Appl. Phys. Rev.* **5** 011301
[9] Zhang J, Shi J, Dong-Chen Q, Chen L and Zhang K H L 2020 Recent progress on the electronic structure, defect and doping properties of Ga_2O_3 *APL Materials* **8** 020906
[10] Holger von W 2018 *Gallium Oxide: Technology, Devices and Applications (Metal Oxides)* Chapter Properties of $(In,Ga)_2O_3$ Alloys (Amsterdam: Elsevier) pp 119–48
[11] Maccioni M B and Fiorentini V 2016 Phase diagram and polarization of stable phases of $(Ga_{1-x}In_x)_2O_3$ *Appl. Phys. Express* **9** 041102
[12] Kneiß M, Storm P, Hassa A, Splith D, von Wenckstern H, Lorenz M and Grundmann M 2020 Growth, structural and optical properties of coherent κ-$(Al_xGa_{1-x})_2O_3$/κ-Ga_2O_3 quantum well superlattice heterostructures *APL Mater.* **8** 051112
[13] Cora Io, Mezzadri F, Boschi F, Bosi M, Caplovicová M, Calestani G, Dódony Ian, Pécz Bela and Fornari R 2017 The real structure of *CrystEngComm* **19** 1509–16 ε-Ga_2O_3 and its relation to κ-phase
[14] Oshima Y, Víllora Eon G, Matsushita Y, Yamamoto S and Shimamura K 2015 Epitaxial growth of phase-pure ε-Ga_2O_3 by halide vapor phase epitaxy *J. Appl. Phys.* **118** 085301
[15] Nikolaev V I, Stepanov S I, Pechnikov A I, Shapenkov S V, Scheglov M P, Chikiryaka A V and Vyvenko O F 2020 HVPE Growth and Characterization of ε-Ga_2O_3 Films on Various Substrates *ECS J. Solid State Sci. Technol.* **9** 045014

[16] Boschi F, Bosi M, Berzina T, Buffagni E, Ferrari C and Fornari R 2016 Hetero-epitaxy of ε-Ga_2O_3 layers by MOCVD and ALD *J. Cryst. Growth* **443** 25–30

[17] Mezzadri F, Calestani G, Boschi F, Delmonte D, Bosi M and Fornari R 2016 Crystal Structure and Ferroelectric Properties of ε-Ga_2O_3 Films Grown on (0001)-Sapphire *Inorg. Chem.* **55** 12079–84

[18] Chen Y, Xia X, Liang H, Abbas Q, Liu Y and Guotong D 2018 Growth Pressure Controlled Nucleation Epitaxy of Pure Phase ε- and β-Ga_2O_3 Films on Al_2O_3 via MOCVD *Crystal Growth Design* **18** 1147–54

[19] Pavesi M, Fabbri F, Boschi F, Piacentini G, Baraldi A, Bosi M, Gombia E, Parisini A and Fornari R 2018 ε-Ga_2O_3 epilayers as a material for solar-blind UV photodetectors *Mater. Chem. Phys.* **205** 502–7

[20] Mulazzi M, Reichmann F, Becker A, Klesse W M, Alippi P, Fiorentini V, Parisini A, Bosi M and Fornari R 2019 The electronic structure of ε-Ga_2O_3 *APL Mater.* **7** 022522

[21] Park S H, Lee H S, Ahn H S and Yang M 2019 Crystal Phase Control of ε-Ga_2O_3 Fabricated using by Metal-Organic Chemical Vapor Deposition *J. Korean Phys. Soc.* **74** 502–7

[22] Tahara D, Nishinaka H, Morimoto S and Yoshimoto M 2017 Stoichiometric control for heteroepitaxial growth of smooth ε-Ga_2O_3 thin films onc-plane AlN templates by mist chemical vapor deposition *Japan. J. Appl. Phys.* **56** 078004

[23] Arata Y, Nishinaka H, Tahara D and Yoshimoto M 2018 Heteroepitaxial growth of single-phase ε-Ga_2O_3 thin films on c-plane sapphire by mist chemical vapor deposition using a NiO buffer layer *CrystEngComm* **20** 6236–42

[24] Vogt P, Brandt O, Riechert H, Lähnemann J and Bierwagen O 2017 Metal-Exchange Catalysis in the Growth of Sesquioxides: Towards Heterostructures of Transparent Oxide Semiconductors *Phys. Rev. Lett.* **119** 196001

[25] Kracht M *et al* 2017 Tin-Assisted Synthesis of $\varepsilon - Ga_2O_3$ by Molecular Beam Epitaxy *Phys. Rev. Appl.* **8** 054002

[26] Orita M, Hiramatsu H, Ohta H, Hirano M and Hosono H 2002 Preparation of highly conductive, deep ultraviolet transparent β-Ga_2O_3 thin film at low deposition temperatures *Thin Solid Films* **411** 134–9

[27] Kneiß M, Hassa A, Splith D, Sturm C, von Wenckstern H, Schultz T, Koch N, Lorenz M and Grundmann M 2019 Tin-assisted heteroepitaxial PLD-growth of κ-Ga_2O_3 thin films with high crystalline quality *APL Mater.* **7** 022516

[28] Hassa A, von Wenckstern H, Splith D, Sturm C, Kneiß M, Prozheeva V and Grundmann M 2019 Structural, optical and electrical properties of orthorhombic κ-$(In_xGa_{1-x})_2O_3$ thin films *APL Mater.* **7** 022525

[29] Storm P, Kneiß M, Hassa A, Schultz T, Splith D, von Wenckstern H, Koch N, Lorenz M and Grundmann M 2019 Epitaxial κ-$(Al_xGa_{1-x})_2O_3$ thin films and heterostructures grown by tin-assisted VCCS-PLD *APL Mater.* **7** 111110

[30] Kneiß M, Hassa A, Splith D, Sturm C, von Wenckstern H, Lorenz M and Grundmann M 2019 Epitaxial stabilization of single phase κ-$(In_xGa_{1-x})_2O_3$ thin films up to $x = 0.28$ on c-sapphire and κ-Ga_2O_3 (001) templates by tin-assisted VCCS-PLD *APL Mater.* **7** 101102

[31] Hassa A, Sturm C, Kneiß M, Splith D, von Wenckstern H, Schultz T, Koch N, Lorenz M and Grundmann M 2020 Solubility limit and material properties of a κ-$(Al_xGa_{1-x})_2O_3$ thin film with a lateral cation gradient on (00.1)Al_2O_3 by tin-assisted PLD *APL Mater.* **8** 021103

[32] Tahara D, Nishinaka H, Morimoto S and Yoshimoto M 2018 Heteroepitaxial growth of ε-$(Al_xGa_{1-x})_2O_3$ alloy films on c-plane AlN templates by mist chemical vapor deposition *Appl. Phys. Lett.* **112** 152102

[33] Nishinaka H, Miyauchi N, Tahara D, Morimoto S and Yoshimoto M 2018 Incorporation of indium into ε-gallium oxide epitaxial thin films grown via mist chemical vapour deposition for bandgap engineering *Crystengcomm* **20** 1882–8

[34] Müller S, von Wenckstern H, Splith D, Schmidt F and Grundmann M 2014 Control of the conductivity of Si-doped β-Ga_2O_3 thin films via growth temperature and pressure *Physica Status Solidi* (a) **211** 34–9

[35] Zhang F B, Saito K, Tanaka T, Nishio M and Guo Q X 2014 Structural and optical properties of Ga_2O_3 films on sapphire substrates by pulsed laser deposition *J. Cryst. Growth* **387** 96–100

[36] Vogt P and Bierwagen O 2015 The competing oxide and sub-oxide formation in metal-oxide molecular beam epitaxy *Appl. Phys. Lett.* **106** 081910

[37] Vogt P and Bierwagen O 2016 Reaction kinetics and growth window for plasma-assisted molecular beam epitaxy of Ga_2O_3: Incorporation of Ga vs. Ga_2O desorption *Appl. Phys. Lett.* **108** 072101

[38] Wakabayashi R, Oshima T, Hattori M, Sasaki K, Masui T, Kuramata A, Yamakoshi S, Yoshimatsu K and Ohtomo A 2015 Oxygen-radical-assisted pulsed-laser deposition of β-Ga_2O_3 and β-$(Al_xGa_{1-x})_2O_3$ films *J. Cryst. Growth* **424** 77–9

[39] Wang X, Chen Z, Zhang F, Saito K, Tanaka T, Nishio M and Guo Q 2016 Influence of substrate temperature on the properties of $(AlGa)_2O_3$ thin films prepared by pulsed laser deposition *Ceram. Int.* **42** 12783–8

[40] Hassa A, von Wenckstern H, Vines L and Grundmann M 2019 Influence of oxygen pressure on growth of Si-doped β-$(Al_xGa_{1-x})_2O_3$ thin films on c-Sapphire substrates by pulsed laser deposition *ECS J. Solid State Sci. Technol.* **8** Q3217–Q3220

[41] Vogt P and Bierwagen O 2016 Kinetics versus thermodynamics of the metal incorporation in molecular beam epitaxy of $(In_xGa_{1-x})_2O_3$ *APL Mater.* **4** 086112

[42] Nakagomi S and Kokubun Y 2012 Crystal orientation of β-Ga_2O_3 thin films formed on c-plane and a-plane sapphire substrate *J. Cryst. Growth* **349** 12–18

[43] Zhang F, Saito K, Tanaka T, Nishio M, Arita M and Guo Q 2014 Wide bandgap engineering of $(AlGa)_2O_3$ films *Appl. Phys. Lett.* **105** 162107

[44] Grundmann M, Scheibe M, Lorenz M, Bläsing J and Krost A 2014 X-ray multiple diffraction of ZnO substrates and heteroepitaxial thin films *Physica Status Solidi* (b) **251** 850–63

[45] Klinger M and Jäger Aš 2015 Crystallographic Tool Box(CrysTBox): automated tools for transmission electron microscopists and crystallographers *J. Appl. Crystallogr.* **48** 2012–18

[46] Playford H Y, Hannon A C, Tucker M G, Dawson D M, Ashbrook S E, Kastiban R J, Sloan J and Walton R I 2014 Characterization of Structural Disorder in γ-Ga_2O_3 *J. Phys. Chem.* C **118** 16188–98

[47] Schewski R *et al* 2014 Epitaxial stabilization of pseudomorphic α-Ga_2O_3 on sapphire (0001) *Appl. Phys. Express* **8** 011101

[48] Lorenz M 2007 *Transparent Conductive Zinc Oxide: Basics and Applications in Thin Film Solar Cells (Springer Series in Materials Science Book 104)* (Berlin: Springer) pp 303–57

Supplemental

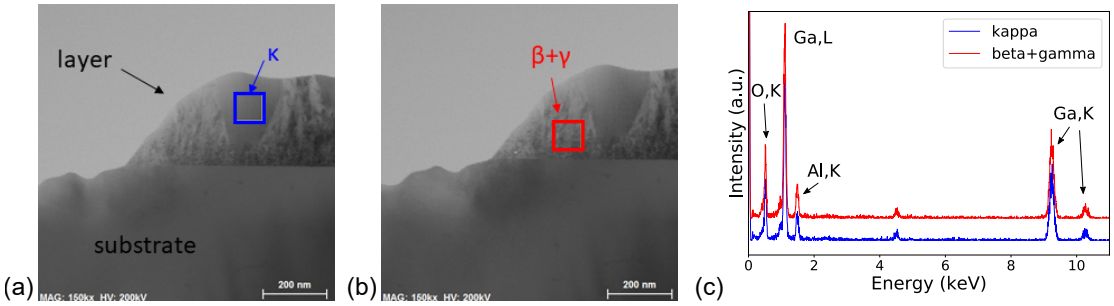

Figure 1: (a & b) STEM images of sample B (coexistence of the κ- and $\beta + \gamma$-phases). (c) STEM-EDXS measurement of the regions marked in (a) and (b). The calculated peak ratios Ga,L to Al,K for the κ- and $\beta + \gamma$ amounts 5.80 and 5.66 respectively, which is not a significant difference and proves the Al/Ga composition is preserved throughout the phase change.

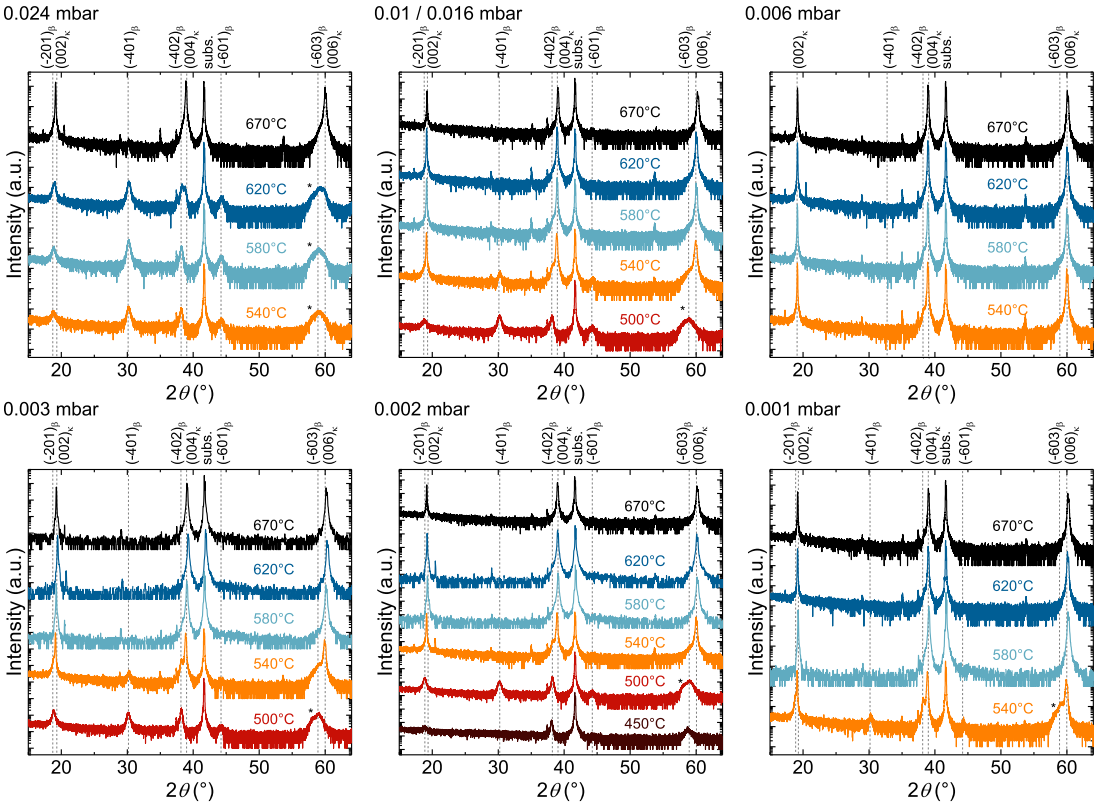

Figure 2: XRD 2θ-ω scans of $(Al_xGa_{1-x})_2O_3$ thin films deposited at oxygen pressures between 0.024 and 0.001 mbar and growth temperatures ranging between 450 and 670°. The respective parameters are provided in the graph. The growth directions of the orthorhombic κ- or monoclinic β-samples are indicated in the graphs. The shoulders highlighted by the asterix can be assigned either to $(\text{-}313)_\beta$ or $(333)_\gamma$ lattice planes. The substrates (00.6) Al_2O_3 reflection peak can be observed at 41.68°. At 20.4° and 29.0° Umweganregung (X-ray double diffraction) of the substrate are visible. Additional reflections are due to the K_β (35.2°, 53.9°) or the tungsten L_α (37.4°) spectral lines.

4.2 Physical Properties of κ-(Al,Ga)$_2$O$_3$, κ-(In,Ga)$_2$O$_3$ and α-(Al,Ga)$_2$O$_3$ thin films

The content of this section has been published in the following two manuscripts:

Reproduced from
A. Hassa, C. Sturm, M. Kneiß, D. Splith, H. von Wenckstern, T. Schultz, N. Koch, M. Lorenz, and M. Grundmann:
Solubility limit and material properties of a κ-$(Al_xGa_{1-x})_2O_3$ thin film with a lateral cation gradient on (00.1)Al_2O_3 by tin-assisted PLD, APL Materials, volume 8, no. 2, page 021103 (2020), with the permission of AIP Publishing.
doi:10.1063/1.5141041

Reproduced from
A. Hassa, H. von Wenckstern, D. Splith, C. Sturm, M. Kneiß, V. Prozheeva and M. Grundmann:
Structural, optical, and electrical properties of orthorhombic κ-$(In_xGa_{1-x})_2O_3$ thin films, APL Materials, volume 7, no. 2, page 022525 (2019), with the permission of AIP Publishing.
doi:10.1063/1.5054394

Reprinted from
A. Hassa, P. Storm, M. Kneiß, Dr. D. Splith, Dr. H. von Wenckstern, Prof. M. Lorenz, Prof. M. Grundmann:
Structural and elastic properties of α-$(Al_xGa_{1-x})_2O_3$ thin films on (11.0)Al_2O_3 substrates for the entire composition range, physica status solidi (b), pages 2000394 (2020).
Available under Public Licence (CC BY-NC 4.0) at:
doi:10.1002/pssb.202000394

APL Materials ARTICLE scitation.org/journal/apm

Solubility limit and material properties of a κ-$(Al_xGa_{1-x})_2O_3$ thin film with a lateral cation gradient on $(00.1)Al_2O_3$ by tin-assisted PLD

Cite as: APL Mater. 8, 021103 (2020); doi: 10.1063/1.5141041
Submitted: 3 December 2019 • Accepted: 14 January 2020 •
Published Online: 3 February 2020

A. Hassa,[1,a)] C. Sturm,[1] M. Kneiß,[1] D. Splith,[1] H. von Wenckstern,[1] T. Schultz,[2,3] N. Koch,[2,3] M. Lorenz,[1] and M. Grundmann[1]

AFFILIATIONS

[1]Universität Leipzig, Felix-Bloch-Institut für Festkörperphysik, Linnéstraße 5, 04103 Leipzig, Germany
[2]Humboldt-Universität zu Berlin, Institut für Physik, Newtonstraße 15, 12489 Berlin, Germany
[3]Helmholtz-Zentrum für Energie und Materialien GmbH, Hahn-Meitner-Platz 1, 14109 Berlin, Germany

[a)]**Author to whom correspondence should be addressed:** anna.hassa@physik.uni-leipzig.de

ABSTRACT

A ternary, orthorhombic κ-$(Al_xGa_{1-x})_2O_3$ thin film was synthesized by combinatorial pulsed laser deposition on a 2 in. in diameter c-sapphire substrate with a composition gradient. Structural, morphological, and optical properties were studied as a function of the alloy composition. The thin film crystallized in the orthorhombic polymorph for Al contents of $0.07 \leq x \leq 0.46$, enabling bandgap engineering from 5.03 eV to 5.85 eV. The direct optical bandgap and the c-lattice constant, as well, show a linear dependence on the cation composition. XRD measurements, especially 2θ-ω- and ϕ-scans, revealed the growth of κ-$(Al_xGa_{1-x})_2O_3$ in [001]-direction and in three rotational domains. The surface morphology was investigated by atomic force microscopy and reveals root mean square surface roughnesses below 1 nm. Furthermore, the dielectric function (DF) and the refractive index, determined by spectroscopic ellipsometry, were investigated in dependence on the Al content. Certain features of the DF show a blue shift with increasing Al concentration.

I. INTRODUCTION

Monoclinic β-Ga_2O_3 can potentially be used in high-power electronics,[1–4] as solar-blind photo detectors,[5] gas sensors,[6] or thin film transistors,[7] because of its beneficial material properties such as a large Baliga's figure of merit, a large breakdown field[8] of 8 MV cm^{-1}, and a high bandgap energy of 4.6–5 eV.[3]

Another interesting polymorph of the wide bandgap material is its orthorhombic modification, denoted as κ-Ga_2O_3 and being isostructural to κ-Al_2O_3, making the growth of κ-$(Al,Ga)_2O_3$ for any cation composition seem possible. Ternary alloying enables the fabrication of thin films with tailored bandgaps[2–4] in a wide range, which leads to an extended application field. Up to now, just a few publications deal with the solubility limit of Al in κ-Ga_2O_3 or Ga in κ-Al_2O_3 as well as the dependence of chemical, structural, and optical properties on the cation composition. First investigations of orthorhombic $(Al_xGa_{1-x})_2O_3$ thin films grown on an AlN buffer layer on $(00.1)Al_2O_3$ for defined x were published by Tahara *et al.*[9] They report single phase thin films up to $x = 0.395$ with a direct optical bandgap of 5.9 eV. Storm *et al.* presented pulsed laser deposition (PLD) grown thin films on $(00.1)Al_2O_3$ with a maximum Al content of $x = 0.38$, which was increased by growth on a κ-Ga_2O_3 template up to $x = 0.65$.[10]

Binary κ-Ga_2O_3 can be fabricated by halide vapor phase epitaxy[11] (HVPE), atomic layer deposition[12] (ALD), metal-organic chemical vapor deposition[13–18] (MOCVD), plasma-assisted,[19] and tin-assisted[20] molecular beam epitaxy (MBE), as well as tin-assisted pulsed-laser deposition[21,22] (PLD). Alloys with In or Al were realized by mist CVD[9,23] and PLD[10,24,25] on c-plane sapphire substrates. The predicted large spontaneous polarization P of 23 $\mu C/cm^2$ along its c-axis[26] turns the orthorhombic structure, e.g., as κ-$(Al_xGa_{1-x})_2O_3$/κ-Ga_2O_3 heterostructure, to a promising alternative for the fabrication of high power devices. At the interface of heterostructures, P will change abruptly, resulting in an accumulation of free charge carriers.

In the present study, a κ-$(Al_xGa_{1-x})_2O_3$ thin film with a lateral variation of the alloy composition was grown by PLD using the continuous composition spread approach (CCS-PLD) described by von Wenckstern *et al.*[27] Tin was offered during growth to induce the orthorhombic phase as shown for binary κ-Ga_2O_3 by Kracht *et al.*[20] (MBE) and Kneiß *et al.*[22] (PLD). The highest achieved Al content in the present work amounts to $x = 0.46$. The chemical, structural, and optical material properties, namely crystal structure, surface morphology, optical bandgap energy, dielectric function, and refractive index will be discussed in dependence on the cation composition.

II. EXPERIMENTAL DETAILS

The ternary $(Al_xGa_{1-x})_2O_3$ thin film was grown by CCS-PLD using a two-fold segmented ceramic target. One segment consists of Ga_2O_3 (purity 99.999%, Alfa Aeser), and the other of Al_2O_3 (purity 99.997%, Alfa Aeser). Both have been admixed with 1.5 at. % SnO_2 to facilitate the growth in the orthorhombic structure. The oxygen partial pressure in the PLD chamber was 0.006 mbar and the growth temperature 640 °C. The KrF excimer laser radiation (248 nm) had an energy density of 2.6 J cm^{-2} on the target, which is located 10 cm away from the 2 in. in diameter (00.1)Al_2O_3 substrate. The pulse repetition frequency was 1 Hz for the first 300 pulses to create a nucleation layer and 10 Hz for the subsequent main layer, for which 30.000 pulses were applied. The chemical cation composition of the whole wafer was determined by energy-dispersive X-ray spectroscopy (EDX) performed with a FEI Nova Nanolab 200 equipped with an Ametek EDAX detector on 49 positions on the 2 in. wafer. Along the gradient, the cation concentration was additionally measured with higher spatial resolution by EDX as well as X-ray photoelectron spectroscopy (XPS). The XPS measurements were done at the Humboldt-Universität zu Berlin utilizing a JEOL JPS-9030 setup using non-monochromated Al K_α radiation for the excitation. The binding energy scale was referenced to C1s at 248.8 eV. The survey in Fig. 2 was recorded at the ENERGIZE endstation at Bessy II, using the Mg anode of a DAR400 X-ray source from ScientaOmicron for the excitation and a DA30 analyzer from ScientaOmicron for detection of the emitted photoelectrons. Here, the O1s peak was set to 531 eV, as the C1s peak was overlapped by Ga Auger peaks. Crystal structure screening was done with X-ray diffraction (XRD) measurements utilizing a PANalytical X'pert PRO MRD diffractometer equipped with a PIXcel^{3D} detector operating in 1D scanning line mode with 255 channels. The c-lattice constant for each detected XRD spectra was determined by fitting the (002), (004), (006), (008), and (0010) reflection peak positions with a pseudo-Voigt function, and subsequently, the lattice plane distances were extrapolated to a diffraction angle of $\theta = 90°$ using the formula $c = f(0.5[\tan(\theta)^{-1} + \cos(\theta)\tan(\theta)^{-1}])$ to minimize the goniometer error.[28] The direct optical bandgaps (E_g) were deduced from transmission measurements utilizing a PerkinElmer Lambda 19 spectrometer equipped with a deuterium lamp for the UV-region and a tungsten-halogen lamp for the visible and near-infrared region. From the transmission spectra (T), the absorption coefficient α was calculated via $\alpha = (-\ln(T)/d)^2$ with d being the film thickness. By extrapolation, the linear part of $(\alpha h\nu)^2$ to zero, E_g was estimated. Spectroscopic ellipsometry was employed to determine also E_g, d, the dielectric functions and refractive indexes utilizing a J.A. Woollam M2000 dual rotating compensator ellipsometer RC2 with a spot size of about $300 \times 500\ \mu m^2$.

III. RESULTS AND DISCUSSION

A. Structural properties

With the implemented CCS technique for thin film preparation, the cation concentration varies across the wafer. The resulting composition and the exact direction of the cation gradient was identified by EDX measurements on positions marked in Fig. 1(a) as black dots to determine the Al incorporation x, locally. In the figure, the compositions between the measurement points were interpolated, indicating the direction of the cation gradient. Additionally, along the gradient EDX and XPS mesurements were employed every mm (EDX) or every second mm (XPS). The Al content ranges from $x = 0.07$ to $x = 0.79$. These in principle identical results are presented in Fig. 1(b). In accordance with the surfactant-mediated growth model described by Kneiß *et al.*,[22] tin is not detected in the bulk (measured by EDX), but with the surface sensitive technique (XPS), tin-related peaks can be observed and are attributed to the Sn surfactant layer. The survey spectrum in Fig. 2 shows these tin peaks as well as peaks assigned to gallium, oxygen, and aluminum, as expected for $(Al_xGa_{1-x})_2O_3$.

The crystal structure was investigated in dependence on the Al content by 55 single XRD 2θ-ω scans recorded along the direction of the composition gradient. All measurements are presented as a false color map in Fig. 3(a). Three single XRD patterns for selected x values are depicted in Fig. 3(b). Over the whole composition range, reflection peaks of the c-sapphire substrate are visible at $2\theta = 41.58°$ and 90.64°. For $x > 0.46$, no additional reflections can be observed, which indicates the amorphous growth of $(Al_xGa_{1-x})_2O_3$ in this composition range. For $x \leq 0.46$, reflection peaks assigned to the (002) n-lattice planes of the orthorhombic crystal structure are visible.

The 2θ angles of these reflections shift with increasing Al content to higher values, due to the smaller ionic radius of Al compared to that of Ga. In accordance to this, the c-lattice constant, presented in Fig. 4(a), decreases with increasing x and shows two slightly different linear dependencies described by

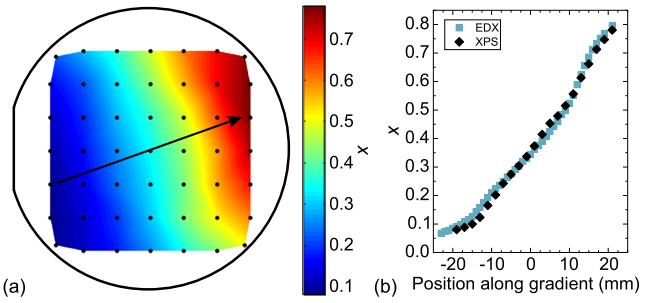

FIG. 1. (a) Al content x at 49 points across the thin film surface, marked in the graph as black dots and determined by EDX. The data between the measurement points was interpolated, the black arrow represents the direction of the gradient. (b) Cation ratio x acquired along the in (a) indicated gradient by EDX and XPS, respectively.

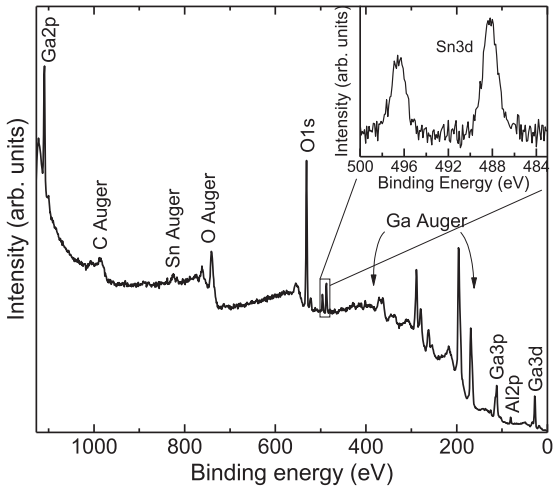

FIG. 2. XPS survey spectrum for $(Al_xGa_{1-x})_2O_3$.

$$c(x)(\text{Å}) = \begin{cases} (9.271 \pm 0.001) - (0.333 \pm 0.008) \cdot x, & \text{for } 0.07 \le x \le 0.13 \\ (9.276 \pm 0.001) - (0.357 \pm 0.002) \cdot x, & \text{for } 0.14 \le x \le 0.46. \end{cases} \quad (1)$$

For higher Al-contents ($x > 0.46$) the c-lattice constant saturates, indicating the solubility limit of κ-$(Al_xGa_{1-x})_2O_3$. Further, to investigate the crystalline quality of the thin film, the full width half maximum (FWHM) of the (004)-lattice plane reflection peaks is plotted in Fig. 4(a) in dependence on x exhibiting an increase from 0.07° for x = 0.07 to 0.15° for x = 0.46, indicating a high crystalline quality over the whole composition range. Comparisons with binary κ-Ga_2O_3 thin films grown by PLD on c-sapphire reveal similarly FWHM's of the (004) reflections below 0.06° for various growth temperatures and pressures.[22] XRD ϕ-scans of the skew-symmetric (131) and asymmetric (206) reflections, exemplarily shown in Fig. 4(b) for an Al concentration of x = 0.13, indicate the epitaxial growth on c-plane sapphire as well as the appearance of three rotational domains of the orthorhombic unit cell separated by 120°,[29] which were also present for κ-Ga_2O_3[22]

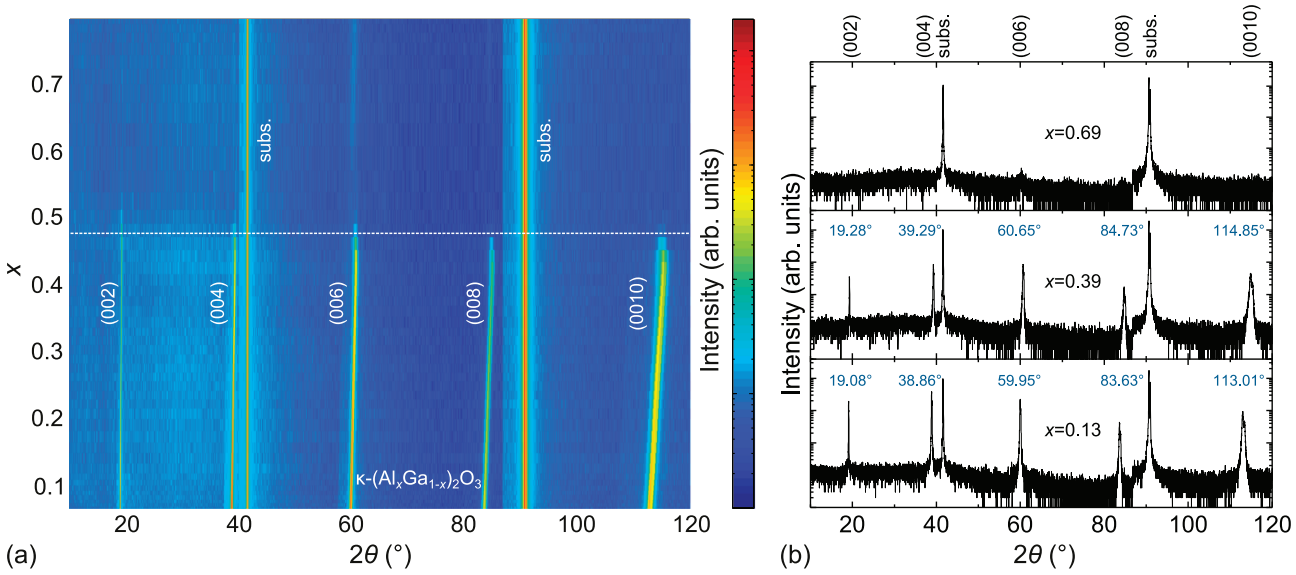

FIG. 3. (a) False color map of 2θ-ω scans of orthorhombic κ-$(Al_xGa_{1-x})_2O_3$ recorded along the composition gradient indicated in Fig. 1(a). (b) XRD patterns for x = 0.13, x = 0.39, and x = 0.69. Peak positions of the (002) n lattice planes as well as the substrate (subs.) reflection are labeled.

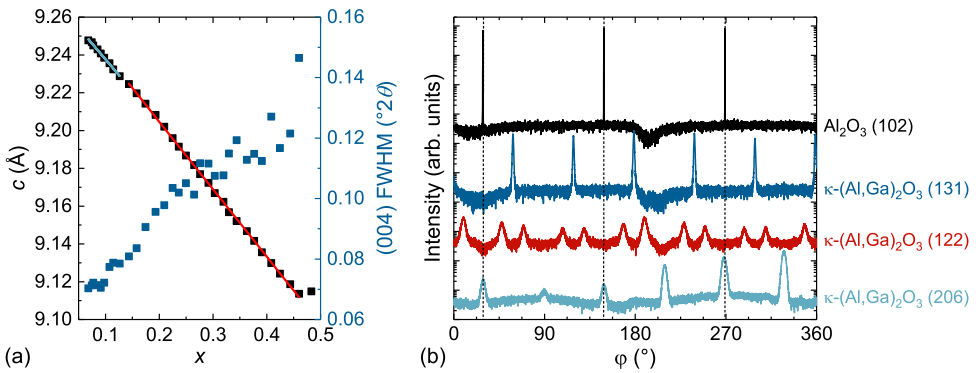

FIG. 4. (a) c lattice constant, estimated from the (002) n (n = 1–5) reflection peaks, as well as FWHM of the (004)-lattice plane reflection peak from XRD patterns determined in dependence on x. (b) XRD ϕ-scans of the (131), (122) and (206) reflections as well as the substrate (102) reflection performed for x = 0.13.

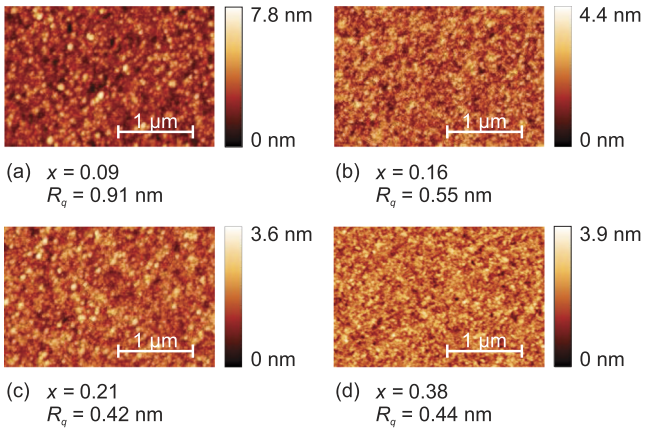

FIG. 5. 2 × 3 μm^2 AFM scans of surface morphologies of κ-$(Al_xGa_{1-x})_2O_3$ for different Al contents x as labeled recorded by AFM. R_q denotes the root mean square surface roughness.

and κ-$(In_xGa_{1-x})_2O_3$[24] thin films grown by PLD. The in-plane epitaxial relationships can be described by κ-$(Al_xGa_{1-x})_2O_3$ ⟨010⟩ ‖ α-Al_2O_3 ⟨10$\bar{1}$0⟩ and κ-$(Al_xGa_{1-x})_2O_3$ ⟨100⟩ ‖ α-Al_2O_3 ⟨2$\bar{1}\bar{1}$0⟩. Furthermore, the twelve-fold (122) reflection, originating from an additional two-fold splitting on mirror planes, proofs the orthorhombic structure of the thin film.

B. Surface morphology

The surface morphology was recorded along the cation gradient by atomic force microscopy. Exemplary images for four different Al-contents (x = 0.09, 0.16, 0.21, and 0.38) are shown in Fig. 5 and exhibit smooth surfaces consisting of spherically shaped grains with diameters of approximately 100 nm. Based on the recorded images, root mean square surface roughnesses (R_q) and corresponding peak-valley-distances (d_{PV}, described by the scale next to the recorded images) were determined. For $x \leq 0.21$, R_q and d_{PV} decrease with increasing x and stay roughly constant for $x > 0.21$.

C. Optical properties

The determination of the direct optical bandgap E_g in dependence on x was performed by two different measurement methods. Along the composition gradient, transmission spectroscopy and spectroscopic ellipsometry measurements were conducted. The first one was performed in 5 mm steps starting after 4 mm (equals 6 positions) and the second one in 1 mm steps (equals 32 positions) only on the κ-phase part of the thin film. Figure 6(a) presents transmission spectra as well as the calculated absorption spectra for different Al contents. The bandgap energies $E_{g,T}$ were obtained by extrapolating the linear part of the absorption spectra expressed as $(\alpha h\nu)^2$ to the zero line. The resulted direct optical bandgaps show a shift to higher energies with increasing x, which is also visible in Fig. 6(b). Linear fitting of $E_{g,T}$ yields

$$E_{g,T}(x)(\mathrm{eV}) = (4.92 \pm 0.06) + (2.17 \pm 0.08) \cdot x. \quad (2)$$

For comparison, the bandgap variation was determined via spectroscopic ellipsometry and is displayed in Fig. 6(b), too. The deduced change of the bandgap energy is almost linear and resulted in the fitting equation,

$$E_{g,E}(x)(\mathrm{eV}) = (4.85 \pm 0.01) + (2.14 \pm 0.03) \cdot x. \quad (3)$$

The resulting maximum bandgap energy is 5.85 eV for x = 0.46. In a previous publication of Schmidt-Grund *et al.*,[30] optical properties of an $(Al_xGa_{1-x})_2O_3$ thin film with the CCS-PLD technique on a 2 in. (001)-oriented MgO substrate was discussed. For $x < 0.4$, they observed the monoclinic β-modification and estimated the direct optical bandgap for this phase from spectroscopic ellipsometry to $E_{g-dir}(x)(\mathrm{eV}) = 4.811 + 2.138 \cdot x$. This is in accordance to the presented $E_{g,E}$ in our study, indicating a similar bandgap dependence of monoclinic and orthorhombic $(Al_xGa_{1-x})_2O_3$. The film thicknesses deduced from the spectroscopic ellipsometry data were divided by the applied pulse number to obtain the composition dependent growth rate $r(x)$ that is displayed in Fig. 6(b), too. It exhibits a maximum of 15.7 pm/pulse for x = 0.07 and decreases to 12.0 pm/pulse for x = 0.46.

Further, the dielectric function (DF) was obtained by using a layer stack model consisting of a c-plane sapphire substrate layer, where the DF was taken from literature,[31] a layer describing the thin film and a surface layer. Due to the presence of rotational domains, the film is effectively optical uniaxial, i.e., the tensor of the film DF is given by $\varepsilon_\perp = \varepsilon_{xx} = \varepsilon_{yy} \neq \varepsilon_\parallel = \varepsilon_{zz}$ and $\varepsilon_{ij} = 0$ for $i \neq j$. The line shape of each tensor component was described by model dielectric functions. Due to the absence of sharp features in the experimental spectra, it was sufficient to describe the onset of the absorption in

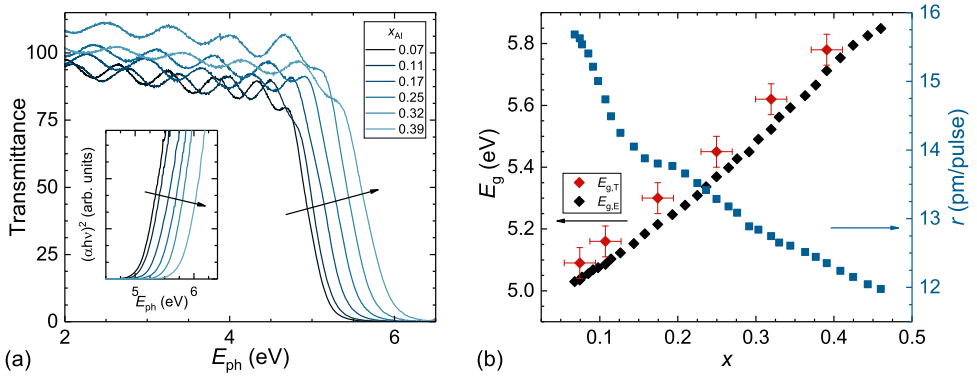

FIG. 6. (a) Transmission spectra for increasing Al contents as labeled. The inset shows corresponding absorption spectra expressed as $(\alpha h\nu)^2$. (b) Direct optical bandgap and growth rate r as a function of x. The values are determined by transmission spectroscopy [$E_{g,T}$, shown in (a)] by and spectroscopic ellipsometry ($E_{g,E}$), respectively.

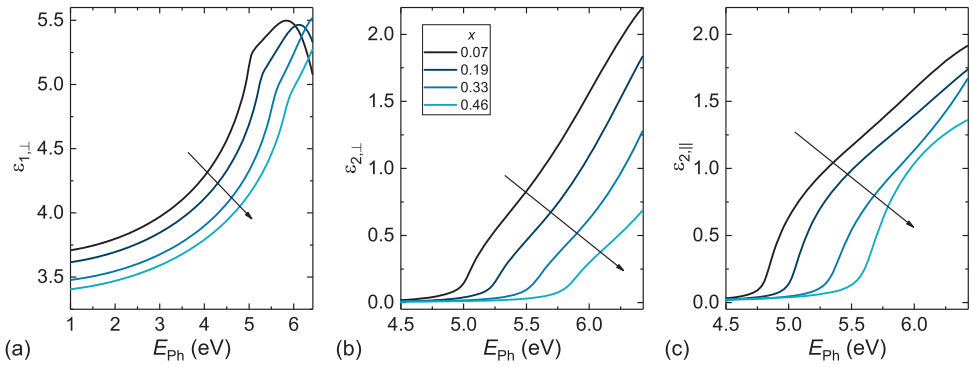

FIG. 7. Real (a) and imaginary part [(b) and (c)] of the dielectric function for different Al concentration as labeled.

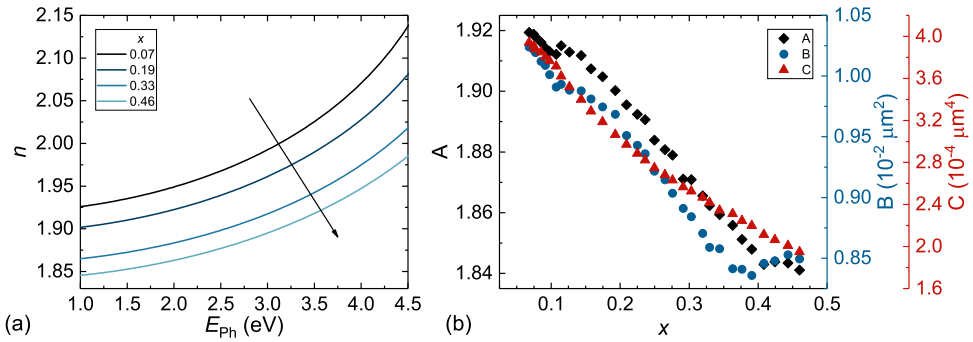

FIG. 8. (a) Refractive index n depending on the photon energy for various x as labeled. (b) Cauchy parameters A, B, and C in dependence of x.

the observed spectral range by band-to-band transitions ($\chi^{\mathrm{CPM_0}}$) as proposed by Adachi.[32] The contributions of the energetic transitions to the imaginary part of the DF is described by Gaussian oscillators (χ^{gauss}), whereas the contributions of these transitions to the real part of the DF was described by means of a pole function (χ^{pole}) due to the Kramers-Kronig transformation. Thus, the entire DF for each component is given by

$$\varepsilon_i = 1 + \sum_{j=1}^{2} \chi_{j,i}^{\mathrm{CPM_0}} + \chi_{j,i}^{\mathrm{gauss}} + \chi_i^{\mathrm{pole}}, \tag{4}$$

with $i = \perp, \parallel$. Finally, the dielectric function of the surface layer was described by an effective medium approach,[33] where the dielectric function of the underlaying $(Al,Ga)_2O_3$ film and void was mixed 1:1.

The DF for various x is presented in Fig. 7 and shows that incorporation of Al leads to a blue shift of the transition energies and thus to a blue shift of the entire dielectric function. This is accompanied by a decrease of the real part of the DF in the visible spectral range and thus of the refractive index displayed in Fig. 8(a). A comparison of the tensor components yields that the absorption sets in at lower energies for light polarized parallel to the surface normal than for light polarized perpendicular to the surface normal. Additionally, the Cauchy function $n = A + B/\lambda^2 + C/\lambda^4$ describes the dispersion of the refractive index up to 4.5 eV. Figure 8(b) presents the Cauchy parameters A, B, and C as a function of x.

IV. CONCLUSION

In this study, an orthorhombic $(Al_xGa_{1-x})_2O_3$ thin film with a lateral varying cation composition gradient ($0.07 \leq x \leq 0.46$) was examined for a variety of structural and optical material properties in dependence on x. For the highest Al incorporation of $x = 0.46$ in the crystalline phase, the optical bandgap at RT is 5.85 eV, which is up to now the highest reported Al content and E_g for κ-$(Al_xGa_{1-x})_2O_3$ thin films grown on c-plane sapphire. Chemical investigations confirmed a tin enrichment on the layer surface, not in the bulk, indicating a surfactant-mediated growth of the thin film. Heteroepitaxial growth in three rotational domains was presented and compared to heteroepitaxial grown monoclinic thin films, the sample shown here has higher crystalline quality, higher growth rates, and lower surface roughnesses. The c-lattice constant exhibits a linear increase with increasing x following Vegard's law. Furthermore, dielectric functions and refractive indexes were investigated in a wide composition range. Based on our findings, κ-$(Al_xGa_{1-x})_2O_3$ seems to be well suited for possible usage, e.g., in high electron mobility transistors, as wave-length selective UV - or quantum-well infrared photodetectors and more. Future investigations should target the suppression of rotational domains as well as doping to achieve electrically conductive samples.

ACKNOWLEDGMENTS

We thank Monika Hahn for PLD target fabrication, Jörg Lenzner for EDX measurements, and Ulrike Teschner for transmission measurements. This work was supported by the European Social Fund within the Young Investigator Group "Oxide Heterostructures" (Grant No. SAB 100310460) and partly by Deutsche Forschungsgemeinschaft in the Framework of Sonderforschungsbereich 762 "Functionality of Oxide Interfaces". A.H. and M.K. acknowledge the Leipzig School for Natural Sciences BuildMoNa.

We acknowledge support from the German Research Foundation (DFG) and Universität Leipzig within the program of Open Access Publishing. The work in Berlin was funded by the Deutsche Forschungsgemeinschaft (DFG) - Projekt No. 182087777-SFB 951.

REFERENCES

[1] M. Higashiwaki, A. Kuramata, H. Murakami, and Y. Kumagai, "State-of-the-art technologies of gallium oxide power devices," J. Phys. D: Appl. Phys. **50**, 333002 (2017).
[2] S. Stepanov, V. Nikolaev, V. Bougrov, and A. Romanov, "Gallium oxide: Properties and applications—A review," Rev. Adv. Mater. Sci. **44**, 63–86 (2016).
[3] H. von Wenckstern, "Group-III sesquioxides: Growth, physical properties and devices," Adv. Electron. Mater. **3**, 1600350 (2017).
[4] S. J. Pearton, J. Yang, P. H. Cary, F. Ren, J. Kim, M. J. Tadjer, and M. A. Mastro, "A review of Ga_2O_3 materials, processing, and devices," Appl. Phys. Rev. **5**, 011301 (2018).
[5] Z. Zhang, H. von Wenckstern, and M. Grundmann, "Monolithic multichannel ultraviolet photodiodes based on (Mg,Zn)O thin films with continuous composition spreads," IEEE J. Sel. Top. Quantum Electron. **20**, 106–111 (2014).
[6] O. Bierwagen, "Indium oxide—A transparent, wide-band gap semiconductor for (opto)electronic applications," Semicond. Sci. Technol. **30**, 024001 (2015).
[7] M. Grundmann, H. Frenzel, A. Lajn, M. Lorenz, F. Schein, and H. von Wenckstern, "Transparent semiconducting oxides: Materials and devices," Phys. Status Solidi A **207**, 1437–1449 (2010).
[8] M. Higashiwaki, K. Sasaki, A. Kuramata, T. Masui, and S. Yamakoshi, "Gallium oxide (Ga_2O_3) metal-semiconductor field-effect transistors on single-crystal β-Ga_2O_3 (010) substrates," Appl. Phys. Lett. **100**, 013504 (2012).
[9] D. Tahara, H. Nishinaka, S. Morimoto, and M. Yoshimoto, "Heteroepitaxial growth of ε-$(Al_xGa_{1-x})_2O_3$ alloy films on c-plane AlN templates by mist chemical vapor deposition," Appl. Phys. Lett. **112**, 152102 (2018).
[10] P. Storm, M. Kneiß, A. Hassa, T. Schultz, D. Splith, H. von Wenckstern, N. Koch, M. Lorenz, and M. Grundmann, "Epitaxial κ-$(Al_xGa_{1-x})_2O_3$ thin films and heterostructures grown by tin-assisted VCCS-PLD," APL Mater. **7**, 111110 (2019).
[11] Y. Oshima, E. G. Víllora, Y. Matsushita, S. Yamamoto, and K. Shimamura, "Epitaxial growth of phase-pure ε-Ga_2O_3 by halide vapor phase epitaxy," J. Appl. Phys. **118**, 085301 (2015).
[12] F. Boschi, M. Bosi, T. Berzina, E. Buffagni, C. Ferrari, and R. Fornari, "Hetero-epitaxy of ε-Ga_2O_3 layers by MOCVD and ALD," J. Cryst. Growth **443**, 25–30 (2016).
[13] I. Cora, F. Mezzadri, F. Boschi, M. Bosi, M. Čaplovičová, G. Calestani, I. Dódony, B. Pécz, and R. Fornari, "The real structure of ε-Ga_2O_3 and its relation to κ-phase," CrystEngComm **19**, 1509–1516 (2017).
[14] X. Xia, Y. Chen, Q. Feng, H. Liang, P. Tao, M. Xu, and G. Du, "Hexagonal phase-pure wide band gap ε-Ga_2O_3 films grown on 6H-SiC substrates by metal organic chemical vapor deposition," Appl. Phys. Lett. **108**, 202103 (2016).
[15] F. Mezzadri, G. Calestani, F. Boschi, D. Delmonte, M. Bosi, and R. Fornari, "Crystal structure and ferroelectric properties of ε-Ga_2O_3 films grown on (0001)-sapphire," Inorg. Chem. **55**, 12079–12084 (2016).
[16] Y. Chen, X. Xia, H. Liang, Q. Abbas, Y. Liu, and G. Du, "Growth pressure controlled nucleation epitaxy of pure phase ε- and β-Ga_2O_3 films on Al_2O_3 via MOCVD," Cryst. Growth Des. **18**, 1147–1154 (2018).
[17] M. Pavesi, F. Fabbri, F. Boschi, G. Piacentini, A. Baraldi, M. Bosi, E. Gombia, A. Parisini, and R. Fornari, "ε-Ga_2O_3 epilayers as a material for solar-blind UV photodetectors," Mater. Chem. Phys. **205**, 502–507 (2018).
[18] M. Mulazzi, F. Reichmann, A. Becker, W. M. Klesse, P. Alippi, V. Fiorentini, A. Parisini, M. Bosi, and R. Fornari, "The electronic structure of ε-Ga_2O_3," APL Mater. **7**, 022522 (2019).
[19] P. Vogt, O. Brandt, H. Riechert, J. Lähnemann, and O. Bierwagen, "Metal-exchange catalysis in the growth of sesquioxides: Towards heterostructures of transparent oxide semiconductors," Phys. Rev. Lett. **119**, 196001 (2017).
[20] M. Kracht, A. Karg, J. Schörmann, M. Weinhold, D. Zink, F. Michel, M. Rohnke, M. Schowalter, B. Gerken, A. Rosenauer, P. J. Klar, J. Janek, and M. Eickhoff, "Tin-assisted synthesis of ε–Ga_2O_3 by molecular beam epitaxy," Phys. Rev. Appl. **8**, 054002 (2017).
[21] M. Orita, H. Hiramatsu, H. Ohta, M. Hirano, and H. Hosono, "Preparation of highly conductive, deep ultraviolet transparent β-Ga_2O_3 thin film at low deposition temperatures," Thin Solid Films **411**, 134–139 (2002).
[22] M. Kneiß, A. Hassa, D. Splith, C. Sturm, H. von Wenckstern, T. Schultz, N. Koch, M. Lorenz, and M. Grundmann, "Tin-assisted heteroepitaxial PLD-growth of κ-Ga_2O_3 thin films with high crystalline quality," APL Mater. **7**, 022516 (2019).
[23] H. Nishinaka, N. Miyauchi, D. Tahara, S. Morimoto, and M. Yoshimoto, "Incorporation of indium into ε-gallium oxide epitaxial thin films grown via mist chemical vapour deposition for bandgap engineering," CrystEngComm **20**, 1882–1888 (2018).
[24] A. Hassa, H. von Wenckstern, D. Splith, C. Sturm, M. Kneiß, V. Prozheeva, and M. Grundmann, "Structural, optical, and electrical properties of orthorhombic κ-$(In_xGa_{1-x})_2O_3$ thin films," APL Mater. **7**, 022525 (2019).
[25] M. Kneiß, A. Hassa, D. Splith, C. Sturm, H. von Wenckstern, M. Lorenz, and M. Grundmann, "Epitaxial stabilization of single phase κ-$(In_xGa_{1-x})_2O_3$ thin films up to $x = 0.28$ on c-sapphire and κ-Ga_2O_3 (001) templates by tin-assisted VCCS-PLD," APL Mater. **7**, 101102 (2019).
[26] M. B. Maccioni and V. Fiorentini, "Phase diagram and polarization of stable phases of $(Ga_{1-x}In_x)_2O_3$," Appl. Phys. Express **9**, 041102 (2016).
[27] H. von Wenckstern, Z. Zhang, F. Schmidt, J. Lenzner, H. Hochmuth, and M. Grundmann, "Continuous composition spread using pulsed-laser deposition with a single segmented target," CrystEngComm **15**, 10020 (2013).
[28] L. Spiess, G. Teichert, R. Schwarzer, H. Behnken, and C. Genzel, *Moderne Röntgenbeugung: Röntgendiffraktometrie für Materialwissenschaftler, Physiker und Chemiker*, German ed. (Vieweg+Teubner Verlag, 2009).
[29] M. Grundmann, "Formation of epitaxial domains: Unified theory and survey of experimental results," Phys. Status Solidi B **248**, 805–824 (2011).
[30] R. Schmidt-Grund, C. Kranert, H. von Wenckstern, V. Zviagin, M. Lorenz, and M. Grundmann, "Dielectric function in the spectral range (0.5–8.5)eV of an $(Al_xGa_{1-x})_2O_3$ thin film with continuous composition spread," J. Appl. Phys. **117**, 165307 (2015).
[31] H. Yao and C. H. Yan, "Anisotropic optical responses of sapphire (α-Al_2O_3) single crystals," J. Appl. Phys. **85**, 6717 (1999).
[32] S. Adachi, "Model dielectric constants of GaP, GaAs, GaSb, InP, InAs, and InSb," Phys. Rev. B **35**, 7454–7463 (1987).
[33] D. A. G. Bruggeman, Ann. Phys. **24**, 636 (1935).

APL Materials ARTICLE scitation.org/journal/apm

Structural, optical, and electrical properties of orthorhombic κ-$(In_xGa_{1-x})_2O_3$ thin films

Cite as: APL Mater. 7, 022525 (2019); doi: 10.1063/1.5054394
Submitted: 31 August 2018 • Accepted: 19 December 2018 •
Published Online: 6 February 2019

A. Hassa,[1] H. von Wenckstern,[1] D. Splith,[1] C. Sturm,[1] M. Kneiß,[1] V. Prozheeva,[2] and M. Grundmann[1]

AFFILIATIONS

[1]Felix Bloch Institute for Solid State Physics, Universität Leipzig, Linnéstraße 5, 04103 Leipzig, Germany
[2]Department of Applied Physics, Aalto University, P.O. Box 15100, FIN-00076 Aalto, Finland

ABSTRACT

Material properties of orthorhombic κ-phase $(In_xGa_{1-x})_2O_3$ thin films grown on a c-plane sapphire substrate by pulsed-laser deposition are reported for an indium content up to $x \sim 0.35$. This extended range of miscibility enables band gap engineering between 4.3 and 4.9 eV. The c-lattice constant as well as the bandgap depends linearly on the In content. For $x > 0.35$, a phase change to the hexagonal $InGaO_3$(II) and the cubic bixbyite structure occurred. The dielectric function and the refractive index were determined by spectroscopic ellipsometry as a function of the alloy composition. We propose zirconium to induce n-type conductivity and have achieved electrically conducting thin films with a room temperature conductivity of up to 0.1 S/cm for samples with a low In content of about $x = 0.01$. Temperature-dependent Hall-effect measurements yielded a thermal activation energy of the free electron density of 190 meV. Schottky barrier diodes with rectification ratios up to 10^6 were investigated by quasi-static capacitance voltage and temperature-dependent current voltage measurements.

Wide band gap semiconducting oxides such as ZnO and SnO_2 or the group-III sesquioxides In_2O_3 and Ga_2O_3 find potential application as photo detectors,[1] gas sensors,[2] thin film transistors[3] and in high-power electronics.[4–7] Research on Ga_2O_3 and its alloys has increased tremendously after the demonstration of a metal-semiconductor field-effect transistor using a Ga_2O_3 layer grown homoepitaxially by molecular beam epitaxy.[8] Ga_2O_3 single crystals are available for the thermodynamically most stable polymorph (beta-gallia structure) having a monoclinic lattice symmetry, and hence, the majority of Ga_2O_3-related publications deal with β-Ga_2O_3. Rhombohedral α-Ga_2O_3 is of interest and investigated as well since it has the same lattice structure as thermodynamically stable α-Al_2O_3 and metastable α-In_2O_3 and would allow band gap engineering in a wide composition range. Recent reviews summarize material properties and devices based on monoclinic and/or rhombohedral $(In,Ga,Al)_2O_3$.[5–7,9] Maccioni and Fiorentini predicted a large polarization of 23 $\mu C/cm^2$ for orthorhombic Ga_2O_3 which is similar to that of $BaTiO_3$ and about three times larger than that of AlN.[10] In 2018, Cho and Mishra[11] predicted an identical polarization for this modification and Kim *et al.*[12] calculated a value of 26.39 $\mu C/cm^2$. The crystal structure of orthorhombic Ga_2O_3 was described in detail by Cora *et al.*, and a much smaller polarization of 0.2 $\mu C/cm^2$ was deduced from the atomic coordinates[13] being in close agreement with the value of 0.18 $\mu C/cm^2$ obtained from dynamic hysteresis measurements.[14] The difference between the predicted and the experimentally determined values needs to be resolved to judge the true potential of orthorhombic Ga_2O_3 for high electron mobility transistors for which band gap engineering is required as well. Binary thin films were obtained by halide vapor phase epitaxy,[15] metal-organic chemical vapor deposition,[13,14,16–18] atomic layer deposition,[17] and tin-assisted growth by pulsed-laser deposition (PLD)[19] or molecular beam epitaxy.[20] In the latter samples, tin does not contribute free electrons at room temperature (RT).[19] So far, successful n-type doping was not reported. In nominally undoped samples, electrical conductivity was observed for $T > 400$ K with a thermal activation energy of 695 meV.[21] Furthermore, such samples were used to fabricate a photo conductive UV-detector. Ternary layers were obtained on a c-plane sapphire substrate [with an AlN

buffer layer for $(Al,Ga)_2O_3$] by mist chemical vapor deposition.[22,23] For $(In_xGa_{1-x})_2O_3$, phase separation was reported for $x > 0.2$ (cubic phase formed).[23] The optical bandgap decreased from 5 eV for $x = 0$ to 4.5 eV for $x = 0.2$. The indium incorporation leads to an increase in the c-lattice constant that can be described by $c(x) = (0.9274 + 0.1075 \cdot x)$ nm.

We have achieved n-conducting κ-phase $(In_{0.01}Ga_{0.99})_2O_3$:Zr thin films with a free electron concentration of $n = 2 \times 10^{16}$ cm^{-3} at RT. The conductivity of such samples was sufficient to achieve Schottky barrier diodes with rectification ratios up to 10^6. Further, we stabilized $(In_xGa_{1-x})_2O_3$ thin films in the κ-phase polymorph up to $x \sim 0.35$ and report structural, morphological, and optical properties as a function of the alloy composition.

$(In_xGa_{1-x})_2O_3$ thin films were grown by pulsed-laser deposition (PLD) at a temperature of 940 K and an oxygen partial pressure of 3×10^{-4} mbar. The c-sapphire substrates were either 2 inch in diameter or 10×10 mm^2 sized quadratic pieces. For investigations of material properties in dependence on the indium content, we used a thin film with laterally continuous composition spread (CCS) that was deposited from a ceramic target consisting of two semi-circular segments. One segment consists of Ga_2O_3 (purity 99.999%, Alfa Aeser) and the other of In_2O_3 (purity 99.994%, Alfa Aeser). Both segments have an admixture of 2.5 wt. % SnO_2 (purity 99.999%, Alfa Aeser), which equals approximately 1.6 at. % in Ga_2O_3 and 2.3 at. % in In_2O_3, to induce the growth of κ-phase thin films as described by Orita *et al.*[19] and by Kracht *et al.*[20] Details about our CCS-PLD approach can be found in Ref. 24. To enhance the n-type conductivity of κ-$(In_{0.01}Ga_{0.99})_2O_3$, zirconium was used as a doping element, resulting in a concentration of approximately 1.3 at. % in the thin film.

The PLD setup consists of a KrF excimer laser (248 nm) focused to an energy density of 2 J cm^{-2} at the target. The distance between the target and the substrate was 10 cm. The composition of the thin films was determined by energy-dispersive X-ray spectroscopy (EDX) using a FEI Nova Nanolab 200 equipped with an Ametek EDAX detector. X-ray diffraction (XRD) measurements were performed with a PANalytical X'pert PRO MRD diffractometer equipped with a PIXcel^{3D} detector operating in a 1D scanning line mode with 255 channels. The surface morphology was determined with a Park Systems XE-150 atomic force microscope in a non-contact mode. The optical properties were investigated by spectroscopic ellipsometry using a J. A. Woollam dual rotating compensator ellipsometer RC2. Electrical properties were investigated by using current-voltage measurements of ohmic and Schottky barrier contacts, which were realized using recipes optimized for monoclinic Ga_2O_3. The ohmic contacts consist of a thermally evaporated layer stack of Ti/Al/Au and were annealed subsequently at 773 K for 10 min in nitrogen ambient.[25] For the Schottky barrier contacts, Pt was reactively sputtered[26] in a peripheral position (off-axis configuration),[27] and finally, a Pt layer was sputtered in an inert Ar ambient to assure current spreading.[26,27]

Temperature-dependent resistivity and Hall-effect measurements were performed for $T \leq 350$ K inside a Quantum Design physical property measurement system (PPMS) at a magnetic field of 1 T using a Keithley current source, switch system, and multimeter. Temperature-dependent resistivity and Hall-effect measurements for $T \geq 350$ K were performed inside a home-built high temperature thermostat at a magnetic field of 0.43 T using a Keithley current source, switch system, and multimeter and a Lakeshore 331 temperature controller.

Current-voltage (IV) measurements and quasi-static capacitance-voltage (CV) measurements on Schottky-contacts (SCs) were performed in a Süss Waferprober System P200 connected to an Agilent 4155C Semiconductor Parameter Analyzer. For temperature-dependent measurement between 100 and 320 K, a piece of one of the samples was mounted on a TO18 socket and a diode was contacted using gold wire and silver epoxy resin. The measurement was performed inside a cryostat using again the Agilent 4155C Semiconductor Parameter Analyzer. For the temperature-dependent measurement between 300 and 700 K, the same piece was removed from the socket and put inside a Linkam HFS600E-PB4 Probe Stage.

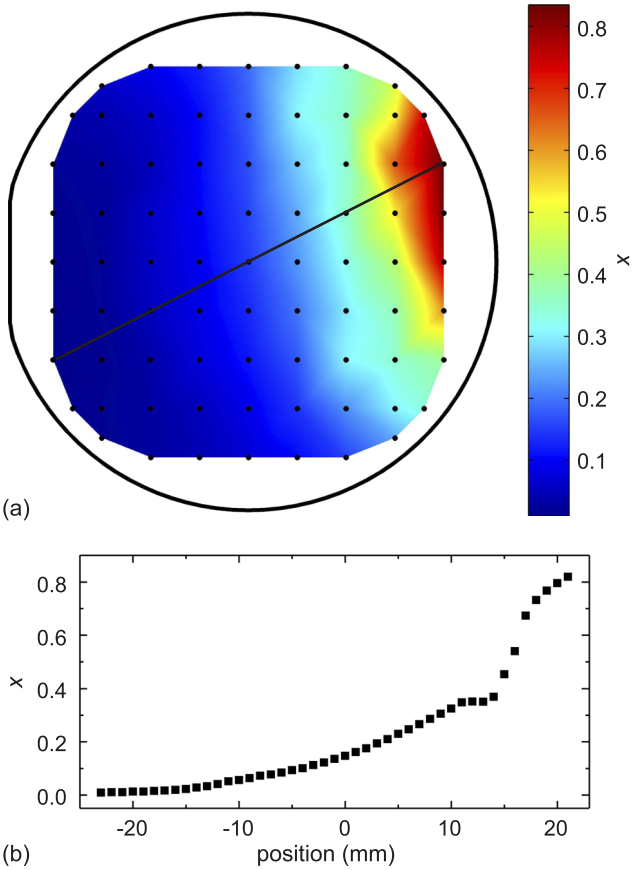

FIG. 1. (a) False color representation of the In content x of a $(In_xGa_{1-x})_2O_3$ thin film grown on a 2 inch diameter c-plane sapphire substrate. The black dots indicate measurement spots, data in between was interpolated. (b) shows the EDX-linescan along the compositional gradient as indicated by the black line in (a).

Inside the stage, the diode was contacted with tungsten probe needles. An Agilent 4156C Semiconductor Parameter Analyzer was used for this measurement. The temperature was calculated from a reference measurement of a Pt100 resistor inside the probe stage.

The lateral variation of the cation composition of the CCS-PLD thin film was determined by EDX measurements and is depicted in Fig. 1(a). It exhibits a non-linear increase in the indium content x along the gradient direction as visible in Fig. 1(b). The strong increase in the gradient, observed for positions $z > 15$ mm, is connected to phase separation as concluded from 55 2θ-ω measurements recorded with a step size of 1 mm along the gradient direction. The results are represented as a false color map in Fig. 2(a). For $x = 0.1$, a single XRD 2θ-ω scan is shown in Fig. 2(c). Around $x \sim 0.35$ (corresponding to the position $z = 15$ mm) and $x \sim 0.5$, changes of the predominant crystallographic phase are evident. In the region of $0.35 < x < 0.5$, the hexagonal $InGaO_3$(II) phase appears, and for higher In concentrations ($x > 0.5$), the cubic bixbyite structure is found. For $x \leq 0.35$, a series of narrow peaks, shifting to lower angles with increasing In content, are observed. The peak positions occur for each In content systematically at higher angles compared to those of monoclinic $(In_xGa_{1-x})_2O_3$ thin films[28–30] indicating growth in the orthorhombic modification. To clarify this assumption, XRD ϕ-scans were recorded for five selected In contents for asymmetric reflections corresponding to the (131), (122), and (206) lattice planes of the κ-phase shown in Fig. 2(b) for $x = 0.01$. The 2θ and χ positions of these reflections were assumed to be the same as for binary κ-Ga_2O_3 based on the unit cell by Cora *et al.*[13] due to a lack of data on composition-dependent lattice constants for the alloy. Both the (131) and (206) reflections occur six-fold with a separation of 60° indicating epitaxial growth on the c-sapphire substrate. Assuming an orthorhombic unit cell, this six-fold symmetry suggests three rotational domains separated by 120°.[31] The orthorhombic symmetry of the unit cell was confirmed by the twelve-fold occurring (122) reflection, where an additional two-fold splitting of the peaks is due to mirror planes in the orthorhombic structure. Furthermore, according to calculations using the VESTA software package,[32] there should be no reflection observable for this specific set of angles in the hexagonal equivalent of this phase, typically referred to as ε-Ga_2O_3[33] instead of κ-Ga_2O_3. These results unambiguously substantiate the growth in orthorhombic modification for $x \leq 0.35$.

The epitaxial relationship deduced from the positions of the film reflections in the XRD ϕ-scans with respect to those of the α-Al_2O_3 (10.2) plane are κ-$(In_xGa_{1-x})_2O_3$ $\langle 010\rangle \| \alpha$-$Al_2O_3$ $\langle 10\bar{1}0\rangle$ and κ-$(In_xGa_{1-x})_2O_3$ $\langle 100\rangle \| \alpha$-$Al_2O_3$ $\langle 2\bar{1}\bar{1}0\rangle$. With that, the peaks in Fig. 2(a) for $x \leq 0.35$ can be assigned to the $(00n)$ reflections of orthorhombic $(In_xGa_{1-x})_2O_3$. Hence, we extended the composition range for which κ-phase thin films were reported; samples grown by mist-CVD showed phase separation for $x > 0.2$.[23]

The dependence of the c-lattice constant on the indium content is shown in Fig. 4. It increases linearly with x and can be modeled in close agreement with the data of Nishinaka *et al.*[23] by $c = [(9.269 \pm 0.004) + (1.097 \pm 0.01) \cdot x\,]$ Å. For a lower indium content, a non-linearity in $c(x)$ is observed that we attribute to slightly different sample alignment between the chemical and the structural analysis.

The growth rate τ was calculated from the sample thickness (deduced from spectroscopic ellipsometry, see below) and starts for the lowest In content at $\tau = 8.7$ pm/pulse and saturates around 7.2 pm/pulse for $x \geq 0.2$. For monoclinic $(In_xGa_{1-x})_2O_3$, the growth rate is only 2 pm/pulse for the lowest In content and saturated at 4 pm/pulse for $x > 0.05$[30] for similar deposition conditions. Since the incident particle flux on the substrate is, except for tin, the same for the CCS-PLD growth of monoclinic $(In_xGa_{1-x})_2O_3$ and orthorhombic

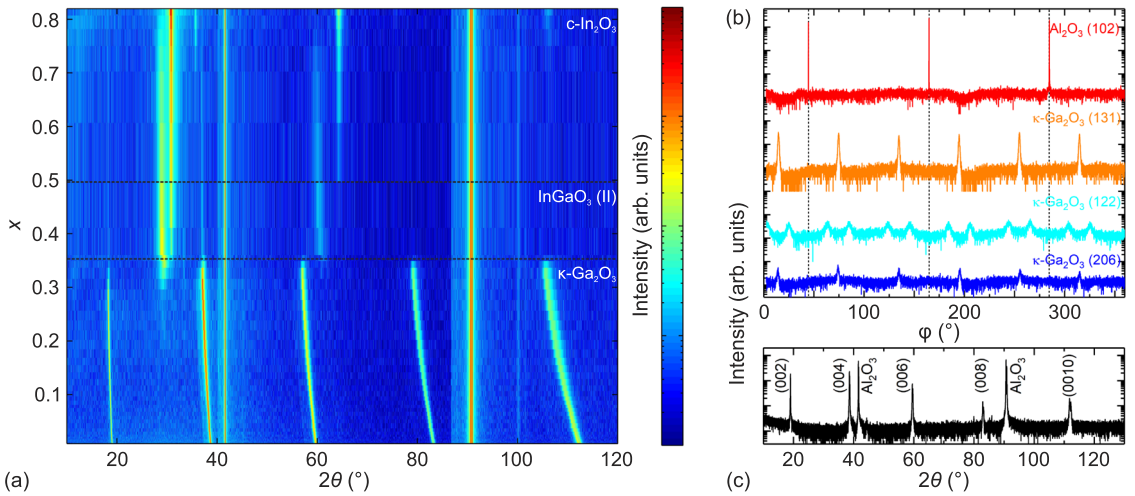

FIG. 2. (a) False color plot of 55 XRD 2θ-ω measurements acquired along a gradient direction. (b) XRD ϕ-scans and (c) single XRD 2θ-ω measurement of a sample piece at $x \sim 0.01$.

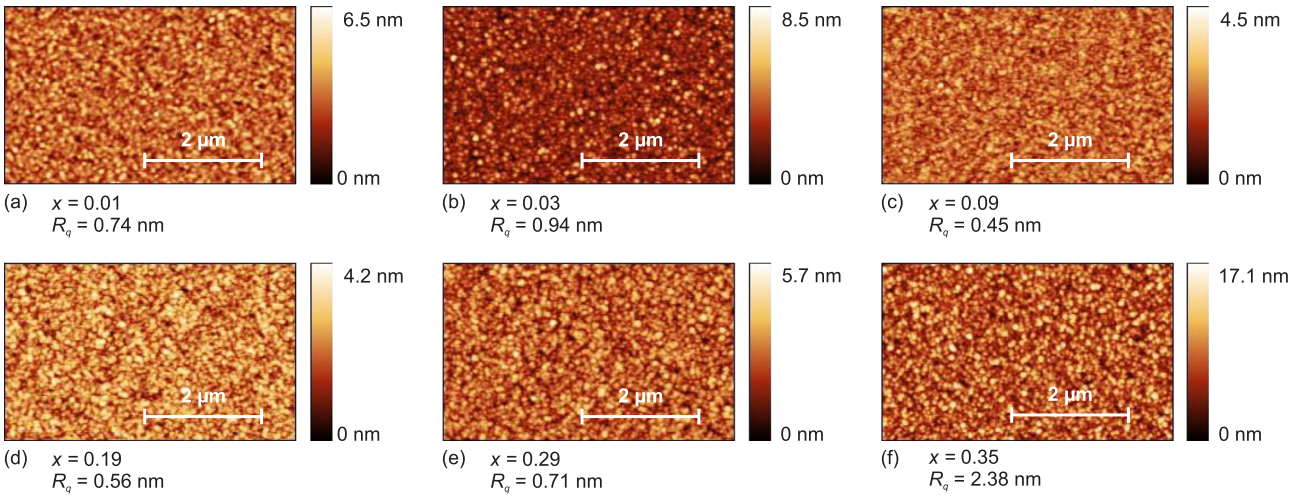

FIG. 3. Surface morphology and corresponding surface roughness R_q measured by atomic force microscopy for In contents x as labeled.

$(In_xGa_{1-x})_2O_3$:Sn, the increased growth rate for the κ-phase is assigned to a strong reduction of the desorption of volatile Ga_2O. This is in line with findings of Kracht *et al.*[20] who proposed an oxidation of gallium suboxides by reducing SnO or SnO_2 at the surface, which leads to an increased incorporation of gallium and with that to higher growth rates compared to tin-free growth. That the presence of tin is beneficial for the stabilization of PLD thin films with an orthorhombic phase was already pointed out in 2002 by Orita *et al.*[19] who investigated tin-doped Ga_2O_3 as a possible transparent conducting oxide (TCO) material. Further, they demonstrated that tin is not contributing to the electrical conductivity at RT likely due to tin-related donor states being too deep to generate free electrons at RT. EDX measurements on our CCS-PLD thin films indicate the presence of about 0.6–0.8 at. % tin in orthorhombic $(In_xGa_{1-x})_2O_3$, however, an electrical conductivity was not measurable corroborating results of Orita *et al.* that tin is not donating free electrons in orthorhombic $(In_xGa_{1-x})_2O_3$:Sn at RT.

The surface morphology was investigated by AFM measurements to deduce the root mean square surface roughness R_q. Figure 3 depicts images of the thin film surfaces of the orthorhombic part for six different In contents. The images show smooth surfaces for $x < 0.35$ with low R_q values ranging between 0.45 nm and 0.94 nm independent of x. For the highest In content in orthorhombic modification, $x = 0.35$, an increased R_q of 2.38 nm caused by the phase transition from orthorhombic into hexagonal $InGaO_3$(II) phase was observed. The grains are spherically shaped with diameters of approximately 100–120 nm for all In contents.

The compositional dependence of the bandgap (Fig. 4) was determined by spectroscopic ellipsometry and shows three regimes with small differences in the slope. In general, the bandgap decreases as expected with increasing In content and allows band gap engineering between about 4.9 eV and 4.3 eV for $0 \leq x \leq 0.35$.

With spectroscopic ellipsometry measurements, the dielectric function (DF) was investigated in the spectral range between 0.74 eV and 6.3 eV for angles of incidence of 50°, 60°, and 70°. In order to reduce the impact of the composition gradient on an individual measurement, the spot size was reduced to about 300 × 500 μm^2 by using focusing optics.

Due to the presence of rotation domains, the optically biaxial films can be described by an uniaxial model with an optical axis parallel to the surface normal. Therefore, standard ellipsometry can be applied,[34] i.e., the ellipsometric parameters Ψ and Δ are given by

$$\rho = \frac{r_p}{r_s} = \tan \Psi e^{i\Delta}. \quad (1)$$

The abbreviations r_p and r_s represent the complex reflection coefficients for light polarized parallel and perpendicular

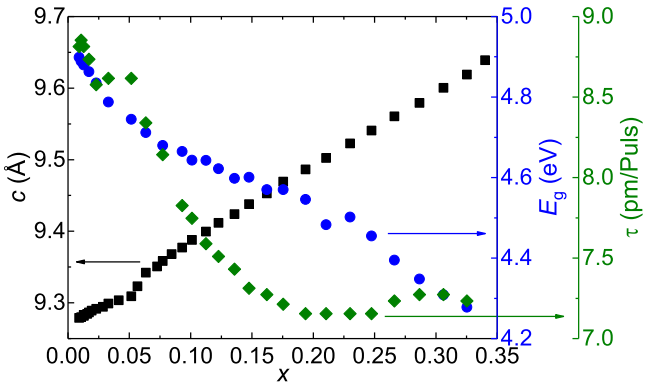

FIG. 4. The c-lattice constant determined from XRD patterns as well as the bandgap and growth rate obtained from spectroscopic ellipsometry measurements as a function of the In content x.

to the plane of incidence. To reduce the dependence of Ψ and Δ on the angle of incidence, it is appropriate to convert these quantities into a pseudodielectric function $\langle\epsilon\rangle$.[35] A layer stack model consisting of a c-plane sapphire substrate, a thin film, and a surface layer was used to obtain the dielectric function (DF). For the c-plane sapphire substrate, the optical constants were taken from Ref. 36. The thin film DF was described to be uniaxial, i.e., the DF tensor is given by $\epsilon_\perp = \epsilon_{xx} = \epsilon_{yy} \neq \epsilon_\parallel = \epsilon_{zz}$. In the analysis of the experimental data, it was found that the contribution of ϵ_{zz} cannot be neglected. The line shape of each tensor component was represented by model dielectric functions. Similar to former calculated DF of β-Ga_2O_3 thin films by Sturm *et al.*,[34] the excitonic contributions (χ^{exc}) were characterized by using a model function, which was developed by Tanguy.[37–39] For the weakly pronounced band-band transitions, which cannot be resolved separately, Gaussian oscillators (χ^{gauss}) were used. Due to the Kramers-Kronig transformation, the contributions of high-energy transitions to the real part of the DF were taken into account by a pole function (χ^{pole}). Since the optical axis is perpendicular to the surface, the sensitivity to $\epsilon_\parallel$ is quite low and the same transitions for $\epsilon_\perp$ and $\epsilon_\parallel$ can be assumed. Thus, the resulting DF is given by

$$\epsilon_i = \sum_{j=1}^{2} \chi_{j,i}^{exc} + \chi_{j,i}^{gauss} + \chi_j^{pole}, \quad (2)$$

with $i = \perp, \parallel$.

Because of the strong correlation between the parameters due to the absence of strong absorption features in the spectra, a further assumption for each transition is that they have the same energy and broadening in $\epsilon_\perp$ and $\epsilon_\parallel$. Finally, the surface roughness was described by an effective medium approach,[40] where the DF of the Ga_2O_3 thin film and air was mixed 1:1. The thickness of this layer was found to be about 2 nm. The experimentally recorded and calculated pseudodielectric functions are well coinciding as exemplary shown in Fig. 5 for selected In concentrations and an angle of incidence of 60°. For energies below 4 eV, the spectra are dominated by thickness oscillations allowing a precise determination of the film thickness, which is in the range of 180–205 nm. For energies larger than 4 eV, absorption sets in and the oscillations vanish such that the spectra are dominated by the excitonic and band-band transitions.

The deduced dielectric function is shown in Fig. 6 for selected In concentrations. As expected, a red shift of the onset of the absorption is observed with increasing In concentration caused by an almost linear red shift of the transition energies with respect to the In concentration. Besides the red shift of the transition energy, we also observe a strong increase in the excitonic broadening from 50 meV for $x \approx 0.01$ up to 350 meV for $x \approx 0.32$ due to alloy broadening. Interestingly, with increasing In concentrations, the difference of the line shape between $\epsilon_\perp$ and $\epsilon_\parallel$ decreases, which leads to a decrease in the optical anisotropy.

Besides the DF, another important quantity, especially for the design of applications, is the refractive index. In the transparent spectral range, the dispersion of the refractive index can be described by the Cauchy function, i.e., $n = A + B/\lambda^2 + C/\lambda$,[4] and the corresponding parameters are depicted in Fig. 2 in the supplementary material. The red shift of the transition energies leads to an increase in the refractive index expressed by an increase in the Cauchy parameters. However, for $x > 0.2$, a decrease in the Cauchy parameters A and C can be observed leading to a decrease in the refractive index especially at small energies. Up to now, the origin of this decrease is not fully understood, but the strong decrease, which is also observable in the real part of the DF as can be seen by the kink at E ~ 1 eV for $x = 0.3$, indicates the presence of free

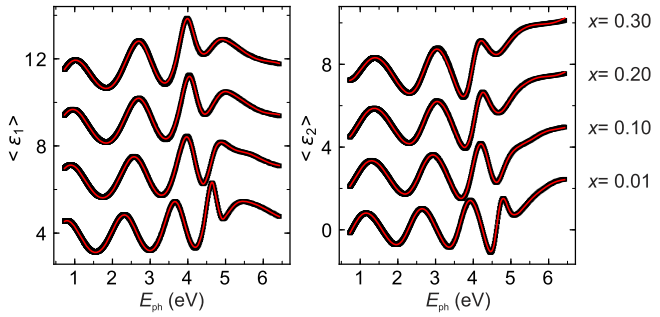

FIG. 5. The experimental (black squares) and calculated (red solid lines) pseudodielectric function for selected In concentration and an angle of incidence of 60°. For a better clarity, the spectra are shifted vertically.

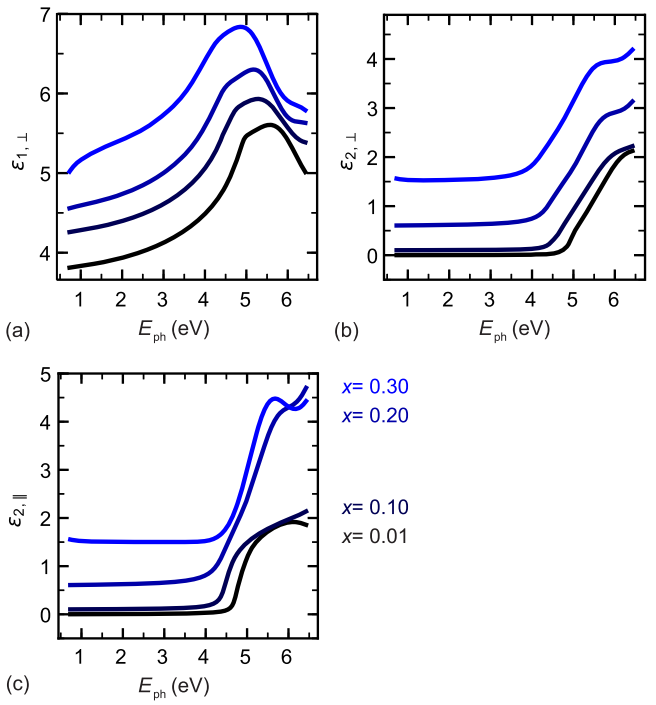

FIG. 6. Dielectric function (a) $\epsilon_{1,\perp}$, (b) $\epsilon_{2,\perp}$ and (c) $\epsilon_{2,\parallel}$ of κ-$(In_xGa_{1-x})_2O_3$ for indium contents as labeled.

charge carriers for these In concentrations, in contrast to Hall effect data. We assume that the transport of the carriers is suppressed due to the existence of potential barriers that cannot be passed at room temperature. The origin of such barriers is likely grain boundaries since rotational domains exist.

As stated above, tin does not contribute free electrons such that it is necessary to add an additional shallow donor in order to achieve n-type conductivity. As a suitable candidate in κ-modification, we identified zirconium and fabricated samples with a low In-content of $x \approx 0.01$ and a Zr content of 1.3 at. %. The band gap and film thickness of the samples were determined by spectroscopic ellipsometry to be 4.97 eV and about 220 nm, respectively.

Resistivity and Hall-effect measurements were performed on a 10 × 10 mm^2 sample using the van-der-Pauw method. The electrical conductivity versus T^{-1} is shown in Fig. 7(a). An almost exponential increase in the conductivity with increasing temperature can be observed. For lower temperatures, the measured conductivity deviates from the simple exponential dependence (dashed line) due to the increase in the free carrier mobility. The free carrier concentration is shown in Fig. 7(b) in dependence on the temperature. An overall trend can be observed: the free carrier concentration increases first exponentially and begins to saturate for $T \geq 400$ K. We fitted the dependence using the equations provided in the supplementary material. The respective fits with and without compensation are shown in Fig. 7(b). The results of both the cases are summarized in Table I. Overall, a better agreement between the measured and the fitted data was achieved if compensation was taken into account and yields values for the donor concentration of $N_D = 3 \times 10^{17}$ cm^{-3} with an activation energy of $E_D = 190$ meV. In principle, we expect compensating centers to be present in our heteroepitaxial thin films, but further experiments are required to understand the nature of donors and compensating acceptors as well as the electric transport phenomena in κ-Ga_2O_3 in more detail. In comparison to the activation energy of 0.695 eV (without compensation) determined by Pavesi *et al.*[21] between 400 ≤ T ≤ 600 K from conductance measurements on nominally undoped κ-Ga_2O_3 thin films, the donor level investigated here is (independent of the compensation case) significantly closer to the conduction band minimum, demonstrating that it increases n-type conductivity even though E_D is higher than for an effective mass donor. Additionally, from the fits, the difference $E_n = E_c - E_F$ between the conduction band minimum E_c and the Fermi level E_F was calculated for room temperature, which can also be found in Table I. From the resistivity and the Hall-effect measurements, the mobility can be calculated. The plot in dependence on the temperature is shown in Fig. 7(c). For low mobilities (gray shaded area), the error of the measurement becomes rather large and since a lower magnetic field was used for the high temperature measurement, the error is even larger here. From the dependence of the mobility on temperature, we deduced polar-optical scattering[41] to be the dominating scattering mechanism in this temperature range. By fitting of the temperature-dependent mobility, the Debye temperature was estimated to be about 1000 K. The used equation can be found in the supplementary material. Despite the data being well modeled by considering only one scattering mechanism over the measured temperature range,

TABLE I. Results of fits of the temperature-dependent free carrier concentration using equations provided in the supplementary material. N_D and N_A are the concentration of the donor and compensating acceptors, respectively, E_D is the thermal activation energy of the donor, and E_n denotes the difference between the Fermi energy and the energy of the conduction band minimum at room temperature.

Compensation	N_D (cm^{-3})	N_A (cm^{-3})	E_D (meV)	E_n (meV)
Without	3×10^{18}	...	310	370
With	3×10^{17}	4×10^{16}	190	490

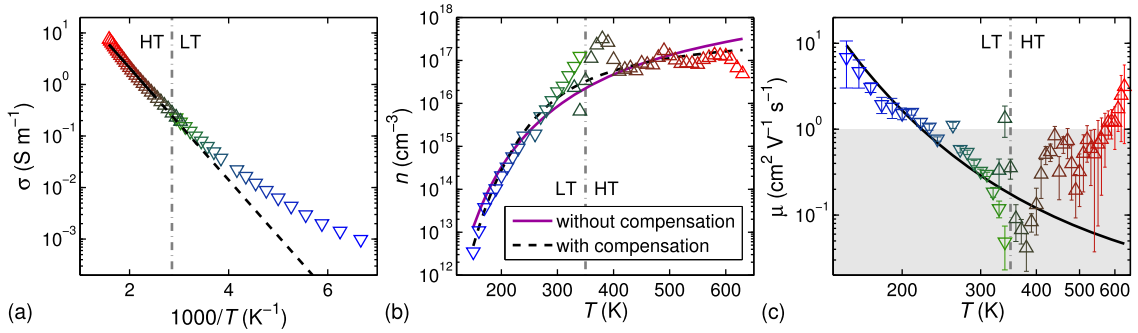

FIG. 7. Results of the temperature dependent resistivity and Hall-effect measurement from low temperatures (labeled LT) to intermediate temperatures and intermediate to high temperatures (labeled HT). (a) shows the conductivity in dependence of T^{-1}. For higher temperatures, the measurements show a linear dependence and for lower temperatures, the measurements deviate from the linear dependence, indicating a more complex behavior. In (b) the free carrier concentration is shown in dependence on the temperature. While the values scatter to some extent due to the noise of the measurement, a clear trend can be seen. The data was fitted with the equation for the cases with and without compensation (see text and Table I for details). (c) shows the mobility in dependence on the temperature. At high temperature, the resulting mobilities are in the range where, especially for the high temperature measurement, the error of the measurement becomes large (gray shaded area). For low temperatures, the mobility may be dominated by polar-optical scattering, as can be seen from the fit of the data.

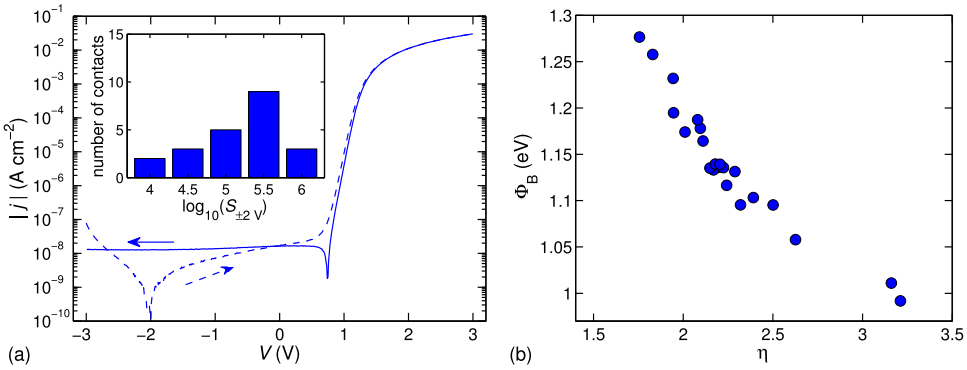

FIG. 8. (a) IV-characteristics of SCs for a bias sweep from negative to positive voltages (dashed lines) and vice versa (solid lines). Instead of the current, the current density j is shown. In the inset, a histogram of the rectification ratios of the rectifying contacts can be found. (b) shows a plot of the effective barrier height vs. the ideality factor determined by fitting the individual characteristics of the rectifying contacts with the thermionic emission model.

it cannot be excluded that other scattering mechanisms also play a role.

In Fig. 8(a), IV characteristics of a representative PtO_δ/κ-$(In,Ga)_2O_3$:Zr Schottky barrier diode is depicted. The plot shows the current density $j = I/A_0$, where A_0 describes the contact area. The first (second) sweep direction is from negative to positive (positive to negative) voltages as indicated by the arrows. The difference between both measurement directions (the position of the zero-crossing) can be explained by a charging current.[42] For the contact shown here, a rectifying behavior is observed and the diode exhibits a low reverse current density of about 1×10^{-8} A cm^{-2}. Overall, 22 contacts were measured and the rectification ratio for V = ±2 V (ratio between the magnitude of the currents measured at these voltages) is depicted as histogram in Fig. 8(a). Some of the contacts exhibit rectification ratios of up to six orders of magnitude. For evaluation of the characteristics, we assumed that the dominating transport mechanism is thermionic emission over the Schottky-barrier, which is reasonable in the mobility and net-doping density range[43,44] discussed above. Since there exists no literature data for the effective mass of κ-Ga_2O_3 and since the ideality factors determined here are too high to evaluate the temperature dependence of the Richardson constant, the effective mass of the free carriers was assumed to be the same as for β-Ga_2O_3 ($m_{eff} = 0.28m_0$[45,46]). The dependence of Φ_B^{eff} on η is plotted in Fig. 8(b) and shows that with the decreasing ideality factor, the effective barrier height increases almost linearly. A similar behavior was observed by Schmitsdorf *et al.*[47,48] and explained by barrier height inhomogeneities using a patch-like inhomogeneity model developed by Tung.[49] The homogeneous barrier height Φ_B^{hom} was determined by linear extrapolation toward $\eta = 1.02$ to be about 1.35 eV.

In order to further investigate the barrier height inhomogeneities, temperature-dependent IV-measurements between $100 \le T \le 320$ K and $300 \le T \le 700$ K were performed. The associated characteristics are displayed in Fig. 9. For temperatures below 100 K, the series resistance becomes so large that almost no rectification can be observed. For temperatures above 575 K, the needle probes of the Linkam probe stage scratched the surface of the contact due to the thermal expansion and damaged it. The difference in the series resistance between the measurement at low and at high temperatures can be explained by the fact that for the low temperature measurement, an ohmic contact close to the edge of the sample was contacted, while for the high temperature measurement, the ohmic contact that surrounds the measured Schottky contact was used. Furthermore, it can be seen that the series resistance increases strongly with decreasing temperatures. Therefore, the determination of the effective barrier height and the ideality factor becomes difficult at low temperatures, since no exponential region is observed. For temperatures of 200 K and higher, the characteristics were fitted with the model of thermionic emission in order to determine the effective barrier height and the ideality

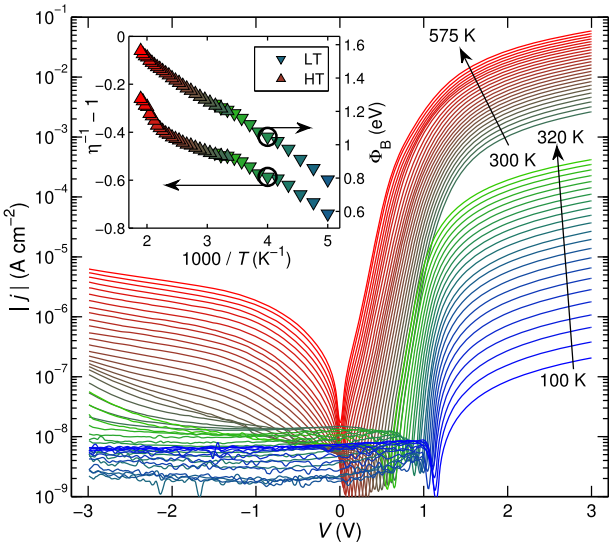

FIG. 9. Temperature-dependent IV-characteristics taken from low temperatures to intermediate temperatures (labeled LT) and intermediate to high temperatures (labeled HT). Here, only the measurement direction going from positive to negative voltages is shown. The higher series resistance in the LT-measurement can be explained by the fact that an ohmic contact on the edge of the sample was used for this measurement. In the inset, the plots of the effective barrier height and $\eta^{-1} - 1$ vs. T^{-1} can be found. Both show an almost linear dependence between 400 K and 200 K.

factor. According to the theory of Werner and Güttler,[50] a linear dependence of Φ_B^{eff} and $(\eta^{-1} - 1)$ on T^{-1} can be expected if the barrier is laterally inhomogeneous with a Gaussian-shaped barrier distribution. The corresponding plots are shown in the inset of Fig. 9. Both, Φ_B^{eff} and $(\eta^{-1} - 1)$, show a linear dependence on T^{-1} over a large temperature range. At temperatures above 400 K, $(\eta^{-1} - 1)$ deviates from the linear dependence, which might be due to annealing effects. From linear fits in the range between 400 K and 200 K ($1000/T = 2.5$ and 5 K^{-1}), the mean barrier height and the standard deviation of the barrier distribution as well as their voltage coefficients ϱ_2 and ϱ_3 can be determined to be 1.95 eV, 0.20 eV, 0.13, and −0.02 eV, respectively.

After temperature cycling (highest T = 700 K), a RT IV-measurement was performed on other contacts on the same sample piece. While the ideality factor and the series resistance of the contacts increased and the characteristic became more "rounded," the contacts remained rectifying with rectification ratios up to 5 orders of magnitude. Overall, the rectification ratio decreased by 0.4 orders of magnitude, while the effective barrier height stayed about constant and the ideality factor increased by about 0.2. A plot showing an IV-characteristic before and after the IVT-measurement is provided in the supplementary material.

Because of the high series resistance of the Schottky contacts, investigation by standard capacitance-voltage measurements was not possible. Nevertheless, quasi-static CV measurements can be performed, due to the low reverse current. Exemplary CV-characteristics are shown in the inset of Fig. 10(a). In the main plot of Fig. 10(a), the C^{-2}–V dependency is shown. Different linear regions with different slopes are observed and fitted in order to estimate the net-doping concentration in the corresponding voltage region. The curve in region 1 was linearly extrapolated toward C = 0 in order to estimate the built-in voltage V_{bi}. The results are summarized in Table II.

By numerical modeling, the net-doping density N_t was calculated in dependence on the space charge region width w for each contact on the sample. The mean value of the doping-profile is plotted in Fig. 10(b) with solid lines. The shaded areas correspond to the standard deviations of the measurements on the contact. Note that the change in the net-doping density not necessarily means, that there exists a real change in the doping concentration.[51] It is also possible that at certain voltages, deeper lying defects are lifted above the Fermi energy and hence contribute to the net-doping density for this and lower voltages. This could mean that the minimum observed in the doping-profiles could be due to a deep lying acceptor (also leading to compensation) similar to the case of β-Ga_2O_3 thin films.[42] However, more detailed investigations are necessary to obtain a full understanding. Further, there are differences in the net-doping density determined by QSCV-measurements and the donor concentration determined by Hall-effect measurements, since deeper lying defects contribute to the QSCV-signal. Therefore, the net doping density may differ from fits of the Hall-effect data, especially if materials with a large band gap and high barrier height are investigated.

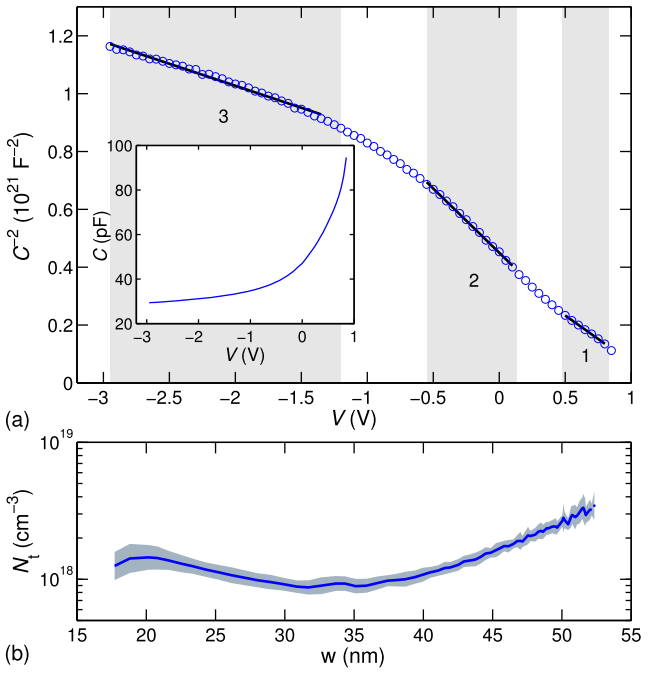

FIG. 10. Results of the quasi-static CV measurement. The inset of (a) shows the capacitance in dependence of the voltage. In (a), C^{-2} vs. V is shown. The differently labeled regions correspond to regions of different linear slope in the plot. The net-doping densities and the built-in potential determined from linear fits can be found in Table II. (b) shows the calculated net-doping profiles. The solid line corresponds to the mean value of measurements on the rectifying contacts and the shaded area to the standard deviation.

In this work we discussed structural, optical, and electrical properties of $(In_xGa_{1-x})_2O_3$ thin films, which were prepared in orthorhombic modification up to $x = 0.35$ using pulsed-laser deposition. The growth rate of κ-$(In_xGa_{1-x})_2O_3$:Sn is higher than that for monoclinic thin films suggesting that desorption processes were suppressed by the tin-assisted PLD growth. Since Sn is not electrically active in the orthorhombic phase, it is necessary to additionally dope κ-$(In_xGa_{1-x})_2O_3$ to create conducting samples. As a suitable donor, we identified Zr and performed electrical transport measurements on a thin film with an admixture of 1.3 at. % Zr. The donor concentration is about 3×10^{17} cm^{-3} and its thermal activation energy is 190 meV. The rectification ratio of Schottky barrier diodes was as high as six orders of magnitude, and the homogeneous barrier height is 1.35 eV. Temperature-dependent measurements revealed a

TABLE II. Results of the linear fits in the different regions seen in Fig. 10(a). For region 1, also the built-in voltage was determined by linear extrapolation.

N_t (10^{18} cm^{-3})	Region 1	1.3
	Region 2	0.74
	Region 3	1.8
V_{bi} (V)	Region 1	1.20

strong increase in series resistance with decreasing temperature. Additionally, the DF and pseudo DF were derived for a wide composition range in this work. Overall, the excellent structural and morphological properties of κ-$(In_xGa_{1-x})_2O_3$ compared to β-$(In_xGa_{1-x})_2O_3$ heteroepitaxial thin films make this material interesting for heterostructure-based devices.

See supplementary material for several fitting equations and additional figures about parameters of the Cauchy function and IV-characteristics of a contact at room temperature before and after a temperature dependent IV-measurement to temperatures up to 700 K.

We thank Monika Hahn for PLD target and SC fabrication. We also thank Jörg Lenzner for EDX measurements and Ulrike Teschner for transmission measurements. This work was supported by the European Social Fund within the Young Investigator Group "Oxide Heterostructures" (No. SAB 100310460) and partly by Deutsche Forschungsgemeinschaft in the Framework of Sonderforschungsbereich 762 "Functionality of Oxide Interfaces". A.H. and M.K. acknowledge the Leipzig School for Natural Sciences BuildMoNa. We acknowledge support from Leipzig University within the program of Open Access Publishing.

REFERENCES

[1] Z. Zhang, H. von Wenckstern, and M. Grundmann, IEEE J. Sel. Top. Quantum Electron. **20**, 106–111 (2014).
[2] O. Bierwagen, Semicond. Sci. Technol. **30**, 024001 (2015).
[3] M. Grundmann, H. Frenzel, A. Lajn, M. Lorenz, F. Schein, and H. von Wenckstern, Phys. Status Solidi A **207**, 1437–1449 (2010).
[4] M. Higashiwaki, A. Kuramata, H. Murakami, and Y. Kumagai, J. Phys. D: Appl. Phys. **50**, 333002 (2017).
[5] S. Stepanov, V. Nikolaev, V. Bougrov, and A. Romanov, Rev. Adv. Mater. Sci. **44**, 63–86 (2016).
[6] H. von Wenckstern, Adv. Electron. Mater. **3**, 1600350 (2017).
[7] S. J. Pearton, J. Yang, P. H. Cary, F. Ren, J. Kim, M. J. Tadjer, and M. A. Mastro, Appl. Phys. Rev. **5**, 011301 (2018).
[8] M. Higashiwaki, K. Sasaki, A. Kuramata, T. Masui, and S. Yamakoshi, Appl. Phys. Lett. **100**, 013504 (2012).
[9] S. Fujita, M. Oda, K. Kaneko, and T. Hitora, Jpn. J. Appl. Phys., Part 1 **55**, 1202A3 (2016).
[10] M. B. Maccioni and V. Fiorentini, Appl. Phys. Express **9**, 041102 (2016).
[11] S. B. Cho and R. Mishra, Appl. Phys. Lett. **112**, 162101 (2018).
[12] J. Kim, D. Tahara, Y. Miura, and B. G. Kim, Appl. Phys. Express **11**, 061101 (2018).
[13] I. Cora, F. Mezzadri, F. Boschi, M. Bosi, M. Čaplovičová, G. Calestani, I. Dódony, B. Pécz, and R. Fornari, CrystEngComm **19**, 1509–1516 (2017).
[14] F. Mezzadri, G. Calestani, F. Boschi, D. Delmonte, M. Bosi, and R. Fornari, Inorg. Chem. **55**, 12079–12084 (2016).
[15] Y. Oshima, E. G. Víllora, Y. Matsushita, S. Yamamoto, and K. Shimamura, J. Appl. Phys. **118**, 085301 (2015).
[16] X. Xia, Y. Chen, Q. Feng, H. Liang, P. Tao, M. Xu, and G. Du, Appl. Phys. Lett. **108**, 202103 (2016).
[17] F. Boschi, M. Bosi, T. Berzina, E. Buffagni, C. Ferrari, and R. Fornari, J. Cryst. Growth **443**, 25–30 (2016).
[18] Y. Chen, X. Xia, H. Liang, Q. Abbas, Y. Liu, and G. Du, Cryst. Growth Des. **18**, 1147–1154 (2018).
[19] M. Orita, H. Hiramatsu, H. Ohta, M. Hirano, and H. Hosono, Thin Solid Films **411**, 134–139 (2002).
[20] M. Kracht, A. Karg, J. Schörmann, M. Weinhold, D. Zink, F. Michel, M. Rohnke, M. Schowalter, B. Gerken, A. Rosenauer, P. J. Klar, J. Janek, and M. Eickhoff, Phys. Rev. Appl. **8**, 054002 (2017).
[21] M. Pavesi, F. Fabbri, F. Boschi, G. Piacentini, A. Baraldi, M. Bosi, E. Gombia, A. Parisini, and R. Fornari, Mater. Chem. Phys. **205**, 502–507 (2018).
[22] D. Tahara, H. Nishinaka, S. Morimoto, and M. Yoshimoto, Appl. Phys. Lett. **112**, 152102 (2018).
[23] H. Nishinaka, N. Miyauchi, D. Tahara, S. Morimoto, and M. Yoshimoto, CrystEngComm **20**, 1882–1888 (2018).
[24] H. von Wenckstern, Z. Zhang, F. Schmidt, J. Lenzner, H. Hochmuth, and M. Grundmann, CrystEngComm **15**, 10020 (2013).
[25] S. Müller, H. von Wenckstern, D. Splith, F. Schmidt, and M. Grundmann, Phys. Status Solidi A **211**, 34–39 (2014).
[26] S. Müller, H. Von Wenckstern, F. Schmidt, D. Splith, F. L. Schein, H. Frenzel, and M. Grundmann, Appl. Phys. Express **8**, 121102 (2015).
[27] S. Müller, H. v. Wenckstern, F. Schmidt, D. Splith, H. Frenzel, and M. Grundmann, Semicond. Sci. Technol. **32**, 065013 (2017).
[28] C. Kranert, J. Lenzner, M. Jenderka, M. Lorenz, H. von Wenckstern, R. Schmidt-Grund, and M. Grundmann, J. Appl. Phys. **116**, 013505 (2014).
[29] H. von Wenckstern, D. Splith, A. Werner, S. Müller, M. Lorenz, and M. Grundmann, ACS Comb. Sci. **17**, 710–715 (2015).
[30] H. von Wenckstern, D. Splith, M. Purfürst, Z. Zhang, C. Kranert, S. Müller, M. Lorenz, and M. Grundmann, Semicond. Sci. Technol. **30**, 024005 (2015).
[31] M. Grundmann, Phys. Status Solidi B **248**, 805–824 (2011).
[32] K. Momma and F. Izumi, J. Appl. Crystallogr. **44**, 1272–1276 (2011).
[33] H. Y. Playford, A. C. Hannon, E. R. Barney, and R. I. Walton, Chem. - Eur. J. **19**, 2803–2813 (2013).
[34] C. Sturm, R. Schmidt-Grund, C. Kranert, J. Furthmüller, F. Bechstedt, and M. Grundmann, Phys. Rev. B **94**, 035148 (2016).
[35] H. Fujiwara, *Spectroscopic Ellipsometry: Principles and Applications*, 1st ed. (John Wiley & Sons, 2007).
[36] H. Yao and C. H. Yan, J. Appl. Phys. **85**, 6717 (1999).
[37] C. Tanguy, Phys. Rev. Lett. **75**, 4090–4093 (1995).
[38] C. Tanguy, Phys. Rev. Lett. **76**, 716 (1996).
[39] C. Tanguy, Phys. Rev. B **60**, 10660–10663 (1999).
[40] D. A. G. Bruggeman, Ann. Phys. **416**, 636 (1935).
[41] M. Grundmann, *Transparent Semiconducting Oxides: Materials and Devices*, 1st ed. (Springer, Berlin and New York, 2006).
[42] D. Splith, S. Müller, H. von Wenckstern, and M. Grundmann, Proc. SPIE **10533**, 105330C (2018).
[43] A. Lajn, H. von Wenckstern, M. Grundmann, G. Wagner, P. Barquinha, E. Fortunato, and R. Martins, J. Appl. Phys. **113**, 044511 (2013).
[44] D. Splith, S. Müller, F. Schmidt, H. von Wenckstern, J. J. van Rensburg, W. E. Meyer, and M. Grundmann, Phys. Status Solidi A **211**, 40–47 (2014).
[45] J. B. Varley, J. R. Weber, A. Janotti, and C. G. Van de Walle, Appl. Phys. Lett. **97**, 142106 (2010).
[46] M. Mohamed, C. Janowitz, I. Unger, R. Manzke, Z. Galazka, R. Uecker, R. Fornari, J. R. Weber, J. B. Varley, and C. G. Van de Walle, Appl. Phys. Lett. **97**, 211903 (2010).
[47] R. F. Schmitsdorf, T. U. Kampen, and W. Mnch, J. Vac. Sci. Technol., B: Microelectron. Nanometer Struct.–Process., Meas., Phenom. **15**, 1221–1226 (1997).
[48] R. Schmitsdorf and W. Mönch, Eur. Phys. J. B **7**, 457–466 (1999).
[49] R. T. Tung, Phys. Rev. B **45**, 13509–13523 (1992).
[50] J. H. Werner and H. H. Güttler, J. Appl. Phys. **69**, 1522–1533 (1991).
[51] L. C. Kimerling, J. Appl. Phys. **45**, 1839–1845 (1974).

Structural, optical and electrical properties of orthorhombic κ-$(In_xGa_{1-x})_2O_3$ thin films

A. Hassa,[1] H. von Wenckstern,[1] D. Splith,[1] C. Sturm,[1] M. Kneiß,[1] V. Prozheeva,[2] and M. Grundmann[1]

[1)] *Universität Leipzig, Felix-Bloch-Institut für Festkörperphysik, Linnéstraße 5, 04103 Leipzig, Germany*

[2)] *Department of Applied Physics, Aalto University, Otakaari 1B, 02150 Espoo, Finland*

Material properties of κ-$(In_xGa_{1-x})_2O_3$

Supplementary material

We fitted the dependence of the free carrier concentration by using the formula[?] :

$$n = \frac{1}{2} N_{\mathrm{C}} \exp\left(-\frac{E_{\mathrm{D}}}{k_{\mathrm{B}}T}\right) \left[\sqrt{\alpha^2 + 4\frac{N_{\mathrm{D}} - N_{\mathrm{A}}}{N_{\mathrm{C}}} \exp\left(\frac{E_{\mathrm{D}}}{k_{\mathrm{B}}T}\right)} - \alpha\right] , \tag{1}$$

with

$$\alpha = 1 + \frac{N_{\mathrm{A}}}{N_{\mathrm{C}}} \exp\left(\frac{E_{\mathrm{D}}}{k_{\mathrm{B}}T}\right) \tag{2}$$

and the effective density of states at the conduction band edge

$$N_{\mathrm{C}} = 2\left(\frac{2\pi m_{\mathrm{eff}} k_{\mathrm{B}} T}{h^2}\right)^{\frac{3}{2}} . \tag{3}$$

Here, N_{D} and N_{A} are the donor and acceptor densities, respectively, and h is Planck's constant. For the uncompensated case N_{A} is assumed to be zero and therefore $\alpha = 1$.

The Fermi energy was calculated from:

$$E_{\mathrm{n}} = E_{\mathrm{D}} - k_{\mathrm{B}}T \log\left[\frac{1}{2}\sqrt{\alpha^2 + 4\frac{N_{\mathrm{D}} - N_{\mathrm{A}}}{N_{\mathrm{C}}} \exp\left(\frac{E_{\mathrm{D}}}{k_{\mathrm{B}}T}\right)} - \frac{\alpha}{2}\right] \tag{4}$$

The IV characteristics were fitted considering thermionic emission:

$$I = A_0 A^* \frac{m_{\mathrm{eff}}}{m_0} T^2 \exp\left(-\frac{\Phi_{\mathrm{B}}^{\mathrm{eff}}}{k_{\mathrm{B}}T}\right) \left[\exp\left(e\frac{V - IR_{\mathrm{s}}}{\eta k_{\mathrm{B}}T}\right) - 1\right] \tag{5}$$

where A^* is the Richardson constant, m_{eff} the effective mass, m_0 the electron mass, T the temperature, k_{B} Boltzmann's constant and R_{s} the series resistance.

To fit the deduced polar-optical scattering for low temperatures compared to the Debye temperature ($T \ll \Theta_{\mathrm{D}}$) we used the formula[?] :

$$\mu_{\mathrm{pol.opt.}} = \frac{e}{2m^*\alpha\omega_0} exp\left(\frac{\Theta_{\mathrm{D}}}{T}\right), \tag{6}$$

with

$$\alpha = \frac{1}{137}\sqrt{\frac{m^* c^2}{2k\Theta_{\mathrm{D}}}} \left(\frac{1}{\epsilon_\infty} - \frac{1}{\epsilon_0}\right) \tag{7}$$

being the dimensionless polar constant.

Material properties of κ-$(In_xGa_{1-x})_2O_3$

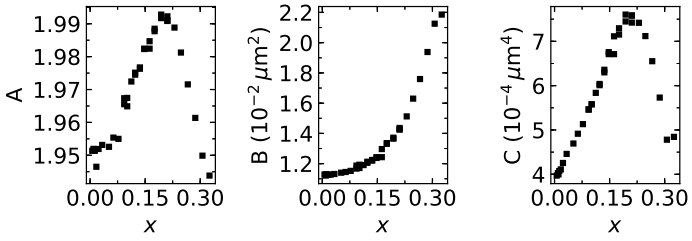

FIG. 1. The parameters of the Cauchy function as a function of the In concentration for $n_\perp = \sqrt{\epsilon_\perp}$.

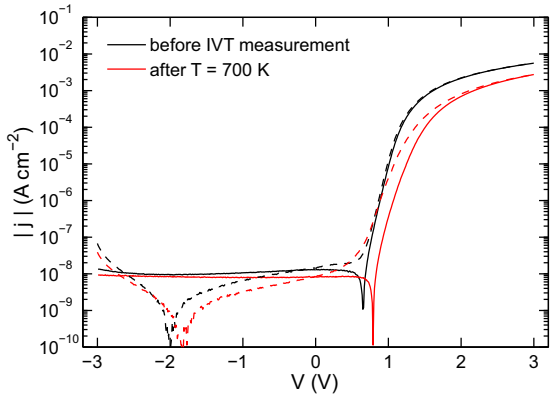

FIG. 2. IV-characteristics of a contact at room temperature before and after the temperature dependent IV-measurement to temperatures up to 700 K. While the ideality factor and rectification ratio slightly change, the contact remains rectifying.

APL Materials ERRATUM scitation.org/journal/apm

Erratum: "Structural, optical, and electrical properties of orthorhombic κ-$(In_xGa_{1-x})_2O_3$ thin films" [APL Mater. 7, 022525 (2019)]

Cite as: APL Mater. 7, 079901 (2019); doi: 10.1063/1.5099518
Submitted: 11 April 2019 • Accepted: 16 April 2019 •
Published Online: 10 July 2019

A. Hassa,[1] H. von Wenckstern,[1] D. Splith,[1] C. Sturm,[1] M. Kneiß,[1] V. Prozheeva,[2] and M. Grundmann[1]

AFFILIATIONS

[1]Felix Bloch Institute for Solid State Physics, Universität Leipzig, Linnéstraße 5, 04103 Leipzig, Germany
[2]Department of Applied Physics, Aalto University, P.O. Box 15100, FIN-00076 Aalto, Finland

https://doi.org/10.1063/1.5099518

Due to a misassignment of EDX and XRD data of the electrically conducting Zr-doped sample, electrical transport data and properties of Schottky barrier diodes reported in the original article[1] were determined for a sample having monoclinic β-gallia structure. The data as well as its analysis are valid; however, it must be attributed to the monoclinic β-phase instead of the orthorhombic κ-phase. The structural and optical data of the ternary κ-$(In_xGa_{1-x})_2O_3$ thin film with lateral spread of the cation composition are valid, and this erratum does not affect these results nor their interpretation.

REFERENCE

[1]A. Hassa *et al.*, APL Mater. 7, 022525 (2019).

ORIGINAL PAPER

physica status solidi pss

www.pss-b.com

Structural and Elastic Properties of α-$(Al_xGa_{1-x})_2O_3$ Thin Films on (11.0) Al_2O_3 Substrates for the Entire Composition Range

Anna Hassa, Philipp Storm, Max Kneiß, Daniel Splith, Holger von Wenckstern, Michael Lorenz, and Marius Grundmann*

Structural properties of rhombohedral α-$(Al_xGa_{1-x})_2O_3$ thin films grown by two combinatorial pulsed laser deposition (PLD) techniques are investigated for the entire composition range. One α-$(Al_xGa_{1-x})_2O_3$ thin film is deposited on a 2 inch in diameter large a-plane sapphire substrate using the continuous composition spread (CCS) PLD technique to fabricate a thin film with varying Al content ranging between $x = 0.13$ and $x = 0.84$. Laterally homogeneous α-$(Al_xGa_{1-x})_2O_3$ thin films exhibiting discrete Al contents are fabricated using radially segmented PLD targets on (11.0) Al_2O_3. Independent of the PLD technique, for $x \approx 0.55$, a change from relaxed to pseudomorphic growth is observed as confirmed by the evolution of in- and out-of-plane lattice constants. The crystal structure is studied depending on the cation composition by X-ray diffraction confirming the fabrication of epitaxial, corundum-structured thin films.

1. Introduction

During the last decade, ultrawide bandgap semiconductors and specifically the group-III sesquioxides attracted increasing scientific interest, especially monoclinic β-Ga_2O_3 triggered by demonstration of a Ga_2O_3 based metal–semiconductor field-effect transistor by Higashiwaki et al. in 2012.[1] Its exceptional material properties, such as a wide bandgap of 4.6–5.0 eV, a large Baliga's figure of merit, and a large breakdown field of 8 MV cm^{-1}[1] make Ga_2O_3 a viable candidate for next-generation power electronic devices. Further applications within solar-blind and quantum-well infrared photodetectors were proposed.[2–5] Apart from the well-studied and thermodynamic stable monoclinic β-gallia structure, Ga_2O_3 can crystallize in various polymorphs.[6] The second-most stable structure is the orthorhombic κ-phase, for which ternary PLD thin films were already reported.[7–11] The third-most stable polymorph is the rhombohedral α-phase.

In comparison to the β-polymorph, α-Ga_2O_3 has a trifle higher bandgap of 5.0–5.3 eV.[12–16] N-type conductivity can be achieved by an additional Sn-doping[17] enabling the preparation of highly rectifying Schottky barrier diodes.[17–19] Consequently, devices operating at high voltages with low on-resistance were already demonstrated.[13] As the corundum structure is the thermodynamically most stable phase of Al_2O_3, the growth of ternary $(Al,Ga)_2O_3$ is feasible without miscibility gap, potentially enabling bandgap engineering between 5.0 and 8.8 eV.[20] The rhombohedral unit cell exhibits six Ga_2O_3 formula units and has space group $R\bar{3}c$. Due to the smaller ionic radii of Al (0.57 Å) compared to that of Ga (0.62 Å), the lattice parameter a (c) can be increased from 4.7617 Å (12.995 Å) for α-Al_2O_3 to 4.9825 Å (13.433 Å)[21] for α-Ga_2O_3.

Successful fabrication of rhombohedral Ga_2O_3 was reported by mist chemical vapor deposition (CVD),[13,17,19,21–23] halide vapor phase epitaxy (HVPE),[14,16,24] metalorganic vapor phase epitaxy (MOVPE),[15] mist epitaxy,[19] and the sol–gel method,[12] whereas ternary α-$(Al_xGa_{1-x})_2O_3$ has been realized by mist CVD,[25–28] PLD,[29,30] and molecular beam epitaxy (MBE)[31] until now. As substrates, *a*-, *c*-, *m*-, or *r*-plane sapphire are possible to use. Typically, the rhombohedral structure forms under high pressures and/or temperatures.[13,32]

In this study, we present the growth of binary α-Ga_2O_3 and ternary α-$(Al_xGa_{1-x})_2O_3$ thin films by PLD using two different combinatorial approaches on a-sapphire. The binary α-Ga_2O_3 thin film was deposited utilizing a single Ga_2O_3 ceramic target. By means of a twofold azimuthally segmented target (Ga_2O_3/Al_2O_3) we created an α-$(Al_xGa_{1-x})_2O_3$ thin film with a laterally varying cation composition on a 2 inch in diameter wafer. The continuous composition spread approach (CCS-PLD) was introduced by von Wenckstern et al.[33] and the resulting cation gradient ranges between $x = 0.13$ and $x = 0.84$ as measured by energy-dispersive X-ray spectroscopy (EDX). The thin-film thickness was determined by spectroscopic ellipsometry and ranges between 230 and 280 nm across the wafer. Further laterally

A. Hassa, P. Storm, M. Kneiß, Dr. D. Splith, Dr. H. von Wenckstern, Prof. M. Lorenz, Prof. M. Grundmann
Felix-Bloch-Institut für Festkörperphysik
Universität Leipzig
Linnéstraße 5, Leipzig 04103, Germany
E-mail: anna.hassa@uni-leipzig.de

The ORCID identification number(s) for the author(s) of this article can be found under https://doi.org/10.1002/pssb.202000394.

DOI: 10.1002/pssb.202000394

homogeneous α-$(Al_xGa_{1-x})_2O_3$ thin films were grown utilizing radially segmented ceramic targets. The usage of such targets allows the creation of a discrete material library and in this case of $(Al_xGa_{1-x})_2O_3$ thin films with a well-defined Al content by changing the radial position of the laser spot.[34] As thin films with a laterally homogeneous, discrete cation composition can thereby be produced, samples fabricated using radially segmented targets are referred to as discrete cation composition samples (DCCS) in the following. Another application of this approach is the synthesis of a thin film having a vertically varying cation composition, and that is why this method is abbreviated with VCCS-PLD. Further information about the implemented PLD approaches can be found in ref. [35].

The rhombohedral crystal structure of the thin films was confirmed by X-ray diffraction (XRD) 2θ-ω scans. Furthermore, epitaxial growth as well as the *a*- and *c*-lattice constants were studied in dependence on the Al content by XRD reciprocal space map (RSM) measurements.

2. Results and Discussion

2.1. Chemical Composition

To identify the cation ratio of the 2 inch in diameter large $(Al_xGa_{1-x})_2O_3$ CCS–PLD thin film, EDX was conducted on 49 positions across the wafer. The measurement points are marked as black dots in **Figure 1**a; the composition between these data points was interpolated and the resulting cation ratio represented as false color map. Along the cation gradient direction, marked with a black arrow, additional EDX measurements were performed in 1 mm steps to obtain the spatial Al dependency with high lateral resolution as shown in Figure 1b. The Al incorporation covers a range of $0.13 \leq x \leq 0.84$.

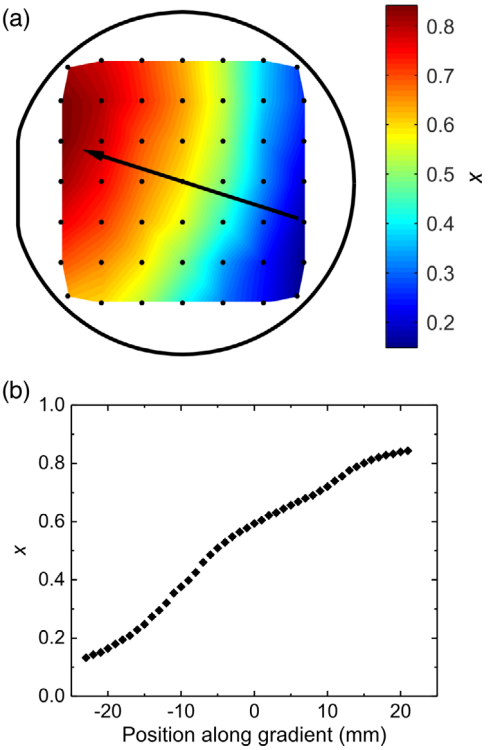

Figure 1. a) Cation composition at 49 points across the surface of an $(Al_xGa_{1-x})_2O_3$ thin film as determined from EDX. The measurement points are marked in the graph as black dots. The spaces between the measurement points were interpolated; the black arrow reveals the gradient direction. b) Al to Ga ratio *x* measured along the gradient direction by EDX.

2.2. Structural Analysis

The crystal structure of each sample was investigated by XRD. In **Figure 2**a, an exemplary 2θ-ω scan of the binary Ga_2O_3 thin film is presented and confirms the rhombohedral α-phase with reflection peaks at $2\theta = 35.96°$ and 76.35°, which can be assigned to the (110)- and (220)-lattice planes. The substrates reflection peaks appear at slightly higher angular positions of $2\theta = 37.80°$ and 80.52°. The XRD ϕ-scans of the asymmetric (113) reflection of the thin film as well as of the substrate confirm single crystalline, epitaxial growth without rotational domains as the reflections occur on the same ϕ-angles for layer and substrate.

To analyze the shift of the (110)- and (220)-lattice plane reflections with increasing Al content, 2θ-ω patterns were recorded every 1 mm along the cation gradient of the 2 inch long $(Al_xGa_{1-x})_2O_3$ thin film shown in Figure 1 and subsequently, the spatial positions were associated with the chemical composition shown in Figure 1b. The resulting false color map is presented in Figure 2c and reveals the crystallization in the rhombohedral phase in the entire investigated Al range. The angular positions of the (110)- and (220)-reflection peaks shift from $2\theta = 36.22°$ and 77.0° for $x = 0.13$ to $2\theta = 37.34°$ and 79.56° for $x = 0.84$, as expected, as the ionic radius of Al is smaller compared to that of Ga. For $x = 1$, the reflection peaks will potentially merge into the substrate peaks detected at $2\theta = 37.80°$ and 80.52°.

2.3. Lattice Constants

RSMs of the asymmetric (226)-reflex were measured as function of the ternary alloy composition to determine in-plane lattice constants as well. Exemplary RSMs of the CCS α-$(Al_xGa_{1-x})_2O_3$ sample are shown in **Figure 3** revealing relaxed growth for $x = 0.14$ and pseudomorphic growth for $x = 0.84$. To determine the transition point from relaxed to pseudomorphic growth as well as the behavior of the lattice constants, 25 RSMs were recorded on various positions along the thin-film gradient. Furthermore, RSMs of the binary Ga_2O_3 thin film as well as of the bare substrate were examined. Hence, the reflection peak positions were identified and are shown in **Figure 4**a in reciprocal space units ($q_{\parallel}$, $q_{\perp}$). The variation of the chemical composition is marked in false colors. Based on the reflection peak positions, the out-of-plane *a*- as well as the in-plane *c*-lattice constants were identified and shown in Figure 4b,c as a function of the Al content. In Figure 4b, the *a*-lattice constants of the lateral homogeneous α-$(Al_xGa_{1-x})_2O_3$ thin films deposited via the DCCS–PLD technique are included additionally. Based on the graphs shown in Figure 4, a distinction of three different

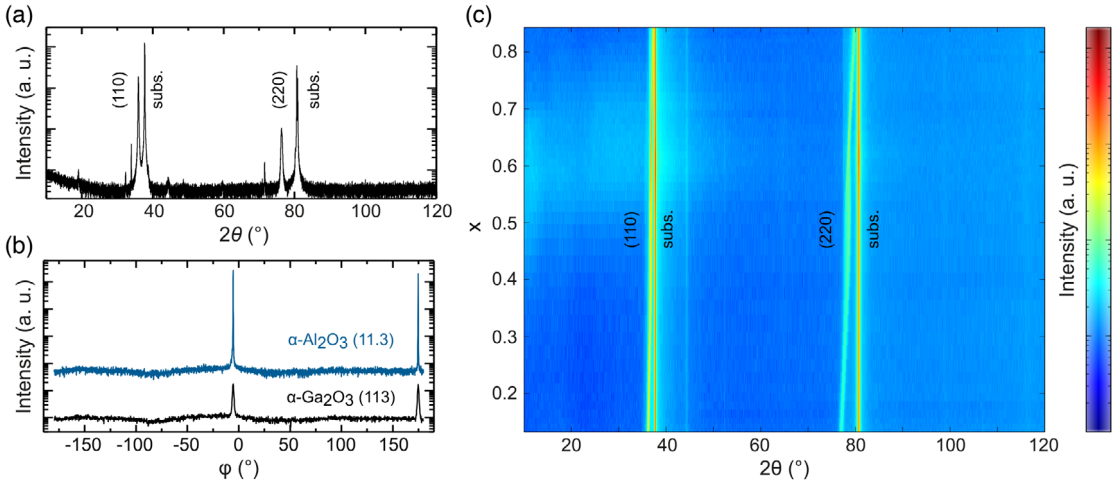

Figure 2. a) XRD 2θ-ω scan of an α-Ga_2O_3 thin film. b) XRD ϕ-scans of the skew-symmetric (113) reflection of the α-Ga_2O_3 layer and the a-plane substrate. c) 55 single 2θ-ω XRD scans presented as false color maps of the α-$(Al_xGa_{1-x})_2O_3$ thin film in dependence on the cation composition recorded along the composition gradient indicated in Figure 1a. Note, that the low-intensity peak at $2\theta = 44.48°$ is caused by the XRD sample holder and can be neglected.

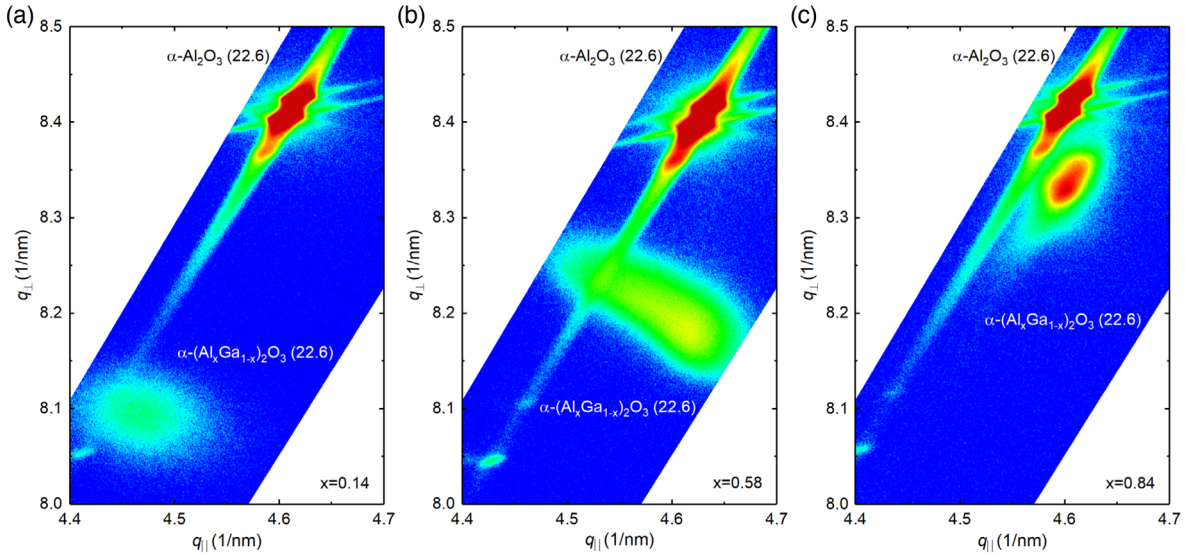

Figure 3. RSMs of the CCS wafer recorded in the vicinity of the α-Al_2O_3 (226) peak for Al contents of a) $x = 0.14$, b) $x = 0.58$, and c) $x = 0.84$.

cation regimes is suggested: 1) $0 \leq x \leq 0.55$, 2) $0.55 < x < 0.6$, and 3) $x \geq 0.6$.

In regime (1) the peak positions of the (226)-thin film reflection in reciprocal space increases along a straight connecting the α-Ga_2O_3 and α-Al_2O_3 binary endpoints indicating relaxed growth of the thin film on the substrate for regime (1). Here, the *a*- and *c*-constants both decrease nearly linearly. Linear fits of the lattice constants yields

$$a_{\text{bulk}}(x) = a_0 + x \cdot (a_1 - a_0) \quad (1)$$

and

$$c_{\text{bulk}}(x) = c_0 + x \cdot (c_1 - c_0) \quad (2)$$

with $a_0 = 4.9825$ Å and $c_0 = 13.433$ Å denoting the lattice constants of α-Ga_2O_3[21] as well as $a_1 = 4.759$ Å and $c_1 = 12.991$ Å of α-Al_2O_3.[36] The experimentally determined lattice constants of the binary sample are with $a = 4.976$ and $c = 13.455$ Å in excellent agreement with literature values.[21] In the second identified regime (2), the reflection peaks broaden strongly as observed in Figure 3b. The evaluation of the peak positions reveals that $q_\perp$ decreases slightly while $q_\parallel$ increases up to the value of binary α-Al_2O_3, indicating compressive in-plane stress of the lattice. Here, the α-$(Al_xGa_{1-x})_2O_3$ lattice adjusts in-plane to the substrate's lattice, which causes the rapid drop of *c* to approximately 12.99 Å, corresponding to the lattice constant of binary α-Al_2O_3. The rapid change is compensated out-of-plane by a small increase in *a*. For even higher Al contents ($x \geq 0.6$), the out-of-plane crystal

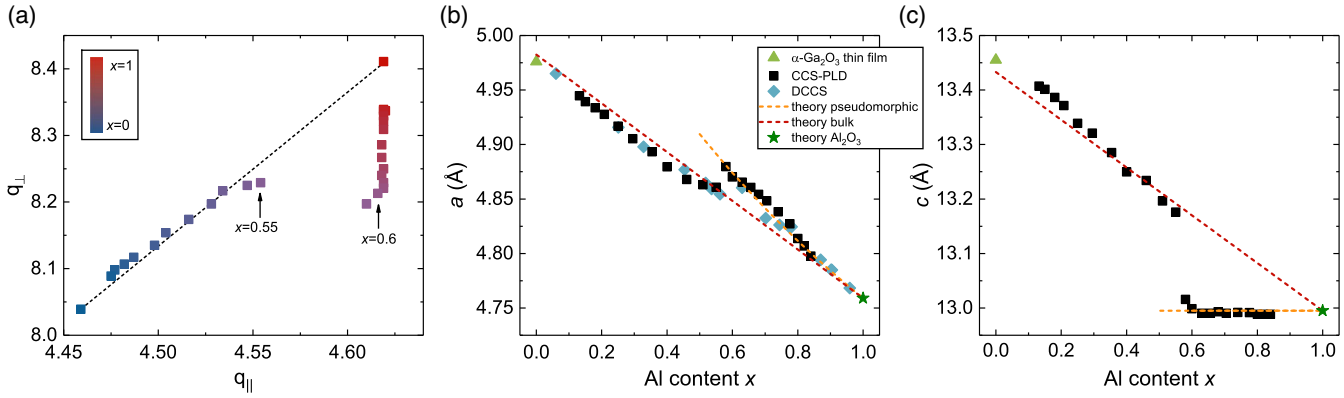

Figure 4. a) From RSM extracted (226) reflection peak positions of the binary and the CCS sample in reciprocal lattice units. The Al content is indicated by false colors. The dashed lines indicated the connection of the peak positions of binary α-Ga_2O_3 and α-Al_2O_3. b) Lattice constants a (out-of-plane) and c) c (in-plane) of α-$(Al_xGa_{1-x})_2O_3$ in dependence on the Al content x. The dashed lines represents the theoretical calculations for the bulk alloy (red) and pseudomorphic growth (orange). The black squares indicate the data received from the thin film deposited by CCS–PLD[33] and the blue diamonds indicate laterally homogeneous thin films with a DCCS grown using radially segmented targets. The light-green triangle represents the α-Ga_2O_3 thin film and the green star the theoretical value of binary Al_2O_3.

lattice contracts leading to an increasing $q_{\parallel}$ value, while $q_{\perp}$ remains constant. Thinking of lattice constants, this means that a decreases to the α-Al_2O_3 data point while c stays constant at around 12.99 Å. A change in relaxed to pseudomorphic growth with increasing Al content was also reported by Grundmann and Lorenz.[30] for α-$(Al_xGa_{1-x})_2O_3$ thin films on r-plane sapphire. Based on this study, the theoretical out-of-plane strain[30,37] given by

$$a = a_{\text{bulk}}\left(1 - \frac{C_{12}\varepsilon_a + C_{13}\varepsilon_c}{C_{11}}\right) \tag{3}$$

with $\varepsilon_a = a_1/a_{\text{bulk}} - 1$, $\varepsilon_c = c_1/c_{\text{bulk}} - 1$, and the elastic constants C_{11}, C_{12}, and C_{13} of the rhombohedral structure,[30] is included in Figure 4b coinciding with the experimental pseudomorphic out-of-plane a-lattice constants. The observable theoretical bowing is caused by the concentration dependence of the elastic constants and fits reasonably well with the experimental data.

The constants derived for the α-$(Al_xGa_{1-x})_2O_3$ thin films coincides for $0 \leq x \leq 0.55$ with literature values[25,28] and follow Vegard's law. The transition to pseudomorphic growth at around $x = 0.55$ is influenced by the thin-film thickness (here 240 nm) and will occur at higher Al concentrations for thicker thin films. In contrast to this current study, Ito et al., Dang et al., and Fujita et al. reported growth of relaxed α-$(Al_xGa_{1-x})_2O_3$ thin films in the entire composition range, pseudomorphic growth was not.[25,28,38] Grundmann et al. reported a similar transition composition for thin films in r-plane sapphire, which might be due to different relaxation mechanisms, e.g., for (01.2)-oriented thin films relaxation may occur via prismatic glide planes which is not possible for the (11.0)-oriented thin films discussed here.

3. Conclusion

In the present study, we investigated the growth as well as the evolution of the lattice parameters with varying Al content of α-$(Al_xGa_{1-x})_2O_3$ thin films. The samples were synthesized by different combinatorial PLD approaches on a-plane Al_2O_3 and the rhombohedral crystal structure was confirmed by XRD 2θ–ω measurements. RSMs reveal a change of relaxed to pseudomorphic growth for an Al content of $x = 0.55$. For $x \leq 0.55$ the out-of-plane a- and in-plane c-lattice constants decreases with increasing Al content following Vegard's law confirming relaxed growth. For the pseudomorphic thin films, the c-constant align at around 12.99 Å corresponding to α-Al_2O_3 and the out-of-plane a-lattice constant first increases step-like ($x \approx 0.6$) and decreases subsequently to the value of α-Al_2O_3.

4. Experimental Section

In this study, we investigated thin films deposited by using various combinatorial pulsed laser deposition (PLD) techniques. A Coherent LPX Pro 305 KrF excimer laser beam (248 nm) with an energy density of 2.6 J cm^{-2} on the target surface is utilized. The target-to-substrate distance is 10 cm. An α-Ga_2O_3 thin film was deposited at a growth temperature (T_g) of ≈640 °C and an oxygen pressure ($p(O_2)$) of 0.001 mbar using a single Ga_2O_3 (purity 99.999%, Alfa Aeser) ceramic target. Further lateral homogeneous thin films were deposited utilizing an elliptically segmented Ga_2O_3/$(Al_{0.4}Ga_{0.6})_2O_3$ (corresponds to Al contents of $x < 0.75$) or an $(Al_{0.4}Ga_{0.6})_2O_3$/Al_2O_3 ($x > 0.75$) target. The cation composition was varied by changing the radial position of the laser spot on the PLD target based on the VCCS–PLD technique.[34] The growth parameters are $T_g = 715$ °C and $p(O_2) = 0.0006$ mbar. As substrates 5 × 5 mm^2 large a-sapphire was used, 10 000 laser pulses were applied with a repetition rate of 10 Hz.

The ternary thin film obtaining a lateral varying cation composition was fabricated by using the CCS aproach for PLD.[33,35] The sample was grown at $T_g = 640$ °C and $p(O_2) = 0.006$ mbar on a 2 inch in diameter large a-sapphire wafer. For this purpose, a twofold segmented ceramic target consisting of one Ga_2O_3 segment and one Al_2O_3 (purity 99.997%, Alfa Aesar) segment was rotated simultaneously with the 2 inch in diameter large substrate. Both segments were additionally doped with 0.1 wt% SiO_2. The applied pulse number was 25 000 with a repetition rate of 10 Hz.

The chemical cation distribution of the 2 inch in diameter large wafer was determined by EDX using a FEI Nova Nanolab 200 equipped with an Ametek EDAX detector. XRD (2θ-ω, ϕ, RSM) measurements were conducted using a PANalytical X'pert PRO MRD diffractometer equipped

with a PIXcel^{3D} detector operating in 1D scanning line mode with 255 channels (for 2θ-ω scans), receiving slit mode (ϕ-scans), and fast 2D frame based mode (RSMs).

The thin-film thickness was deduced by spectroscopic ellipsometry using a dual rotating compensator ellipsometer (RC2, J.A. Woollam M2000) with a spot size of about $300 \times 500\,\mu m^2$.

Acknowledgements

The authors thank Monika Hahn for PLD target fabrication, Jörg Lenzner for EDX measurements, Chris Sturm for the determination of the thin film thickness, and Catharina Krömmelbein for the fabrication of a binary α-Ga_2O_3 thin film. This work was supported by European Social Fund within the Young Investigator Group "Oxide Heterostructures" (No. SAB 100310460) and partly by Deutsche Forschungsgemeinschaft in the Framework of Sonderforschungsbereich 762 "Functionality of Oxide Interfaces". A.H. and M.K. acknowledge the Leipzig School for Natural Sciences BuildMoNa. The authors acknowledge support from the German Research Foundation (DFG) and Universität Leipzig within the program of Open Access Publishing. Open access funding enabled and organized by Projekt DEAL.

Conflict of Interest

The authors declare no conflict of interest.

Keywords

combinatorial synthesis, pulsed laser deposition, X-ray diffraction, α-$(Al_xGa_{1-x})_2O_3$, α-Ga_2O_3

Received: July 17, 2020
Revised: September 18, 2020
Published online:

[1] M. Higashiwaki, K. Sasaki, A. Kuramata, T. Masui, S. Yamakoshi, *Appl. Phys. Lett.* **2012**, *100*, 013504.
[2] S. Stepanov, V. Nikolaev, V. Bougrov, A. Romanov, *Rev. Adv. Mater. Sci.* **2016**, *44*, 63.
[3] H. von Wenckstern, *Adv. Electron. Mater.* **2017**, *3*, 1600350.
[4] S. J. Pearton, J. Yang, P. H. Cary, F. Ren, J. Kim, M. J. Tadjer, M. A. Mastro, *Appl. Phys. Rev.* **2018**, *5*, 011301.
[5] Z. Liu, P.-G. Li, Y.-S. Zhi, X.-L. Wang, X.-L. Chu, W.-H. Tang, *Chin. Phys. B* **2019**, *28*, 017105.
[6] R. Roy, V. G. Hill, E. F. Osborn, *J. Am. Chem. Soc.* **1952**, *74*, 719.
[7] A. Hassa, H. von Wenckstern, D. Splith, C. Sturm, M. Kneiß, V. Prozheeva, M. Grundmann, *APL Mater.* **2019**, *7*, 022525.
[8] M. Kneiß, A. Hassa, D. Splith, C. Sturm, H. von Wenckstern, M. Lorenz, M. Grundmann, *APL Mater.* **2019**, *7*, 101102.
[9] P. Storm, M. Kneiß, A. Hassa, T. Schultz, D. Splith, H. von Wenckstern, N. Koch, M. Lorenz, M. Grundmann, *APL Mater.* **2019**, *7*, 111110.
[10] A. Hassa, C. Sturm, M. Kneiß, D. Splith, H. von Wenckstern, T. Schultz, N. Koch, M. Lorenz, M. Grundmann, *APL Mater.* **2020**, *8*, 021103.
[11] A. Hassa, C. Wouters, M. Kneiß, D. Splith, C. Sturm, H. von Wenckstern, M. Albrecht, M. Lorenz, M. Grundmann, *J. Phys. D: Appl. Phys.* **2020**, *53*, 48.
[12] G. Sinha, K. Adhikary, S. Chaudhuri, *J. Cryst. Growth* **2005**, *276*, 204.
[13] D. Shinohara, S. Fujita, *Jpn. J. Appl. Phys.* **2008**, *47*, 7311.
[14] Y. Oshima, E. G. Vllora, K. Shimamura, *Appl. Phys. Express* **2015**, *8*, 055501.
[15] V. Gottschalch, S. Merker, S. Blaurock, M. Kneiß, U. Teschner, M. Grundmann, H. Krautscheid, *J. Cryst. Growth* **2019**, *510*, 76.
[16] A. I. Pechnikov, S. I. Stepanov, A. V. Chikiryaka, M. P. Scheglov, M. A. Odnobludov, V. I. Nikolaev, *Semiconductors* **2019**, *53*, 780.
[17] K. Akaiwa, S. Fujita, *Jpn. J. Appl. Phys.* **2012**, *51*, 070203.
[18] M. Oda, R. Tokuda, H. Kambara, T. Tanikawa, T. Sasaki, T. Hitora, *Appl. Phys. Express* **2016**, *9*, 021101.
[19] K. Kaneko, S. Fujita, T. Hitora, *Jpn. J. Appl. Phys.* **2018**, *57*, 02CB18.
[20] S.-D. Mo, W. Y. Ching, *Phys. Rev. B* **1998**, *57*, 15219.
[21] M. Marezio, J. P. Remeika, *J. Chem. Phys.* **1967**, *46*, 1862.
[22] T. Kawaharamura, G. T. Dang, M. Furuta, *Jpn. J. Appl. Phys.* **2012**, *51*, 040207.
[23] R. Cuscó, N. Domènech-Amador, T. Hatakeyama, T. Yamaguchi, T. Honda, L. Artús, *J. Appl. Phys.* **2015**, *117*, 185706.
[24] Y. Oshima, K. Kawara, T. Shinohe, T. Hitora, M. Kasu, S. Fujita, *APL Mater.* **2019**, *7*, 022503.
[25] H. Ito, K. Kaneko, S. Fujita, *Jpn. J. Appl. Phys.* **2012**, *51*, 100207.
[26] S. Fujita, K. Kaneko, *J. Cryst. Growth* **2014**, *401*, 588.
[27] K. Kaneko, K. Suzuki, Y. Ito, S. Fujita, *J. Cryst. Growth* **2016**, *436*, 150.
[28] G. T. Dang, T. Yasuoka, Y. Tagashira, T. Tadokoro, W. Theiss, T. Kawaharamura, *Appl. Phys. Lett.* **2018**, *113*, 062102.
[29] M. Lorenz, S. Hohenberger, E. Rose, M. Grundmann, *Appl. Phys. Lett.* **2018**, *113*, 231902.
[30] M. Grundmann, M. Lorenz, *APL Mater.* **2020**, *8*, 021108.
[31] R. Kumaran, T. Tiedje, S. E. Webster, S. Penson, W. Li, *Opt. Lett.* **2010**, *35*, 3793.
[32] J. P. Remeika, M. Marezio, *Appl. Phys. Lett.* **1966**, *8*, 87.
[33] H. von Wenckstern, Z. Zhang, F. Schmidt, J. Lenzner, H. Hochmuth, M. Grundmann, *CrystEngComm* **2013**, *15*, 10020.
[34] M. Kneiß, P. Storm, G. Benndorf, M. Grundmann, H. von Wenckstern, *ACS Comb. Sci.* **2018**, *20*, 643.
[35] H. von Wenckstern, M. Kneiß, A. Hassa, P. Storm, D. Splith, M. Grundmann, *Phys. Status Solidi B* **2020**, *257*, 1900626.
[36] E. R. Dobrovinskaya, L. A. Lytvynov, V. Pishchik, *Sapphire: Material, Manufacturing, Applications*, Springer Science+Business Media, LLC **2009**.
[37] M. Grundmann, *J. Appl. Phys.* **2018**, *124*, 185302.
[38] S. Fujita, M. Oda, K. Kaneko, T. Hitora, *Jpn. J. Appl. Phys.* **2016**, *55*, 1202A3.

Correction to: Structural and elastic properties of α-$(Al_xGa_{1-x})_2O_3$ thin films on (11.0)Al_2O_3 substrates for the entire composition range

Anna Hassa Philipp Storm Max Kneiß Daniel Splith Holger von Wenckstern Michael Lorenz Marius Grundmann*

Felix Bloch Institute for Solid State Physics, Universität Leipzig, Linnéstraße 5, 04103 Leipzig, Germany

Due to a typo in our theoretical calculations of the pseudomorphic out-of-plane lattice constant a, the "theory pseudomorphic" curve (orange dashed line) in Figure 4b) of the original article[1] was unfortunately plotted incorrectly. We corrected our calculations and plotted the modified graph below, which replaces the original Figure 4b). This correction has no consequences on the results of this study or modifies the discussion of the behavior of the lattice constants and strain states of the layers.

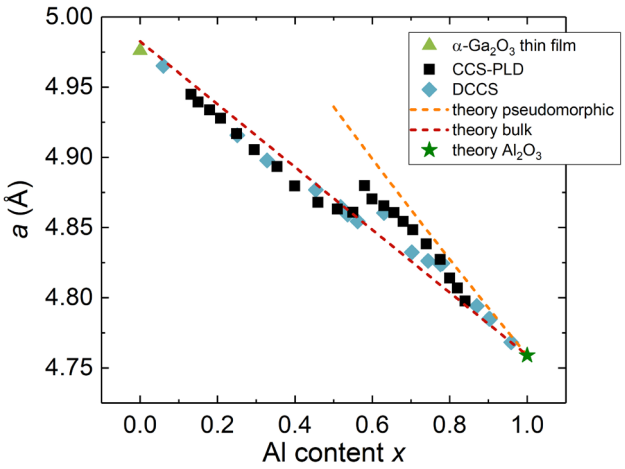

References

[1] Hassa *et al.*, physica status solidi (b), 2000394 (2020)

4.3 Progression of Group-III Sesquioxides: Epitaxy, Solubility and Desorption

The content of this section has been published in the following manuscript:

Reprinted from
A. Hassa, M. Grundmann and H. von Wenckstern:
Progression of Group-III Sesquioxides: Epitaxy, Solubility and Desorption, Journal of Physics D: Applied Physics, accepted manuscript (2020). Available under Public Licence (CC BY 3.0 licence) at:
doi:10.1088/1361-6463/abd4a4

Progression of Group-III Sesquioxides: Epitaxy, Solubility and Desorption

A. Hassa,[1] M. Grundmann,[1] and H. von Wenckstern[1]
Universität Leipzig, Felix-Bloch-Institut für Festkörperphysik, Linnéstraße 5, 04103 Leipzig, Germany

(Dated: 11th December 2020)

In recent years, ultra-wide bandgap semiconductors have increasingly moved into scientific focus due to their outstanding material properties, making them promising candidates for future applications within high-power electronics or solar-blind photo detectors. The group-III-sesquioxides can appear in various polymorphs, which influences, for instance, the energy of the optical bandgap. In gallium oxide, the optical bandgap ranges between 4.6 eV and 5.3 eV depending on the polymorph. For each polymorph it can be increased or decreased by alloying with aluminum oxide (8.8 eV) or indium oxide (2.7-3.75 eV), respectively, enabling bandgap engineering and thus leading to an extended application field. For this purpose, an overview of miscibility limits, the variation of bandgap and lattice constants as a function of the alloy composition are reviewed for the rhombohedral, monoclinic, orthorhombic and cubic polymorph. Further, the effect of formation and desorption of volatile suboxides on growth rates is described with respect to chemical trends of the discussed ternary materials.

I. INTRODUCTION

In the last decades, an increasing number of studies on ultra-wide bandgap semiconductors have been reported and more and more oxide semiconductors have come into focus. In this process a variety of publications and reviews on structural, optical and electrical properties of monoclinic β-Ga_2O_3 [1–5] appeared. Up to now, successful implementations of β-Ga_2O_3 based devices, such as high-power switches and transistors [2–4,6], solar-blind photo detectors [7], gas sensors [8], or thin film transistors [1], have been reported. The group-III-sesquioxides and their ternary alloys can crystallize in different crystal structures. The growth of the respective structure can be specifically influenced by the choice of growth parameters (e.g. substrate temperature, pressure, metal flux, etc.), substrate material and orientation, additional doping (e.g. tin for the orthorhombic polymorph), or others. The electrically insulating Al_2O_3 grows in thermodynamic equilibrium in a rhombohedral crystal lattice where it has a very large optical bandgap of 8.7-8.8 eV. Due to its optical transparency, high temperature and chemical stability, high mechanical strength [9] and its low cost industrial manufacturing capabilities, α-Al_2O_3 is used commonly as substrate material. Binary Ga_2O_3 can be synthesized in four different polymorphs identified as rhombohedral α-, monoclinic β-, defective spinel γ-, or orthorhombic κ-phase (also referred to as ε). Often a cubic δ-phase [10] is mentioned, but Playford *et al.* showed that this polymorph is just a nanocrystalline form of ε-Ga_2O_3 and not a distinct polymorph [11]. The monoclinic β-gallia structure is the thermodynamically most stable phase for which high-quality bulk single crystals are commercially available and hence most Ga_2O_3 based publications deal with the β-gallia polymorph. The remaining polymorphs are metastable and can change their structure at different transition temperatures, resulting in a ranking of their thermodynamical stability described by $\beta > \kappa > \alpha > \gamma$ [10]. Depending on the polymorph, the bandgap of Ga_2O_3 can range between 4.6-5.3 eV. The group-III sesquioxide with the smallest direct bandgap is In_2O_3 with 3.6-3.8 eV [12–14], which crystallizes in the cubic bixbyite structure in thermodynamical equilibrium.

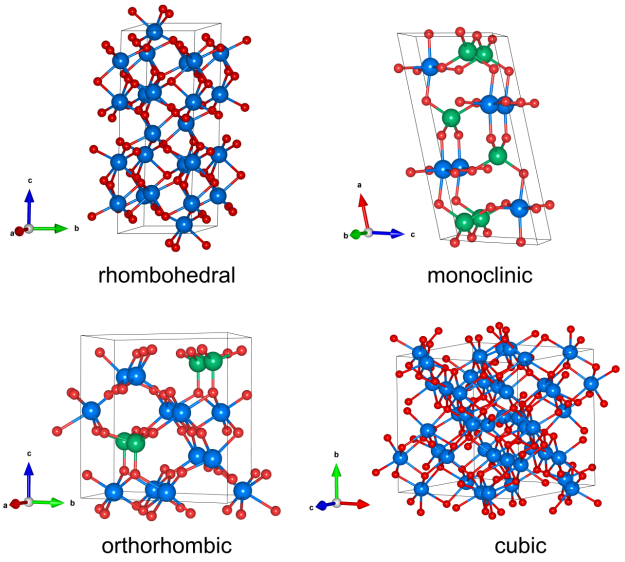

Figure 1. Ball-and-stick representation of the rhombohedral (corundum) α-, the monoclinic β-gallia, the orthorhombic κ-, and the cubic bixbyite crystal structure. The blue marked atoms denote the octahedral (O_h) and the green ones the tetrahedral (T_d) cation sites. The red atoms indicate the oxygen atoms. The structure models were created with VESTA [15].

Ball-and-stick models of the rhombohedral, monoclinic, orthorhombic and cubic polymorphs are presented in Fig. 1. In Tab. I the space groups, lattice constants and optical bandgap energies of the binary materials, originating in these polymorphs, are summarized.

The fabrication of Ga_2O_3 thin films can be realized by a variety of growth techniques such as mist chemical vapour deposition [17,24–31] (mist CVD), metal organic CVD [22,32–45] (MOCVD), halide vapour phase epitaxy [46–56] (HVPE), metalorganic vapour phase epitaxy [57–59] (MOVPE), pulsed laser deposition [57,60–69] (PLD), molecular beam epitaxy [57,70–76] (MBE), atomic layer deposition [77–79] (ALD), mist epitaxy,[80], the sol-gel method [81], and magnetron sputtering [82]. Be-

Table I. Space group, lattice parameter and optical bandgap for various binary polymorphs of the group-II sesquioxides.

Structure	Space group	Polymorph	Lattice constants	Optical bandgap
rhombohedral	$R\bar{3}c$	α-Al_2O_3	$a = 4.7617$ Å [16] $c = 12.995$ Å [16]	8.7-8.8 eV
		α-Ga_2O_3	$a = 4.9825$ Å [17] $c = 13.433$ Å [17]	5.2-5.3 eV
		α-In_2O_3	$a = 5.487$ Å [18] $c = 14.510$ Å [18]	3.7 eV
monoclinic	$C2/m$	θ-Al_2O_3	$a = 11.854$ Å [19] $b = 2.904$ Å [19] $c = 5.622$ Å [19] $\beta = 103.83°$ [19]	no exp. values
		β-Ga_2O_3	$a = 12.214$ Å [20] $b = 3.037$ Å [20] $c = 5.798$ Å [20] $\beta = 103.83°$ [20]	4.6-5.0 eV
orthorhombic	$Pna2_1$	κ-Al_2O_3	$a = 4.8437$ Å [21] $b = 8.3300$ Å [21] $c = 8.9547$ Å [21]	no exp. values
		κ-Ga_2O_3	$a = 5.046$ Å [22] $b = 8.702$ Å [22] $c = 9.283$ Å [22]	4.9 eV
cubic	$Ia3$	c-In_2O_3	$a = 10.117$ Å [23]	3.75 eV

sides, crystalline β-Ga_2O_3 bulk crystals can be grown by floating-zone (FZ) [83–85], the edge-defined film-fed growth (EFG) [86], the Czochralski (CZ) [87,88], the Verneuil [89,90] and the flux [20,91–93] methods. In studies about In_2O_3, the semiconductor was inter alia fabricated by MOCVD [94–96], PLD [97–101], MBE [102–107], or sputtering [108–110]. The growth of bulk In_2O_3 from melt was developed and described by the IKZ Berlin [111]. The growth techniques of the ternary alloys used for $(Al,Ga,In)_2O_3$ are summarized for the α-, β-, κ- and cubic bixbyite phase in Tab. II.

In the present work we review the dependencies of lattice constants and optical bandgaps as a function of the alloy composition of the rhombohedral, monoclinic, orthorhombic, and cubic group-III-sesquioxide polymorphs. The review contains published data as well as own results that we obtained on our thin films grown by PLD. Furthermore, we point out how formation and desorption of volatile suboxides influence the cation composition and under which growth conditions in the PLD chamber desorption can be suppressed. In the course of this, we present thin films with a lateral varying composition, including a short description of the combinatorial PLD approach used.

II. COMBINATORIAL THIN FILM SYNTHESIS

Investigations of entire mixtures of ternary solid-solutions within a single thin film sample of ternary $(Al,Ga)_2O_3$ or $(In,Ga)_2O_3$ is possible by employing a composition spread approach, e.g., by pulsed laser deposition (PLD). A combinatorial PLD thin film synthesis was introduced by the semiconductor physics group of the Universität Leipzig (UL) [148], which allows the growth of thin films that exhibit a lateral variation of the cation composition. For a thin film with a compositional gradient, a two-fold segmented target has to be utilized. A synchronized rotation speed of target and substrate used in the PLD chamber is a precondition for our approach. The geometric arrangement of target and substrate influences the cation composition as described in detail in Ref. 149.

In general, these thin films were synthesized by employing a KrF excimer laser (248 nm) with an energy density of 2.6 Jcm^{-2} on the target surface. The ceramic targets used are composed of one half of Ga_2O_3 (purity 99.999%, Alfa Aeser) and one half of Al_2O_3 (purity 99.997%, Alfa Aeser) or In_2O_3 (purity 99.994%, Alfa Aeser), respectively. In addition, the segments can be doped, e.g. to induce electrical conductivity or to stabilize the growth of the κ-phase [69,76] (tin doping is decisive). The target material is ball-milled and the homogenized powders are sintered in air and high temperatures between 1150 and 1350°C for 72 h. 2 in. diameter c-plane sapphire substrates are placed in a heatable substrate holder located at a distance of 10 cm opposite to the target. The lateral offset between laser spot position on the target and the substrate center is 16-17 mm. Besides the oxygen pressure, the growth temperature in the PLD chamber can be adjusted. Further details on our growth facilities are summarized in Ref. 150. The pulse repetition number of the samples discussed ranges between 25000 and 30000 at a pulse frequency of 10 Hz.

The cation distribution was determined by energy-dispersive X-ray spectroscopy (EDX) using a FEI Nova Nanolab 200 equipped with an Ametek EDAX detector. The crys-

Table II. Growth methods and highest reported cation incorporation for rhombohedral, monoclinic, orthorhombic, and cubic polymorphs of $(Al,Ga,In)_2O_3$ alloys.

Polymorph	Growth method	Reported alloy range
α-$(Al_xGa_{1-x})_2O_3$	mist CVD [112–115], PLD [116–118], MBE [119]	entire composition range
α-$(In_yGa_{1-y})_2O_3$	mist CVD [113,120,121]	$y \leq 0.08$, $y \geq 0.67$ [120]
β-$(Al_xGa_{1-x})_2O_3$	PLD [122–125], MBE [126–129], sputtering [130]	$x \leq 0.61$ [128]
β-$(In_yGa_{1-y})_2O_3$	MOCVD [131], PLD [101,132–135], MBE [71,75,136], sol gel method [137]	$y \leq 0.35$ [138]
κ-$(Al_xGa_{1-x})_2O_3$	mist CVD [139], PLD [140–142]	$x \leq 0.65$ [140]
κ-$(In_yGa_{1-y})_2O_3$	mist CVD [143], PLD [144,145]	$y \leq 0.35$ [144]
c-$(Ga_zIn_{1-z})_2O_3$	MOCVD [146,147], PLD [132,134], MBE [138], sol-gel method [137]	$z \leq 0.5$ [146,147]

tal structure was identified by XRD 2θ-ω scans conducted with a PANalytical X'pert PRO MRD diffractometer equipped with a PIXcel^{3D} detector with 255 channels operating in 1D scanning line mode. The thin film thickness (d) was determined by spectroscopic ellipsometry employing a dual rotating compensator ellipsometer (RC2, J.A. Woollam M2000) with a spot size of about $300 \times 500\,\mu m^2$. Then the growth rate r was calculated by dividing d by the number of pulses during deposition.

III. FORMATION AND DESORPTION OF VOLATILE SUBOXIDES

In several publications the influence of growth conditions on growth rates (r) during deposition of Ga_2O_3 and its ternary alloys with In or Al was studied systematically. The investigations revealed that under high growth temperatures (T_g) and oxygen-poor growth conditions volatile suboxides forms and desorbs leading to lower r and that in ternary alloys a non-stoichiometric incorporation of the provided cations into the thin film can be observed.

Vogt *et al.* examined the influence of the O- and Me-fluxes (Me = Ga, In) ratio for binary Ga_2O_3 and In_2O_3, respectively, during MBE growth [73,136]. In Ga_2O_3 for oxygen-rich conditions the growth rates are determined by the offered metal flux and no desorption of cation species was observed, which leads to the assumption that all metal atoms are incorporated into the thin film layer. In a oxygen-poor regime volatile Me_2O suboxides are formed, which were not incorporated into the thin film. Consistent studies of PLD grown Ga_2O_3 thin films also revealed the influence of oxygen pressure ($p(O_2)$) and growth temperature on the growth rate. Lower growth rates are observed for decreasing oxygen pressure [65] or increasing growth temperatures,[66], respectively.

In the ternary alloys $(Al,Ga)_2O_3$ and $(In,Ga)_2O_3$ the desorption of volatile suboxides manifests itself in such a way that, besides decreasing r, the cation ratio of Al to Ga or In to Ga is altered. For PLD grown $(Al,Ga)_2O_3$ thin films a high growth temperature and/or low oxygen pressure result in lower r and higher Al incorporation into the layer [123,124,142,151]. Due to the lower dissociation energy of the Ga-O bond compared to the Al-O bond, in an oxygen poor regime Ga atoms form volatile sub-oxides being desorbed, which leads to a preferential incorporation of the Al atoms. In the $(In,Ga)_2O_3$ alloy desorption of volatile suboxides can be observed, too [131,136]: the Ga atoms are preferentially incorporated on account of the higher dissociation energy of the Ga-O bond compared to the In-O bond. In addition, a metal-exchange has to be taken into account for this alloy. In $(In,Ga)_2O_3$ the Ga atoms etches already existing In-O bonds and then replace In [136]. As a result, the released In atoms form either droplets on the thin film surface at low T_g or will be desorbed as In_2O suboxide at high T_g, leading to a further reduction of the In incorporation as well as lower growth rates[136]. To investigate systematically the influence of $p(O_2)$ on $(Al,Ga)_2O_3$ and $(In,Ga)_2O_3$, CCS-PLD thin films grown with well-defined lateral variation of the cation flux at a constant temperature of 640°C and either an oxygen poor regime of $p(O_2) = 0.0003$ mbar or an oxygen rich regime of $p(O_2) = 0.01$ mbar on c-plane sapphire were studied. The composition gradients were determined by EDX and the resulting Al and In contents in terms of the gradient position are presented in Fig. 2. Position 0 indicates the center of the wafer and the gray solid lines, the calculated model curve of the CCS-PLD approach [149].

For oxygen rich conditions, the spatial resolution of the alloy composition fits quite well to the model curve, which indicates a stoichiometric target-to-layer transfer with growth rates between 9 and 10 pm/pulse for all Al contents and low In content ($y = 0.1$). For higher y the growth rates range between 12.9 and 13.8 pm/pulse as visible in Fig. 3. In an oxygen poor regime a strong deviation from the stoichiometric cation incorporation in $(Al,Ga)_2O_3$ and $(In,Ga)_2O_3$, respectively, can be observed as well as a strong decrease in growth rates. For the $(Al,Ga)_2O_3$ sample the Al content increases suddenly in the first quarter from 45 at.% to around 80 at.% and increases in the last three quarters slightly up to 99 at.%. The narrow Al valley at position -14/-13 is caused by phase separation, which is not within the scope of this work for which reason this is not discussed further. A similar behaviour is given for the $(In,Ga)_2O_3$ sample: for oxygen poor conditions the In content increases in the first three quarters only up to approximately 20 at.% and jumps in the last quarter up to 80 at.% (see Fig. 2).

The strong non-stoichiometric cation incorporation is caused by the low supply of oxygen atoms during growth leading to the formation and subsequent desorption of volatile sub-

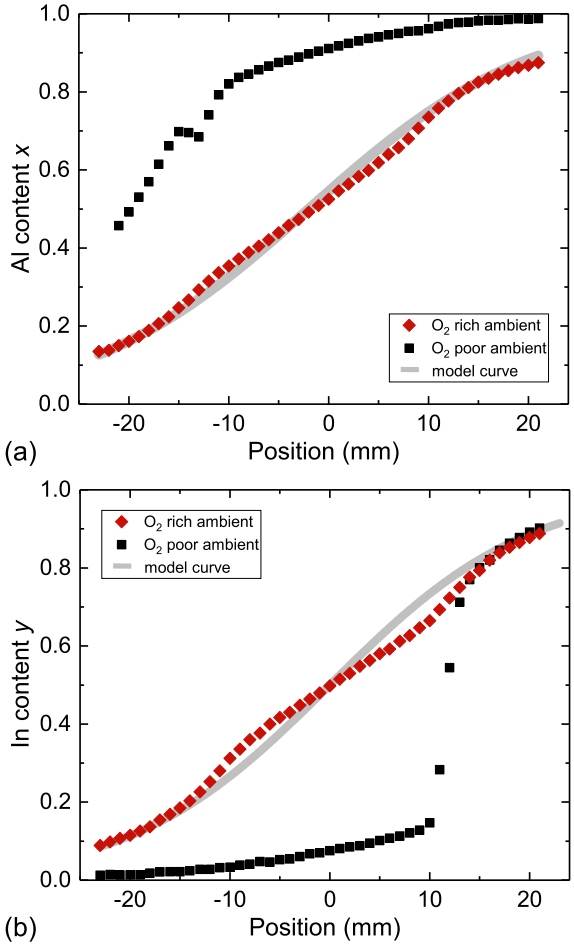

Figure 2. (a) Al cation ratio x and (b) Al cation ratio y recorded along the gradient direction of CCS-PLD $(Al_xGa_{1-x})_2O_3$ and $(In_yGa_{1-y})_2O_3$ thin films on c-sapphire substrates. The growth temperature of each sample was around 640°C and the oxygen regimes are indicated in the graphs.

oxides, which can be further approved by the low grates being $\approx 6-7$ pm/pulse below the values of the oxygen rich samples. The growth rates of the $(In,Ga)_2O_3$ sample in the oxygen regime increases with increasing In content, which is caused on the one hand by the higher ionic radii of In compared to Ga and on the other hand by a kinetically favored formation of In_2O_3 leading to a faster reaction with O_2 and thereby to higher r.

Interestingly, the cation ratio of the $(In_xGa_{1-x})_2O_3$ thin film fits in the last quarter ($y > 0.6$) with the model curve due to an observable phase separation to the cubic bixbyite phase (for further details see Ref. 132), which allows the assumption that despite formation and desorption of volatile suboxides, both, Ga and In, are incorporated stoichiometrically in this phase.

In summary, it has been shown in this part that in the $(In,Ga)_2O_3$ alloy mainly In_2O forms and desorbs, why proportionately more Ga atoms are detected in the layer. Against it, in the $(Al,Ga)_2O_3$ alloy the significantly higher Al incorporation is due to a stronger Ga_2O formation and desorption.

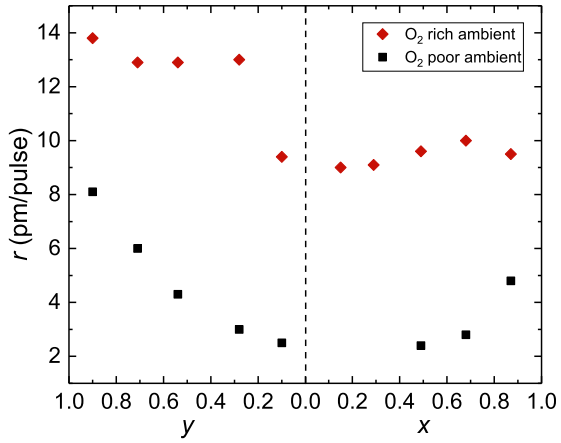

Figure 3. Growth rates r for different cation compositions of $(Al_xGa_{1-x})_2O_3$ and $(In_yGa_{1-y})_2O_3$ thin films grown on c-plane sapphire at 640°C and oxygen rich ($p(O_2) = 0.01$ mbar) or poor ($p(O_2) = 0.0003$ mbar) conditions, respectively.

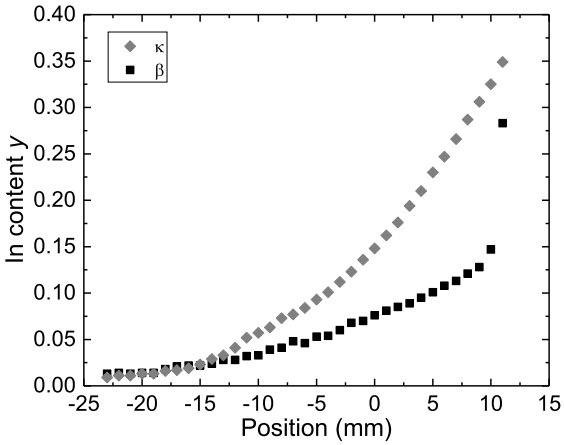

Figure 4. In content y in terms of the spatial location on the wafer for a β- and a κ-$(In_yGa_{1-y})_2O_3$ thin film on c-plane sapphire. Both thin films were deposited in an oxygen poor regime ($p(O_2) = 0.0003$ mbar) at $T_g = 640$°C.

Studies of the influence of T_g and $p(O_2)$ on β- and κ-$(Al,Ga)_2O_3$ thin films, published in Ref. 142,151, demonstrate that desorption occurs for both polymorphs. A direct comparison showed that the formation and desorption of volatile suboxides is stronger in the monoclinic alloy, resulting in an increased Al incorporation in the layer under same growth conditions. A potential reason for the slightly suppressed desorption in the orthorhombic polymorph is surfactant-mediated growth. An additional tin supply during growth, both for PLD and MBE, is necessary to synthesize orthorhombic thin films [69,76]. Tin acts as a surfactant in the growth process and is not incorporated into the thin film [69,141].

Figure 4 presents β- and κ-$(In,Ga)_2O_3$ thin films grown at $T_g = 640$°C and oxygen poor conditions ($p(O_2) = 0.0003$ mbar). The κ-$(In,Ga)_2O_3$ thin film was already discussed in Ref. 144 and a comparable β-$(In,Ga)_2O_3$

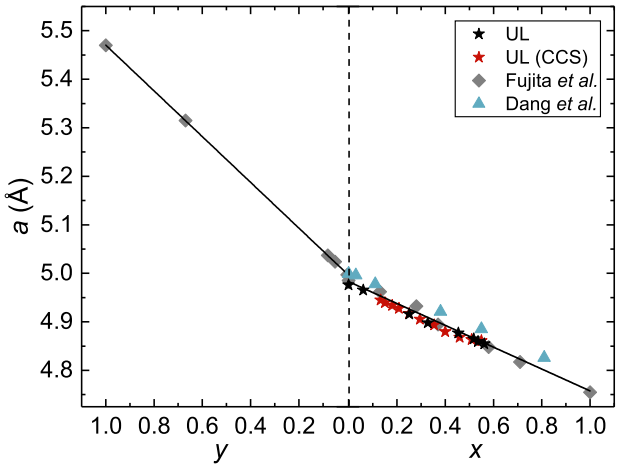

Figure 5. Lattice constant a of α-$(In_yGa_{1-y})_2O_3$ and α-$(Al_xGa_{1-x})_2O_3$ as a function of the alloy composition. The data was taken from Hassa *et al.* [118], Fujita *et al.* [113] and Dang *et al.* [115]. Recent data from our PLD thin films are shown by star-shaped (for lateral homogeneous thin films) or diamond-shaped (for CCS-PLD) markers and are denoted by UL.

thin film in Ref. 132 by the University of Leipzig (UL). The β-phase crystallized up to approximately $y = 0.28$ and the κ-phase up to $y = 0.35$. For higher In contents phase separation proceeds to the hexagonal InGaO (II) as well as to the cubic $(Ga,In)_2O_3$ phase (crystal structure determined by X-ray diffraction [132,144]). From position -23 to -12, the increase of y of both polymorphs is equal. After this point it can be observed that the content gap of y becomes larger with ongoing positions. At position 11 the gap is $\Delta y = 0.17$, which indicates a more extensive formation and desorption of volatile suboxides in the β-phase.

IV. CRYSTAL STRUCTURE

The group-III sesquioxides (Al_2O_3, Ga_2O_3 and In_2O_3) have different ground state crystal structures, namely the rhombohedral corundum, the monoclinic β-gallia and the cubic bixbyite structure, respectively. The rhombohedral corundum-structure has been reported as the only polymorph for all of the group-III sesquioxides and hence it should in principle be possible to stabilize the α-phase throughout the entire composition range [121]. Phase separation in the $(Al,Ga,In)_2O_3$ alloys is expected for all other polymorphs. The miscibility gap will likely depend on the polymorph considered. In Tab. II the actual reported maximum cation compositions of the thermodynamically most stable polymorphs are shown. Since Al, Ga and In have different ionic radii the lattice constants will change within ternary alloys. An incorporation of Al into Ga_2O_3 leads to decreasing lattice parameters, while In incorporation causes an increase. The cation sites have a coordination number of 4 or 6 depending on the distinct polymorph. The ratio and arrangement of the octahedral (O_h) or tetrahedral (T_d) lattice sites differs in the polymorphs discussed below and is distinguished by color in Fig. 1.

A. Rhombohedral crystal structure

In the corundum structure (space group $R\bar{3}c$) all Me^{3+} (Me = Al, Ga, In) cations occupy O_h lattice sites and grow within a hexagonal close-packed O^{2-} array. The unit cell presented in Fig. 1 contains six Me_2O_3 formula units with the space group $R\bar{3}c$. As indicated, all group-III-sesquioxides can be synthesized in the rhombohedral structure and alloying in the whole composition range should be possible as observed for α-$(Al_xGa_{1-x})_2O_3$. It is interesting that so far In in α-Ga_2O_3 has only been reported up to 8 at.%, while Ga has been incorporated up to 33 at.% into α-In_2O_3 [120]. The pseudo-hexagonal lattice constants (a/c) in the corundum-structured $(Al,Ga,In)_2O_3$ thin films range between $a = 4.7617$ Å / $c = 12.995$ Å [113] for Al_2O_3, $a = 4.9825$ Å / $c = 13.433$ Å for Ga_2O_3 [17], and $a = 5.487$ Å / $c = 14.510$ Å for In_2O_3 [18]. Figure 5 presents the evolution of the a-lattice constant as a function of the composition for relaxed thin films [113,115,118], which follow Vegard's law. The linear fit of the a-lattice constant can be found in Tab. III. The slope in β-$(In_yGa_{1-y})_2O_3$ is much higher than for β-$(Al_xGa_{1-x})_2O_3$ due to a higher relative percentage difference in the atomic radii of In with respect to Ga (14% larger) compared to Al to Ga (6.5% smaller).

B. Monoclinic β-gallia crystal structure

Monoclinic β-Ga_2O_3 belongs to space group $C2/m$ [20] and the unit cell is formed by four Ga_2O_3 molecules, where the Ga atoms occupy either the O_h or the T_d lattice site with a ratio of 1:1. By alloying β-Ga_2O_3 with In or Al, these cations prefer the O_h lattice sites [92,154]. After Al has occupied all O_h lattice sites (50 at.%), the T_d lattice sites are then also occupied [154]. There exist three possibilities of connections between the octahedrally and tetrahedrally ordered cations. In the [010]-direction the T_d are connected with each other as well as the O_h. The O_h are also connected along the [102]-direction. In the remaining directions, there exists only linkings between the T_d and O_h cation sites [156]. The oxygen atoms can occupy three different lattice sites, two of them, namely O(1) and O(2), are threefold and O(3) is fourfold coordinated.

Since only Ga_2O_3 crystallizes in the β-phase, the solubility of Al and In in this structure is limited. The highest reported Al content in β-$(Al_xGa_{1-x})_2O_3$ thin films is $x = 0.61$ [128] and $x = 0.78$ in ceramic samples [157]. The maximum In incorporation into β-$(In_yGa_{1-y})_2O_3$ thin films is $y = 0.35$ [71] and $y = 0.44$ [23] in ceramic samples. The lattice constants of β-Ga_2O_3 are $a = 12.214$ Å, $b = 3.037$ Å, $c = 5.798$ Å and $\beta = 103.83°$ [20]. Figure 6 presents published lattice parameters of monoclinic $(Al,Ga)_2O_3$ and $(In,Ga)_2O_3$ alloys as a function of the Al or In content, respectively [23,92,137,152,154,155]. The data points exhibit a linear dependency and thus follow Vegard's law. The fits of each lattice parameter are shown in Tab. III. Interestingly, for $x = 0$ the lattice constants are in close agreement with the values of binary β-Ga_2O_3, while for

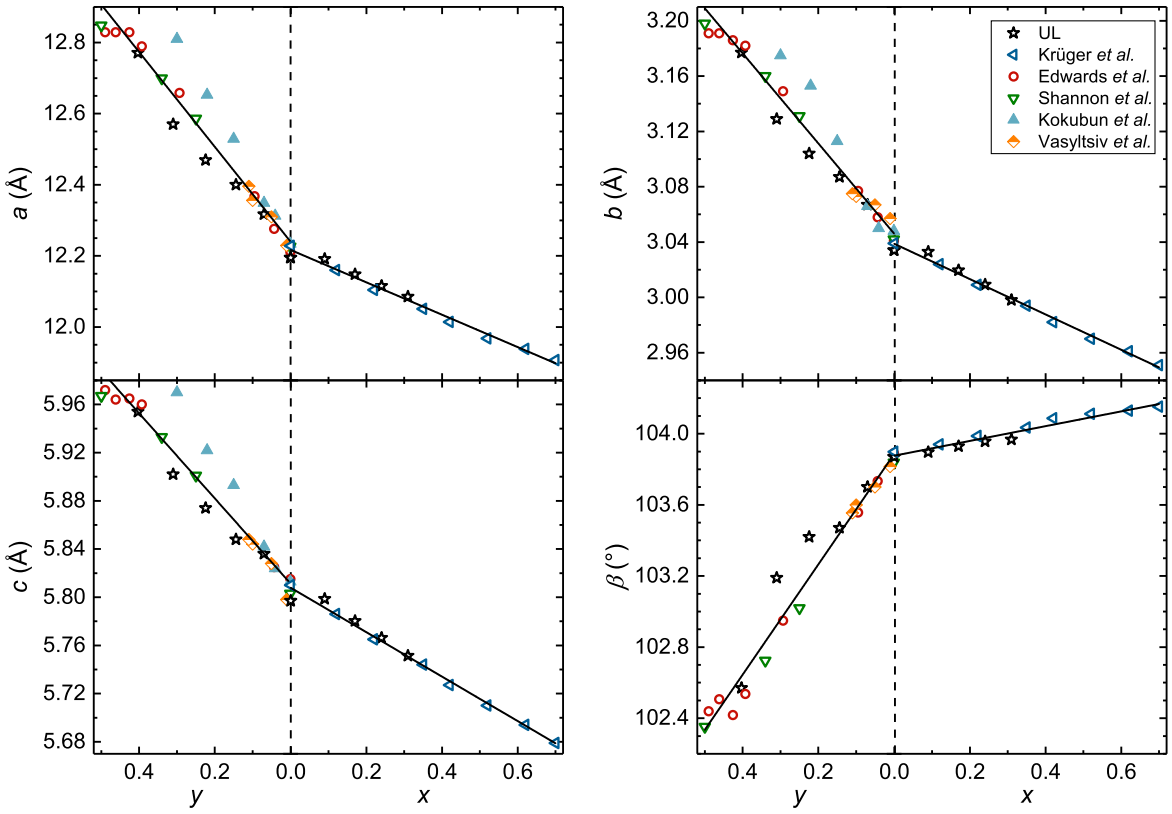

Figure 6. Lattice constants a, b, c and β in dependence on the cation composition for monoclinic β-$(In_yGa_{1-y})_2O_3$ and β-$(Al_xGa_{1-x})_2O_3$. Literature data were compiled for powder samples (Kranert [152,153], Krüger [154], Edwards [23], Shannon [92]), thin films (Kokubun [137]) and bulk crystals (Vasyltsiv [155]). The Recent data from our PLD thin films are shown by star-shaped markers and are denoted by UL.

$y = 0$ the lattice constants a, b and c are 1 to 1.7% higher. The angle β is for both alloys the same of about 103.88° fitting well to the binary value of 103.83° [20]. Extrapolations to $x = 1$ show a close agreement of the lattice parameters with those of monoclinic θ-Al_2O_3, with the exception of the lattice parameter β, which should be nearly identical for both materials.

C. Orthorhombic crystal structure

In the orthorhombic structure the T_d to O_h coordinated cations exhibit a ratio of 1:3 and are formed by six molecules in space group $Pna2_1$. Often the orthorhombic polymorph of Ga_2O_3 is also denoted as ε-phase. Since some literature, probably Cora or Kneiß *et al.*, the isostructurality to κ-Al_2O_3 demonstrated, the orthorhombic polymorph is named κ and not ε [22,69]. The Me^{3+} cations can be arranged as pure O_h or mixed T_d and O_h layer along the [001]-direction or as zig-zag ribbons consisting of edge-shared O_h and corner-shared T_d layers [21,22]. The oxygen atoms arrange themselves as an ABAC pseudo-close-packed stacking [21].

Since the Al_2O_3 can form an orthorhombic lattice, the whole composition range of κ-$(Al_xGa_{1-x})_2O_3$ should be feasible. Actually the highest reported Al content on c-sapphire substrates is $x = 0.46$ [141], which can be significantly increased

Table III. Dependence of the lattice constants of rhombohedral, monoclinic, orthorhombic, and cubic $(Al,Ga,In)_2O_3$ thin films on the cation incorporation. The equations represent the linear fittings from Fig. 5, Fig. 6, Fig. 7 and Ref. 23,158,159.

Material	Lattice parameter
α-$(Al_xGa_{1-x})_2O_3$	$a(x) = (4.983 - 0.225x)$ Å
α-$(In_yGa_{1-y})_2O_3$	$a(y) = (4.999 + 0.471y)$ Å
β-$(Al_xGa_{1-x})_2O_3$	$a(x) = (12.217 - 0.455x)$ Å
	$b(x) = (3.039 - 0.128x)$ Å
	$c(x) = (5.808 - 0.184x)$ Å
	$\beta(x) = (103.88 + 0.415x)$ Å
β-$(In_yGa_{1-y})_2O_3$	$a(y) = (12.241 + 1.332y)$ Å
	$b(y) = (3.046 + 0.325y)$ Å
	$c(y) = (5.812 + 0.353y)$
	$\beta(y) = (103.88 - 3.098y)$ Å
κ-$(Al_xGa_{1-x})_2O_3$	$c(x) = (9.274 - 0.347x)$ Å
κ-$(In_yGa_{1-y})_2O_3$	$c(y) = (9.268 + 1.121y)$ Å
c-$(Ga_zIn_{1-z})_2O_3$	$a(z) = (10.113 - 0.803z)$ Å

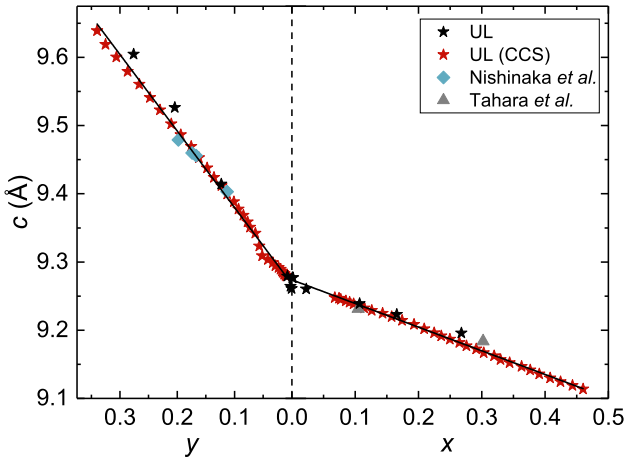

Figure 7. Lattice constant c of κ-$(In_yGa_{1-y})_2O_3$ and κ-$(Al_xGa_{1-x})_2O_3$ as a function of the alloy composition. The data was taken from: Hassa *et al.* [141,144], Kneiß *et al.* [145], Nishinaka *et al.* [143], Tahara [139], and Storm *et al.* [140].

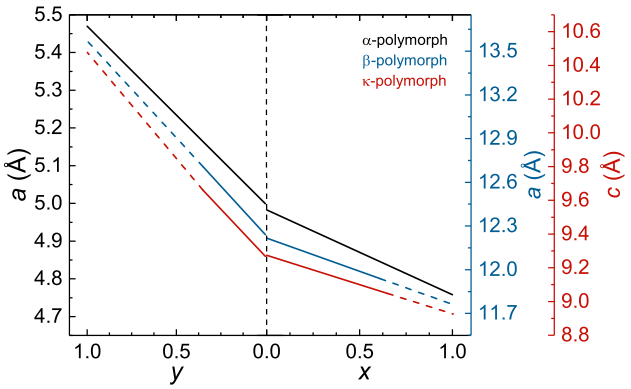

Figure 8. Lattice constants of the rhombohedral, monoclinic and orthorhombic polymorph of $(Al_xGa_{1-x})_2O_3$ and $(In_xGa_{1-x})_2O_3$ as function of the alloy composition. The graphs are based on the equations depicted in Tab. III. The solid lines mark the maximum experimental cation ratio and the dashed lines are extrapolated to Al_2O_3 ($x = 1$) and In_2O_3 ($y = 1$).

up to $x = 0.65$ using a κ-Ga_2O_3 buffer layer between substrate and thin film [140]. For κ-$(In_yGa_{1-y})_2O_3$ on c-sapphire a maximum In incorporation of $x = 0.35$ [144] was realized, up to now.

The lattice constants for κ-Al_2O_3 are identified to be $a = 4.8437$ Å, $b = 8.3300$ Å and $c = 8.9547$ Å [21] and for κ-Ga_2O_3 as $a = 5.046$ Å, $b = 8.702$ Å and $c = 9.283$ Å [22]. The influence of the Al content [139–141] or rather In content [143–145] on the lattice parameter c is presented in Fig. 7. As for the monoclinic alloys causes the Al (In) incorporation a linear decrease (increase) of c according to Vegard's law. Linear fittings of the experimental values results in the equations listed in Tab. III. Assuming again $x = 0$ and $y = 0$, c fits well with the experimental result of binary κ-Ga_2O_3. By extrapolating the lattice constant up to $x = 1$, 8.927 Å is obtained being in close agreement with binary κ-Al_2O_3 [21], too.

Table IV. Linear fits of the optical bandgaps in dependence on the Al incorporation x or In content y for the α-, β-, κ- and cubic phase of $(Al,Ga,In)_2O_3$. The data are taken for α from Ref. 112,115, for β from Ref. 122,133,134,137,155,160,161, and for κ from Ref. 139–141,143–145.

Material	Bandgap (eV)
α-$(Al_xGa_{1-x})_2O_3$	$E_g(x) = 5.25 + 3.31x$
β-$(Al_xGa_{1-x})_2O_3$	$E_g(x) = 4.98 + 1.56x$
β-$(In_yGa_{1-y})_2O_3$	$E_g(y) = 4.99 - 2.32y$
κ-$(Al_xGa_{1-x})_2O_3$	$E_g(x) = 4.91 + 2.10x$
κ-$(In_yGa_{1-y})_2O_3$	$E_g(y) = 4.90 - 1.85y$
c-$(Ga_zIn_{1-z})_2O_3$	$E_g(z) = 3.73 + 0.56z$

D. Cubic crystal structure

The cubic structure, also called bixbyite, is body-centered cubic (bcc) and belongs to the space group $Ia3$. The bcc unit cell consists of 16 molecules. The sixfold coordinated cations can occupy the Wyckhoff position 8b (cation lies on the space diagonal between two oxygen vacancies) or the Wyckhoff position 24d (within the bcc cell with the oxygen vacancies located on the surface diagonal), respectively. The ratio of the b to d cation positions is 8:24 in the unit cell. As substrates (100)ZrO_2 or (006)Al_2O_3 are mostly used. The solubility limit of Ga atoms into phase pure cubic In_2O_3 is 50 at.%[146,147]. For higher Ga contents an additional phase, usually the monoclinic β-gallia and/or hexagonal $InGaO_3$ phase can be observed. The lattice parameter in binary In_2O_3 is $a = 10.117 \pm 0.001$ Å [158] and can be decreased by alloying with Ga [23,159] following for the a-lattice constant Vegard's law presented in Tab. III.

V. OPTICAL BANDGAP

One of the most important aspects of the group-III sesquioxides is the possibility of bandgap engineering in a broad range. Actually, Al_2O_3 and Ga_2O_3 are indirect semiconductors, but with such a small difference in the band-to-band transition that both behave much as direct bandgap semiconductors [3,162]. For In_2O_3 a distinct classification of direct or indirect bandgap is also possible and widely discussed. As introduced by Weiher and Ley, In_2O_3 can exhibit an indirect, forbidden band-to-band transition of $E_g^{\text{indirect}} = 2.62$ eV and a direct transition of $E_g^{\text{direct}} = 3.75$ eV [13]. Further investigations of Walsh *et al.* showed that the direct optical band-to-band transitions are parity-forbidden, resulting in an upper bandgap limit of 2.9 eV [163]. The first dipole allowed band-to-band transition can be observed at 3.7 eV, which could be experimentally confirmed [13,164].

For Ga_2O_3 the bandgap energy depends strongly on the respective formed polymorph. For instance, the bandgap of the monoclinic polymorph can range between 4.6 and 5.0 eV [3]. Due to the optical anisotropy, the bandgap depends strongly

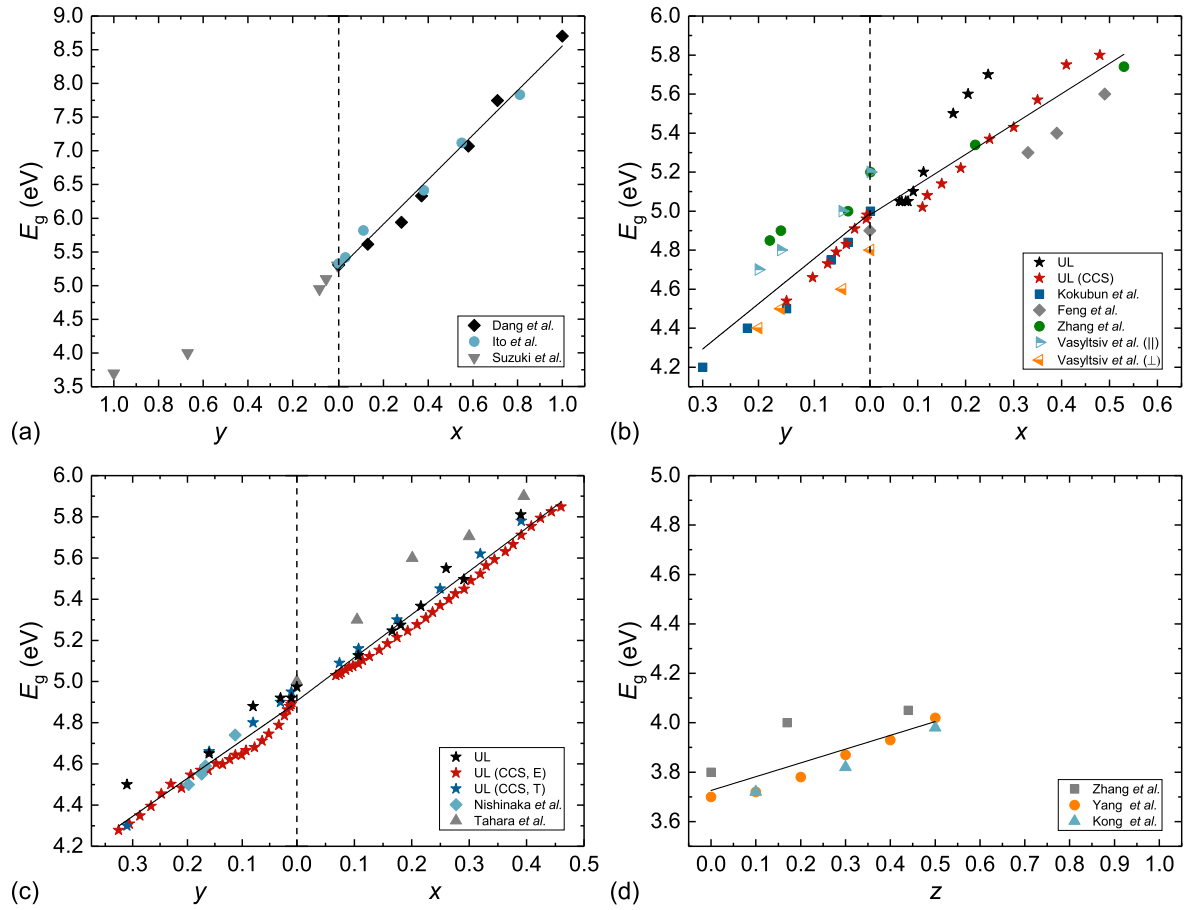

Figure 9. Optical bandgap as function of the Al, In or Ga incorporation x, y or z for the (a) rhombohedral, (b) monoclinic, (c) orthorhombic and (d) cubic polymorphs of the group-III sesquioxides. The data were extracted for the α-polymorph from Ref. 112,115,120, for β- from Ref. 122,133,134,137,151,155,160,161, for κ- from Ref. 139–141,143–145, and for the cubic phase from Ref. 134,146,147.

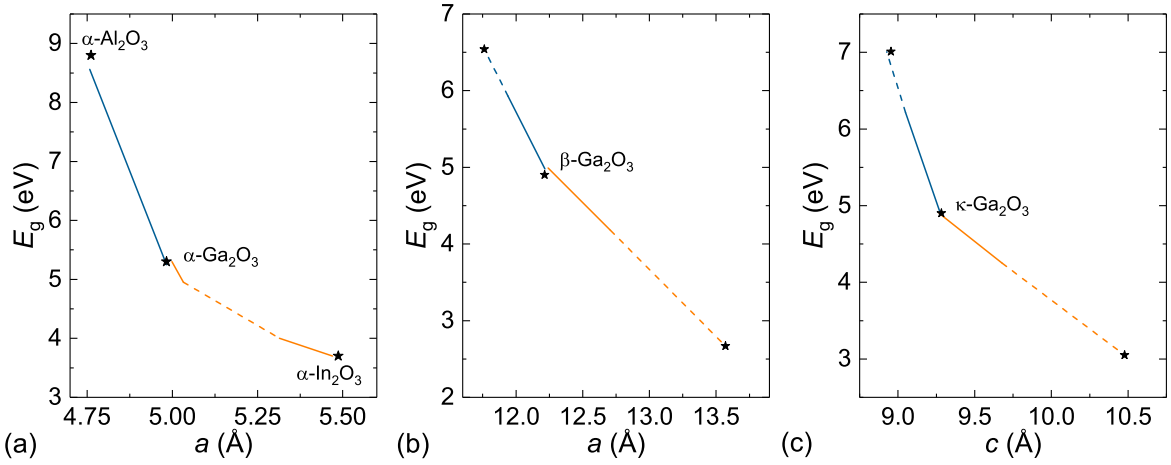

Figure 10. Optical bandgap in dependence on the lattice parameter (a) a for rhombohedral, (b) a for monoclinic and (b) c for orthorhombic $(Al,Ga)_2O_3$ and $(In,Ga)_2O_3$. The solid line presents linear fittings of recently published data. The dashed lines shows the extrapolation to binary Al_2O_3 and In_2O_3. The lattice parameters and bandgap energies for α-, β- and κ-Ga_2O_3 as well as for α-Al_2O_3 and In_2O_3 are taken from Tab. I.

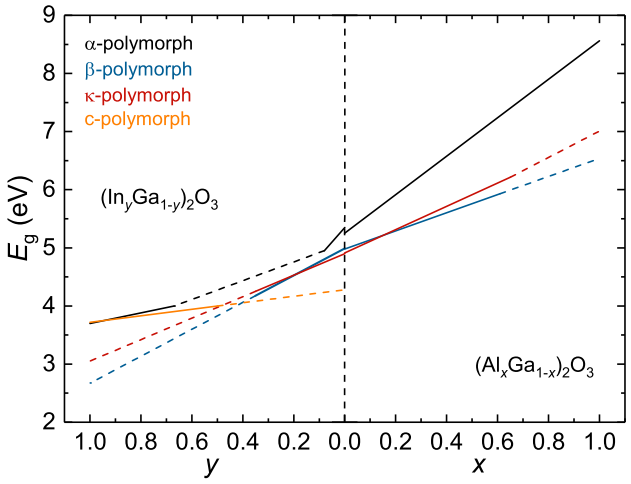

Figure 11. Optical bandgap in dependence on the cation incorporation x or y based on Tab. IV for the rhombohedral (black), monoclinic (blue), orthorhombic (red) and cubic polymorphs (orange) of the sesquioxides. The solid lines represents the maximum reported cation incorporation for the distinct polymorphs and the dashed lines are extrapolated to the binary sesquioxides.

on the orientation and polarization [165]. The orthorhombic Ga_2O_3 exhibits an optical bandgap of 4.9 eV [38,55,69] and the rhombohedral phase a slightly higher one of 5.2 to 5.3 eV [24,46,48,58]. The optical bandgap of α-Al_2O_3 was found to be 8.7-8.8 eV [115,166] and for binary κ-Al_2O_3 no experimental bandgaps are available. Figure 9 summarizes experimental results of optical bandgaps as a function of the alloy composition for rhombohedral (α), monoclinic (β), orthorhombic (κ) and cubic polymorphs of $(Al,Ga,In)_2O_3$ thin films. The linear fits of the separate polymorphs are summarized in Tab. IV. The highest bandgap variance is observed in the rhombohedral α-phase, since each sesquioxide can crystallize in the rhombohedral structure allowing bandgap engineering between 3.7 eV [120] and 8.7 eV [115], except a range of $4 < E_g < 4.95$ eV [120]. For the β- and κ-phase alloys is the bandgap engineering limited by the solubility and therefore phase separation.

Using the linear fits (see Tab. IV), extrapolations to the current maximum Al and In incorporation allows declaration of the possible bandgap engineering. It follows that for β-$(Al,Ga,In)_2O_3$ thin films the bandgap can be varied between approximately 4.2 and 5.9 eV corresponding to an In content of 35 at.% and an Al content of 61 at.% into β-Ga_2O_3. For the ternary alloys of the orthorhombic structure ensues a similar range of about 4.25 to 6.2 eV (35 at.% In, 65 at.% Al). For phase pure cubic $(Ga_zIn_{1-z})_2O_3$ amounts the maximum reported Ga incorporation $z = 0.5$ [146,147] leading to a small bandgap variation of 3.7 eV to 4.05 eV. Figure 11 illustrates the actual possible and extrapolated bandgap energies of all polymorphs discussed in dependence on the alloy compound. In addition, Fig. 10 summarizes the data fits from Tab. III and IV for α-, β- and κ-Ga_2O_3 alloyed with Al or In and represents the relation of the optical bandgap as a function of the lattice parameter. For this purpose, these equations were resolved according to x/y and then put on a par. Assuming that monoclinic and orthorhombic $(Al,Ga,In)_2O_3$ thin films are achievable up to binary Al_2O_3 and In_2O_3, the plots (E_g vs. x/y and E_g vs. lattice constant) were extrapolated up to the maximum and minimum possible values of $x = 1$ or $y = 1$ (dashed lines in Fig. 11), respectively. As a result of these extrapolations for the monoclinic phase a maximum bandgap range of $2.67 - 6.54$ eV and for the orthorhombic polymorph a range of $3.05 - 7.01$ eV. Compared with experimental results of α-Al_2O_3 (8.7-8.8 eV [115,166]), the extrapolated monoclinic and orthorhombic Al_2O_3 bandgaps are much smaller. The extrapolated values for β-In_2O_3 reflect the value of the parity-forbidden direct bandgap of cubic In_2O_3, whereby the extrapolated value of κ-In_2O_3 is near the fundamental bandgap [163].

In contrast, the alloy of cubic In_2O_3 with Ga exhibits direct band-to-band transistions with a possible bandgap range of 3.7 eV to an extrapolated maximum of 4.28 eV for cubic Ga_2O_3. A possible reason for the strong difference of the extrapolated values for β- and κ-In_2O_3 with the actual cubic In_2O_3 bandgaps can be that the calculation for the β- and κ-polymorph starts at the Ga_2O_3 of the phase diagram where no parity-forbidden transitions were reported. Since the graphs intersect each other at an average In content of 40 at.%, this could indicate the critical cation composition where phase separations proceeds.

However, for α-$(In,Ga)_2O_3$ and cubic $(Ga,In)_2O_3$ thin films, a bandgap bowing of $b = 1.69$ eV [167] can be observed resulting in a minimum bandgap of 3.7 eV [113,120,146]. Such a bowing cannot be excluded for the monoclinic and orthorhombic polymorph, so it should be kept in mind for higher potential In contents.

VI. SUMMARY AND OUTLOOK

In this report, we pointed out that for the group-III-sesquioxides, oxygen pressure has a strong influence on the alloy composition and cation incorporation of PLD grown thin films. At low oxygen pressures, volatile suboxides are formed and desorb. Due to different dissociation energies of the Me-O bonds, the provided cations are incorporated with different preferences. The dissociation energy of the Al-O bond is higher as the Ga-O bond, which is higher than the In-O bond, resulting in a preferentially incorporation of Al into the $(Al,Ga)_2O_3$ alloy or Ga into the $(In,Ga)_2O_3$ alloy.

Besides, we have reviewed the dependence of lattice constants and optical bandgap on the group-III sesquioxide alloy composition for the rhombohedral, monoclinic, orthorhombic, and cubic crystal structures. The summarized data revealed different solubility limits of the distinct polymorphs of $(Al_xGa_{1-x})_2O_3$ and $(In_yGa_{1-y})_2O_3$ due to different ground state crystal structures of the binary materials. For instance, in the rhombohedral structure the cation incorporation of Ga in α-Al_2O_3 or Al in α-Ga_2O_3 is possible in the entire compositional range, while Ga in α-In_2O_3 was only reported up to 33 at.% and In in α-Ga_2O_3 has a solubility limit of around 8 at.%. For the monoclinic and orthorhombic poly-

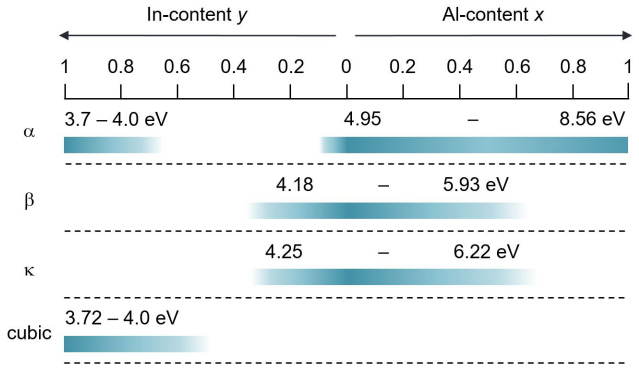

Figure 12. Current miscibility limits and corresponding optical bandgap energies for the rhombohedral α-, monoclinic β- and orthorhombic κ-polymorph of $(Al_xGa_{1-x})_2O_3$ and $(In_yGa_{1-y})_2O_3$ as well as for cubic $(In_yGa_{1-y})_2O_3$. The graph was adapted and extended from Ref. 168.

morphs of Ga_2O_3, which are not reported for binary Al_2O_3 and In_2O_3, the maximum reported cation incorporations are similar: The Al content reaches a maximum of 61 to 65 at.% and In is included up to 35 at.% in β- or κ-Ga_2O_3. The highest reported Ga content in the cubic In_2O_3 phase was reported to be 50 at.%. Starting from Ga_2O_3 the lattice constants decreases (increases) with increasing Al (In) incorporation and follow for all reviewed polymorphs Vegard's law. We also reviewed the evolution of the bandgap, which leads to bandgap ranges from 3.7-4 eV and 4.95-8.7 eV for the α-polymorph, 4.2-5.9 eV for the β-polymorph, 4.2-5.7 eV for the κ-polymorph, and 3.7-4.05 eV for the cubic phase. The bandgaps and corresponding miscibility limits are summarized in Fig. 12 for all polymorphs discussed.

Future studies and investigations should continue to focus on expanding the phase limits of the ternary alloys for each polymorph of the group-III sesquioxides. Since the α-phase can be stabilized across the entire composition range of the $(Al,Ga)_2O_3$ alloy and this is also - at least theoretically - feasible for the $(In_xGa_{1-x})_2O_3$ alloy, this structure is particularly suitable for the realization of of wavelength-selective photodetectors, such as deep UV-photodetectors or QWIP's. With the availability of native β-Ga_2O_3 substrates, alloys of this phase are a prime candidate for the realization of high performance power devices and possibly QWIP's. The κ-phase is due to it's spontaneous polarization especially interesting for confining extremely high 2DEG densities, which can be potentially exploited in HEMT's. The emphasis should also remain on optimizing or realizing the electrical conductivity of all polymorphs of $(In_xGa_{1-x})_2O_3$ or $(Al_xGa_{1-x})_2O_3$, respectively.

ACKNOWLEDGEMENTS

We thank Monika Hahn for PLD target fabrication, Jörg Lenzner and Daniel Splith for EDX measurements, and Chris Sturm for the determination of the thin film thicknesses using ellipsometry. This work was supported by European Social Fund within the Young Investigator Group "Oxide Heterostructures" (No. SAB 100310460). This work was funded by the Deutsche Forschungsgemeinschaft (DFG,German Research Foundation)—project number 31047526, SFB762, project B04. A.H. acknowledge the Leipzig School for Natural Sciences BuildMoNa. We acknowledge support from the German Research Foundation (DFG) and Universität Leipzig within the program of Open Access Publishing.

REFERENCES

[1] M. Higashiwaki, H. Murakami, Y. Kumagai, and A. Kuramata, 'Current status of Ga_2O_3 power devices,' Japanese Journal of Applied Physics **55**, 1202A1 (2016).
[2] S. Stepanov, V. Nikolaev, V. Bougrov, and A. Romanov, 'Gallium oxide: Properties and applications - A review,' Rev. Adv. Mater. Sci. **44**, 63–86 (2016).
[3] H. von Wenckstern, 'Group-III Sesquioxides: Growth, Physical Properties and Devices,' Advanced Electronic Materials **3**, 1600350 (2017).
[4] S. J. Pearton, J. Yang, P. H. Cary, F. Ren, J. Kim, M. J. Tadjer, and M. A. Mastro, 'A review of Ga_2O_3 materials, processing, and devices,' Applied Physics Reviews **5**, 011301 (2018), https://doi.org/10.1063/1.5006941.
[5] J. Zhang, J. Shi, D.-C. Qi, L. Chen, and K. H. L. Zhang, 'Recent progress on the electronic structure, defect, and doping properties of Ga_2O_3,' APL Materials **8**, 020906 (2020).
[6] M. Higashiwaki, A. Kuramata, H. Murakami, and Y. Kumagai, 'State-of-the-art technologies of gallium oxide power devices,' Journal of Physics D: Applied Physics **50**, 333002 (2017).
[7] Z. Zhang, H. von Wenckstern, and M. Grundmann, 'Monolithic Multichannel Ultraviolet Photodiodes Based on (Mg,Zn)O Thin Films With Continuous Composition Spreads,' Selected Topics in Quantum Electronics, IEEE Journal of **20**, 106–111 (2014).
[8] O. Bierwagen, 'Indium oxide - a transparent, wide-band gap semiconductor for (opto)electronic applications,' Semiconductor Science and Technology **30**, 024001 (2015).
[9] E. Thune, A. Fakih, C. Matringe, D. Babonneau, and R. Guinebretière, 'Understanding of one dimensional ordering mechanisms at the (001) sapphire vicinal surface,' Journal of Applied Physics **121**, 015301 (2017).
[10] R. Roy, V. G. Hill, and E. F. Osborn, 'Polymorphism of Ga_2O_3 and the System Ga_2O_3-H_2O,' Journal of the American Chemical Society **74**, 719–722 (1952).
[11] H. Y. Playford, A. C. Hannon, M. G. Tucker, D. M. Dawson, S. E. Ashbrook, R. J. Kastiban, J. Sloan, and R. I. Walton, 'Characterization of Structural Disorder in γ-Ga_2O_3,' The Journal of Physical Chemistry C **118**, 16188–16198 (2014).
[12] H. K. Müller, 'Electrical and Optical Properties of Sputtered In_2O_3 films. I. Electrical Properties and Intrinsic Absorption,' Physica Status Solidi (b) **27**, 723–731 (1968).
[13] R. L. Weiher and R. P. Ley, 'Optical Properties of Indium Oxide,' Journal of Applied Physics **37**, 299–302 (1966).
[14] P. D. C. King, T. D. Veal, F. Fuchs, C. Y. Wang, D. J. Payne, A. Bourlange, H. Zhang, G. R. Bell, V. Cimalla, O. Ambacher, R. G. Egdell, F. Bechstedt, and C. F. McConville, 'Band gap, electronic structure, and surface electron accumulation of cubic and rhombohedral In_2O_3,' Phys. Rev. B **79**, 205211 (2009).
[15] K. Momma and F. Izumi, 'VESTA 3 for three-dimensional visualization of crystal, volumetric and morphology data,' J. Appl. Crystallogr. **44**, 1272–1276 (2011).
[16] E. R. Dobrovinskaya, L. A. Lytvynov, and V. Pishchik, *Sapphire: Material, Manufacturing, Applications* (Springer Science+Business Media, 2009).
[17] M. Marezio and J. P. Remeika, 'Bond Lengths in the α-Ga_2O_3 Structure and the High-Pressure Phase of $Ga_{2-x}Fe_xO_3$,' The Journal of Chemical Physics **46**, 1862–1865 (1967).
[18] C. T. Prewitt, R. D. Shannon, D. B. Rogers, and A. W. Sleight, 'C rare earth oxide-corundum transition and crystal chemistry of oxides having

the corundum structure,' Inorganic Chemistry **8**, 1985–1993 (1969).

[19] R.-S. Zhou and R. L. Snyder, 'Structures and transformation mechanisms of the β, γ and θ transition aluminas,' Acta Crystallographica Section B Structural Science **47**, 617–630 (1991).

[20] J. Åhman, G. Svensson, and J. Albertsson, 'A Reinvestigation of β-Gallium Oxide,' Acta Crystallographica Section C Crystal Structure Communications **52**, 1336–1338 (1996).

[21] B. Ollivier, R. Retoux, P. Lacorre, D. Massiot, and G. Férey, 'Crystal structure of κ-alumina: an X-ray powder diffraction, TEM and NMR study,' Journal of Materials Chemistry **7**, 1049–1056 (1997).

[22] I. Cora, F. Mezzadri, F. Boschi, M. Bosi, M. Čaplovičová, G. Calestani, I. Dódony, B. Pécz, and R. Fornari, 'The real structure of ε-Ga_2O_3 and its relation to κ-phase,' CrystEngComm **19**, 1509–1516 (2017).

[23] D. D. Edwards, P. E. Folkins, and T. O. Mason, 'Phase Equilibria in the Ga_2O_3 In_2O_3 System,' Journal of the American Ceramic Society **80**, 253–257 (1997).

[24] D. Shinohara and S. Fujita, 'Heteroepitaxy of Corundum-Structured α-Ga_2O_3 Thin Films on α-Al_2O_3 Substrates by Ultrasonic Mist Chemical Vapor Deposition,' Japanese Journal of Applied Physics **47**, 7311 (2008).

[25] T. Kawaharamura, G. T. Dang, and M. Furuta, 'Successful Growth of Conductive Highly Crystalline Sn-Doped α-Ga_2O_3 Thin Films by Fine-Channel Mist Chemical Vapor Deposition,' Japanese Journal of Applied Physics **51**, 040207 (2012).

[26] R. Cuscó, N. Domènech-Amador, T. Hatakeyama, T. Yamaguchi, T. Honda, and L. Artús, 'Lattice dynamics of a mist-chemical vapor deposition-grown corundum-like Ga_2O_3 single crystal,' Journal of Applied Physics **117**, 185706 (2015).

[27] K. Kaneko, H. Kawanowa, H. Ito, and S. Fujita, 'Evaluation of Misfit Relaxation in α-Ga_2O_3 Epitaxial Growth on α-Al_2O_3 Substrate,' Japanese Journal of Applied Physics **51**, 020201 (2012).

[28] K. Akaiwa, K. Kaneko, K. Ichino, and S. Fujita, 'Conductivity control of Sn-doped α-Ga_2O_3thin films grown on sapphire substrates,' Japanese Journal of Applied Physics **55**, 1202BA (2016).

[29] K. Shimazoe, H. Nishinaka, Y. Arata, D. Tahara, and M. Yoshimoto, 'Phase control of α- and κ-Ga_2O_3 epitaxial growth on $LiNbO_3$ and $LiTaO_3$ substrates using α-Fe_2O_3 buffer layers,' AIP Advances **10**, 055310 (2020).

[30] S. dong Lee, K. Kaneko, and S. Fujita, 'Homoepitaxial growth of beta gallium oxide films by mist chemical vapor deposition,' Japanese Journal of Applied Physics **55**, 1202B8 (2016).

[31] D. Tahara, H. Nishinaka, S. Morimoto, and M. Yoshimoto, 'Stoichiometric control for heteroepitaxial growth of smooth ε-Ga_2O_3 thin films oncplane AlN templates by mist chemical vapor deposition,' Japanese Journal of Applied Physics **56**, 078004 (2017).

[32] G. Battiston, R. Gerbasi, M. Porchia, R. Bertoncello, and F. Caccavale, 'Chemical vapour deposition and characterization of gallium oxide thin films,' Thin Solid Films **279**, 115–118 (1996).

[33] L. Kong, J. Ma, C. Luan, and Z. Zhu, 'Structural and optical properties of Ga_2O_3: In films deposited on MgO (100) substrates by MOCVD,' Journal of Solid State Chemistry **184**, 1946–1950 (2011).

[34] W. Mi, J. Ma, C. Luan, Y. Lv, H. Xiao, and Z. Li, 'Characterization of β-Ga_2O_3 epitaxial films grown on MgO (111) substrates by metal-organic chemical vapor deposition,' Materials Letters **87**, 109–112 (2012).

[35] D. Gogova, G. Wagner, M. Baldini, M. Schmidbauer, K. Irmscher, R. Schewski, Z. Galazka, M. Albrecht, and R. Fornari, 'Structural properties of Si-doped β-Ga_2O_3 layers grown by MOVPE,' Journal of Crystal Growth **401**, 665–669 (2014).

[36] S. Rafique, L. Han, M. J. Tadjer, J. A. Freitas, N. A. Mahadik, and H. Zhao, 'Homoepitaxial growth of β-Ga_2O_3 thin films by low pressure chemical vapor deposition,' Applied Physics Letters **108**, 182105 (2016).

[37] M. Baldini, M. Albrecht, A. Fiedler, K. Irmscher, D. Klimm, R. Schewski, and G. Wagner, 'Semiconducting Sn-doped β-Ga_2O_3 homoepitaxial layers grown by metal organic vapour-phase epitaxy,' Journal of Materials Science **51**, 3650–3656 (2016).

[38] Y. Zhuo, Z. Chen, W. Tu, X. Ma, Y. Pei, and G. Wang, 'β-Ga_2O_3 versus ε-Ga_2O_3: Control of the crystal phase composition of gallium oxide thin film prepared by metal-organic chemical vapor deposition,' Applied Surface Science **420**, 802–807 (2017).

[39] Y. Chen, X. Xia, H. Liang, Q. Abbas, Y. Liu, and G. Du, 'Growth Pressure Controlled Nucleation Epitaxy of Pure Phase ε- and β-Ga_2O_3 Films on Al_2O_3 via MOCVD,' Crystal Growth & Design **18**, 1147–1154 (2018), https://doi.org/10.1021/acs.cgd.7b01576.

[40] F. Alema, B. Hertog, A. Osinsky, P. Mukhopadhyay, M. Toporkov, and W. V. Schoenfeld, 'Fast growth rate of epitaxial β-Ga_2O_3 by close coupled showerhead MOCVD,' Journal of Crystal Growth **475**, 77–82 (2017).

[41] X. Xia, Y. Chen, Q. Feng, H. Liang, P. Tao, M. Xu, and G. Du, 'Hexagonal phase-pure wide band gap ε-Ga_2O_3 films grown on 6H-SiC substrates by metal organic chemical vapor deposition,' Applied Physics Letters **108**, 202103 (2016).

[42] F. Mezzadri, G. Calestani, F. Boschi, D. Delmonte, M. Bosi, and R. Fornari, 'Crystal Structure and Ferroelectric Properties of ε-Ga_2O_3 Films Grown on (0001)-Sapphire,' Inorganic chemistry **55**, 12079–12084 (2016).

[43] M. Pavesi, F. Fabbri, F. Boschi, G. Piacentini, A. Baraldi, M. Bosi, E. Gombia, A. Parisini, and R. Fornari, 'ε-Ga_2O_3 epilayers as a material for solar-blind UV photodetectors,' Materials Chemistry and Physics **205**, 502 – 507 (2018).

[44] M. Mulazzi, F. Reichmann, A. Becker, W. M. Klesse, P. Alippi, V. Fiorentini, A. Parisini, M. Bosi, and R. Fornari, 'The electronic structure of ε-Ga_2O_3,' APL Materials **7**, 022522 (2019).

[45] S. H. Park, H. S. Lee, H. S. Ahn, and M. Yang, 'Crystal Phase Control of ε-Ga_2O_3 Fabricated using by Metal-Organic Chemical Vapor Deposition,' Journal of the Korean Physical Society **74**, 502–507 (2019).

[46] Y. Oshima, E. G. Víllora, and K. Shimamura, 'Halide vapor phase epitaxy of twin-free α-Ga_2O_3 on sapphire (0001) substrates,' Applied Physics Express **8**, 055501 (2015).

[47] Y. Oshima, K. Kawara, T. Shinohe, T. Hitora, M. Kasu, and S. Fujita, 'Epitaxial lateral overgrowth of α-Ga_2O_3 by halide vapor phase epitaxy,' APL Materials **7**, 022503 (2019).

[48] A. I. Pechnikov, S. I. Stepanov, A. V. Chikiryaka, M. P. Scheglov, M. A. Odnobludov, and V. I. Nikolaev, 'Thick α-Ga_2O_3 Layers on Sapphire Substrates Grown by Halide Epitaxy,' Semiconductors **53**, 780–783 (2019).

[49] J. H. Leach, K. Udwary, J. Rumsey, G. Dodson, H. Splawn, and K. R. Evans, 'Halide vapor phase epitaxial growth of β-Ga_2O_3 and α-Ga_2O_3 films,' APL Materials **7**, 022504 (2019).

[50] M. Orita, H. Ohta, M. Hirano, and H. Hosono, 'Deep-ultraviolet transparent conductive β-Ga_2O_3 thin films,' Applied Physics Letters **77**, 4166–4168 (2000).

[51] H. Murakami, K. Nomura, K. Goto, K. Sasaki, K. Kawara, Q. T. Thieu, R. Togashi, Y. Kumagai, M. Higashiwaki, A. Kuramata, S. Yamakoshi, B. Monemar, and A. Koukitu, 'Homoepitaxial growth of β-Ga_2O_3 layers by halide vapor phase epitaxy,' Applied Physics Express **8**, 015503 (2014).

[52] K. Nomura, K. Goto, R. Togashi, H. Murakami, Y. Kumagai, A. Kuramata, S. Yamakoshi, and A. Koukitu, 'Thermodynamic study of β-Ga_2O_3 growth by halide vapor phase epitaxy,' Journal of Crystal Growth **405**, 19–22 (2014).

[53] Y. Oshima, E. G. Víllora, and K. Shimamura, 'Quasi-heteroepitaxial growth of β-Ga_2O_3 on off-angled sapphire (0 0 0 1) substrates by halide vapor phase epitaxy,' Journal of Crystal Growth **410**, 53–58 (2015).

[54] V. Nikolaev, A. Pechnikov, S. Stepanov, I. Nikitina, A. Smirnov, A. Chikiryaka, S. Sharofidinov, V. Bougrov, and A. Romanov, 'Epitaxial growth of β-Ga_2O_3 on (0001) sapphire substrates by halide vapour phase epitaxy,' Materials Science in Semiconductor Processing **47**, 16–19 (2016).

[55] Y. Oshima, E. G. Víllora, Y. Matsushita, S. Yamamoto, and K. Shimamura, 'Epitaxial growth of phase-pure ε-Ga_2O_3 by halide vapor phase epitaxy,' Journal of Applied Physics **118**, 085301 (2015).

[56] V. I. Nikolaev, S. I. Stepanov, A. I. Pechnikov, S. Shapenkov, M. P. Scheglov, A. Chikiryaka, and O. F. Vyvenko, 'HVPE Growth and Characterization of ε-Ga_2O_3 Films on Various Substrates,' ECS Journal of Solid State Science and Technology **9**, 045014 (2020).

[57] R. Schewski, G. Wagner, M. Baldini, D. Gogova, Z. Galazka, T. Schulz, T. Remmele, T. Markurt, H. von Wenckstern, M. Grundmann, O. Bierwagen, P. Vogt, and M. Albrecht, 'Epitaxial stabilization of pseudomorphic α-Ga_2O_3 on sapphire (0001),' Applied Physics Express **8**, 011101 (2014).

[58] V. Gottschalch, S. Merker, S. Blaurock, M. Kneiß, U. Teschner, M. Grundmann, and H. Krautscheid, 'Heteroepitaxial growth of α-, β-, γ- and κ-Ga_2O_3 phases by metalorganic vapor phase epitaxy,' Journal of Crystal Growth **510**, 76–84 (2019).

[59] G. Wagner, M. Baldini, D. Gogova, M. Schmidbauer, R. Schewski, M. Albrecht, Z. Galazka, D. Klimm, and R. Fornari, 'Homoepitaxial growth of β-Ga_2O_3 layers by metal-organic vapor phase epitaxy,' physica status solidi (a) **211**, 27–33 (2013).

[60] M. Orita, H. Hiramatsu, H. Ohta, M. Hirano, and H. Hosono, 'Preparation of highly conductive, deep ultraviolet transparent β-Ga_2O_3 thin film at low deposition temperatures,' Thin Solid Films **411**, 134–139 (2002).

[61] K. Matsuzaki, H. Hiramatsu, K. Nomura, H. Yanagi, T. Kamiya, M. Hirano, and H. Hosono, 'Growth, structure and carrier transport properties of Ga_2O_3 epitaxial film examined for transparent field-effect transistor,' Thin Solid Films **496**, 37–41 (2006).

[62] A. Petitmangin, C. Hébert, J. Perrière, B. Gallas, L. Binet, P. Barboux, and P. Vermaut, 'Metallic clusters in nonstoichiometric gallium oxide films,' Journal of Applied Physics **109**, 013711 (2011).

[63] C. Hebert, A. Petitmangin, J. Perrière, E. Millon, A. Petit, L. Binet, and P. Barboux, 'Phase separation in oxygen deficient gallium oxide films grown by pulsed-laser deposition,' Materials Chemistry and Physics **133**, 135–139 (2012).

[64] A. Petitmangin, B. Gallas, C. Hebert, J. Perrière, L. Binet, P. Barboux, and X. Portier, 'Characterization of oxygen deficient gallium oxide films grown by PLD,' Applied Surface Science **278**, 153–157 (2013).

[65] S. Müller, H. von Wenckstern, D. Splith, F. Schmidt, and M. Grundmann, 'Control of the conductivity of Si-doped β-Ga_2O_3 thin films via growth temperature and pressure,' physica status solidi (a) **211**, 34–39 (2014).

[66] F. B. Zhang, K. Saito, T. Tanaka, M. Nishio, and Q. X. Guo, 'Structural and optical properties of Ga_2O_3 films on sapphire substrates by pulsed laser deposition,' Journal of Crystal Growth **387**, 96–100 (2014).

[67] W. Seiler, M. Selmane, K. Abdelouhadi, and J. Perrière, 'Epitaxial growth of gallium oxide films on c-cut sapphire substrate,' Thin Solid Films **589**, 556–562 (2015).

[68] K. D. Leedy, K. D. Chabak, V. Vasilyev, D. C. Look, K. Mahalingam, J. L. Brown, A. J. Green, C. T. Bowers, A. Crespo, D. B. Thomson, and G. H. Jessen, 'Si content variation and influence of deposition atmosphere in homoepitaxial Si-doped β-Ga_2O_3 films by pulsed laser deposition,' APL Materials **6**, 101102 (2018).

[69] M. Kneiß, A. Hassa, D. Splith, C. Sturm, H. von Wenckstern, T. Schultz, N. Koch, M. Lorenz, and M. Grundmann, 'Tin-assisted heteroepitaxial PLD-growth of κ-Ga_2O_3 thin films with high crystalline quality,' APL Materials **7**, 022516 (2019).

[70] T. Oshima, T. Okuno, and S. Fujita, 'Ga_2O_3 Thin Film Growth on c-Plane Sapphire Substrates by Molecular Beam Epitaxy for Deep-Ultraviolet Photodetectors,' Japanese Journal of Applied Physics **46**, 7217–7220 (2007).

[71] T. Oshima, N. Arai, N. Suzuki, S. Ohira, and S. Fujita, 'Surface morphology of homoepitaxial β-Ga_2O_3 thin films grown by molecular beam epitaxy,' Thin Solid Films **516**, 5768–5771 (2008).

[72] H. Okumura, M. Kita, K. Sasaki, A. Kuramata, M. Higashiwaki, and J. S. Speck, 'Systematic investigation of the growth rate of β-Ga_2O_3(010) by plasma-assisted molecular beam epitaxy,' Applied Physics Express **7**, 095501 (2014).

[73] P. Vogt and O. Bierwagen, 'The competing oxide and sub-oxide formation in metal-oxide molecular beam epitaxy,' Applied Physics Letters **106**, 081910 (2015).

[74] A. Mauze, Y. Zhang, T. Itoh, F. Wu, and J. S. Speck, 'Metal oxide catalyzed epitaxy (MOCATAXY) of β-Ga_2O_3 films in various orientations grown by plasma-assisted molecular beam epitaxy,' APL Materials **8**, 021104 (2020).

[75] P. Vogt, O. Brandt, H. Riechert, J. Lähnemann, and O. Bierwagen, 'Metal-Exchange Catalysis in the Growth of Sesquioxides: Towards Heterostructures of Transparent Oxide Semiconductors,' Phys. Rev. Lett. **119**, 196001 (2017).

[76] M. Kracht, A. Karg, J. Schörmann, M. Weinhold, D. Zink, F. Michel, M. Rohnke, M. Schowalter, B. Gerken, A. Rosenauer, P. J. Klar, J. Janek, and M. Eickhoff, 'Tin-Assisted Synthesis of $\varepsilon-Ga_2O_3$ by Molecular Beam Epitaxy,' Physical Review Applied **8**, 054002 (2017).

[77] D. won Choi, K.-B. Chung, and J.-S. Park, 'Low temperature Ga_2O_3 atomic layer deposition using gallium tri-isopropoxide and water,' Thin Solid Films **546**, 31–34 (2013).

[78] H. Altuntas, I. Donmez, C. Ozgit-Akgun, and N. Biyikli, 'Electrical characteristics of β-Ga_2O_3 thin films grown by PEALD,' Journal of Alloys and Compounds **593**, 190–195 (2014).

[79] F. Boschi, M. Bosi, T. Berzina, E. Buffagni, C. Ferrari, and R. Fornari, 'Hetero-epitaxy of ε-Ga_2O_3 layers by MOCVD and ALD,' Journal of Crystal Growth **443**, 25–30 (2016).

[80] K. Kaneko, S. Fujita, and T. Hitora, 'A power device material of corundum-structured α-Ga_2O_3 fabricated by MIST EPITAXY®technique,' Japanese Journal of Applied Physics **57**, 02CB18 (2018).

[81] G. Sinha, K. Adhikary, and S. Chaudhuri, 'Sol–gel derived phase pure α-Ga_2O_3 nanocrystalline thin film and its optical properties,' Journal of Crystal Growth **276**, 204–207 (2005).

[82] S. Li, S. Jiao, D. Wang, S. Gao, and J. Wang, 'The influence of sputtering power on the structural, morphological and optical properties of β-Ga_2O_3 thin films,' Journal of Alloys and Compounds **753**, 186–191 (2018).

[83] N. Ueda, H. Hosono, R. Waseda, and H. Kawazoe, 'Synthesis and control of conductivity of ultraviolet transmitting β-Ga_2O_3 single crystals,' Applied Physics Letters **70**, 3561–3563 (1997).

[84] E. G. Víllora, K. Shimamura, Y. Yoshikawa, K. Aoki, and N. Ichinose, 'Large-size β-Ga_2O_3 single crystals and wafers,' Journal of Crystal Growth **270**, 420–426 (2004).

[85] N. Suzuki, S. Ohira, M. Tanaka, T. Sugawara, K. Nakajima, and T. Shishido, 'Fabrication and characterization of transparent conductive Sn-doped β-Ga_2O_3 single crystal,' physica status solidi (c) **4**, 2310–2313 (2007).

[86] H. Aida, K. Nishiguchi, H. Takeda, N. Aota, K. Sunakawa, and Y. Yaguchi, 'Growth of β-Ga_2O_3 Single Crystals by the Edge-Defined, Film Fed Growth Method,' Japanese Journal of Applied Physics **47**, 8506–8509 (2008).

[87] Y. Tomm, P. Reiche, D. Klimm, and T. Fukuda, 'Czochralski grown Ga_2O_3 crystals,' Journal of Crystal Growth **220**, 510–514 (2000).

[88] Z. Galazka, R. Uecker, K. Irmscher, M. Albrecht, D. Klimm, M. Pietsch, M. Brützam, R. Bertram, S. Ganschow, and R. Fornari, 'Czochralski growth and characterization of β-Ga_2O_3 single crystals,' Crystal Research and Technology **45**, 1229–1236 (2010).

[89] M. Lorenz, J. Woods, and R. Gambino, 'Some electrical properties of the semiconductor β-Ga_2O_3,' Journal of Physics and Chemistry of Solids **28**, 403–404 (1967).

[90] T. Harwig and J. Schoonman, 'Electrical properties of β-Ga_2O_3 single crystals. II,' Journal of Solid State Chemistry **23**, 205–211 (1978).

[91] M. Schieber, 'Growth of oxide crystals by the flux method,' Journal of the American Ceramic Society **47**, 655–655 (1964).

[92] R. Shannon and C. Prewitt, 'Synthesis and structure of phases in the In_2O_3 - Ga_2O_3 system,' Journal of Inorganic and Nuclear Chemistry **30**, 1389 – 1398 (1968).

[93] G. Frank, L. Brock, and H. Bausen, 'The solubilities of Sn in In_2O_3 and of In in SnO_2 crystals grown from Sn—In melts,' Journal of Crystal Growth **36**, 179–180 (1976).

[94] C. Y. Wang, V. Cimalla, H. Romanus, T. Kups, G. Ecke, T. Stauden, M. Ali, V. Lebedev, J. Pezoldt, and O. Ambacher, 'Phase selective growth and properties of rhombohedral and cubic indium oxide,' Applied Physics Letters **89**, 011904 (2006).

[95] C. Y. Wang, V. Lebedev, V. Cimalla, T. Kups, K. Tonisch, and O. Ambacher, 'Structural studies of single crystalline In_2O_3 films epitaxially grown on InN (0001),' Applied Physics Letters **90**, 221902 (2007).

[96] L. Kong, J. Ma, C. Luan, Z. Zhu, and Q. Yu, 'Domain structure and optical property of epitaxial indium oxide film deposited on MgO (100) substrate,' Surface Science **605**, 977–981 (2011).

[97] E. J. Tarsa, J. H. English, and J. S. Speck, 'Pulsed laser deposition of oriented In_2O_3 on (001) InAs, MgO, and yttria-stabilized zirconia,' Applied Physics Letters **62**, 2332–2334 (1993).

[98] T. Koida and M. Kondo, 'High electron mobility of indium oxide grown on yttria-stabilized zirconia,' Journal of Applied Physics **99**, 123703 (2006).

[99] C.-Y. Park, S.-G. Yoon, Y.-H. Jo, and S.-C. Shin, 'Room-temperature ferromagnetism observed in Mo-doped indium oxide films,' Applied Physics Letters **95**, 122502 (2009).

[100] C. Kranert, R. Schmidt-Grund, and M. Grundmann, 'Raman active phonon modes of cubic In_2O_3,' physica status solidi (RRL) - Rapid Research Letters **8**, 554–559 (2014).

[101] R. Schmidt-Grund, H. Krauß, C. Kranert, M. Bonholzer, and M. Grundmann, 'Temperature dependence of the dielectric function in the spectral range (0.5–8.5) eV of an In_2O_3 thin film,' Applied Physics Letters

105, 111906 (2014).

[102] N. Taga, M. Maekawa, Y. Shigesato, I. Yasui, M. Kamei, and T. E. Haynes, 'Deposition of Heteroepitaxial In_2O_3 Thin Films by Molecular Beam Epitaxy,' Japanese Journal of Applied Physics **37**, 6524–6529 (1998).

[103] A. Bourlange, D. J. Payne, R. G. Egdell, J. S. Foord, P. P. Edwards, M. O. Jones, A. Schertel, P. J. Dobson, and J. L. Hutchison, 'Growth of In_2O_3 (100) on Y-stabilized ZrO_2 (100) by O-plasma assisted molecular beam epitaxy,' Applied Physics Letters **92**, 092117 (2008).

[104] E. H. Morales, Y. He, M. Vinnichenko, B. Delley, and U. Diebold, 'Surface structure of Sn-doped In_2O_3 (111) thin films by STM,' New Journal of Physics **10**, 125030 (2008).

[105] O. Bierwagen, M. E. White, M.-Y. Tsai, and J. S. Speck, 'Plasma-assisted molecular beam epitaxy of high quality In_2O_3 (001) thin films on Y-stabilized ZrO_2 (001) using In as an auto surfactant,' Applied Physics Letters **95**, 262105 (2009).

[106] O. Bierwagen and J. S. Speck, 'Nucleation of islands and continuous high-quality In_2O_3 (001) films during plasma-assisted molecular beam epitaxy on Y-stabilized ZrO_2 (001),' Journal of Applied Physics **107**, 113519 (2010).

[107] K. H. L. Zhang, V. K. Lazarov, P. L. Galindo, F. E. Oropeza, D. J. Payne, H. H.-C. Lai, and R. G. Egdell, 'Domain Matching Epitaxial Growth of In_2O_3 Thin Films on α-Al_2O_3 (0001),' Crystal Growth & Design **12**, 1000–1007 (2012).

[108] M. Kamei, Y. Shigesato, and S. Takaki, 'Origin of characteristic grain-subgrain structure of tin-doped indium oxide films,' Thin Solid Films **259**, 38–45 (1995).

[109] N. Taga, H. Odaka, Y. Shigesato, I. Yasui, M. Kamei, and T. E. Haynes, 'Electrical properties of heteroepitaxial grown tin-doped indium oxide films,' Journal of Applied Physics **80**, 978–984 (1996).

[110] C. Xirouchaki, G. Kiriakidis, T. F. Pedersen, and H. Fritzsche, 'Photoreduction and oxidation of as-deposited microcrystalline indium oxide,' Journal of Applied Physics **79**, 9349–9352 (1996).

[111] Z. Galazka, R. Uecker, K. Irmscher, D. Schulz, D. Klimm, M. Albrecht, M. Pietsch, S. Ganschow, A. Kwasniewski, and R. Fornari, 'Melt growth, characterization and properties of bulk In_2O_3 single crystals,' Journal of Crystal Growth **362**, 349–352 (2013).

[112] H. Ito, K. Kaneko, and S. Fujita, 'Growth and Band Gap Control of Corundum-Structured α-$(AlGa)_2O_3$ Thin Films on Sapphire by Spray-Assisted Mist Chemical Vapor Deposition,' Japanese Journal of Applied Physics **51**, 100207 (2012).

[113] S. Fujita and K. Kaneko, 'Epitaxial growth of corundum-structured wide band gap III-oxide semiconductor thin films,' Journal of Crystal Growth **401**, 588–592 (2014).

[114] K. Kaneko, K. Suzuki, Y. Ito, and S. Fujita, 'Growth characteristics of corundum-structured α-$(Al_xGa_{1-x})_2O_3$/Ga_2O_3 heterostructures on sapphire substrates,' Journal of Crystal Growth **436**, 150–154 (2016).

[115] G. T. Dang, T. Yasuoka, Y. Tagashira, T. Tadokoro, W. Theiss, and T. Kawaharamura, 'Bandgap engineering of α-$(Al_xGa_{1-x})_2O_3$ by a mist chemical vapor deposition two-chamber system and verification of Vegard's Law,' Applied Physics Letters **113**, 062102 (2018).

[116] M. Lorenz, S. Hohenberger, E. Rose, and M. Grundmann, 'Atomically stepped, pseudomorphic, corundum-phase $(Al_{1-x}Ga_x)_2O_3$ thin films ($0 \leq x < 0.08$) grown on R-plane sapphire,' Applied Physics Letters **113**, 231902 (2018).

[117] M. Grundmann and M. Lorenz, 'Anisotropic strain relaxation through prismatic and basal slip in α-$(Al,Ga)_2O_3$ on R-plane Al_2O_3,' APL Materials **8**, 021108 (2020).

[118] A. Hassa, P. Storm, M. Kneiß, D. Splith, H. von Wenckstern, M. Lorenz, and M. Grundmann, 'Structural and Elastic Properties of α-$(Al_xGa_{1-x})_2O_3$ Thin Films on (11.0) Al_2O_3 Substrates for the Entire Composition Range,' physica status solidi (b) (2020), 10.1002/pssb.202000394.

[119] R. Kumaran, T. Tiedje, S. E. Webster, S. Penson, and W. Li, 'Epitaxial Nd-doped α-$(Al_{1-x}Ga_x)_2O_3$ films on sapphire for solid-state waveguide lasers,' Optics Letters **35**, 3793 (2010).

[120] N. Suzuki, K. Kaneko, and S. Fujita, 'Growth of corundum-structured $(In_xGa_{1-x})_2O_3$ alloy thin films on sapphire substrates with buffer layers,' Journal of Crystal Growth **401**, 670–672 (2014).

[121] S. Fujita, M. Oda, K. Kaneko, and T. Hitora, 'Evolution of corundum-structured III-oxide semiconductors: Growth, properties, and devices,' Japanese Journal of Applied Physics Part 1-Regular Papers Short Notes & Review Papers **55**, 1202A3 (2016).

[122] F. Zhang, K. Saito, T. Tanaka, M. Nishio, M. Arita, and Q. Guo, 'Wide bandgap engineering of $(AlGa)_2O_3$ films,' Applied Physics Letters **105**, 162107 (2014).

[123] R. Wakabayashi, T. Oshima, M. Hattori, K. Sasaki, T. Masui, A. Kuramata, S. Yamakoshi, K. Yoshimatsu, and A. Ohtomo, 'Oxygen-radical-assisted pulsed-laser deposition of β-Ga_2O_3 and β-$(Al_xGa_{1-x})_2O_3$ films,' Journal of Crystal Growth **424**, 77–79 (2015).

[124] X. Wang, Z. Chen, F. Zhang, K. Saito, T. Tanaka, M. Nishio, and Q. Guo, 'Influence of substrate temperature on the properties of $(AlGa)_2O_3$ thin films prepared by pulsed laser deposition,' Ceramics International **42**, 12783–12788 (2016).

[125] Q. Feng, Z. Feng, Z. Hu, X. Xing, G. Yan, J. Zhang, Y. Xu, X. Lian, and Y. Hao, 'Temperature dependent electrical properties of pulse laser deposited Au/Ni/β-$(AlGa)_2O_3$ Schottky diode,' Applied Physics Letters **112**, 072103 (2018).

[126] A. Vaidya, J. Sarker, Y. Zhang, L. Lubecki, J. Wallace, J. D. Poplawsky, K. Sasaki, A. Kuramata, A. Goyal, J. A. Gardella, B. Mazumder, and U. Singisetti, 'Structural, band and electrical characterization of β-$(Al_{0.19}Ga_{0.81})_2O_3$ films grown by molecular beam epitaxy on Sn doped β-Ga_2O_3 substrate,' Journal of Applied Physics **126**, 095702 (2019).

[127] H. Okumura, Y. Kato, T. Oshima, and T. Palacios, 'Demonstration of lateral field-effect transistors using Sn-doped β-$(AlGa)_2O_3$ (010),' Japanese Journal of Applied Physics **58**, SBBD12 (2019).

[128] T. Oshima, T. Okuno, N. Arai, Y. Kobayashi, and S. Fujita, 'β-$Al_{2x}Ga_{2-2x}O_3$ Thin Film Growth by Molecular Beam Epitaxy,' Japanese Journal of Applied Physics **48**, 070202 (2009).

[129] E. Ahmadi, Y. Oshima, F. Wu, and J. S. Speck, 'Schottky barrier height of Ni to β-$(Al_xGa_{1-x})_2O_3$ with different compositions grown by plasma-assisted molecular beam epitaxy,' Semiconductor Science and Technology **32**, 035004 (2017).

[130] C.-C. Wang, S.-H. Yuan, S.-L. Ou, S.-Y. Huang, K.-Y. Lin, Y.-A. Chen, P.-W. Hsiao, and D.-S. Wuu, 'Growth and characterization of co-sputtered aluminum-gallium oxide thin films on sapphire substrates,' Journal of Alloys and Compounds **765**, 894–900 (2018).

[131] M. Baldini, D. Gogova, K. Irmscher, M. Schmidbauer, G. Wagner, and R. Fornari, 'Heteroepitaxy of $Ga_{2(1-x)}In_{2x}O_3$ layers by MOVPE with two different oxygen sources,' Crystal Research and Technology **49**, 552–557 (2014).

[132] H. von Wenckstern, D. Splith, A. Werner, S. Müller, M. Lorenz, and M. Grundmann, 'Properties of Schottky Barrier Diodes on $(In_xGa_{1-x})_2O_3$ for $0.01 \leq x \leq 0.85$ Determined by a Combinatorial Approach,' ACS Combinatorial Science **17**, 710–715 (2015).

[133] H. von Wenckstern, D. Splith, M. Purfürst, Z. Zhang, C. Kranert, S. Müller, M. Lorenz, and M. Grundmann, 'Structural and optical properties of $(In,Ga)_2O_3$ thin films and characteristics of Schottky contacts thereon,' Semiconductor Science and Technology **30**, 024005 (2015).

[134] F. Zhang, K. Saito, T. Tanaka, M. Nishio, and Q. Guo, 'Wide bandgap engineering of $(GaIn)_2O_3$ films,' Solid State Communications **186**, 28–31 (2014).

[135] Z. Zhang, H. von Wenckstern, J. Lenzner, M. Lorenz, and M. Grundmann, 'Visible-blind and solar-blind ultraviolet photodiodes based on $(In_xGa_{1-x})_2O_3$,' Applied Physics Letters **108**, 123503 (2016).

[136] P. Vogt and O. Bierwagen, 'Kinetics versus thermodynamics of the metal incorporation in molecular beam epitaxy of $(In_xGa_{1-x})_2O_3$,' APL Materials **4**, 086112 (2016).

[137] Y. Kokubun, T. Abe, and S. Nakagomi, 'Sol-gel prepared $(Ga_{1-x}In_x)_2O_3$ thin films for solar-blind ultraviolet photodetectors,' physica status solidi (a) **207**, 1741–1745 (2010).

[138] T. Oshima and S. Fujita, 'Properties of Ga_2O_3-based $(In_xGa_{1-x})_2O_3$ alloy thin films grown by molecular beam epitaxy,' physica status solidi (c) **5**, 3113–3115 (2008).

[139] D. Tahara, H. Nishinaka, S. Morimoto, and M. Yoshimoto, 'Heteroepitaxial growth of ε-$(Al_xGa_{1-x})_2O_3$ alloy films on c-plane AlN templates by mist chemical vapor deposition,' Applied Physics Letters **112**, 152102 (2018).

[140] P. Storm, M. Kneiß, A. Hassa, T. Schultz, D. Splith, H. von Wenckstern, N. Koch, M. Lorenz, and M. Grundmann, 'Epitaxial κ-$(Al_xGa_{1-x})_2O_3$ thin films and heterostructures grown by tin-assisted VCCS-PLD,' APL

Materials **7**, 111110 (2019).

[141] A. Hassa, C. Sturm, M. Kneiß, D. Splith, H. von Wenckstern, T. Schultz, N. Koch, M. Lorenz, and M. Grundmann, 'Solubility limit and material properties of a κ-$(Al_xGa_{1-x})_2O_3$ thin film with a lateral cation gradient on $(00.1)Al_2O_3$ by tin-assisted PLD,' APL Materials **8**, 021103 (2020).

[142] A. Hassa, C. Wouters, M. Kneiß, D. Splith, C. Sturm, H. von Wenckstern, M. Albrecht, M. Lorenz, and M. Grundmann, 'Control of phase formation of $(Al_xGa_{1-x})_2O_3$ thin films on c-plane Al_2O_3,' Journal of Physics D: Applied Physics **53** (2020), 10.1088/1361-6463/abaf7d.

[143] H. Nishinaka, N. Miyauchi, D. Tahara, S. Morimoto, and M. Yoshimoto, 'Incorporation of indium into ε-gallium oxide epitaxial thin films grown via mist chemical vapour deposition for bandgap engineering,' Crystengcomm **20**, 1882–1888 (2018).

[144] A. Hassa, H. von Wenckstern, D. Splith, C. Sturm, M. Kneiß, V. Prozheeva, and M. Grundmann, 'Structural, optical, and electrical properties of orthorhombic κ-$(In_xGa_{1-x})_2O_3$ thin films,' APL Materials **7**, 022525 (2019).

[145] M. Kneiß, A. Hassa, D. Splith, C. Sturm, H. von Wenckstern, M. Lorenz, and M. Grundmann, 'Epitaxial stabilization of single phase κ-$(In_xGa_{1-x})_2O_3$ thin films up to $x = 0.28$ on c-sapphire and κ-Ga_2O_3 (001) templates by tin-assisted VCCS-PLD,' APL Materials **7**, 101102 (2019).

[146] F. Yang, J. Ma, C. Luan, and L. Kong, 'Structural and optical properties of $Ga_{2(1-x)}In_{2x}O_3$films prepared on α-Al_2O_3 (0001) by MOCVD,' Applied Surface Science **255**, 4401–4404 (2009).

[147] L. Kong, J. Ma, F. Yang, C. Luan, and Z. Zhu, 'Preparation and characterization of $Ga_{2x}In_{2(1-x)}O_3$ films deposited on ZrO_2 (100) substrates by MOCVD,' Journal of Alloys and Compounds **499**, 75–79 (2010).

[148] H. von Wenckstern, Z. Zhang, F. Schmidt, J. Lenzner, H. Hochmuth, and M. Grundmann, 'Continuous composition spread using pulsed-laser deposition with a single segmented target,' CrystEngComm **15**, 10020 (2013).

[149] H. von Wenckstern, M. Kneiß, A. Hassa, P. Storm, D. Splith, and M. Grundmann, 'A Review of the Segmented-Target Approach to Combinatorial Material Synthesis by Pulsed-Laser Deposition,' physica status solidi (b) , 1900626 (2019).

[150] M. Lorenz, 'Transparent Conductive Zinc Oxide: Basics and Applications in Thin Film Solar Cells (Springer Series in Materials Science Book 104),' (Springer, 2007) Chap. Pulsed Laser Deposition of ZnO-Based Thin Films, pp. 303–357.

[151] A. Hassa, H. von Wenckstern, L. Vines, and M. Grundmann, 'Influence of Oxygen Pressure on Growth of Si-Doped β-$(Al_xGa_{1-x})_2O_3$ Thin Films on c-Sapphire Substrates by Pulsed Laser Deposition,' ECS Journal of Solid State Science and Technology **8**, Q3217–Q3220 (2019).

[152] C. Kranert, J. Lenzner, M. Jenderka, M. Lorenz, H. von Wenckstern, R. Schmidt-Grund, and M. Grundmann, 'Lattice parameters and Raman-active phonon modes of $(In_xGa_{1-x})_2O_3$ for $x < 0.4$,' Journal of Applied Physics **116**, 013505 (2014).

[153] C. Kranert, M. Jenderka, J. Lenzner, M. Lorenz, H. von Wenckstern, R. Schmidt-Grund, and M. Grundmann, 'Lattice parameters and Raman-active phonon modes of β-$(Al_xGa_{1-x})_2O_3$,' Journal of Applied Physics **117**, 125703 (2015).

[154] B. W. Krueger, C. S. Dandeneau, E. M. Nelson, S. T. Dunham, F. S. Ohuchi, M. A. Olmstead, and J. Jones, 'Variation of Band Gap and Lattice Parameters of β-$(Al_xGa_{1-x})_2O_3$ Powder Produced by Solution Combustion Synthesis,' Journal of the American Ceramic Society **99**, 2467–2473 (2016).

[155] V. I. Vasyltsiv, Y. I. Rym, and Y. M. Zakharko, 'Optical absorption and photoconductivity at the band edge of β-$Ga_{2-x}In_xO_3$,' physica status solidi (b) **195**, 653–658 (1996).

[156] S. Geller, 'Crystal Structure of β-Ga_2O_3,' The Journal of Chemical Physics **33**, 676–684 (1960).

[157] A. L. Jaromin and D. D. Edwards, 'Subsolidus Phase Relationships in the Ga_2O_3-Al_2O_3-TiO_2 System,' Journal of the American Ceramic Society **88**, 2573–2577 (2005).

[158] M. Marezio, 'Refinement of the crystal structure of In_2O_3 at two wavelengths,' Acta Crystallographica **20**, 723–728 (1966).

[159] A. Regoutz, R. Egdell, D. Morgan, R. Palgrave, H. Téllez, S. Skinner, D. Payne, G. Watson, and D. Scanlon, 'Electronic and surface properties of Ga-doped In_2O_3 ceramics,' Applied Surface Science **349**, 970–982 (2015).

[160] R. Schmidt-Grund, C. Kranert, H. von Wenckstern, V. Zviagin, M. Lorenz, and M. Grundmann, 'Dielectric function in the spectral range (0.5–8.5)eV of an $(Al_xGa_{1-x})_2O_3$ thin film with continuous composition spread,' Journal of Applied Physics **117**, 165307 (2015).

[161] Z. Feng, Q. Feng, J. Zhang, X. Li, F. Li, L. Huang, H.-Y. Chen, H.-L. Lu, and Y. Hao, 'Band alignment of $SiO_2/(Al_xGa_{1-x})_2O_3$ ($0 \leq x \leq 0.49$) determined by X-ray photoelectron spectroscopy,' Applied Surface Science **434**, 440–444 (2018).

[162] Y. Yourdshahyan, C. Ruberto, L. Bengtsson, and B. I. Lundqvist, 'First-principles calculations on the atomic and electronic structure of κ-Al_2O_3,' Physical Review B **56**, 8553–8558 (1997).

[163] A. Walsh, J. L. F. D. Silva, S.-H. Wei, C. Körber, A. Klein, L. F. J. Piper, A. DeMasi, K. E. Smith, G. Panaccione, P. Torelli, D. J. Payne, A. Bourlange, and R. G. Egdell, 'Nature of the Band Gap of In_2O_3Revealed by First-Principles Calculations and X-Ray Spectroscopy,' Physical Review Letters **100** (2008), 10.1103/physrevlett.100.167402.

[164] H. Köstlin, R. Jost, and W. Lems, 'Optical and electrical properties of doped In_2O_3 films,' Physica Status Solidi (a) **29**, 87–93 (1975).

[165] C. Sturm, R. Schmidt-Grund, C. Kranert, J. Furthmüller, F. Bechstedt, and M. Grundmann, 'Dipole analysis of the dielectric function of color dispersive materials: Application to monoclinic Ga_2O_3,' Physical Review B **94** (2016), 10.1103/physrevb.94.035148.

[166] S.-D. Mo and W. Y. Ching, 'Electronic and optical properties of θ-Al_2O_3 and comparison to α-Al_2O_3,' Physical Review B **57**, 15219–15228 (1998).

[167] H. Peelaers, D. Steiauf, J. B. Varley, A. Janotti, and C. G. V. de Walle, '$(InxGa_{1-x})_2O_3$ alloys for transparent electronics,' Physical Review B **92** (2015), 10.1103/physrevb.92.085206.

[168] H. von Wenckstern, D. Splith, and M. Grundmann, 'Pulsed Laser Deposition 2,' in *Gallium Oxide: Materials Properties, Crystal Growth, and Devices*, edited by M. Higashiwaki and S. Fujita (Springer International Publishing, Cham, 2020) pp. 273–291.

[169] A. Kohn, G. Katz, and J. D. Broder, 'Characterization of Ga_2O_3 Characterization of β-Ga_2O_3 and its alumina isomorph, θ-Al_2O_3,' Am. Mineral **42**, 398 (1957).

[170] H. He, R. Orlando, M. A. Blanco, R. Pandey, E. Amzallag, I. Baraille, and M. Rérat, 'First-principles study of the structural, electronic, and optical properties of Ga_2O_3 in its monoclinic and hexagonal phases,' Physical Review B **74** (2006), 10.1103/physrevb.74.195123.

[171] S. Yoshioka, H. Hayashi, A. Kuwabara, F. Oba, K. Matsunaga, and I. Tanaka, 'Structures and energetics of Ga_2O_3 polymorphs,' Journal of Physics: Condensed Matter **19**, 346211 (2007).

[172] K. Shimamura, E. G. Víllora, T. Ujiie, and K. Aoki, 'Excitation and photoluminescence of pure and Si-doped β-Ga_2O_3 single crystals,' Applied Physics Letters **92**, 201914 (2008).

[173] K. Akaiwa and S. Fujita, 'Electrical Conductive Corundum-Structured α-Ga_2O_3 Thin Films on Sapphire with Tin-Doping Grown by Spray-Assisted Mist Chemical Vapor Deposition,' Japanese Journal of Applied Physics **51**, 070203 (2012).

[174] L. Spiess, G. Teichert, R. Schwarzer, H. Behnken, and C. Genzel, *Moderne Röntgenbeugung: Röntgendiffraktometrie für Materialwissenschaftler, Physiker und Chemiker (German Edition)* (Vieweg+Teubner Verlag, 2009).

[175] F. Fuchs and F. Bechstedt, 'Indium-oxide polymorphs from first principles: Quasiparticle electronic states,' Physical Review B **77** (2008), 10.1103/physrevb.77.155107.

[176] J. P. Remeika and M. Marezio, 'GROWTH OF α-Ga_2O_3 SINGLECRYSTALS AT 44 KBARS,' Applied Physics Letters **8**, 87–88 (1966).

[177] X. Feng, C. Zhao, Z. Li, Y. Luo, and J. Ma, 'Ternary $Al_{2x}In_{2-2x}O_3$ films with tunable optical band gap prepared on YSZ (100) substrates by metal organic chemical vapor deposition,' Journal of Alloys and Compounds **637**, 257–260 (2015).

[178] X. Feng, C. Zhao, Z. Li, Y. Luo, and J. Ma, 'Influence of Al content on the properties of ternary $Al_{2x}In_{2-2x}O_3$ alloy films prepared on YSZ (111) substrates by MOCVD,' Materials Research Bulletin **70**, 354–357 (2015).

[179] Z. Li, C. Zhao, X. Du, W. Mi, C. Luan, X. Feng, and J. Ma, 'Structural and optical properties of $Al_{2x}In_{2-2x}O_3$ films prepared by metal-organic chemical vapor deposition,' RSC Adv. **4**, 54300–54306 (2014).

[180] Z. Li, J. Ma, C. Zhao, X. Du, W. Mi, C. Luan, and X. Feng, 'Preparation and characterization of $Al_{2x}In_{2-2x}O_3$ films deposited on MgO (100) by MOCVD,' Materials Research Bulletin **67**, 14–19 (2015).

[181] L. M. Foster and H. C. Stumpf, 'Analogies in the Gallia and Alumina Systems. The Preparation and Properties of Some Low-Alkali Gallates,' Journal of the American Chemical Society **73**, 1590–1595 (1951).

[182] L. Binet, D. Gourier, and C. Minot, 'Relation between Electron Band Structure and Magnetic Bistability of Conduction Electrons in β-Ga_2O_3,' Journal of Solid State Chemistry **113**, 420–433 (1994).

[183] H. von Wenckstern, 'Gallium Oxide: Technology, Devices and Applications (Metal Oxides),' (Elsevier, 2018) Chap. Properties of $(In,Ga)_2O_3$ alloys, pp. 119–148.

[184] H. Peelaers, J. B. Varley, J. S. Speck, and C. G. V. de Walle, 'Structural and electronic properties of Ga_2O_3-Al_2O_3 alloys,' Applied Physics Letters **112**, 242101 (2018).

[185] P. Liu and J. Skogsmo, 'Space-group determination and structure model for κ-Al_2O_3 by convergent-beam electron diffraction (CBED),' Acta Crystallographica Section B Structural Science **47**, 425–433 (1991).

[186] Y. Yourdshahyan, C. Ruberto, M. Halvarsson, L. Bengtsson, V. Langer, B. I. Lundqvist, S. Ruppi, and U. Rolander, 'Theoretical Structure Determination of a Complex Material: κ-Al_2O_3,' Journal of the American Ceramic Society **82**, 1365–1380 (2004).

[187] M. Kneiß, P. Storm, A. Hassa, D. Splith, H. von Wenckstern, M. Lorenz, and M. Grundmann, 'Growth, structural and optical properties of coherent κ-$(Al_xGa_{1-x})_2O_3$/κ-Ga_2O_3 quantum well superlattice heterostructures,' APL Materials **8**, 051112 (2020).

[188] M. Grundmann, H. Frenzel, A. Lajn, M. Lorenz, F. Schein, and H. von Wenckstern, 'Transparent semiconducting oxides: materials and devices,' phys. stat. sol. (a) **207**, 1437–1449 (2010).

[189] M. Baldini, M. Albrecht, D. Gogova, R. Schewski, and G. Wagner, 'Effect of indium as a surfactant in $(Ga_{1-x}In_x)_2O_3$ epitaxial growth on β-Ga_2O_3 by metal organic vapour phase epitaxy,' Semiconductor Science and Technology **30**, 024013 (2015).

CHAPTER5

Summary and Outlook

This thesis summarizes studies of the epitaxy and physical properties of various Ga_2O_3 based alloys with In_2O_3 or Al_2O_3, respectively. The best growth conditions were determined to suppress the formation and desorption of volatile suboxides and to obtain high quality samples. The κ-phase was successfully stabilized and maximum cation contents of $x_{\mathsf{In}} = 0.35$ in the κ-$(In,Ga)_2O_3$ alloy and $x_{\mathsf{Al}} = 0.46$ in the κ-$(Al,Ga)_2O_3$ alloy were achieved, allowing bandgap engineering of about 4.3 to 5.8 eV. The growth of α-$(Al,Ga)_2O_3$ was successfully realized over the whole composition range. All obtained data were summarized together with recent literature data.

Desorption processes during growth of the β- and κ-phases of $(Al,Ga)_2O_3$ and $(In,Ga)_2O_3$ thin films

The choice of deposition conditions directly influences the growth of the ternary alloys of the sesquioxides investigated. Within the PLD technique, both, $p(O_2)$ and T_{g}, can be set as mentioned. To investigate the impact of these conditions on the monoclinic and orthorhombic polymorphs, $(Al,Ga)_2O_3$ and $(In,Ga)_2O_3$ thin films were deposited by different PLD approaches and systematically changed growth conditions. Two $(Al,Ga)_2O_3$ sample series were fabricated using a Si-doped or a Sn doped Ga_2O_3+8.8 at.%Al_2O_3 ceramic target, respectively. The resulting monoclinic and orthorhombic thin films exhibit systematically divergent physical properties: Decreasing $p(O_2)$ and/or increasing T_{g} leads to an enhanced incorporation of Al atoms compared to Ga atoms and considerably lower growth rates due to the formation and subsequent desorption of volatile Ga suboxides (Ga_2O). At low $p(O_2)$ there is a small amount of oxygen atoms in the PLD chamber, which favors an increased formation of energetically more beneficial volatile suboxides. These suboxides desorbs and are not incorporated in the thin film. Since the dissociation energies of the Al-O bond is higher than that of the Ga-O bond, the Al atoms are incorporated preferentially into the layer. As a

consequence, lower growth rates with higher Al-contents were observed.

For further investigations of the desorption process $(In,Ga)_2O_3$ and $(Al,Ga)_2O_3$ thin films were fabricated applying the CCS-PLD approach with low and high $p(O_2)$. Also in this case, low $p(O_2)$ leads to changed cation compositions and low growth rates. However, the Ga-content in the $(In,Ga)_2O_3$ alloy is higher than the In-content due to the weaker dissociation energy of the In-O bond compared to the Ga-bond.

Studies of $(Al,Ga)_2O_3$ and $(In,Ga)_2O_3$ thin films under systematically changed ambient conditions are presented in a total of three publications [E2, E3, E7].

Physical properties and Phase formation of orthorhombic $(Al,Ga)_2O_3$ and $(In,Ga)_2O_3$ thin films

Investigations on $(Al,Ga)_2O_3$ thin films, prepared under systematically changed growth conditions, revealed that the formation of the orthorhombic polymorph strongly depends on $p(O_2)$ and T_g. For that, $p(O_2)$ below 0.016 mbar, a high T_g above 580°C and an additional amount of tin in the PLD target are required. The tin probably acts as surfactant by creating a liquid tin layer on the sample surface. Conducted XPS measurements revealed tin residues only on the sample surface and not in the layer, which supports the surfactant-mediated growth. An exact confirmation of this assumed growth process was not possible under the given measurement setups and should be part of future investigations. Further growth conditions lead to monoclinic thin films or a mixture of the β-, γ- and κ-phases.

Based on this study, 2 inch in diameter large samples were prepared by the CCS-PLD approach applying circular half-segmented Ga_2O_3/Al_2O_3 or Ga_2O_3/In_2O_3 ceramic targets to fabricate thin films with a lateral varying cation composition. The targets were doped with tin to induce the κ-phase. In $(Al_xGa_{1-x})_2O_3$, the κ-phase was obtained in the range of $0.07 \leq x_{Al} \leq 0.46$ [E4], which was the highest reported value at that time. Later, a maximum Al-content of $x = 0.65$ was achieved by introducing a κ-Ga_2O_3 buffer layer between substrate and layer [E13]. For κ-$(In_xGa_{1-x})_2O_3$, the κ-phase was achieved up to $x_{In} = 0.35$ being the highest reported In-content so far [E5]. XRD ϕ-scans on these thin films demonstrates epitaxial growth in three rotational domains for the orthorhombic alloys. Optical bandgap measurements showed a minimum achievable value of 4.3 eV for κ-$(In_{0.35}Ga_{0.65})_2O_3$ and a maximum achievable bandgap of 5.8 eV for κ-$(Al_{0.46}Ga_{0.54})_2O_3$.

Furthermore, the dielectric functions and refractive indexes for both mentioned alloys were derived. The κ-phase exhibits for the entire realized composition range excellent structural and morphological properties compared to similar monoclinic thin films.

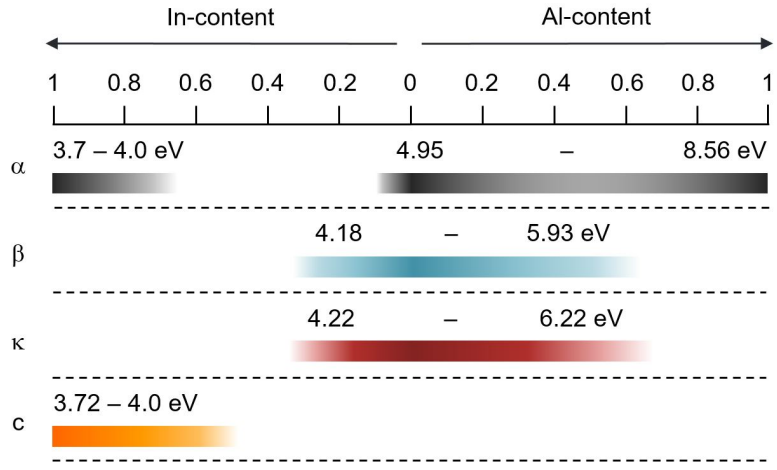

Figure 5.1: Current miscibility limits and corresponding optical bandgap energies for the different polymorphs of the group-III sesquioxides. The graph can be found in a similar way within the cumulative part of this work [E7].

In the cummulative part of this work, are the studies dealing with the orthorhombic alloys presented in a total of three publications [E3-E5]. Further studies performed on the κ-modification within the semiconductor physics group were published in Refs. [E1, E11-E13, E15].

Physical properties of rhombohedral $(Al,Ga)_2O_3$ thin films

In the $(Al_xGa_{1-x})_2O_3$ alloy the successful stabilization of the rhombohedral α-structure in the entire composition range was demonstrated. The evolution of the in-plane and out-of plane lattice parameters revealed that the thin films grow for low Al-contents relaxed and switched for $x = 0.55$ to pseudomorphic growth. The c-lattice constant followed in the relaxed grown part Vegard's law and aligned in the pseudomorphic part at around 12.99 Å, which corresponds to the value of α-Al_2O_3.

Evolution of the optical bandgaps and lattice constants of the sesquioxides

Optical bandgaps as well as lattice constants presented discussed in the course of this thesis were published in an topical review together with the current literature on the α-, β-, κ- and cubic (c) crystal structure for the $(Al,Ga)_2O_3$ and $(In,Ga)_2O_3$ alloys in dependence on the cation composition. The range of the optical bandgaps in dependence on the current miscibility limits are presented in fig. 5.1.

Outlook

In this thesis, various polymorphs of Ga_2O_3 based alloys were prepared by PLD and extensively investigated for their suitability in various device applications. In order to fabricate high quality and reproducible samples, the best growth conditions were identified. However, studies are still needed to further improve thin film growth. For instance, this can include the suppression of the three rotational domains in the κ-modification. Investigations can also be carried out on the α-phase focused on a more in-depth analysis of the relaxed or pseudomorphic growth as a function of layer thickness or the substrate used or the realization of the α-$(In,Ga)_2O_3$ alloy. Stabilization of higher phase boundaries should also continue in the other alloys mentioned for the prospective realization of devices where tailored bandgaps are required, such as deep UV-PDs or QWIPs. Future studies should also deal with the examination of spontaneous polarization in κ-Ga_2O_3 based heterostructures as well as a demonstration of the formation of 2DEGs. Furthermore, the focus should still be on optimizing or realizing the electrical conductivity of all polymorphs of the $(In_xGa_{1-x})_2O_3$ or $(Al_xGa_{1-x})_2O_3$ alloy, respectively.

List of Abbreviations

2DEG two-dimensional electron gas

AFM atomic force microscope

ALD atomic layer deposition

ARPES angle-resolved photoemission spectroscopy

CBM conduction band minimum

CCS continuous composition spread

CVD chemical vapour deposition

CZ Czochralski

DCS discrete compositional screening

DFT density functional theory

EDX energy dispersive X-ray spectroscopy

FZ floating-zone technique

HEMT high-electron mobility transistor

HVPE halide vapor phase epitaxy

IR infrared

MBE molecular beam epitaxy

MOCVD metal organic chemical vapour deposition

MOVPE metal organic chemical vapor phase epitaxy

PD photodetector

PLD pulsed laser deposition

QWIP quantum-well infrared photodetector

RSM reciprocal space map

RT room temperature

TEM transmission electron microscopy

UV ultraviolet

VBM valence band maximum

VCCS vertical continuous composition spread

XPS X-ray photoelectron spectroscopy

XRD X-ray diffraction

Bibliography

[1] **H. von Wenckstern**: *Group-III Sesquioxides: Growth, Physical Properties and Devices*, Advanced Electronic Materials, volume 3, no. 9: page 1600350 (2017). doi:10.1002/aelm.201600350

[2] **S. Fujita and K. Kaneko**: *Epitaxial growth of corundum-structured wide band gap III-oxide semiconductor thin films*, Journal of Crystal Growth, volume 401: pages 588–592 (2014). doi:10.1016/j.jcrysgro.2014.02.032

[3] **C. Haberstroh, R. Helbig and R. A. Stein**: *Some new features of the photoluminescence of SiC(6H), SiC(4H), and SiC(15R)*, Journal of Applied Physics, volume 76, no. 1: pages 509–513 (1994). doi:10.1063/1.357103

[4] **N. Kaminski and O. Hilt**: *SiC and GaN devices - wide bandgap is not all the same*, IET Circuits, Devices & Systems, volume 8, no. 3: pages 227–236 (2014). doi:10.1049/iet-cds.2013.0223

[5] **S. D. Mo and W. Y. Ching**: *Electronic and optical properties of θ-Al_2O_3 and comparison to α-Al_2O_3*, Physical Review B, volume 57, no. 24: pages 15219–15228 (1998). doi:10.1103/PhysRevB.57.15219

[6] **C. T. Prewitt, R. D. Shannon, D. B. Rogers and A. W. Sleight**: *C rare earth oxide-corundum transition and crystal chemistry of oxides having the corundum structure*, Inorganic Chemistry, volume 8, no. 9: pages 1985–1993 (1969). doi:10.1021/ic50079a033

[7] **M. Higashiwaki, K. Sasaki, A. Kuramata, T. Masui and S. Yamakoshi**: *Gallium oxide (Ga_2O_3) metal-semiconductor field-effect transistors on single-crystal β-Ga_2O_3 (010) substrates*, Applied Physics Letters, volume 100, no. 1: page 013504 (2012). doi:10.1063/1.3674287

[8] **M. Higashiwaki, A. Kuramata, H. Murakami and Y. Kumagai**: *State-of-the-art technologies of gallium oxide power devices*, Journal of Physics D: Applied Physics, volume 50, no. 33: page 333002 (2017)

[9] **S. Stepanov, V. Nikolaev, V. Bougrov and A. Romanov**: *Gallium oxide: Properties and applications - A review*, Rev. Adv. Mater. Sci., volume 44: pages 63–86 (2016)

[10] **S. J. Pearton, J. Yang, P. H. Cary, F. Ren, J. Kim, M. J. Tadjer and M. A. Mastro**: *A review of Ga_2O_3 materials, processing, and devices*, Applied Physics Reviews, volume 5, no. 1: page 011301 (2018). doi:10.1063/1.5006941

[11] **T. Oshima, T. Okuno, N. Arai, N. Suzuki, S. Ohira and S. Fujita**: *Vertical Solar-Blind Deep-Ultraviolet Schottky Photodetectors Based on β-Ga_2O_3 Substrates*, Applied Physics Express, volume 1, no. 1: page 011202 (2008). doi:10.1143/apex.1.011202

[12] **S. Nakagomi, T. Momo, S. Takahashi and Y. Kokubun**: *Deep ultraviolet photodiodes based on β-Ga_2O_3/SiC heterojunction*, Applied Physics Letters, volume 103, no. 7: page 072105 (2013). doi:10.1063/1.4818620

[13] **Z. Zhang, H. von Wenckstern and M. Grundmann**: *Monolithic Multichannel Ultraviolet Photodiodes Based on (Mg,Zn)O Thin Films With Continuous Composition Spreads*, Selected Topics in Quantum Electronics, IEEE Journal of, volume 20, no. 6: pages 106–111 (2014)

[14] **O. Bierwagen**: *Indium oxide - a transparent, wide-band gap semiconductor for (opto)electronic applications*, Semiconductor Science and Technology, volume 30, no. 2: page 024001 (2015)

[15] **M. Grundmann, H. Frenzel, A. Lajn, M. Lorenz, F. Schein and H. von Wenckstern**: *Transparent semiconducting oxides: materials and devices*, phys. stat. sol. (a), volume 207, no. 6: pages 1437–1449 (2010)

[16] **R. Roy, V. G. Hill and E. F. Osborn**: *Polymorphism of Ga_2O_3 and the System Ga_2O_3-H_2O*, Journal of the American Chemical Society, volume 74, no. 3: pages 719–722 (1952)

[17] **J. Zhang, J. Shi, D.-C. Qi, L. Chen and K. H. L. Zhang**: *Recent progress on the electronic structure, defect, and doping properties of Ga_2O_3*, APL Materials, volume 8, no. 2: page 020906 (2020). doi:10.1063/1.5142999

[18] **M. B. Maccioni and V. Fiorentini**: *Phase diagram and polarization of stable phases of* $(Ga_{1-x}In_x)_2O_3$, Applied Physics Express, volume 9, no. 4: page 041102 (2016). doi:10.7567/apex.9.041102

[19] **S. B. Cho and R. Mishra**: *Epitaxial engineering of polar* ϵ-Ga_2O_3 *for tunable two-dimensional electron gas at the heterointerface*, Applied Physics Letters, volume 112, no. 16: page 162101 (2018). doi:10.1063/1.5019721

[20] **J. Kim, D. Tahara, Y. Miura and B. G. Kim**: *First-principle calculations of electronic structures and polar properties of* (κ, ϵ)-Ga_2O_3, Applied Physics Express, volume 11, no. 6: page 061101 (2018)

[21] **P. Ranga, S. B. Cho, R. Mishra and S. Krishnamoorthy**: *Highly tunable, polarization-engineered two-dimensional electron gas in* ϵ-$AlGaO_3$/ϵ-Ga_2O_3 *heterostructures*, Applied Physics Express, volume 13, no. 6: page 061009 (2020). doi:10.35848/1882-0786/ab9168

[22] **D. Guo, X. Zhao, Y. Zhi, W. Cui, Y. Huang, Y. An, P. Li, Z. Wu and W. Tang**: *Epitaxial growth and solar-blind photoelectric properties of corundum-structured* α -Ga_2O_3 *thin films*, Materials Letters, volume 164: pages 364–367 (2016). doi:10.1016/j.matlet.2015.11.001

[23] **J. Moloney, O. Tesh, M. Singh, J. W. Roberts, J. C. Jarman, L. C. Lee, T. N. Huq, J. Brister, S. Karboyan, M. Kuball, P. R. Chalker, R. A. Oliver and F. C.-P. Massabuau**: *Atomic layer deposited* α-Ga_2O_3 *solar-blind photodetectors*, Journal of Physics D: Applied Physics, volume 52, no. 47: page 475101 (2019). doi:10.1088/1361-6463/ab3b76

[24] **H. von Wenckstern, Z. Zhang, F. Schmidt, J. Lenzner, H. Hochmuth and M. Grundmann**: *Continuous composition spread using pulsed-laser deposition with a single segmented target*, CrystEngComm, volume 15, no. 46: page 10020 (2013). doi:10.1039/c3ce41327f

[25] **S. Müller, H. von Wenckstern, D. Splith, F. Schmidt and M. Grundmann**: *Control of the conductivity of Si-doped* β-Ga_2O_3 *thin films via growth temperature and pressure*, physica status solidi (a), volume 211, no. 1: pages 34–39 (2014). doi:10.1002/pssa.201330025

[26] **F. B. Zhang, K. Saito, T. Tanaka, M. Nishio and Q. X. Guo**: *Structural and optical properties of* Ga_2O_3 *films on sapphire substrates by pulsed laser deposition*, Journal of Crystal Growth, volume 387: pages 96–100 (2014). doi:10.1016/j.jcrysgro.2013.11.022

[27] **P. Vogt and O. Bierwagen**: *The competing oxide and sub-oxide formation in metal-oxide molecular beam epitaxy*, Applied Physics Letters, volume 106, no. 8: page 081910 (2015). doi:10.1063/1.4913447

[28] **P. Vogt and O. Bierwagen**: *Reaction kinetics and growth window for plasma-assisted molecular beam epitaxy of Ga_2O_3: Incorporation of Ga vs. Ga_2O desorption*, Applied Physics Letters, volume 108, no. 7: page 072101 (2016). doi:10.1063/1.4942002

[29] **Y.-R. Luo**: *Comprehensive Handbook of Chemical Bond Energies*, 1. edition, CRC Press (2007). doi:10.1201/9781420007282

[30] **M. Purfürst**: *Herstellung und Charakterisierung von Ultraviolett-Photodetektoren auf Indium-Galliumoxid-Basis*, Masterarbeit, Universität Leipzig (2013)

[31] **A. Werner**: *Charakterisierung von Gallium-Aluminiumoxid-Dünnfilmen*, Masterarbeit, Universität Leipzig (2017)

[32] **E. Thune, A. Fakih, C. Matringe, D. Babonneau and R. Guinebretière**: *Understanding of one dimensional ordering mechanisms at the (001) sapphire vicinal surface*, Journal of Applied Physics, volume 121, no. 1: page 015301 (2017). doi:10.1063/1.4973341

[33] **Y. Yourdshahyan, C. Ruberto, L. Bengtsson and B. I. Lundqvist**: *First-principles calculations on the atomic and electronic structure of κ-Al_2O_3*, Physical Review B, volume 56, no. 14: pages 8553–8558 (1997). doi:10.1103/physrevb.56.8553

[34] **J. Åhman, G. Svensson and J. Albertsson**: *A Reinvestigation of β-Gallium Oxide*, Acta Crystallographica Section C Crystal Structure Communications, volume 52, no. 6: pages 1336–1338 (1996). doi:10.1107/S0108270195016404

[35] **I. Cora, F. Mezzadri, F. Boschi, M. Bosi, M. Čaplovičová, G. Calestani, I. Dódony, B. Pécz and R. Fornari**: *The real structure of ϵ-Ga_2O_3 and its relation to κ-phase*, CrystEngComm, volume 19, no. 11: pages 1509–1516 (2017). doi:10.1039/c7ce00123a

[36] **M. Marezio and J. P. Remeika**: *Bond Lengths in the α-Ga_2O_3 Structure and the High-Pressure Phase of $Ga_{2-x}Fe_xO_3$*, The Journal of Chemical Physics, volume 46, no. 5: pages 1862–1865 (1967). doi:10.1063/1.1840945

[37] **H. He, R. Orlando, M. A. Blanco, R. Pandey, E. Amzallag, I. Baraille and M. Rérat**: *First-principles study of the structural, electronic, and optical properties of Ga_2O_3 in its monoclinic and hexagonal phases*, Physical Review B, volume 74, no. 19 (2006). doi:10.1103/physrevb.74.195123

[38] **H. Y. Playford, A. C. Hannon, M. G. Tucker, D. M. Dawson, S. E. Ashbrook, R. J. Kastiban, J. Sloan and R. I. Walton**: *Characterization of Structural Disorder in γ-Ga_2O_3*, The Journal of Physical Chemistry C, volume 118, no. 29: pages 16188–16198 (2014). doi:10.1021/jp5033806

[39] **T. Oshima, T. Nakazono, A. Mukai and A. Ohtomo**: *Epitaxial growth of γ-Ga_2O_3 films by mist chemical vapor deposition*, Journal of Crystal Growth, volume 359: pages 60–63 (2012). doi:10.1016/j.jcrysgro.2012.08.025

[40] **M. Higashiwaki, H. Murakami, Y. Kumagai and A. Kuramata**: *Current status of Ga_2O_3 power devices*, Japanese Journal of Applied Physics, volume 55, no. 12: page 1202A1 (2016). doi:10.7567/JJAP.55.1202A1

[41] **M. Orita, H. Ohta, M. Hirano and H. Hosono**: *Deep-ultraviolet transparent conductive β-Ga_2O_3 thin films*, Applied Physics Letters, volume 77, no. 25: pages 4166–4168 (2000). doi:10.1063/1.1330559

[42] **K. Momma and F. Izumi**: *VESTA3 for three-dimensional visualization of crystal, volumetric and morphology data*, Journal of Applied Crystallography, volume 44, no. 6: pages 1272–1276 (2011). doi:10.1107/S0021889811038970

[43] **M. Orita, H. Hiramatsu, H. Ohta, M. Hirano and H. Hosono**: *Preparation of highly conductive, deep ultraviolet transparent β-Ga_2O_3 thin film at low deposition temperatures*, Thin Solid Films, volume 411, no. 1: pages 134–139 (2002). doi:10.1016/S0040-6090(02)00202-X

[44] **K. Matsuzaki, H. Hiramatsu, K. Nomura, H. Yanagi, T. Kamiya, M. Hirano and H. Hosono**: *Growth, structure and carrier transport properties of Ga2O3 epitaxial film examined for transparent field-effect transistor*, Thin Solid Films, volume 496, no. 1: pages 37–41 (2006). doi:10.1016/j.tsf.2005.08.187

[45] **A. Petitmangin, C. Hébert, J. Perrière, B. Gallas, L. Binet, P. Barboux and P. Vermaut**: *Metallic clusters in nonstoichiometric gallium oxide films*, Journal of Applied Physics, volume 109, no. 1: page 013711 (2011). doi:10.1063/1.3531536

[46] **C. Hebert, A. Petitmangin, J. Perrière, E. Millon, A. Petit, L. Binet and P. Barboux**: *Phase separation in oxygen deficient gallium oxide films grown by pulsed-laser deposition*, Materials Chemistry and Physics, volume 133, no. 1: pages 135–139 (2012). doi:10.1016/j.matchemphys.2011.12.078

[47] **A. Petitmangin, B. Gallas, C. Hebert, J. Perrière, L. Binet, P. Barboux and X. Portier**: *Characterization of oxygen deficient gallium oxide films grown by PLD*, Applied Surface Science, volume 278: pages 153–157 (2013). doi:10.1016/j.apsusc.2012.10.136

[48] **W. Seiler, M. Selmane, K. Abdelouhadi and J. Perrière**: *Epitaxial growth of gallium oxide films on c-cut sapphire substrate*, Thin Solid Films, volume 589: pages 556–562 (2015). doi:10.1016/j.tsf.2015.06.034

[49] **K. D. Leedy, K. D. Chabak, V. Vasilyev, D. C. Look, K. Mahalingam, J. L. Brown, A. J. Green, C. T. Bowers, A. Crespo, D. B. Thomson and G. H. Jessen**: *Si content variation and influence of deposition atmosphere in homoepitaxial Si-doped β-Ga_2O_3 films by pulsed laser deposition*, APL Materials, volume 6, no. 10: page 101102 (2018). doi:10.1063/1.5047214

[50] **G. Battiston, R. Gerbasi, M. Porchia, R. Bertoncello and F. Caccavale**: *Chemical vapour deposition and characterization of gallium oxide thin films*, Thin Solid Films, volume 279, no. 1-2: pages 115–118 (1996). doi:10.1016/0040-6090(95)08161-5

[51] **L. Kong, J. Ma, C. Luan and Z. Zhu**: *Structural and optical properties of Ga_2O_3: In films deposited on MgO (100) substrates by MOCVD*, Journal of Solid State Chemistry, volume 184, no. 8: pages 1946–1950 (2011). doi:10.1016/j.jssc.2011.05.048

[52] **W. Mi, J. Ma, C. Luan, Y. Lv, H. Xiao and Z. Li**: *Characterization of β-Ga_2O_3 epitaxial films grown on MgO (111) substrates by metal-organic chemical vapor deposition*, Materials Letters, volume 87: pages 109–112 (2012). doi:10.1016/j.matlet.2012.07.106

[53] **D. Gogova, G. Wagner, M. Baldini, M. Schmidbauer, K. Irmscher, R. Schewski, Z. Galazka, M. Albrecht and R. Fornari**: *Structural properties of Si-doped β-Ga_2O_3 layers grown by MOVPE*, Journal of Crystal Growth, volume 401: pages 665–669 (2014). doi:10.1016/j.jcrysgro.2013.11.056

[54] **S. Rafique, L. Han, M. J. Tadjer, J. A. Freitas, N. A. Mahadik and H. Zhao**: *Homoepitaxial growth of β-Ga_2O_3 thin films by low pressure chemical*

vapor deposition, Applied Physics Letters, volume 108, no. 18: page 182105 (2016). doi:10.1063/1.4948944

[55] **M. Baldini, M. Albrecht, A. Fiedler, K. Irmscher, D. Klimm, R. Schewski and G. Wagner**: *Semiconducting Sn-doped β-Ga_2O_3 homoepitaxial layers grown by metal organic vapour-phase epitaxy*, Journal of Materials Science, volume 51, no. 7: pages 3650–3656 (2016). doi:10.1007/s10853-015-9693-6

[56] **Y. Zhuo, Z. Chen, W. Tu, X. Ma, Y. Pei and G. Wang**: *β-Ga_2O_3 versus ϵ-Ga_2O_3: Control of the crystal phase composition of gallium oxide thin film prepared by metal-organic chemical vapor deposition*, Applied Surface Science, volume 420: pages 802–807 (2017). doi:10.1016/j.apsusc.2017.05.241

[57] **Y. Chen, X. Xia, H. Liang, Q. Abbas, Y. Liu and G. Du**: *Growth Pressure Controlled Nucleation Epitaxy of Pure Phase ϵ- and β-Ga_2O_3 Films on Al_2O_3 via MOCVD*, Crystal Growth & Design, volume 18, no. 2: pages 1147–1154 (2018). doi:10.1021/acs.cgd.7b01576

[58] **F. Alema, B. Hertog, A. Osinsky, P. Mukhopadhyay, M. Toporkov and W. V. Schoenfeld**: *Fast growth rate of epitaxial β-Ga_2O_3 by close coupled showerhead MOCVD*, Journal of Crystal Growth, volume 475: pages 77–82 (2017). doi:10.1016/j.jcrysgro.2017.06.001

[59] **T. Kawaharamura, G. T. Dang and M. Furuta**: *Successful Growth of Conductive Highly Crystalline Sn-Doped α-Ga_2O_3 Thin Films by Fine-Channel Mist Chemical Vapor Deposition*, Japanese Journal of Applied Physics, volume 51: page 040207 (2012). doi:10.1143/jjap.51.040207

[60] **S. dong Lee, K. Kaneko and S. Fujita**: *Homoepitaxial growth of beta gallium oxide films by mist chemical vapor deposition*, Japanese Journal of Applied Physics, volume 55, no. 12: page 1202B8 (2016). doi:10.7567/jjap.55.1202b8

[61] **T. Oshima, T. Okuno and S. Fujita**: *Ga_2O_3 Thin Film Growth on c-Plane Sapphire Substrates by Molecular Beam Epitaxy for Deep-Ultraviolet Photodetectors*, Japanese Journal of Applied Physics, volume 46, no. 11R: page 7217 (2007)

[62] **T. Oshima and S. Fujita**: *Properties of Ga_2O_3-based $(In_xGa_{1-x})_2O_3$ alloy thin films grown by molecular beam epitaxy*, physica status solidi (c), volume 5, no. 9: pages 3113–3115 (2008). doi:10.1002/pssc.200779297

[63] **H. Okumura, M. Kita, K. Sasaki, A. Kuramata, M. Higashiwaki and J. S. Speck**: *Systematic investigation of the growth rate of β-Ga_2O_3(010) by*

plasma-assisted molecular beam epitaxy, Applied Physics Express, volume 7, no. 9: page 095501 (2014). doi:10.7567/apex.7.095501

[64] **H. Murakami, K. Nomura, K. Goto, K. Sasaki, K. Kawara, Q. T. Thieu, R. Togashi, Y. Kumagai, M. Higashiwaki, A. Kuramata, S. Yamakoshi, B. Monemar and A. Koukitu**: *Homoepitaxial growth of β-Ga_2O_3 layers by halide vapor phase epitaxy*, Applied Physics Express, volume 8, no. 1: page 015503 (2014). doi:10.7567/apex.8.015503

[65] **K. Nomura, K. Goto, R. Togashi, H. Murakami, Y. Kumagai, A. Kuramata, S. Yamakoshi and A. Koukitu**: *Thermodynamic study of β-Ga_2O_3 growth by halide vapor phase epitaxy*, Journal of Crystal Growth, volume 405: pages 19–22 (2014). doi:10.1016/j.jcrysgro.2014.06.051

[66] **Y. Oshima, E. G. Víllora and K. Shimamura**: *Quasi-heteroepitaxial growth of β-Ga_2O_3 on off-angled sapphire (0 0 0 1) substrates by halide vapor phase epitaxy*, Journal of Crystal Growth, volume 410: pages 53–58 (2015). doi:10.1016/j.jcrysgro.2014.10.038

[67] **V. Nikolaev, A. Pechnikov, S. Stepanov, I. Nikitina, A. Smirnov, A. Chikiryaka, S. Sharofidinov, V. Bougrov and A. Romanov**: *Epitaxial growth of β-Ga_2O_3 on (0001) sapphire substrates by halide vapour phase epitaxy*, Materials Science in Semiconductor Processing, volume 47: pages 16–19 (2016). doi:10.1016/j.mssp.2016.02.008

[68] **G. Wagner, M. Baldini, D. Gogova, M. Schmidbauer, R. Schewski, M. Albrecht, Z. Galazka, D. Klimm and R. Fornari**: *Homoepitaxial growth of β-Ga_2O_3 layers by metal-organic vapor phase epitaxy*, physica status solidi (a), volume 211, no. 1: pages 27–33 (2013). doi:10.1002/pssa.201330092

[69] **D. won Choi, K.-B. Chung and J.-S. Park**: *Low temperature Ga_2O_3 atomic layer deposition using gallium tri-isopropoxide and water*, Thin Solid Films, volume 546: pages 31–34 (2013). doi:10.1016/j.tsf.2013.03.066

[70] **H. Altuntas, I. Donmez, C. Ozgit-Akgun and N. Biyikli**: *Electrical characteristics of β-Ga_2O_3 thin films grown by PEALD*, Journal of Alloys and Compounds, volume 593: pages 190–195 (2014). doi:10.1016/j.jallcom.2014.01.029

[71] **N. Ueda, H. Hosono, R. Waseda and H. Kawazoe**: *Synthesis and control of conductivity of ultraviolet transmitting β-Ga_2O_3 single crystals*, Applied Physics Letters, volume 70, no. 26: pages 3561–3563 (1997). doi:10.1063/1.119233

[72] **E. G. Víllora, K. Shimamura, Y. Yoshikawa, K. Aoki and N. Ichinose**: *Large-size β-Ga_2O_3 single crystals and wafers*, Journal of Crystal Growth, volume 270, no. 3-4: pages 420–426 (2004). doi:10.1016/j.jcrysgro.2004.06.027

[73] **N. Suzuki, S. Ohira, M. Tanaka, T. Sugawara, K. Nakajima and T. Shishido**: *Fabrication and characterization of transparent conductive Sn-doped β-Ga_2O_3 single crystal*, physica status solidi (c), volume 4, no. 7: pages 2310–2313 (2007). doi:10.1002/pssc.200674884

[74] **H. Aida, K. Nishiguchi, H. Takeda, N. Aota, K. Sunakawa and Y. Yaguchi**: *Growth of β-Ga_2O_3 Single Crystals by the Edge-Defined, Film Fed Growth Method*, Japanese Journal of Applied Physics, volume 47, no. 11: pages 8506–8509 (2008). doi:10.1143/jjap.47.8506

[75] **Y. Tomm, P. Reiche, D. Klimm and T. Fukuda**: *Czochralski grown Ga_2O_3 crystals*, Journal of Crystal Growth, volume 220, no. 4: pages 510–514 (2000). doi:10.1016/s0022-0248(00)00851-4

[76] **Z. Galazka, R. Uecker, K. Irmscher, M. Albrecht, D. Klimm, M. Pietsch, M. Brützam, R. Bertram, S. Ganschow and R. Fornari**: *Czochralski growth and characterization of β-Ga_2O_3 single crystals*, Crystal Research and Technology, volume 45, no. 12: pages 1229–1236 (2010). doi:10.1002/crat.201000341

[77] **K. Yamaguchi**: *First principles study on electronic structure of β-Ga_2O_3*, Solid State Communications, volume 131, no. 12: pages 739–744 (2004). doi:10.1016/j.ssc.2004.07.030

[78] **S. Yoshioka, H. Hayashi, A. Kuwabara, F. Oba, K. Matsunaga and I. Tanaka**: *Structures and energetics of Ga_2O_3 polymorphs*, Journal of Physics: Condensed Matter, volume 19, no. 34: page 346211 (2007). doi:10.1088/0953-8984/19/34/346211

[79] **J. B. Varley, J. R. Weber, A. Janotti and C. G. Van de Walle**: *Oxygen vacancies and donor impurities in β-Ga_2O_3*, Applied Physics Letters, volume 97, no. 14: page 142106 (2010). doi:10.1063/1.3499306

[80] **H. Peelaers and C. G. V. de Walle**: *Brillouin zone and band structure of β-Ga_2O_3*, physica status solidi (b), volume 252, no. 4: pages 828–832 (2015). doi:10.1002/pssb.201451551

[81] **J. L. Lyons**: *Electronic Properties of Ga_2O_3 Polymorphs*, ECS Journal of Solid State Science and Technology, volume 8, no. 7: pages Q3226–Q3228 (2019). doi:10.1149/2.0331907jss

[82] **T. Matsumoto, M. Aoki, A. Kinoshita and T. Aono**: *Absorption and Reflection of Vapor Grown Single Crystal Platelets of β-Ga_2O_3*, Japanese Journal of Applied Physics, volume 13, no. 10: page 1578 (1974)

[83] **N. Ueda, H. Hosono, R. Waseda and H. Kawazoe**: *Anisotropy of electrical and optical properties in β-Ga_2O_3 single crystals*, Applied Physics Letters, volume 71, no. 7: pages 933–935 (1997). doi:10.1063/1.119693

[84] **Y. Zhang, F. Alema, A. Mauze, O. S. Koksaldi, R. Miller, A. Osinsky and J. S. Speck**: *MOCVD grown epitaxial β-Ga_2O_3 thin film with an electron mobility of 176 cm^2/V s at room temperature*, APL Materials, volume 7, no. 2: page 022506 (2019). doi:10.1063/1.5058059

[85] **C. Joishi, S. Rafique, Z. Xia, L. Han, S. Krishnamoorthy, Y. Zhang, S. Lodha, H. Zhao and S. Rajan**: *Low-pressure CVD-grown β-Ga_2O_3 bevel-field-plated Schottky barrier diodes*, Applied Physics Express, volume 11, no. 3: page 031101 (2018). doi:10.7567/apex.11.031101

[86] **Y. Zhang, C. Joishi, Z. Xia, M. Brenner, S. Lodha and S. Rajan**: *Demonstration of β-$(Al_xGa_{1-x})_2O_3/Ga_2O_3$ double heterostructure field effect transistors*, Applied Physics Letters, volume 112, no. 23: page 233503 (2018). doi:10.1063/1.5037095

[87] **K. Sasaki, A. Kuramata, T. Masui, E. G. Víllora, K. Shimamura and S. Yamakoshi**: *Device-Quality β-Ga_2O_3 Epitaxial Films Fabricated by Ozone Molecular Beam Epitaxy*, Applied Physics Express, volume 5, no. 3: page 035502 (2012)

[88] **M. Baldini, M. Albrecht, A. Fiedler, K. Irmscher, R. Schewski and G. Wagner**: *Si- and Sn-Doped Homoepitaxial β-Ga_2O_3 Layers Grown by MOVPE on (010)-Oriented Substrates*, ECS Journal of Solid State Science and Technology, volume 6, no. 2: pages Q3040–Q3044 (2017). doi:10.1149/2.0081702jss

[89] **F. Mezzadri, G. Calestani, F. Boschi, D. Delmonte, M. Bosi and R. Fornari**: *Crystal Structure and Ferroelectric Properties of ϵ-Ga_2O_3 Films Grown on (0001)-Sapphire*, Inorganic chemistry, volume 55, no. 22: pages 12079–12084 (2016). doi:10.1021/acs.inorgchem.6b02244

[90] **M. Kracht, A. Karg, J. Schörmann, M. Weinhold, D. Zink, F. Michel, M. Rohnke, M. Schowalter, B. Gerken, A. Rosenauer, P. J. Klar, J. Janek and M. Eickhoff**: *Tin-Assisted Synthesis of $\epsilon-Ga_2O_3$ by Molecular Beam Epitaxy*, Physical Review Applied, volume 8, no. 5: page 054002 (2017). doi:10.1103/PhysRevApplied.8.054002

[91] **M. Mulazzi, F. Reichmann, A. Becker, W. M. Klesse, P. Alippi, V. Fiorentini, A. Parisini, M. Bosi and R. Fornari**: *The electronic structure of ϵ-Ga_2O_3*, APL Materials, volume 7, no. 2: page 022522 (2019). doi:10.1063/1.5054395

[92] **D. Tahara, H. Nishinaka, S. Morimoto and M. Yoshimoto**: *Stoichiometric control for heteroepitaxial growth of smooth ϵ-Ga_2O_3 thin films onc-plane AlN templates by mist chemical vapor deposition*, Japanese Journal of Applied Physics, volume 56, no. 7: page 078004 (2017). doi:10.7567/jjap.56.078004

[93] **K. Shimazoe, H. Nishinaka, Y. Arata, D. Tahara and M. Yoshimoto**: *Phase control of α- and κ-Ga_2O_3 epitaxial growth on $LiNbO_3$ and $LiTaO_3$ substrates using α-Fe_2O_3 buffer layers*, AIP Advances, volume 10, no. 5: page 055310 (2020). doi:10.1063/5.0006137

[94] **X. Xia, Y. Chen, Q. Feng, H. Liang, P. Tao, M. Xu and G. Du**: *Hexagonal phase-pure wide band gap ε-Ga_2O_3 films grown on 6H-SiC substrates by metal organic chemical vapor deposition*, Applied Physics Letters, volume 108, no. 20: page 202103 (2016)

[95] **M. Pavesi, F. Fabbri, F. Boschi, G. Piacentini, A. Baraldi, M. Bosi, E. Gombia, A. Parisini and R. Fornari**: *ϵ-Ga_2O_3 epilayers as a material for solar-blind UV photodetectors*, Materials Chemistry and Physics, volume 205: pages 502 – 507 (2018). doi:https://doi.org/10.1016/j.matchemphys.2017.11.023

[96] **S. H. Park, H. S. Lee, H. S. Ahn and M. Yang**: *Crystal Phase Control of ϵ-Ga_2O_3 Fabricated using by Metal-Organic Chemical Vapor Deposition*, Journal of the Korean Physical Society, volume 74, no. 5: pages 502–507 (2019). doi:10.3938/jkps.74.502

[97] **Y. Oshima, E. G. Víllora, Y. Matsushita, S. Yamamoto and K. Shimamura**: *Epitaxial growth of phase-pure ϵ-Ga_2O_3 by halide vapor phase epitaxy*, Journal of Applied Physics, volume 118, no. 8: page 085301 (2015). doi:10.1063/1.4929417

[98] **V. I. Nikolaev, S. I. Stepanov, A. I. Pechnikov, S. Shapenkov, M. P. Scheglov, A. Chikiryaka and O. F. Vyvenko**: *HVPE Growth and Characterization of ϵ-Ga_2O_3 Films on Various Substrates*, ECS Journal of Solid State Science and Technology, volume 9, no. 4: page 045014 (2020). doi:10.1149/2162-8777/ab8b4c

[99] **P. Vogt, O. Brandt, H. Riechert, J. Lähnemann and O. Bierwagen**: *Metal-Exchange Catalysis in the Growth of Sesquioxides: Towards Heterostructures of Transparent Oxide Semiconductors*, Phys. Rev. Lett., volume 119: page 196001 (2017). doi:10.1103/PhysRevLett.119.196001

[100] **F. Boschi, M. Bosi, T. Berzina, E. Buffagni, C. Ferrari and R. Fornari**: *Hetero-epitaxy of ϵ-Ga_2O_3 layers by MOCVD and ALD*, Journal of Crystal Growth, volume 443: pages 25–30 (2016). doi:10.1016/j.jcrysgro.2016.03.013

[101] **A. Parisini, A. Bosio, V. Montedoro, A. Gorreri, A. Lamperti, M. Bosi, G. Garulli, S. Vantaggio and R. Fornari**: *Si and Sn doping of ϵ-Ga_2O_3 layers*, APL Materials, volume 7, no. 3: page 031114 (2019). doi:10.1063/1.5050982

[102] **D. Shinohara and S. Fujita**: *Heteroepitaxy of Corundum-Structured α-Ga_2O_3 Thin Films on α-Al_2O_3 Substrates by Ultrasonic Mist Chemical Vapor Deposition*, Japanese Journal of Applied Physics, volume 47, no. 9R: page 7311 (2008). doi:10.1143/JJAP.47.7311

[103] **K. Akaiwa and S. Fujita**: *Electrical Conductive Corundum-Structured α-Ga_2O_3 Thin Films on Sapphire with Tin-Doping Grown by Spray-Assisted Mist Chemical Vapor Deposition*, Japanese Journal of Applied Physics, volume 51: page 070203 (2012). doi:10.1143/jjap.51.070203

[104] **R. Cuscó, N. Domènech-Amador, T. Hatakeyama, T. Yamaguchi, T. Honda and L. Artús**: *Lattice dynamics of a mist-chemical vapor deposition-grown corundum-like Ga_2O_3 single crystal*, Journal of Applied Physics, volume 117, no. 18: page 185706 (2015). doi:10.1063/1.4921060

[105] **K. Kaneko, H. Kawanowa, H. Ito and S. Fujita**: *Evaluation of Misfit Relaxation in α-Ga_2O_3 Epitaxial Growth on α-Al_2O_3 Substrate*, Japanese Journal of Applied Physics, volume 51: page 020201 (2012). doi:10.1143/jjap.51.020201

[106] **K. Akaiwa, K. Kaneko, K. Ichino and S. Fujita**: *Conductivity control of Sn-doped α-Ga_2O_3thin films grown on sapphire substrates*, Japanese Journal of Applied Physics, volume 55, no. 12: page 1202BA (2016). doi:10.7567/jjap.55.1202ba

[107] **K. Kaneko, S. Fujita and T. Hitora**: *A power device material of corundum-structured α-Ga_2O_3 fabricated by MIST EPITAXY®technique*, Japanese Journal of Applied Physics, volume 57, no. 2S2: page 02CB18 (2018). doi:10.7567/jjap.57.02cb18

[108] **Y. Oshima, E. G. Víllora and K. Shimamura**: *Halide vapor phase epitaxy of twin-free α-Ga_2O_3 on sapphire (0001) substrates*, Applied Physics Express, volume 8, no. 5: page 055501 (2015). doi:10.7567/apex.8.055501

[109] **Y. Oshima, K. Kawara, T. Shinohe, T. Hitora, M. Kasu and S. Fujita**: *Epitaxial lateral overgrowth of α-Ga_2O_3 by halide vapor phase epitaxy*, APL Materials, volume 7, no. 2: page 022503 (2019). doi:10.1063/1.5051058

[110] **A. I. Pechnikov, S. I. Stepanov, A. V. Chikiryaka, M. P. Scheglov, M. A. Odnobludov and V. I. Nikolaev**: *Thick α-Ga_2O_3 Layers on Sapphire Substrates Grown by Halide Epitaxy*, Semiconductors, volume 53, no. 6: pages 780–783 (2019). doi:10.1134/s1063782619060150

[111] **V. I. Nikolaev, A. I. Pechnikov, V. V. Nikolaev, M. P. Scheglov, A. V. Chikiryaka, S. I. Stepanov, O. S. Medvedev, S. V. Shapenkov, E. V. Ubyivovk and O. F. Vyvenko**: *HVPE growth of α- and ϵ-Ga_2O_3 on patterned sapphire substrates*, Journal of Physics: Conference Series, volume 1400: page 055049 (2019). doi:10.1088/1742-6596/1400/5/055049

[112] **V. Gottschalch, S. Merker, S. Blaurock, M. Kneiß, U. Teschner, M. Grundmann and H. Krautscheid**: *Heteroepitaxial growth of α-, β-, γ- and κ-Ga_2O_3 phases by metalorganic vapor phase epitaxy*, Journal of Crystal Growth, volume 510: pages 76–84 (2019). doi:10.1016/j.jcrysgro.2019.01.018

[113] **G. Sinha, K. Adhikary and S. Chaudhuri**: *Sol–gel derived phase pure α-Ga_2O_3 nanocrystalline thin film and its optical properties*, Journal of Crystal Growth, volume 276, no. 1-2: pages 204–207 (2005). doi:10.1016/j.jcrysgro.2004.11.375

[114] **R. Schewski, G. Wagner, M. Baldini, D. Gogova, Z. Galazka, T. Schulz, T. Remmele, T. Markurt, H. von Wenckstern, M. Grundmann, O. Bierwagen, P. Vogt and M. Albrecht**: *Epitaxial stabilization of pseudomorphic α-Ga_2O_3 on sapphire (0001)*, Applied Physics Express, volume 8, no. 1: page 011101 (2014). doi:10.7567/apex.8.011101

[115] **G. T. Dang, S. Sato, Y. Tagashira, T. Yasuoka, L. Liu and T. Kawaharamura**: *α-$(Al_xGa_{1-x})_2O_3$ single-layer and heterostructure buffers for the*

growth of conductive Sn-doped α-Ga_2O_3 thin films via mist chemical vapor deposition, APL Materials, volume 8, no. 10: page 101101 (2020). doi:10.1063/5.0023041

[116] **T. Uchida, K. Kaneko and S. Fujita**: *Electrical characterization of Si-doped n-type α-Ga2O3 on sapphire substrates*, MRS Advances, volume 3, no. 3: pages 171–177 (2018). doi:10.1557/adv.2018.45

[117] **S. Morimoto, H. Nishinaka and M. Yoshimoto**: *Growth and characterization of F-doped α-Ga_2O_3 thin films with low electrical resistivity*, Thin Solid Films, volume 682: pages 18–23 (2019). doi:10.1016/j.tsf.2019.04.051

[118] **M. Oda, R. Tokuda, H. Kambara, T. Tanikawa, T. Sasaki and T. Hitora**: *Schottky barrier diodes of corundum-structured gallium oxide showing on-resistance of 0.1 mΩ·cm^2 grown by MIST EPITAXY® T2 - Applied Physics Express*, Applied Physics Express, volume 9, no. 2: page 021101 (2016)

[119] **H. Y. Playford, A. C. Hannon, E. R. Barney and R. I. Walton**: *Structures of uncharacterised polymorphs of gallium oxide from total neutron diffraction*, Chem. - A Eur. J., volume 19, no. 8: pages 2803–2813 (2013). doi:10.1002/chem.201203359

[120] **H. Hayashi, R. Huang, H. Ikeno, F. Oba, S. Yoshioka, I. Tanaka and S. Sonoda**: *Room temperature ferromagnetism in Mn-doped γ-Ga_2O_3 with spinel structure*, Applied Physics Letters, volume 89, no. 18: page 181903 (2006). doi:10.1063/1.2369541

[121] **Y. Huang, Z. Liu, J. Wang, Z. Yusong, D. Guo, X. Wang, W. Xiaolong, Z. Chen, P. Li and W.-H. Tang**: *The effect of Mn dopant on structural and optoelectronic properties of γ-Ga_2O_3 thin film photodetectors*, ECS Journal of Solid State Science and Technology, volume 9: page 055010 (2020). doi:10.1149/2162-8777/ab9ab3

[122] **Y. Huang, A. Gao, D. Guo, X. Lu, X. Zhang, Y. Huang, J. Yu, S. Li, P. Li and W. Tang**: *Fe doping-stabilized γ-Ga_2O_3 thin films with a high room temperature saturation magnetic moment*, Journal of Materials Chemistry C, volume 8, no. 2: pages 536–542 (2020). doi:10.1039/c9tc05823k

[123] **I. Cora, Z. Fogarassy, R. Fornari, M. Bosi, A. Rečnik and B. Pécz**: *In situ TEM study of κ→β and κ→γ phase transformations in Ga_2O_3* , Acta Materialia, volume 183: pages 216–227 (2020). doi:10.1016/j.actamat.2019.11.019

[124] **M. Marezio**: *Refinement of the crystal structure of In_2O_3 at two wavelengths*, Acta Crystallographica, volume 20, no. 6: pages 723–728 (1966). doi:10.1107/s0365110x66001749

[125] **E. J. Tarsa, J. H. English and J. S. Speck**: *Pulsed laser deposition of oriented In_2O_3 on (001) InAs, MgO, and yttria-stabilized zirconia*, Applied Physics Letters, volume 62, no. 19: pages 2332–2334 (1993). doi:10.1063/1.109408

[126] **T. Koida and M. Kondo**: *High electron mobility of indium oxide grown on yttria-stabilized zirconia*, Journal of Applied Physics, volume 99, no. 12: page 123703 (2006). doi:10.1063/1.2203722

[127] **C.-Y. Park, S.-G. Yoon, Y.-H. Jo and S.-C. Shin**: *Room-temperature ferromagnetism observed in Mo-doped indium oxide films*, Applied Physics Letters, volume 95, no. 12: page 122502 (2009). doi:10.1063/1.3232243

[128] **C. Kranert, R. Schmidt-Grund and M. Grundmann**: *Raman active phonon modes of cubic In_2O_3*, physica status solidi (RRL) - Rapid Research Letters, volume 8, no. 6: pages 554–559 (2014). doi:10.1002/pssr.201409004

[129] **R. Schmidt-Grund, H. Krauß, C. Kranert, M. Bonholzer and M. Grundmann**: *Temperature dependence of the dielectric function in the spectral range (0.5–8.5) eV of an In_2O_3 thin film*, Applied Physics Letters, volume 105, no. 11: page 111906 (2014). doi:10.1063/1.4896321

[130] **N. Taga, M. Maekawa, Y. Shigesato, I. Yasui, M. Kamei and T. E. Haynes**: *Deposition of Heteroepitaxial In_2O_3 Thin Films by Molecular Beam Epitaxy*, Japanese Journal of Applied Physics, volume 37, no. Part 1, No. 12A: pages 6524–6529 (1998). doi:10.1143/jjap.37.6524

[131] **A. Bourlange, D. J. Payne, R. G. Egdell, J. S. Foord, P. P. Edwards, M. O. Jones, A. Schertel, P. J. Dobson and J. L. Hutchison**: *Growth of In_2O_3 (100) on Y-stabilized ZrO_2 (100) by O-plasma assisted molecular beam epitaxy*, Applied Physics Letters, volume 92, no. 9: page 092117 (2008). doi:10.1063/1.2889500

[132] **E. H. Morales, Y. He, M. Vinnichenko, B. Delley and U. Diebold**: *Surface structure of Sn-doped In_2O_3 (111) thin films by STM*, New Journal of Physics, volume 10, no. 12: page 125030 (2008). doi:10.1088/1367-2630/10/12/125030

[133] **O. Bierwagen, M. E. White, M.-Y. Tsai and J. S. Speck**: *Plasma-assisted molecular beam epitaxy of high quality In_2O_3 (001) thin films on Y-stabilized ZrO_2*

(001) using In as an auto surfactant, Applied Physics Letters, volume 95, no. 26: page 262105 (2009). doi:10.1063/1.3276910

[134] **O. Bierwagen and J. S. Speck**: *Nucleation of islands and continuous high-quality In_2O_3 (001) films during plasma-assisted molecular beam epitaxy on Y-stabilized ZrO_2 (001)*, Journal of Applied Physics, volume 107, no. 11: page 113519 (2010). doi:10.1063/1.3415539

[135] **K. H. L. Zhang, V. K. Lazarov, P. L. Galindo, F. E. Oropeza, D. J. Payne, H. H.-C. Lai and R. G. Egdell**: *Domain Matching Epitaxial Growth of In_2O_3 Thin Films on α-Al_2O_3 (0001)*, Crystal Growth & Design, volume 12, no. 2: pages 1000–1007 (2012). doi:10.1021/cg201474h

[136] **C. Y. Wang, V. Cimalla, H. Romanus, T. Kups, G. Ecke, T. Stauden, M. Ali, V. Lebedev, J. Pezoldt and O. Ambacher**: *Phase selective growth and properties of rhombohedral and cubic indium oxide*, Applied Physics Letters, volume 89, no. 1: page 011904 (2006). doi:10.1063/1.2219125

[137] **C. Y. Wang, V. Lebedev, V. Cimalla, T. Kups, K. Tonisch and O. Ambacher**: *Structural studies of single crystalline In_2O_3 films epitaxially grown on InN (0001)*, Applied Physics Letters, volume 90, no. 22: page 221902 (2007). doi:10.1063/1.2743907

[138] **L. Kong, J. Ma, C. Luan, Z. Zhu and Q. Yu**: *Domain structure and optical property of epitaxial indium oxide film deposited on MgO (100) substrate*, Surface Science, volume 605, no. 9-10: pages 977–981 (2011). doi:10.1016/j.susc.2011.02.017

[139] **M. Kamei, Y. Shigesato and S. Takaki**: *Origin of characteristic grain-subgrain structure of tin-doped indium oxide films*, Thin Solid Films, volume 259, no. 1: pages 38–45 (1995). doi:10.1016/0040-6090(94)06390-7

[140] **N. Taga, H. Odaka, Y. Shigesato, I. Yasui, M. Kamei and T. E. Haynes**: *Electrical properties of heteroepitaxial grown tin-doped indium oxide films*, Journal of Applied Physics, volume 80, no. 2: pages 978–984 (1996). doi:10.1063/1.362910

[141] **. Xirouchaki, G. Kiriakidis, T. F. Pedersen and H. Fritzsche**: *Photoreduction and oxidation of as-deposited microcrystalline indium oxide*, Journal of Applied Physics, volume 79, no. 12: pages 9349–9352 (1996). doi:10.1063/1.362612

[142] **R. L. Weiher and R. P. Ley**: *Optical Properties of Indium Oxide*, Journal of Applied Physics, volume 37, no. 1: pages 299–302 (1966). doi:10.1063/1.1707830

[143] **A. Walsh, J. L. F. D. Silva, S.-H. Wei, C. Körber, A. Klein, L. F. J. Piper, A. DeMasi, K. E. Smith, G. Panaccione, P. Torelli, D. J. Payne, A. Bourlange and R. G. Egdell**: *Nature of the Band Gap of In_2O_3 Revealed by First-Principles Calculations and X-Ray Spectroscopy*, Physical Review Letters, volume 100, no. 16 (2008). doi:10.1103/physrevlett.100.167402

[144] **H. Köstlin, R. Jost and W. Lems**: *Optical and electrical properties of doped In_2O_3 films*, Physica Status Solidi (a), volume 29, no. 1: pages 87–93 (1975). doi:10.1002/pssa.2210290110

[145] **R. L. Weiher**: *Electrical Properties of Single Crystals of Indium Oxide*, Journal of Applied Physics, volume 33, no. 9: pages 2834–2839 (1962). doi:10.1063/1.1702560

[146] **V. G. Hill, R. Roy and E. F. Osborn**: *The System Alumina-Gallia-Water*, Journal of the American Ceramic Society, volume 35, no. 6: pages 135–142 (1952). doi:10.1111/j.1151-2916.1952.tb13087.x

[147] **M. Mizuno, T. Yamada and T. No**: *The liquidus curve in the system Al_2O_3-Ga_2O_3 as measured with a solar furnace*, Journal of the Ceramic Association, Japan, volume 83, no. 956: pages 175–177 (1975). doi:10.2109/jcersj1950.83.956_175

[148] **A. L. Jaromin and D. D. Edwards**: *Subsolidus Phase Relationships in the Ga_2O_3-Al_2O_3-TiO_2 System*, Journal of the American Ceramic Society, volume 88, no. 9: pages 2573–2577 (2005). doi:10.1111/j.1551-2916.2005.00484.x

[149] **T. Oshima, T. Okuno, N. Arai, Y. Kobayashi and S. Fujita**: *β-$Al_{2x}Ga_{2-2x}O_3$ Thin Film Growth by Molecular Beam Epitaxy*, Japanese Journal of Applied Physics, volume 48, no. 7: page 070202 (2009). doi:10.1143/JJAP.48.070202

[150] **M. Lorenz, S. Hohenberger, E. Rose and M. Grundmann**: *Atomically stepped, pseudomorphic, corundum-phase $(Al_{1-x}Ga_x)_2O_3$ thin films ($0 \leq x < 0.08$) grown on R-plane sapphire*, Applied Physics Letters, volume 113, no. 23: page 231902 (2018). doi:10.1063/1.5059374

[151] **H. Ito, K. Kaneko and S. Fujita**: *Growth and Band Gap Control of Corundum-Structured α-$(AlGa)_2O_3$ Thin Films on Sapphire by Spray-Assisted Mist Chemical Vapor Deposition*, Japanese Journal of Applied Physics, volume 51: page 100207 (2012). doi:10.1143/JJAP.51.100207

[152] **K. Kaneko, K. Suzuki, Y. Ito and S. Fujita**: *Growth characteristics of corundum-structured α-$(Al_xGa_{1-x})_2O_3/Ga_2O_3$ heterostructures on sapphire substrates*, Journal of Crystal Growth, volume 436: pages 150–154 (2016). doi:10.1016/j.jcrysgro.2015.12.013

[153] **G. T. Dang, T. Yasuoka, Y. Tagashira, T. Tadokoro, W. Theiss and T. Kawaharamura**: *Bandgap engineering of α-$(Al_xGa_{1-x})_2O_3$ by a mist chemical vapor deposition two-chamber system and verification of Vegard's Law*, Applied Physics Letters, volume 113, no. 6: page 062102 (2018). doi:10.1063/1.5037678

[154] **M. Grundmann and M. Lorenz**: *Anisotropic strain relaxation through prismatic and basal slip in α-$(Al,Ga)_2O_3$ on R-plane Al_2O_3*, APL Materials, volume 8, no. 2: page 021108 (2020). doi:10.1063/1.5144744

[155] **R. Kumaran, T. Tiedje, S. E. Webster, S. Penson and W. Li**: *Epitaxial Nd-doped α-$(Al_{1-x}Ga_x)_2O_3$ films on sapphire for solid-state waveguide lasers*, Optics Letters, volume 35, no. 22: page 3793 (2010). doi:10.1364/ol.35.003793

[156] **F. Zhang, K. Saito, T. Tanaka, M. Nishio, M. Arita and Q. Guo**: *Wide bandgap engineering of $(AlGa)_2O_3$ films*, Applied Physics Letters, volume 105, no. 16: page 162107 (2014). doi:10.1063/1.4900522

[157] **R. Wakabayashi, T. Oshima, M. Hattori, K. Sasaki, T. Masui, A. Kuramata, S. Yamakoshi, K. Yoshimatsu and A. Ohtomo**: *Oxygen-radical-assisted pulsed-laser deposition of β-Ga_2O_3 and β-$(Al_xGa_{1-x})_2O_3$ films*, Journal of Crystal Growth, volume 424: pages 77–79 (2015). doi:10.1016/j.jcrysgro.2015.05.005

[158] **X. Wang, Z. Chen, F. Zhang, K. Saito, T. Tanaka, M. Nishio and Q. Guo**: *Influence of substrate temperature on the properties of $(AlGa)_2O_3$ thin films prepared by pulsed laser deposition*, Ceramics International, volume 42, no. 11: pages 12783–12788 (2016). doi:10.1016/j.ceramint.2016.05.039

[159] **Q. Feng, Z. Feng, Z. Hu, X. Xing, G. Yan, J. Zhang, Y. Xu, X. Lian and Y. Hao**: *Temperature dependent electrical properties of pulse laser deposited Au/Ni/β-$(AlGa)_2O_3$ Schottky diode*, Applied Physics Letters, volume 112, no. 7: page 072103 (2018). doi:10.1063/1.5019310

[160] **A. Vaidya, J. Sarker, Y. Zhang, L. Lubecki, J. Wallace, J. D. Poplawsky, K. Sasaki, A. Kuramata, A. Goyal, J. A. Gardella, B. Mazumder and U. Singisetti**: *Structural, band and electrical characterization of β-$(Al_{0.19}Ga_{0.81})_2O_3$ films grown by molecular beam epitaxy on Sn doped β-Ga_2O_3 substrate*, Journal of Applied Physics, volume 126, no. 9: page 095702 (2019). doi:10.1063/1.5113509

[161] **H. Okumura, Y. Kato, T. Oshima and T. Palacios**: *Demonstration of lateral field-effect transistors using Sn-doped β-$(AlGa)_2O_3$ (010)*, Japanese Journal of Applied Physics, volume 58, no. SB: page SBBD12 (2019). doi:10.7567/1347-4065/ab002b

[162] **E. Ahmadi, Y. Oshima, F. Wu and J. S. Speck**: *Schottky barrier height of Ni to β-$(Al_xGa_{1-x})_2O_3$ with different compositions grown by plasma-assisted molecular beam epitaxy*, Semiconductor Science and Technology, volume 32, no. 3: page 035004 (2017). doi:10.1088/1361-6641/aa53a7

[163] **C.-C. Wang, S.-H. Yuan, S.-L. Ou, S.-Y. Huang, K.-Y. Lin, Y.-A. Chen, P.-W. Hsiao and D.-S. Wuu**: *Growth and characterization of co-sputtered aluminum-gallium oxide thin films on sapphire substrates*, Journal of Alloys and Compounds, volume 765: pages 894–900 (2018). doi:10.1016/j.jallcom.2018.06.270

[164] **D. Tahara, H. Nishinaka, S. Morimoto and M. Yoshimoto**: *Heteroepitaxial growth of ε-$(Al_xGa_{1-x})_2O_3$ alloy films on c-plane AlN templates by mist chemical vapor deposition*, Applied Physics Letters, volume 112, no. 15: page 152102 (2018)

[165] **N. Suzuki, K. Kaneko and S. Fujita**: *Growth of corundum-structured $(In_xGa_{1-x})_2O_3$ alloy thin films on sapphire substrates with buffer layers*, Journal of Crystal Growth, volume 401: pages 670–672 (2014). doi:10.1016/j.jcrysgro.2014.02.051

[166] **S. Fujita, M. Oda, K. Kaneko and T. Hitora**: *Evolution of corundum-structured III-oxide semiconductors: Growth, properties, and devices*, Japanese Journal of Applied Physics Part 1-Regular Papers Short Notes & Review Papers, volume 55, no. 12: page 1202A3 (2016)

[167] **M. Baldini, D. Gogova, K. Irmscher, M. Schmidbauer, G. Wagner and R. Fornari**: *Heteroepitaxy of $Ga_{2(1-x)}In_{2x}O_3$ layers by MOVPE with two different oxygen sources*, Crystal Research and Technology, volume 49, no. 8: pages 552–557 (2014). doi:10.1002/crat.201300410

[168] **H. von Wenckstern, D. Splith, M. Purfürst, Z. Zhang, C. Kranert, S. Müller, M. Lorenz and M. Grundmann**: *Structural and optical properties of $(In,Ga)_2O_3$ thin films and characteristics of Schottky contacts thereon*, Semiconductor Science and Technology, volume 30, no. 2: page 024005 (2015). doi:10.1088/0268-1242/30/2/024005

[169] **F. Zhang, K. Saito, T. Tanaka, M. Nishio and Q. Guo**: *Wide bandgap engineering of $(GaIn)_2O_3$ films*, Solid State Communications, volume 186: pages 28–31 (2014). doi:10.1016/j.ssc.2014.01.024

[170] **Z. Zhang, H. von Wenckstern, J. Lenzner, M. Lorenz and M. Grundmann**: *Visible-blind and solar-blind ultraviolet photodiodes based on $(In_xGa_{1-x})_2O_3$*, Applied Physics Letters, volume 108, no. 12: page 123503 (2016). doi:10.1063/1.4944860

[171] **P. Vogt and O. Bierwagen**: *Kinetics versus thermodynamics of the metal incorporation in molecular beam epitaxy of $(In_xGa_{1-x})_2O_3$*, APL Materials, volume 4, no. 8: page 086112 (2016). doi:10.1063/1.4961513

[172] **Y. Kokubun, T. Abe and S. Nakagomi**: *Sol-gel prepared $(Ga_{1-x}In_x)_2O_3$ thin films for solar-blind ultraviolet photodetectors*, physica status solidi (a), volume 207, no. 7: pages 1741–1745 (2010). doi:10.1002/pssa.200983712

[173] **H. Nishinaka, N. Miyauchi, D. Tahara, S. Morimoto and M. Yoshimoto**: *Incorporation of indium into ϵ-gallium oxide epitaxial thin films grown via mist chemical vapour deposition for bandgap engineering*, Crystengcomm, volume 20, no. 13: pages 1882–1888 (2018)

[174] **F. Yang, J. Ma, C. Luan and L. Kong**: *Structural and optical properties of $Ga_{2(1-x)}In_{2x}O_3$films prepared on α-Al_2O_3 (0001) by MOCVD*, Applied Surface Science, volume 255, no. 8: pages 4401–4404 (2009). doi:10.1016/j.apsusc.2008.10.129

[175] **L. Kong, J. Ma, F. Yang, C. Luan and Z. Zhu**: *Preparation and characterization of $Ga_{2x}In_{2(1-x)}O_3$ films deposited on ZrO_2 (100) substrates by MOCVD*, Journal of Alloys and Compounds, volume 499, no. 1: pages 75–79 (2010). doi:10.1016/j.jallcom.2010.02.092

[176] **V. M. Goldschmidt, T. Barth and G. Lunde.**: *Geochemische Verteilungsgesetze der Elemente*, Skr. norske Vidensk.-Akad. Mat.-Naturv. KI, volume Band 7 (1925)

[177] **R. Shannon and C. Prewitt**: *Synthesis and structure of phases in the In_2O_3 - Ga_2O_3 system*, Journal of Inorganic and Nuclear Chemistry, volume 30: pages 1389 – 1398 (1968)

[178] **R. J. Cava, J. M. Phillips, J. Kwo, G. A. Thomas, R. B. van Dover, S. A. Carter, J. J. Krajewski, W. F. Peck, J. H. Marshall and D. H. Rapkine**: *$GaInO_3$: A new transparent conducting oxide*, Applied Physics Letters, volume 64, no. 16: pages 2071–2072 (1994). doi:10.1063/1.111686

[179] **J. M. Phillips, J. Kwo, G. A. Thomas, S. A. Carter, R. J. Cava, S. Y. Hou, J. J. Krajewski, J. H. Marshall, W. F. Peck, D. H. Rapkine and R. B. van Dover**: *Transparent conducting thin films of $GaInO_3$*, Applied Physics Letters, volume 65, no. 1: pages 115–117 (1994). doi:10.1063/1.113052

[180] **M. Lorenz**: *Pulsed Laser Deposition of ZnO-Based Thin Films*, in *Transparent Conductive Zinc Oxide*, pages 303–357, Springer Berlin Heidelberg (2008). doi:10.1007/978-3-540-73612-7_7

[181] **M. Kneiß**: *Combinatorial Pulsed Laser Deposition Employing Radially-Segmented Targets: Exploring Orthorhombic $(In_xGa_{1-x})_2O_3$ and $(Al_xGa_{1-x})_2O_3$ Towards Superlattice Heterostructures*, PhD thesis, Universität Leipzig (2020)

[182] **M. Kneiß, P. Storm, G. Benndorf, M. Grundmann and H. von Wenckstern**: *Combinatorial Material Science and Strain Engineering Enabled by Pulsed Laser Deposition Using Radially Segmented Targets*, ACS Combinatorial Science, volume 20, no. 11: pages 643–652 (2018). doi:10.1021/acscombsci.8b00100

[183] **J. I. Goldstein, D. E. Newbury, J. R. Michael, N. W. Ritchie, J. H. J. Scott and D. C. Joy**: *Scanning Electron Microscopy and X-Ray Microanalysis*, 4. edition, Springer New York, ISBN 978-1-4939-6674-5 (2018). doi:10.1007/978-1-4939-6676-9

[184] **D. Necas and P. Klapetek**: *Gwyddion: an open-source software for SPM data analysis*, Central European Journal of Physics, volume 10, no. 1: pages 181–188 (2012)

[185] **M. Grundmann**: *The physics of semiconductors: An introduction including devices and nanophysics*, 3. edition, Springer, Berlin and New York, ISBN 978-3-319-23880-7 (2016). doi:0.1007/3-540-34661-9

[186] **C. Sturm, R. Schmidt-Grund, C. Kranert, J. Furthmüller, F. Bechstedt and M. Grundmann**: *Dipole analysis of the dielectric function of color*

dispersive materials: Application to monoclinic Ga_2O_3, Phys. Rev. B, volume 94: page 035148 (2016). doi:10.1103/PhysRevB.94.035148

[187] **H. Fujiwara**: *Spectroscopic Ellipsometry: Principles and Applications*, 1. edition, John Wiley & Sons, ISBN 9780470016084 (2007)

List of Publications

The references [E2-E7] are part of this cumulative thesis.

[E1] **M. Kneiß, P. Storm, A. Hassa, D. Splith, H. von Wenckstern, M. Lorenz and M. Grundmann**: *Growth, structural and optical properties of coherent κ-$(Al_xGa_{1-x})_2O_3$/κ-Ga_2O_3 quantum well superlattice heterostructures*, APL Materials, volume 8, no. 5: page 051112 (2020). doi:10.1063/5.0007137

[E2] **A. Hassa, H. von Wenckstern, L. Vines and M. Grundmann**: *Influence of Oxygen Pressure on Growth of Si-Doped β-$(Al_xGa_{1-x})_2O_3$ Thin Films on c-Sapphire Substrates by Pulsed Laser Deposition*, ECS Journal of Solid State Science and Technology, volume 8, no. 7: pages Q3217–Q3220 (2019). doi:10.1149/2.0411907jss

[E3] **A. Hassa, C. Wouters, M. Kneiß, D. Splith, C. Sturm, H. von Wenckstern, M. Albrecht, M. Lorenz and M. Grundmann**: *Control of phase formation of $(Al_xGa_{1-x})_2O_3$ thin films on c-plane Al_2O_3*, Journal of Physics D: Applied Physics, volume 53, no. 48 (2020). doi:10.1088/1361-6463/abaf7d

[E4] **A. Hassa, C. Sturm, M. Kneiß, D. Splith, H. von Wenckstern, T. Schultz, N. Koch, M. Lorenz and M. Grundmann**: *Solubility limit and material properties of a κ-$(Al_xGa_{1-x})_2O_3$ thin film with a lateral cation gradient on (00.1)Al_2O_3 by tin-assisted PLD*, APL Materials, volume 8, no. 2: page 021103 (2020). doi:10.1063/1.5141041

[E5] **A. Hassa, H. von Wenckstern, D. Splith, C. Sturm, M. Kneiß, V. Prozheeva and M. Grundmann**: *Structural, optical, and electrical properties of orthorhombic κ-$(In_xGa_{1-x})_2O_3$ thin films*, APL Materials, volume 7, no. 2: page 022525 (2019). doi:10.1063/1.5054394

[E6] **A. Hassa, P. Storm, M. Kneiß, D. Splith, H. von Wenckstern, M. Lorenz and M. Grundmann**: *Structural and Elastic Properties of α-*

$(Al_xGa_{1-x})_2O_3$ Thin Films on (11.0) Al_2O_3 Substrates for the Entire Composition Range, physica status solidi (b), page 2000394 (2020). doi:10.1002/pssb.202000394

[E7] **A. Hassa, M. Grundmann and H. von Wenckstern**: *Progression of Group-III Sesquioxides: Epitaxy, Solubility and Desorption*, Journal of Physics D: Applied Physics (2020). doi:10.1088/1361-6463/abd4a4

[E8] **H. von Wenckstern, D. Splith, A. Werner, S. Müller, M. Lorenz and M. Grundmann**: *Properties of Schottky Barrier Diodes on $(In_xGa_{1-x})_2O_3$ for $0.01 \leq x \leq 0.85$ Determined by a Combinatorial Approach*, ACS Combinatorial Science, volume 17, no. 12: pages 710–715 (2015). doi:10.1021/acscombsci.5b00084

[E9] **C. Wouters, C. Sutton, L. M. Ghiringhelli, T. Markurt, R. Schewski, A. Hassa, H. von Wenckstern, M. Grundmann, M. Scheffler and M. Albrecht**: *Investigating the ranges of (meta)stable phase formation in $(In_xGa_{1-x})_2O_3$: Impact of the cation coordination*, Physical Review Materials, volume 4, no. 12 (2020). doi:10.1103/physrevmaterials.4.125001

[E10] **J. E. N. Swallow, R. G. Palgrave, P. A. E. Murgatroyd, A. Regoutz, M. Lorenz, A. Hassa, M. Grundmann, H. von Wenckstern, J. B. Varley and T. D. Veal**: *Indium Gallium Oxide Alloys: Electronic Structure, Optical Gap, Surface Space Charge, and Chemical Trends within Common-Cation Semiconductors*, ACS Appl. Mater. Interfaces (2021). doi:10.1021/acsami.0c16021

[E11] **M. Kneiß, A. Hassa, D. Splith, C. Sturm, H. von Wenckstern, T. Schultz, N. Koch, M. Lorenz and M. Grundmann**: *Tin-assisted heteroepitaxial PLD-growth of κ-Ga_2O_3 thin films with high crystalline quality*, APL Materials, volume 7, no. 2: page 022516 (2019). doi:10.1063/1.5054378

[E12] **M. Kneiß, A. Hassa, D. Splith, C. Sturm, H. von Wenckstern, M. Lorenz and M. Grundmann**: *Epitaxial stabilization of single phase κ-$(In_xGa_{1-x})_2O_3$ thin films up to $x = 0.28$ on c-sapphire and κ-Ga_2O_3 (001) templates by tin-assisted VCCS-PLD*, APL Materials, volume 7, no. 10: page 101102 (2019). doi:10.1063/1.5120578

[E13] **P. Storm, M. Kneiß, A. Hassa, T. Schultz, D. Splith, H. von Wenckstern, N. Koch, M. Lorenz and M. Grundmann**: *Epitaxial κ-$(Al_xGa_{1-x})_2O_3$ thin films and heterostructures grown by tin-assisted VCCS-*

PLD, APL Materials, volume 7, no. 11: page 111110 (2019). doi:10.1063/1.5124231

[E14] **H. von Wenckstern, M. Kneiß, A. Hassa, P. Storm, D. Splith and M. Grundmann**: *A Review of the Segmented-Target Approach to Combinatorial Material Synthesis by Pulsed-Laser Deposition*, physica status solidi (b), page 1900626 (2019). doi:10.1002/pssb.201900626

[E15] **M. Kneiß, P. Storm, A. Hassa, D. Splith, H. von Wenckstern, M. Lorenz and M. Grundmann**: *Epitaxial Growth of κ-$(Al_xGa_{1-x})_2O_3$ Layers and Superlattice Heterostructures up to $x = 0.48$ on Highly Conductive Al-Doped ZnO Thin-Film Templates by Pulsed Laser Deposition*, physica status solidi (b), page 2000359 (2020). doi:10.1002/pssb.202000359

Author Contributions

A. Hassa, H. von Wenckstern, L. Vines, and M. Grundmann: *Influence of Oxygen Pressure on Growth of Si-Doped β-$(Al_xGa_{1-x})_2O_3$ Thin Films on c-Sapphire Substrates by Pulsed Laser Deposition*, ECS Journal of Solid State Science and Technology, volume 8, no. 7, pages Q3217–Q3220 (2019). doi:10.1149/2.0411907jss

The concept of this manuscript was created by H. von Wenckstern and me. Sample preparation (by PLD), XRD and AFM measurements were performed by me. EDX measurements were conducted by J. Lenzner, transmission measurements by U. Teschner and the PLD target was prepared by M. Hahn. The implantation was done by L. Vines within a collaboration with the University of Oslo. The subsequent annealing of the implanted samples was executed by me. I analyzed and evaluated the data series received on EDX, XRD, AFM, and transmission measurements. Within the scope of this work, I conceived and implemented electrical transport measurements, such as Hall-Effect and Schottky-diode measurements, including the required preparations. All figures were prepared by me. The manuscript was written by me and all authors critically revised and approved the manuscript, and contributed significantly by discussions on the interpretation of the data. Project supervision and scientific guidance was provided by H. von Wenckstern and M. Grundmann. The project was funded within the framework of the Young Investigator Group "Oxide Heterostructure" (SAB100310460) and partly by the Deutsche Forschungsgemeinschaft (DFG, German Research Foundation) - project number 31047525, SFB762, project B04.

A. Hassa, C. Wouters, M. Kneiß, D. Splith, C. Sturm, H. von Wenckstern, M. Albrecht, M. Lorenz, and M. Grundmann: *Control of phase formation of $(Al_xGa_{1-x})_2O_3$ thin films on c-plane Al_2O_3*, Journal of Physics D: Applied Physics, volume 53, no. 48 (2020). doi:10.1088/1361-6463/abaf7d

The manuscript was conceived and written by me, except the section dealing with the TEM, which was written by C. Wouters. The samples were fabricated by me. The XRD and AFM measurements were conducted be me. EDX measurements were performed by J. Lenzner, spectroscopic ellipsometry measurements by C. Sturm and the PLD target was prepared by M. Hahn. The TEM measurements were performed at the Leibniz-Institut für Kristallzüchtung in Berlin from C. Wouters. The experiment design, evaluation and creation of the figures was carried out in cooperation with C. Wouters. I analyzed and evaluated the data series received on EDX, XRD, AFM, and ellipsometry measurements. The corresponding figures were created by me. All authors critically revised and approved the manuscript, and contributed significantly by discussions on the interpretation of the data. Project supervision and scientific guidance was provided by D. Splith, H. von Wenckstern and M. Grundmann. The project was funded within the framework of the Young Investigator Group "Oxide Heterostructure" (SAB100310460) and partly by the Deutsche Forschungsgemeinschaft (DFG, German Research Foundation) - project number 31047525, SFB762, project B04.

A. Hassa, C. Sturm, M. Kneiß, D. Splith, H. von Wenckstern, T. Schultz, N. Koch, M. Lorenz, and M. Grundmann: *Solubility limit and material properties of a κ-$(Al_xGa_{1-x})_2O_3$ thin film with a lateral cation gradient on (00.1)Al_2O_3 by tin-assisted PLD*, APL Materials, volume 8, no. 2, page 021103 (2020). doi:10.1063/1.5141041

The manuscript was conceived and written by me. The sample was fabricated by me and the XRD and AFM measurements were conducted by me, too. EDX measurements were performed by J. Lenzner, spectroscopic ellipsometry measurements by C. Sturm, transmission measurements by U. Teschner and the PLD target was prepared by M. Hahn. XPS measurements were executed and evaluated at the Humboldt Universität zu Berlin by T. Schultz and the experiment was designed by me and T. Schultz. I analyzed and evaluated the data series received on EDX, XRD, AFM, and transmission measurements. The spectroscopic ellipsometry measurements were evaluated by C. Sturm. All figures were prepared by me, except Fig.2 (XPS measurement) which was prepared by T. Schultz and adjusted by me. All authors critically revised and approved the manuscript, and contributed significantly by discussions on the interpretation of the data. Project supervision and scientific guidance was provided by D. Splith, H. von Wenckstern and M. Grundmann. The project was funded within the framework of the Young Investigator Group "Oxide Heterostructure" (SAB100310460) and partly by the Deutsche Forschungsgemeinschaft (DFG, German Research Foundation) - project number 31047525, SFB762, project B04.

A. Hassa, H. von Wenckstern, D. Splith, C. Sturm, M. Kneiß, V. Prozheeva, and M. Grundmann: *Structural, optical, and electrical properties of orthorhombic κ-$(In_xGa_{1-x})_2O_3$ thin films*, APL Materials, volume 7, no. 2, page 022525 (2019). doi:10.1063/1.5054394

This work was created in collaboration with the co-authors. The concept was developed by H. von Wenckstern and me. The sample investigated was fabricated by me. The XRD and AFM measurements were conducted by me, EDX measurements by J. Lenzner, the spectroscopic ellipsometry measurements by C. Sturm, transmission measurements by U. Teschner and the PLD target was prepared by M. Hahn. The parts about alloy composition, crystal structure, surface morphology, bandgap engineering as well as abstract and conclusion were written by me. The data were evaluated and the corresponding graphs compiled by me. The introduction was written in cooperation with H. von Wenckstern, and the description of the dielectric function by C. Sturm. M. Kneiß provided discussions on the interpretation of the XRD data wrote a paragraph on the interpretation of XRD data. The electrical thin film characterization (resistivity, Hall-effect, temperature I-V, and quasi C-V measurements) were realized and written in cooperation with D. Splith. All authors critically revised and approved the manuscript, and contributed significantly by discussions on the interpretation of the data. Project supervision and scientific guidance was provided by D. Splith, H. von Wenckstern and M. Grundmann. The project was funded within the framework of the Young Investigator Group "Oxide Heterostructure" (SAB100310460) and partly by the Deutsche Forschungsgemeinschaft (DFG, German Research Foundation) - project number 31047525, SFB762, project B04.

A. Hassa, P. Storm, M. Kneiß, D. Splith, H. von Wenckstern, M. Lorenz, and M. Grundmann: *Structural and elastic properties of α-$(Al_xGa_{1-x})_2O_3$ thin films on (11.0)Al_2O_3 substrates for the entire composition range*, physica status solidi (b), pages 2000394 (2020). doi:10.1002/pssb.202000394

The manuscript was conceived and written by me. The sample was fabricated by me. XRD $2\theta - \omega$- and ϕ-scans were conducted and evaluated be me. EDX measurements were performed by D. Splith. Reciprocal space map measurements were performed, analyzed and evaluated in collaboration with P. Storm and M. Kneiß. M. Grundmann provided theoretical calculations about the evolution of the out-of-plane a-lattice con-

stant. All figures were prepared by me, except of Figure 3, which was prepared by P. Storm. All authors critically revised and approved the manuscript, and contributed significantly by discussions on the interpretation of the data. Project supervision and scientific guidance was provided by D. Splith, H. von Wenckstern and M. Grundmann. The project was funded within the framework of the Young Investigator Group "Oxide Heterostructure" (SAB100310460) and partly by the Deutsche Forschungsgemeinschaft (DFG, German Research Foundation) - project number 31047525, SFB762, project B04.

A. Hassa, M. Grundmann and H. von Wenckstern: *Progression of Group-III Sesquioxides: Epitaxy, Solubility and Desorption*, Journal of Physics D: Applied Physics, accepted manuscript (2020). doi:10.1088/1361-6463/abd4a4

The manuscript was conceived and written by me. The samples discussed in the first part were fabricated by me. The EDX measurements were performed by D. Splith. The growth rates were calculated from the thin film thickness, which were determined by spectroscopic ellipsometry measurements performed by C. Sturm. All data (internal and external) contained in the review were collected by me. The resulting formulas were calculated by me. All figures were prepared by me. H. von Wenckstern provided valuable discussions on the manuscript. All authors critically revised and approved the manuscript. Project supervision and scientific guidance was provided by H. von Wenckstern and M. Grundmann. The project was funded within the framework of the Young Investigator Group "Oxide Heterostructure" (SAB100310460) and partly by the Deutsche Forschungsgemeinschaft (DFG, German Research Foundation) - project number 31047525, SFB762, project B04.

Zusammenfassung nach Promotionsordnung §11(4)

Zusammenfassung der Dissertation

Epitaxy and Physical Properties of Group-III Sesquioxide Alloys

der Fakultät für Physik und Geowissenschaften der Universität Leipzig

eingereicht von
M. Sc. Anna Hassa, geb. Werner

angefertigt am
Felix-Bloch-Institut für Festkörperphysik

Januar 2021

Semiconductor-based technology has become an integral part of today's life and is used in smartphones and tablets, among other things. The primarily utilized semiconductor silicon has reached its fundamental technological limits in some, more specialized areas of application - such as the detection of UV radiation - which has brought semiconductors with ultra-wide bandgaps into focus. Gallium oxide (Ga_2O_3) is a particularly promising candidate to enable device performance beyond that of silicon based devices, e.g. in high power electronics or in deep-UV photodetectors (PDs). Due to its ultra-wide bandgap of about 4.6–5.3 eV, Ga_2O_3 is transparent to the human eye. By alloying with other group-III sesquioxides, namely Al_2O_3 (8.8 eV [1]) or In_2O_3 (3.7 eV [2]), the optical bandgap of Ga_2O_3 can be enlarged or reduced and hence enable the fabrication of heterostructures. Further unique properties of Ga_2O_3 are an about three times larger breakdown field of $8\,\mathrm{MV\,cm^{-1}}$ [3] and a high thermal stability.

Ga_2O_3 can crystallize in a rhombohedral (α), monoclinic (β), defective spinel (γ) or orthorhombic (κ) crystal structure [4]. So far, most publications and reviews (in the field of Ga_2O_3) deal with the thermodynamically most stable β-modification [5–9]. In combination with the availability of large native substrates, β-Ga_2O_3 is a suitable candidate for the realization of high performance power devices and UV-PDs, as well. Additional to the promising properties of the β-polymorph, the orthorhombic κ-phase has another outstanding feature: a predicted spontaneous polarization P of 23–26 $\mu\mathrm{C/cm^2}$ [10–12]. At the interface of heterostructures (e.g. Ga_2O_3 / $(Al,Ga)_2O_3$), an abrupt and large change of P causes a charge accumulation and thus extremely 2DEG densities [13], and hence this phase is well suited for high electron mobility transistors. Therefore, a significant part of this work will be devoted to study the κ-phase. The special feature about the rhombohedral α-modification is that this phase can also occur for Al_2O_3 and In_2O_3, which allows a potential bandgap engineering over the entire composition range rendering this polymorph interesting for wavelength-selective PDs, such as deep UV-PDs or quantum-well infrared PDs.

Since all of the mentioned sesquioxides can appear in different crystallographic modifications, alloys of the individual phases can only be stabilized up to certain chemical compositions of the alloy systems. The phase limits influence directly the potential bandgap range and differ for the various distinct polymorphs. For the purpose of isostructural bandgap engineering, it is crucial to determine the phase boundaries and enhance current miscibility gaps, if possible. Connected with this directly is the value of the optical bandgap and thus constitutes an essential part of this thesis for the α-, β- and κ-modification of the $(Al,Ga)_2O_3$ or $(In,Ga)_2O_3$ alloys. Furthermore, the crystalline quality and surface morphology of the different alloys are of particular interest and were determined as a function of the alloy composition within this work. In order to fabricate high quality samples, the best growth conditions have to be defined. All in the scope of this thesis presented

and discussed thin films were grown by pulsed laser deposition (PLD). With this growth method, the substrate temperature (T_g) as well as the oxygen pressure ($p(O_2)$) in the PLD chamber can be set. Previous studies Ga_2O_3 thin films by PLD revealed that the choice of T_g and $p(O_2)$ have a significant impact on the formation of the thin films [14, 15]. How the choice of conditions affects the growth of the respective alloy will therefore be a main part of this work. After analyzing the potential research areas of Ga_2O_3 based alloys as stated above, the resulting main research aspects for this doctor's thesis are as follows:

(I) Analysis of phase formation and desorption processes of the β- and κ-modifications of $(Al,Ga)_2O_3$ and $(In,Ga)_2O_3$ thin films in dependence on $p(O_2)$ and/or T_g

(II) Determination of physical properties of κ-$(Al_xGa_{1-x})_2O_3$, κ-$(In_xGa_{1-x})_2O_3$ as well as α-$(Al_xGa_{1-x})_2O_3$ thin films as a function of the cation composition x

(III) Extension of the phase limits and thus an expanded optical bandgap range of the sesquioxides

For processing these topics, thin films were deposited by different PLD approaches and systematically changed growth conditions. On the one hand, single ceramic targets with a distinct chemical composition were utilized in order to investigate the influence of $p(O_2)$ and T_g on physical properties on the sesquioxide alloys. On the other hand, circular half-segmented (Ga_2O_3/Al_2O_3 or Ga_2O_3/In_2O_3) ceramic targets were used to prepare 2 inch in diameter large thin films with a lateral varying cation composition (CCS-PLD) [16].
During the elaboration of the first point, $p(O_2)$ and T_g were changed systemically and the impact on, e.g., the target-to-layer cation transfer ratio or the growth rate were studied. Low $p(O_2)$, resulting in an oxygen poor growth regime, lead to the formation and subsequent desorption of volatile suboxides. Since the Al-O, Ga-O, and In-O bonds possess different dissociation energies, the cations offered are incorporated into the layer in a different preferential order. The highest dissociation energy has the Al-O bond followed by the Ga-O bond and then by the In-O bond, resulting in a preferentially Al [Ga] incorporation into the $(Al,Ga)_2O_3$ [$(In,Ga)_2O_3$] alloy.
With an additional Sn-doping in the PLD target and under distinct growth conditions, the κ-phase was stabilized. The determination of the required growth window for the facilitation of κ-$(Al,Ga)_2O_3$ was focused in the scope of this thesis, as well, and was defined by $T_g \geq 580°C$ and $p(O_2) \leq 0.016\,mbar$. Other growth parameters lead to thin films with β- and γ-phase impurities or monoclinic thin films. Further, physical properties of κ-$(Al,Ga)_2O_3$ and κ-$(In,Ga)_2O_3$ thin films grown by CCS-PLD on $(00.1)Al_2O_3$ were investigated as a function of the chemical composition. To date, the highest In-content into κ-Ga_2O_3 of 35 at.% is achieved. In combination with the maximum Al-content of 46 at.%, bandgap engineering between 4.3 and 5.9 eV is possible. XRD investigations reveal epitaxially grown thin films with (001)-orientation in three rotational domains. Furthermore, α-$(Al,Ga)_2O_3$ was in the entire composition range successful stabilized. For about 240 nm thick samples, relaxed growth was shown for $x_{Al} < 0.55$, which turns for higher Al-contents to pseudomorphic growth.
In the last part of this thesis, a topical review summarizes literature data together with the data collected during the procession of this work on the progression of current miscibility limits, optical band gaps and lattice constants as a function of the cation composition for the different polymorphs of the sesquioxide alloys.
In conclusion, the extensive data on the physical properties of the different phases of the alloys is very significant and allows, among other things, to control the phase formation or suppress the formation and desorption of volatile suboxides in the sesquioxide alloys.

References

[1] **S. D. Mo and W. Y. Ching**: *Electronic and optical properties of θ-Al_2O_3 and comparison to α-Al_2O_3*, Physical Review B, volume 57, no. 24: pages 15219–15228 (1998). doi: 10.1103/PhysRevB.57.15219

[2] **C. T. Prewitt, R. D. Shannon, D. B. Rogers and A. W. Sleight**: *C rare earth oxide-corundum transition and crystal chemistry of oxides having the corundum structure*, Inorganic Chemistry, volume 8, no. 9: pages 1985–1993 (1969). doi: 10.1021/ic50079a033

[3] **M. Higashiwaki, K. Sasaki, A. Kuramata, T. Masui and S. Yamakoshi**: *Gallium oxide (Ga_2O_3) metal-semiconductor field-effect transistors on single-crystal β-Ga_2O_3 (010) substrates*, Applied Physics Letters, volume 100, no. 1: page 013504 (2012). doi: 10.1063/1.3674287

[4] **R. Roy, V. G. Hill and E. F. Osborn**: *Polymorphism of Ga_2O_3 and the System Ga_2O_3-H_2O*, Journal of the American Chemical Society, volume 74, no. 3: pages 719–722 (1952)

[5] **S. Stepanov, V. Nikolaev, V. Bougrov and A. Romanov**: *Gallium oxide: Properties and applications - A review*, Rev. Adv. Mater. Sci., volume 44: pages 63–86 (2016)

[6] **H. von Wenckstern**: *Group-III Sesquioxides: Growth, Physical Properties and Devices*, Advanced Electronic Materials, volume 3, no. 9: page 1600350 (2017). doi: 10.1002/aelm.201600350

[7] **M. Higashiwaki, A. Kuramata, H. Murakami and Y. Kumagai**: *State-of-the-art technologies of gallium oxide power devices*, Journal of Physics D: Applied Physics, volume 50, no. 33: page 333002 (2017)

[8] **S. J. Pearton, J. Yang, P. H. Cary, F. Ren, J. Kim, M. J. Tadjer and M. A. Mastro**: *A review of Ga_2O_3 materials, processing, and devices*, Applied Physics Reviews, volume 5, no. 1: page 011301 (2018). doi: 10.1063/1.5006941

[9] **J. Zhang, J. Shi, D.-C. Qi, L. Chen and K. H. L. Zhang**: *Recent progress on the electronic structure, defect, and doping properties of Ga_2O_3*, APL Materials, volume 8, no. 2: page 020906 (2020). doi: 10.1063/1.5142999

[10] **M. B. Maccioni and V. Fiorentini**: *Phase diagram and polarization of stable phases of $(Ga_{1-x}In_x)_2O_3$*, Applied Physics Express, volume 9, no. 4: page 041102 (2016). doi: 10.7567/apex.9.041102

[11] **S. B. Cho and R. Mishra**: *Epitaxial engineering of polar ϵ-Ga_2O_3 for tunable two-dimensional electron gas at the heterointerface*, Applied Physics Letters, volume 112, no. 16: page 162101 (2018). doi: 10.1063/1.5019721

[12] **J. Kim, D. Tahara, Y. Miura and B. G. Kim**: *First-principle calculations of electronic structures and polar properties of (κ, ϵ)-Ga_2O_3*, Applied Physics Express, volume 11, no. 6: page 061101 (2018)

[13] **P. Ranga, S. B. Cho, R. Mishra and S. Krishnamoorthy**: *Highly tunable, polarization-engineered two-dimensional electron gas in ϵ-$AlGaO_3$/ϵ-Ga_2O_3 heterostructures*, Applied Physics Express, volume 13, no. 6: page 061009 (2020). doi: 10.35848/1882-0786/ab9168

[14] **S. Müller, H. von Wenckstern, D. Splith, F. Schmidt and M. Grundmann**: *Control of the conductivity of Si-doped β-Ga_2O_3 thin films via growth temperature and pressure*, physica status solidi (a), volume 211, no. 1: pages 34–39 (2014). doi: 10.1002/pssa.201330025

[15] **F. B. Zhang, K. Saito, T. Tanaka, M. Nishio and Q. X. Guo**: *Structural and optical properties of Ga_2O_3 films on sapphire substrates by pulsed laser deposition*, Journal of Crystal Growth, volume 387: pages 96–100 (2014). doi: 10.1016/j.jcrysgro.2013.11.022

[16] **H. von Wenckstern, Z. Zhang, F. Schmidt, J. Lenzner, H. Hochmuth and M. Grundmann**: *Continuous composition spread using pulsed-laser deposition with a single segmented target*, CrystEngComm, volume 15, no. 46: page 10020 (2013). doi: 10.1039/c3ce41327f

Publication list of the author

Publications as part of the cumulative thesis

[C1] **A. Hassa, H. von Wenckstern, L. Vines, and M. Grundmann:** *Influence of Oxygen Pressure on Growth of Si-Doped β-$(Al_xGa_{1-x})_2O_3$ Thin Films on c-Sapphire Substrates by Pulsed Laser Deposition*, ECS Journal of Solid State Science and Technology, volume 8, no. 7, pages Q3217–Q3220 (2019). doi:10.1149/2.0411907jss

The concept of this manuscript was created by H. von Wenckstern and me. Sample preparation (by PLD), XRD and AFM measurements were performed by me. EDX measurements were conducted by J. Lenzner, transmission measurements by U. Teschner and the PLD target was prepared by M. Hahn. The implantation was done by L. Vines within a collaboration with the University of Oslo. The subsequent annealing of the implanted samples was executed by me. I analyzed and evaluated the data series received on EDX, XRD, AFM, and transmission measurements. Within the scope of this work, I conceived and implemented electrical transport measurements, such as Hall-Effect and Schottky-diode measurements, including the required preparations. All figures were prepared by me. The manuscript was written by me and all authors critically revised and approved the manuscript, and contributed significantly by discussions on the interpretation of the data. Project supervision and scientific guidance was provided by H. von Wenckstern and M. Grundmann. The project was funded within the framework of the Young Investigator Group "Oxide Heterostructure" (SAB100310460) and partly by the Deutsche Forschungsgemeinschaft (DFG, German Research Foundation) - project number 31047525, SFB762, project B04.

[C2] **A. Hassa, C. Wouters, M. Kneiß, D. Splith, C. Sturm, H. von Wenckstern, M. Albrecht, M. Lorenz, and M. Grundmann:** *Control of phase formation of $(Al_xGa_{1-x})_2O_3$ thin films on c-plane Al_2O_3*, Journal of Physics D: Applied Physics, volume 53, no. 48 (2020). doi:10.1088/1361-6463/abaf7d

The manuscript was conceived and written by me, except the section dealing with the TEM, which was written by C. Wouters. The samples were fabricated by me. The XRD and AFM measurements were conducted be me. EDX measurements were performed by J. Lenzner, spectroscopic ellipsometry measurements by C. Sturm and the PLD target was prepared by M. Hahn. The TEM measurements were performed at the Leibniz-Institut für Kristallzüchtung in Berlin from C. Wouters. The experiment design, evaluation and creation of the figures was carried out in cooperation with C. Wouters. I analyzed and evaluated the data series received on EDX, XRD, AFM, and ellipsometry measurements. The corresponding figures were created by me. All authors critically revised and approved the manuscript, and contributed significantly by discussions on the interpretation of the data. Project supervision and scientific guidance was provided by D. Splith, H. von Wenckstern and M. Grundmann. The project was funded within the framework of the Young Investigator Group "Oxide Heterostructure" (SAB100310460) and partly by the Deutsche Forschungsgemeinschaft (DFG, German Research Foundation) - project number 31047525, SFB762, project B04.

[C3] A. Hassa, C. Sturm, M. Kneiß, D. Splith, H. von Wenckstern, T. Schultz, N. Koch, M. Lorenz, and M. Grundmann: *Solubility limit and material properties of a κ-$(Al_xGa_{1-x})_2O_3$ thin film with a lateral cation gradient on (00.1)Al_2O_3 by tin-assisted PLD*, APL Materials, volume 8, no. 2, page 021103 (2020). doi:10.1063/1.5141041

The manuscript was conceived and written by me. The sample was fabricated by me and the XRD and AFM measurements were conducted by me, too. EDX measurements were performed by J. Lenzner, spectroscopic ellipsometry measurements by C. Sturm, transmission measurements by U. Teschner and the PLD target was prepared by M. Hahn. XPS measurements were executed and evaluated at the Humboldt Universität zu Berlin by T. Schultz and the experiment was designed by me and T. Schultz. I analyzed and evaluated the data series received on EDX, XRD, AFM, and transmission measurements. The spectroscopic ellipsometry measurements were evaluated by C. Sturm. All figures were prepared by me, except Fig.2 (XPS measurement) which was prepared by T. Schultz and adjusted by me. All authors critically revised and approved the manuscript, and contributed significantly by discussions on the interpretation of the data. Project supervision and scientific guidance was provided by D. Splith, H. von Wenckstern and M. Grundmann. The project was funded within the framework of the Young Investigator Group "Oxide Heterostructure" (SAB100310460) and partly by the Deutsche Forschungsgemeinschaft (DFG, German Research Foundation) - project number 31047525, SFB762, project B04.

[C4] A. Hassa, H. von Wenckstern, D. Splith, C. Sturm, M. Kneiß, V. Prozheeva, and M. Grundmann: *Structural, optical, and electrical properties of orthorhombic κ-$(In_xGa_{1-x})_2O_3$ thin films*, APL Materials, volume 7, no. 2, page 022525 (2019). doi:10.1063/1.5054394

This work was created in collaboration with the co-authors. The concept was developed by H. von Wenckstern and me. The sample investigated was fabricated by me. The XRD and AFM measurements were conducted by me, EDX measurements by J. Lenzner, the spectroscopic ellipsometry measurements by C. Sturm, transmission measurements by U. Teschner and the PLD target was prepared by M. Hahn. The parts about alloy composition, crystal structure, surface morphology, bandgap engineering as well as abstract and conclusion were written by me. The data were evaluated and the corresponding graphs compiled by me. The introduction was written in cooperation with H. von Wenckstern, and the description of the dielectric function by C. Sturm. M. Kneiß provided discussions on the interpretation of the XRD data wrote a paragraph on the interpretation of XRD data. The electrical thin film characterization (resistivity, Hall-effect, temperature I-V, and quasi C-V measurements) were realized and written in cooperation with D. Splith. All authors critically revised and approved the manuscript, and contributed significantly by discussions on the interpretation of the data. Project supervision and scientific guidance was provided by D. Splith, H. von Wenckstern and M. Grundmann. The project was funded within the framework of the Young Investigator Group "Oxide Heterostructure" (SAB100310460) and partly by the Deutsche Forschungsgemeinschaft (DFG, German Research Foundation) - project number 31047525, SFB762, project B04.

[C5] A. Hassa, P. Storm, M. Kneiß, D. Splith, H. von Wenckstern, M. Lorenz, and M. Grundmann: *Structural and elastic properties of α-$(Al_xGa_{1-x})_2O_3$ thin films on (11.0)Al_2O_3 substrates for the entire composition range*, physica status solidi (b), pages 2000394 (2020). doi:10.1002/pssb.202000394

The manuscript was conceived and written by me. The sample was fabricated by me. XRD $2\theta-\omega$- and ϕ-scans were conducted and evaluated be me. EDX measurements were performed by D. Splith. Reciprocal space map measurements were performed, analyzed and evaluated in collaboration with P. Storm and M. Kneiß. M. Grundmann provided theoretical calculations about the evolution of the out-of-plane a-lattice constant. All figures were prepared by me, except of Figure 3, which was prepared by P. Storm. All authors critically revised and approved the manuscript, and contributed significantly by discussions on the interpretation of the data. Project supervision and scientific guidance was provided by D. Splith, H. von Wenckstern and M. Grundmann. The project was funded within the framework of the Young Investigator Group "Oxide Heterostructure" (SAB100310460) and partly by the Deutsche Forschungsgemeinschaft (DFG, German Research Foundation) - project number 31047525, SFB762, project B04.

[C6] A. Hassa, M. Grundmann and H. von Wenckstern: *Progression of Group-III Sesquioxides: Epitaxy, Solubility and Desorption*, Journal of Physics D: Applied Physics, accepted manuscript (2020). doi:10.1088/1361-6463/abd4a4

The manuscript was conceived and written by me. The samples discussed in the first part were fabricated by me. The EDX measurements were performed by D. Splith. The growth rates were calculated from the thin film thickness, which were determined by spectroscopic ellipsometry measurements performed by C. Sturm. All data (internal and external) contained in the review were collected by me. The resulting formulas were calculated by me. All figures were prepared by me. H. von Wenckstern provided valuable discussions on the manuscript. All authors critically revised and approved the manuscript. Project supervision and scientific guidance was provided by H. von Wenckstern and M. Grundmann. The project was funded within the framework of the Young Investigator Group "Oxide Heterostructure" (SAB100310460) and partly by the Deutsche Forschungsgemeinschaft (DFG, German Research Foundation) - project number 31047525, SFB762, project B04.

Other publications with contribution by the author

[P1] H. von Wenckstern, D. Splith, A. Werner, S. Müller, M.Lorenz and M. Grundmann: *Properties of Schottky Barrier Diodes on* $(In_xGa_{1-x})_2O_3$ *for* $0.01 \leq x \leq 0.85$ *Determined by a Combinatorial Approach*, ACS Combinatorial Science, volume 17, no. 12: pages 710–715 (2015). doi:10.1021/acscombsci.5b00084

I fabricated the Schottky-contacts, performed I-V measurements on these contacts along the thin film cation gradient and evaluated data.

[P2] H. von Wenckstern, M. Kneiß, A. Hassa, P. Storm, D. Splith and M. Grundmann: *A Review of the Segmented-Target Approach to Combinatorial Material Synthesis by Pulsed-Laser Deposition*, Physica Status Solidi (B) Basic Research, volume 1900626: pages 1–13 (2019). doi:10.1002/pssb.201900626

I provided data concerning the CCS thin films. All authors critically revised and approved the manuscript.

[P3] M. Kneiß, A. Hassa, D. Splith, C. Sturm, H. von Wenckstern, T. Schultz, N. Koch, M. Lorenz and M. Grundmann: *Tin-assisted heteroepitaxial PLD-growth of* κ-Ga_2O_3 *thin films with high crystalline quality, APL Materials*, volume 7, no. 2: page 022516 (2019). doi:10.1063/1.5054378

I prepared and performed XRD measurements on a temperature sample series. All authors critically revised and approved the manuscript.

[P4] M. Kneiß, A. Hassa, D. Splith, C. Sturm, H. Von Wenckstern, M. Lorenz and M. Grundmann: *Epitaxial stabilization of single phase* κ-$(In_xGa_{1-x})_2O_3$ *thin films up to* $x = 0.28$ *on c-sapphire and* κ-Ga_2O_3, APL Materials, volume 7, no. 10: page 101102 (2019). doi:10.1063/1.5120578

All authors critically revised and approved the manuscript.

[P5] P. Storm, M. Kneiß, A. Hassa, T. Schultz, D. Splith, H. Von Wenckstern, N. Koch, M. Lorenz and M. Grundmann: *Epitaxial* κ-$(Al_xGa_{1-x})_2O_3$ *thin films and heterostructures grown by tin-assisted VCCS-PLD*, APL Materials, volume 7, no. 11: page 111110 (2019). doi:10.1063/1.5124231

I provided discussions on the stabilization of the κ-phase. All authors critically revised and approved the manuscript.

[P6] M. Kneiß, P. Storm, A. Hassa, D. Splith, H. von Wenckstern, M. Lorenz and M. Grundmann: *Growth, Structural and Optical Properties of Coherent* κ-$(Al_xGa_{1-x})_2O_3$/κ-Ga_2O_3 *Quantum Well Superlattice Heterostructures*, APL Materials, volume 8, no. 5: page 051112 (2020). doi:10.1063/5.0007137

All authors critically revised and approved the manuscript.

[P7] M. Kneiß, P. Storm, A. Hassa, D. Splith, H. von Wenckstern, M. Lorenz and M. Grundmann: *Epitaxial Growth of κ-$(Al_xGa_{1-x})_2O_3$ Layers and Superlattice Heterostructures up to $x = 0.48$ on Highly Conductive Al-Doped ZnO Thin-Film Templates by Pulsed Laser Deposition*, physica status solidi (b), volume n/a, no. n/a: page 2000359 (2020). doi:10.1002/pssb.202000359

I provided discussions. All authors critically revised and approved the manuscript.

[P8] C. Wouters, C. Sutton, L. M. Ghiringhelli, T. Markurt, R. Schewski, A. Hassa, H. von Wenckstern, M. Grundmann, M. Scheffler, and M. Albrecht: *Investigating the ranges of (meta)stable phase formation in $(In_xGa_{1-x})_2O_3$: Impact of the cation coordination*, Physical Review Materials, volume 4, no. 12 (2020). doi:10.1103/physrevmaterials.4.125001

I prepared the thin film sample and provided the cation composition data by EDX. I examined and evaluated the crystal structure by XRD. All authors critically revised and approved the manuscript.

[P9] J. E. N. Swallow, R. G. Palgrave, P. A. E. Murgatroyd, A. Regoutz, M. Lorenz, A. Hassa, M. Grundmann, H. von Wenckstern, J. B. Varley, and T. D. Veal: *Indium Gallium Oxide Alloys: Electronic Structure, Optical Gap, Surface Space Charge, and Chemical Trends within Common-Cation Semiconductors*, ACS Appl. Mater. Interfaces (2021). doi: 10.1021/acsami.0c16021

I prepared the thin film investigated, evaluated the crystal structure by XRD as well as the cation composition data by EDX and created the corresponding graphs. All authors critically revised and approved the manuscript.

Collaborations and third-party services

Collaborations within the Felix Bloch Institute of Solid State Physics, Semiconductor Physics Group:

- Max Kneiß provided thin film samples, XRD measurements and assisted by discussions on the interpretation of data on κ-Ga_2O_3 and the alloy systems
- Holger von Wenckstern provided fruitful discussions around the sesquioxides during the procession of this thesis
- Daniel Splith managed the Young Investigator Group and supported in particular with electrical measurements
- Chris Sturm performed and evaluated ellipsometry measurements
- Ulrike Teschner performed transmission spectroscopy measurements
- Monika Hahn and Gabriele Ramm fabricated ceramic targets
- Holger Hochmuth introduced me to the PLD setup
- Jörg Lenzner and Daniel Splith measured and evaluated EDX spectra
- Michael Lorenz introduced me to the XRD measurement technique and equipment setup
- Philipp Storm plotted RSM measurements
- Within the scope of this thesis, bachelor thesis of Mario Klebahn and master thesis of Catharina Krömmelbein and Clemens Petersen were supervised
- This thesis was funded within the framework of the Young Investigator Group "Oxide Heterostructure" (SAB100310460) and partly by the Deutsche Forschungsgemeinschaft (DFG, German Research Foundation) - project number 31047525, SFB762, project B04, which were acquired by Holger von Wenckstern, Michael Lorenz and Marius Grundmann
- This work further was funded by Leipzig School of Natural Sciences BuildMoNa

External collaborations:

- Implantations of Sn and Si to potentially induce electrical conductivity in β-$(Al,Ga)_2O_3$ thin films were performed by Lasse Vines at the University of Oslo
- TEM measurements were performed and evaluated by Charlotte Wouters at the Leibniz-Institut für Kristallzüchtung in Berlin
- XPS measurements were performed and evaluated by Thorsten Schultz, Department of Physics, Humboldt Universität zu Berlin
- First deposition and investigations of a κ-$(In_xGa_{1-x})_2O_3$ thin films were executed in collaboration with Vera Prozheeva from the Aalto University

Supervisors

This thesis was supervised by PD Dr. habil. Holger von Wenckstern and Prof. Dr. Marius Grundmann. Project supervision was further provided by Dr. Daniel Splith and PD Dr. habil. Holger von Wenckstern as project leader and mentor of the Young Investigator Group "Oxide Heterostructure" (SAB100310460), respectively.

Institutes

This thesis was developed between August 2017 and December 2020 at
University Leipzig
Felix Bloch Institute for Solid State Physics
Semiconductor Physics Group
Linnestraße 5
04103 Leipzig, Germany

Dopant implantation (tin, silicon) as part of this thesis were performed by Prof. Lasse Vines at
University of Oslo
Department of Physics/Centre for Materials Science and Nanotechnology
Blindern, P.O. Box 1048
Oslo N-0316, Norway

TEM measurements as part of this thesis were performed and evaluated by M.Sc. Charlotte Wouters under supervision by Prof. Dr. Martin Albrecht at
Leibniz-Institut für Kristallzüchtung
Max-Born-Str. 2
12489 Berlin, Germany

XPS measurements as part of this thesis were performed and evaluated by Dr. Thorsten Schultz under supervision by Prof. Dr. Norbert Koch at
Humboldt Universität zu Berlin
Department of Physics
Newtonstraße 15
12489 Berlin, Germany
and
Helmholtz-Zentrum für Materialien und Energie GmbH
Hahn-Meitner-Platz 1
14109 Berlin, Germany

Discussion and first investigations of κ-$(In,Ga)_2O_3$ were provided in collaboration with Dr. Vera Prozheeva from
Aalto University
Department of Applied Physics
P.O. Box 15100
FIN-00076 Aalto, Finland

Selbständigkeitserklärung

Hiermit erkläre ich, dass ich die vorliegende Dissertation mit dem Titel:

"Epitaxy and Physical Properties of Group-III Sesquioxide Alloys"

ohne unzulässige Hilfe und ohne Benutzung anderer, als der angegebenen Hilfsmittel, angefertigt habe. Weiterhin erkläre ich, dass Gedanken, die aus fremden Quellen direkt oder indirekt übernommenen wurden, als solche in der Arbeit gekennzeichnet wurden. Ich versichere, dass außer den in der Dissertation genannten Personen, keine weiteren Personen bei der geistigen Anfertigung dieser Arbeit beteiligt waren und ich insbesondere nicht die Hilfe eines Promotionsberaters in Anspruch genommen habe. Weiterhin erkläre ich, dass keine weiteren Personen von mir oder in meinem Auftrag unmittelbar oder mittelbar geldwerte Leistungen für Arbeiten erhalten haben, die im Zusammenhang mit dem Inhalt der vorgelegten Dissertation stehen. Ich versichere, dass die vorgelegte Arbeit weder im Inland noch im Ausland in gleicher oder in ähnlicher Form in einer anderen Prüfungsbehörde zum Zwecke einer Promotion oder eines anderen Prüfungsverfahrens vorgelegt und in ihrer Gesamtheit noch nicht veröffentlicht wurde. Ich erkläre, dass ich bisher keine erfolglosen Promotionsversuche unternommen habe.

Leipzig, den 20.01.2021

Anna Hassa

Curriculum Vitae

Persönliche Daten

Name	Anna Hassa, geb. Werner
geboren am	01.05.1991 in Görlitz
Nationalität	deutsch

Ausbildung

Seit 10/2017	Mitglied der Graduiertenschule BuildMoNa
Seit 08/2017	Wissenschaftlicher Mitarbeiter und Doktorand am Felix-Bloch-Institut für Festkörperphysik, Abteilung Halbleiterphysik, Universität Leipzig
2014 – 2017	Masterstudiengang Physik an der Universität Leipzig Abschluss: Master of Science Titel: *Charakterisierung von Gallium-Aluminiumoxid-Dünnfilmen*
2010 – 2014	Bachelorstudiengang Physik an der Universität Leipzig Abschluss: Bachelor of Science Titel: *Strukturelle und elektrische Eigenschaften von Si-dotierten* $(Ga,In)_2O_3$ *Dünnfilmen*
2009 – 2010	Bachelorstudiengang Chemie an der Universität Leipzig
2001 – 2009	Schulbesuch am Augustum-Annengymnasium in Görlitz Abschluss: Abitur
1997 – 2001	Schulbesuch an der Diesterwegschule in Görlitz